The Hong Kong Polytechnic University

Interdisciplinary Division of Biomedical Engineering

DEVELOPMENT OF 3D ULTRASOUND SYSTEM FOR ASSESSING ADOLESCENT IDIOPATHIC SCOLIOSIS

Cheung Chung Wai James

A thesis submitted in partial fulfillment of the requirements

for the degree of Doctor of Philosophy

February 2013

CERTIFCATE OF ORIGINALITY

I hereby declare that this thesis is my own work and that, to the best of my knowledge and belief, it reproduces no material previously published or written, nor material that has been accepted for the award of any other degree or dimple, except where due acknowledgement has been made in the text.

__________________________________ (Signed)

____Cheung_Chung_Wai_James___ (Name of student)

ABSTRACT OF THESIS

"Development of 3D Ultrasound System for Assessing Adolescent Idiopathic Scoliosis"

Submitted by **Cheung Chung Wai James**

for the degree of Doctor Philosophy in Biomedical Engineering at The Hong Kong Polytechnic University in February 2013

Adolescent idiopathic scoliosis (AIS) is a common spinal disease. The prevalence of AIS is 2 to 4 % of the youngster population between 10 and 16 years old in the US. In Hong Kong, the prevalence of AIS is about 3%. With spinal deformity in coronal plane more than 10° measured by Cobb's method, the medical condition is defined as scoliosis. Cobb's method has been regarded as a gold standard in scoliosis diagnosis over decades. The major reason causing etiology of AIS is still remained unclearly. For the patients with more skeletally and sexually immature, the spinal curvature progression occurs in greater probability. Curve progression is one of the most common long-term sequelae of untreated AIS. Bracing and physiotherapy are common non-surgical treatment for preventing curve progression. The patients warrant a series of X-ray examination in which the patient undergoes regularly radiograph of whole spine every 4 to 6 months until skeletal maturity is reached. Surprisingly, less than 1% of the screened population and less than 10% of those patients with Cobb angle greater than 10° are warranted treatment. This previous finding suggests that 90% or more AIS patients are subject to unnecessary radiation. As radiation hazard of radiograph, frequency of assessment is limited, making disease progression monitoring and treatment outcome measure more difficult. Clearly, screen of teenager, monitoring of AIS, lifelong follow-up, outcome measure of therapy and

treatment of scoliosis using non-radiation technologies are the glaring need to be achieved.

Non-radiation approaches for curvature assessment have been developed such as Quantec system using surface topographical technology, Orthoscan Ortelius 800 using electromagnetic spatial sensing technology, and Upright multi-position MRI. However, none of them have been widely used due to the low accuracy or high cost. Ultrasound imaging is a low cost, radiation-free, and widely available modality, and thus it is a potential method for assessing scoliosis. The objective of this study is to develop a freehand 3D ultrasound system for the assessment of scoliosis and to establish the measurement protocol of using the system.

The 3D ultrasound system was comprised of an ultrasound scanner using a probe with a width 92 mm and frequency range of 5-10 MHz, a custom-made supporting frame, an electromagnetic spatial sensing device, a desktop PC installed with a video capture card and a dedicated program for image and data collection, processing, visualization, volume reconstruction, analysis, and assessment. Using the obtained ultrasound images and their corresponding spatial data, different methods have been developed to measure the spine deformity, including 3D image stack approach and volume project approach. The 3D image stack approach used the manually identified transverse processes (TP) for measurement, while the volume project approach used reconstructed image to form an X-ray like projection to identify TP and spine column profile. Tests on spine phantoms and human subjects were conducted for evaluating the system performance. Four flexible spinal column phantoms featured with soft intervertebral discs allowing deformation were used in the phantom tests. The spine phantom was deformed to simulate scoliosis, and each was deformed four times to stimulate different spinal curvatures and imaged using X-ray. Therefore, a total of 16 phantom stimulated spinal curvatures were tested, using both X-ray Cobb's method and the 3D ultrasound method. 36 subjects (age: 31.1 ± 14.7) were recruited for scoliosis measurement tests, and another 11 subjects participated in the intra- and inter- observer tests for both scanning and image analysis. The results obtained using the 3D ultrasound method was compared with the Cobb's angle obtained using X-ray measurement.

The results of the phantom tests showed that there was a strong correlation ($R^2 = 0.7586$, $p<0.001$) between the Cobb’s angle and the angle obtained using the 3D image stack approach where TP was used as a reference. The results also demonstrated excellent intra-observer (ICC=0.99, $p<0.001$) and inter-observer (ICC = 0.89) repeatability. For the subjects, the results also demonstrate good correlation ($R^2 = 0.6806$, $p<0.001$) between the results obtained by the two methods. Intra-observer (ICC=0.565) and inter-observer (ICC = 0.75) repeatability were relatively poor in comparison with those of phantom tests. For the subject tests using the volume projection approach with the spine column profile as a reference for measurement, the results showed that there was a strong correlation ($R^2 = 0.7903$, $p<0.001$) between the Cobb’s angle and the result obtained by the new method. The intra-observer (ICC=0.99, $p<0.001$) and inter-observer (ICC = 0.919, $p<0.001$) repeatability were very high for this method. For the volume projection approach using TP as a reference, the results showed a strong correlation ($R^2 = 0.7779$, $p<0.001$) between the Cobb’s angle and the new measurement. The intra-observer (ICC=0.98, $p<0.001$) and inter-observer (ICC = 0.961, $p<0.001$) repeatability were also very high. Further analysis also demonstrated that intra- and inter-observer repeatability was very high for both scanning and data analysis when they were analyzed separately.

Using 3D ultrasound techniques, a non-radiation AIS assessment system has been successfully developed together with a number of novel image analysis approaches for the measurement of spine curvature. It has been demonstrated that the measurement using the new system was very reliable when the volume project approach was used and the correlation between the Cobb's angle and the result obtained using the new method was very high. The results suggested that the 3D ultrasound system could be a potential complementary tool for Cobb’s method. Future improvement is necessary to facilitate the new system to be a clinical tool for the screening and assessment of scoliosis, particularly AIS. The future development works should include a portable version of the system, automatic angle calculation algorithm, real-time volume reconstruction and projection, etc. It is believed that the developed system integrated with the new features will provide clinicians with an unprecedented powerful imaging and analyzing tool for the assessment of scoliosis.

PUBLICATIONS ARISING FROM THE THESIS

Patents

1. Zheng YP, Cheung CW. A three-dimensional (3D) ultrasound imaging system for assessing scoliosis. US and PCT patent pending. No. 12/509,705.Jul 2009.

2. Zheng YP, Cheung CW, Method and device for 3D ultrasound imaging. Chinese patent filed No.201210163528.1 May 2012

Journal Papers

1. Cheung CWJ, Zheng YP, Law SY. Development of 3-D Ultrasound System for Assessment of Adolescent Idiopathic Scoliosis (AIS) and preliminary clinical trials. (Preparing for submission)

Conference proceedings

1. Cheung CWJ, Zheng YP. Radiation-free Assessment of Adolescent Idiopathic Scoliosis (AIS) Using 3D Ultrasound with Image Stack Approach, 6th World Congress on Bioengineering (WACBE), Beijing, presented 2013

2. Cheung CWJ, Zheng YP, Law SY. Development of 3-D Ultrasound System for Assessment of Adolescent Idiopathic Scoliosis (AIS) and System Validation, 35th Annual International Conference of the IEEE Engineering in Medicine and Biology Society (IEEE EMBC 2013), Osaka, Japan, presented 2013

3. Cheung CWJ, Zheng YP. Development of 3-D Ultrasound System for Assessment of Adolescent Idiopathic Scoliosis (AIS): Formation of X-ray Type of Images, BME 2012 Conference, Hong Kong, P-2, Dec. 2012

4. Cheung CWJ, Zheng YP. Development of 3-D Ultrasound System for Assessment of Adolescent Idiopathic Scoliosis, BME 2010 Conference, Hong Kong, Nov. 2010

5. Cheung CWJ, Zheng YP. Development of 3-D Ultrasound System for Assessment of Adolescent Idiopathic Scoliosis, 6th World Congress of Biomechanics (WCB 2010), Singapore, pp. 584–587, Aug. 2010

6. Cheung CWJ, Zheng YP. Assessment of Adolescent Idiopathic Scoliosis (AIS) Using 3D Ultrasound System, 4th World Congress on Bioengineering (WACBE), Hong Kong, pp. 125, Jul. 2009

ACADEMIC AWARDS

IEEE EMBS Hong Kong Chapter Student Paper Competition 2010, Engineering in Medicine & Biology Society (EMBS) Hong Kong Chapter, First Prize Winner, Aug 2010.

The Research Symposium organized by Department of Health Technology and Informatics (BME section), The Hong Kong Polytechnic University, First Prize Winner, Jun 2010

Hong Kong Medical and Healthcare Device Industries Association (HKMHDIA), Student Research Award, Second Runner-up, Nov 2009.

ACKNOWLEDGEMENTS

This thesis would not have been possible without the guidance and help from the academic staff and colleagues in Interdisciplinary division of Biomedical Engineering and Department of Health Technology and Informatics who in one way or another contributed and extended their valuable assistance in the preparation and completion of this study.

First and foremost, I would like to take this unique opportunity to express my deepest gratitude to my supervisor, Professor Yong-ping Zheng, who provided me with invaluable comments, sincere supports, kind guidance, encouragement, and necessary funding. With his remarkable tolerance, tremendous experience and outstanding leadership, this thesis was produced. His unique view points and sense of humor profoundly changed my way to handle work. He will always be my captain for the journey to the future.

I wish to give my deepest thank to Mr. Wong Ming Sun for his assistance in recruiting subjects and providing necessary first-aid. His professional practice and knowledge provided me deeper understanding of the unique clinical problems and needs.

Thanks are given for my colleagues Ms. Yen Law, Ms. Kelly Lai, Ms. Wei-Wei Jiang, Mr. Tim Tang, for their patience and the professional knowledge they shared. I would also like to thank Mr. Jun- Fung He, Mr. Zheng-Ming Huang, Mr. Louis Lee for their technical supports and encouragement.

I also wish to thank Prof. Daniel Chow for his unique comments and suggestions on the frame design, and Mr. Kung-Chee Chen for his suggestions and guidance on the frame fabrication. Great thanks are given to Ms. Yen Law and Ms. Kelly Lai again for them help in proof reading. I also wish to thank Mr. Man Mak for his work on prototype-2 fabrication.

I gratefully acknowledge all staff in Interdisciplinary of Biomedical Engineering for collaborating circumstances. I'd also like to thank Dr. Patrick Lai in Department of Health Technology and Informatics for his kindness in producing phantom radiograph.

I am very grateful to all subjects who participated in the preliminary clinical trial. Their contributions would pave the road for future development and probably bring a new approach to the clinical field. Hopefully, the developed system could help more people in near future.

Last but not the least, I would like to extend my deepest thanks to my wife, April, for her great support and encouragements.

TABLE OF CONTENTS

LIST OF FIGURES

LIST OF TABLES

LIST OF ABBRAVIATIONS

1D — One-Dimensional
1.5D — One and half Dimensional
2D — Two-Dimensional
3D — Three-Dimensional
4D — Four-Dimensional
AC — Alternating Current
AIS —Adolescent Idiopathic Scoliosis
ASIS — Anterior Superior Iliac Spine
ATR — Axial Truck Rotation
B-mode — Two-dimensional Brightness-mode Ultrasound Image
BMI — Body Mass Index
C — Cervical Vertebra
CRT — Cathode Ray Tube
CT — Computerized Tomography
DS — Distribution Step
EM — Electromagnetic
FBM — Function-Based Method
FBT — Forward Blend Test
HFS — Hole-Filling Step
ICC — Intraclass Correlation Co
L — Lumbar Vertebra
LA — Lateral
LAN — Local Area Network
MEMS — Microelectromechanical System
MRI — Magnetic Resonance Imaging
PA — Posterior-Anterior
PACS — Picture Archive and Communication System
PBM — Pixel-Based Method
PC — Personal Computer
PNN — Pixel Nearest Neighbor
MPR — Multi-Planar Reformatting
PVC — PolyVinyl Chloride
RMS — Root Mean Square
S — Sacral
SDV — Sante Dicom Viewer
SD — Standard Deviation

SR — Surface Rendering
T — Thoracic vertebra
TP — Transverse Process
US — Ultrasound
VBM — Voxel-Based Method
VNN — Voxel Nearest Neighbor
VR — Volume Rendering

CHAPTER 1 INTRODUCTION

1.1 Background

Idiopathic scoliosis stands for a pathological entity of unknown etiology and is characterized by severe deformations of spine and skeleton. It was first described by Hippocrates in ancient Greek. The term was introduced in nineteenth century and defined by Whitman in 1922 (Lowe et al. 2000), included by Cobb (1948) in classification and adopted by Scoliosis Research Society lately in 1966 as the standard method for quantification of scoliotic deformities. Adolescent idiopathic scoliosis (AIS) is a subset of scoliosis with patients aged 10-16 years. No single causative factor has been identified for the cause of AIS. It was suggested that the condition is multi-factorial (Kouwenhoven et al. 2008). The degree of severity is indicated by Cobb's angle measured in term of degree as a gold standard. Yong et al. (2009) reported that the prevalence rates for 9 to 13 years old female AIS patients were 0.27%, 0.64%, 1.58%, 2.22% and 2.49%, respectively. The study showed a significant increasing trend in the prevalence rate with increasing age. Basically, the degree of the spine curvature tends to increase over the patient's whole lifetime, but the degree of progression over the lifetime and the time-at-risk depends on many factors (Weinstein et al. 2008). Thoracic curve with 60° or greater at the growth completed will continuously progress up to 29.4° in average on a follow up of 40 years. Similarly, lumbar curve and thoracolumbar curves of 45° to 50° will gently progress on an average of 15° to 20° on a follow up of 40 years (Weinstein et al. 1981; Weinstein et al. 1983). These curvature progression predicting factors include maturity age at diagnosis, menarchal status, and the amount of skeletal growth remaining, position of the curve apex, and curve size. For the patients with more skeletally and sexually immature, the curve progression is probably greater (Bunnell 1986). Curve progression, back pain, cardiopulmonary problems, and psychosocial concerns are the most common long-term sequelae of untreated AIS. The severity of these sequelae impacts on patients’ health is very variable. Clinical observation is recommended for AIS patients with a Cobb’s angle of 20° or less. The patients with immature skeletal and a Cobb’s angle of between 20° to 40° are warranted for brace treatment. For those patients with Cobb’s angle greater than 40° and immature skeletal or Cobb’s angle greater than 50° and mature skeletal are warranted for surgical management (Kim et al. 2010). Bracing and physiotherapy are common non-surgical treatment for preventing curve progression. Theirs effectiveness, however, has never been rigorously assessed (Weinstein et al. 2008). With technological advances for surgical treatment, surgeons can correct the deformity and restore the balance. But, no long-term results of these changing surgical treatments have been reported (Weinstein et al. 2008). Clearly, screen of teenager, monitoring of AIS, lifelong follow-up, outcome measure of therapy and treatment of scoliosis are the glaring goals to be addressed.

However, the gold standard for scoliosis examination is chest X-ray radiography, which is radiation in nature, hampering the usage with limiting frequency of use and time interval. Other modalities including Computerized Tomography (CT) and Magnetic Resonance Imaging (MRI) can perform the same purpose. CT can also provide three dimensional (3D) information, but it produces significant more radiation and should be conducted in supine posture. Similarly, MRI can also provide 3D information but it is time consuming and also in supine posture. In addition, CT and

MRI imaging are limited by available and expensive. All of these modalities, therefore, are not suitable for mass-screening or frequently therapy outcome measurement. For these reasons, equipment with non-radiation nature and examination in standing posture have been developed including Quantec system (Quantec Image Processing, Warrington, Chesshire, UK), based on surface topographical technology, and Orthoscan Ortelius 800 (Orthoscan Technologies, Inc., USA), based on electromagnetic sensing. In these imaging modalities, the back bone deformity is not directly measured, and measurement outcomes are different from radiographs.

Ultrasound imaging is a low cost, non-radiation, and widely available modality. Surprisingly, advancement relevant to scoliosis diagnosis using ultrasound imaging techniques has been scanty. Two dimensional (2D) Ultrasound B-mode image has been reported to measure vertebra rotation (Suzuki et al. 1989). 3D ultrasound was first developed by Olaf von Ramm and Stephen Smith at Duke University in 1987. The most successful application is fetal examination. Recently, freehand 3D systems have been successfully developed by different research groups (Nelson and Pretoius 1998; Fenster et al. 2001; Gee et al. 2003; Huang et al. 2005, Cheung CWJ et al. 2010; Purnama et al. 2010). 3D Freehand ultrasound can provide image on large extent such as ultrasound extended view, allowing probably generating a whole spine image. An innovative approach using freehand 3D ultrasound imaging system for assessing scoliosis has been developed.

1.2 Objectives of this study

The overall objective of this study is to develop an innovative approach using freehand 3D ultrasound imaging system for accurate evaluation of the scoliotic curvature in posterior-anterior views to provide a 3D radiation-free measurement for scoliosis. To achieve this overall objective, some specific tasks would be conducted in this study, including software development for data collection, rapid volume reconstruction, landmark marking, dimension measurement, angle calculation, and visualization.

The tasks would also include experiments using spine phantoms with different deformity to simulate different degrees of scoliosis. The results would be compared with those obtained by X-ray measurement.

After demonstrating the potential of the new method using phantoms, clinical procedures and a supporting frame, which allows scanning subjects in stand posture, would be developed as another task.

Different algorithms would be explored to process the 3D ultrasound images data to find an optimized method to extract spine deformity information.

Finally, preliminary clinical study would be conducted with normal and scoliotic subjects and the results would be compared with those obtained by X-ray measurement. Intra-observer and inter-observer repeatability of the new measurement would also be conducted.

CHAPTER 2 LITERATURE REVIEW

Over decades, researchers have been refining and developing different imaging techniques for the spine deformity assessment. Although many research works have been undertaken, the gold standard for clinical scoliosis assessment is still Cobb's method (Cobb 1948), which has radiation hazard. This chapter begins with a review of literature on AIS. Currently available methods for assessment of scoliosis and their limitations are then reviewed. 3D ultrasound imaging technique is introduced as potential solution. An overall summary is then made to summarize all the approaches and methods to tackling the problem.

2.1 AIS etiology, diagnosis, and treatment

Scoliosis is a medical condition of persons with lateral curvature in their spines, and it is often associated with the abnormality in the sagittal plane profile and the axial rotational deformities (Figure 2.1). It is also regarded as a musculoskeletal disorder manifested as a three-dimensional spinal deformity.

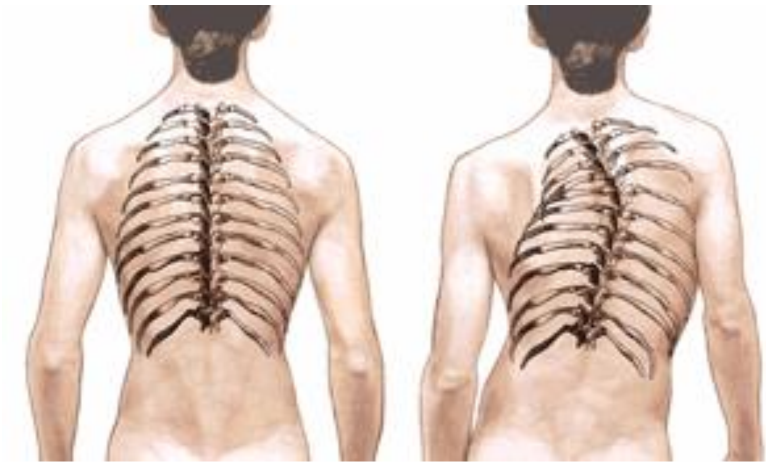

Figure 2.1. The normal spine (left) and AIS (right) (www.scoliosisassociates.com).

The spinal curvature is a vital quantitative parameter for the evaluation of scoliosis; it is particularly helpful for surgical plan, monitoring curve progression, treatment outcome, and diagnosis (Vrtovec et al. 2009). The most prevalent form of scoliosis among the youngsters (10 to 16 years old) is adolescent idiopathic scoliosis (AIS). In the United States, approximately 20 million people are suffered from scoliosis, and the prevalence of AIS in general population in US is 2% to 4% (Good 2009). The prevalence of AIS is about 3% in Hong Kong (Tang et al. 2003). AIS is found more commonly affecting girls than boys. For the patients warranted treatment, the ratio of girls to boys is 8:1 (Bunnell 1988). It was reported that scoliosis patients suffer from various problems including higher mortality, more common backaches, decreased physical capacity, and the deteriorated pulmonary function, resulting in negative impact on the patient quality of life (Pehrsson et al. 1992; Weinstein et al. 1981; Weinstein et al. 2003). AIS is classified with various factors such as its etiology, magnitude, location, direction, and age of onset.

The major reason causing etiology of AIS still remains unclear, possibly largely due to its multi-factorial origin (Figure 2.2) (Weinstein et al., 2008). Researchers suggested that it may be highly dependent on genetic and spine biomechanics. Good (2009) reported that 11% of first-degree relatives of AIS patients are also suffered from scoliosis. A clear genetic basis, however, is still lacking (Miller 2007). AIS is also found partly correlated with abnormal levels of tyrosine, sex and growth hormones, dysfunction of the melatonin-signaling pathway, and calcium-binding receptor protein calmodulin (Ahn et al., 2002; Moreau et al., 2004; Azeddine et al., 2007; Cheung et al., 2008). Kindsfater et al. (1994) and Machida et al. (2009), however, suggested that these biochemical abnormalities might be possibly more related to the progression instead of the origin of AIS. In biomechanical aspect, Castelein et al. (2005) suggested that spine backward inclination in the sagittal place led to presence of dorsal shear forces in certain regions of spine, contributing rotational instability of spine and AIS progression. The other possibly linked factors to AIS etiology have also been suggested such as growth disturbance, hormonal dysfunction, skeletal muscle abnormality, bone mineral density, abnormality in connective tissue, abnormal platelet calmodulin levels, and central nervous system abnormality (Tang et al. 2003). In addition, it has been hypothesized that an abnormality of the paravertebral muscles causes the development of AIS. No definitive conclusion, however, has been drawn (Weinstein et al. 2008).

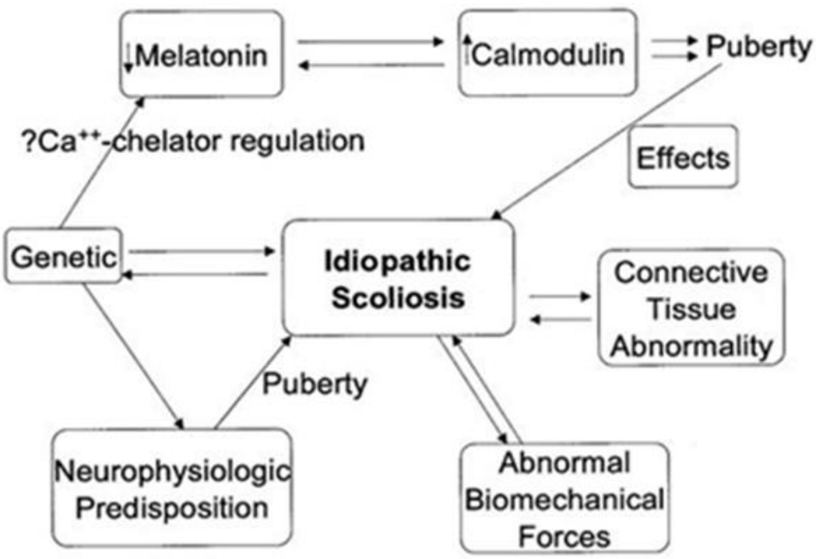

Figure 2.2. Suggested interrelationships among various factors that have a potential role in the etiology of idiopathic scoliosis (Lowe et al. 2000).

With the constraint of conventional radiography, concept of scoliosis is defined by the coronal view of curvature and limiting the measurement approach. By definition, AIS describes those patients with the lateral curvature of the spine more than 10° in the coronal plane, as measured using Cobb's method based on X-ray images (Cobb 1948).

With respect to the anatomical level of the apical vertebra, scoliotic curve can further be described as cervical, thoracic, thoracolumbar and lumbar curves. According to the recommendation of the Scoliosis Research Society, the Cobb's angle is defined as the angle between of the two most tilted end-plates of the vertebral bodies in a standing radiograph (Figure 2.3). The Cobb' method is currently the gold standard for measuring the severity of scoliosis and exploiting to predict its progression, despite many researchers found it error-prone and unreliable (Loder et al. 1995; loder et al. 2004; Morrissy et al. 1990, Shea et al. 1998, Wills et al. 2007). In accompany with Cobb's method, the degree of vertebral rotation is measured with the Nash-Moe method (Nash 1969). These measurements are very important for physician to develop patients' treatment plan, and provide information for delineating coronal and sagittal curves, and progression of deformity. Any delay in diagnosis and management of lateral curvature may lead to serious deformity, resulting in negative impact on psychological well-being, cardiopulmonary function, and physical appearance. It has been shown that the negative impact of pulmonary function for AIS patients is found strongly and consistently associated with degree of curvature. The degree of lateral curvature, high degree of thoracic lordosis, vertebral rotation, decreased respiratory muscle strength, and other factors also affect pulmonary function (Kafer 1977; Kearon et al. 1993; Lin et al. 2001). As the importance of progression monitoring, various progression equations have also been devised to quantify the risk of progression with different reference parameters. For instance, Risser sign, level of apex, presence of trunk imbalance, and chronological age were formulated by Peterson et al. (1995); Cobb's angle, Risser sign, and chronological age were developed by Lonstein et al. (1984). These equations and methods could assist clinicians to formulate a base of reference for their patients' treatment plan on the risk of progression (Weinstein et al. 2008).

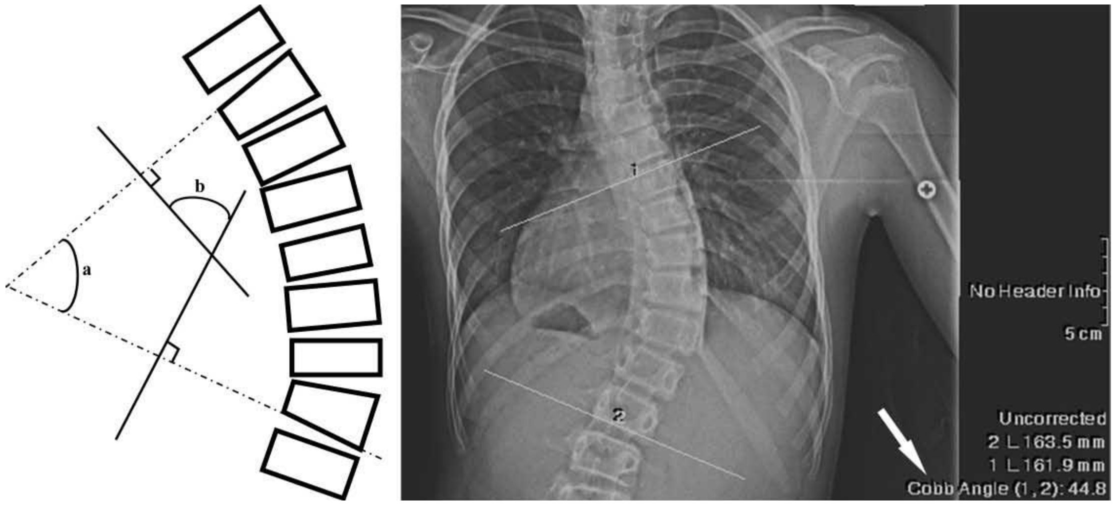

(a) (b)

Figure 2.3. (a) Cobb's Method measurement is demonstrated. (b) Screen capture from picture archive and communication system (PACS) shows the use of software to measure the Cobb's angle from radiograph (Kim et al. 2010).

There are few options for AIS treatment including observation and bracing as a non-operative treatment, and surgical treatment in general. The selection of treatments is determined by degree of Cobb's angle. The objective of non-operative treatment during adolescence is to prevent curve progression particularly for small Cobb's angle, making early examination and monitor more important; whereas, the objective of surgical treatment is curve correction and maintenance (Weinstein et al. 2008). In Europe, physical therapy has been recommended for preventing aggravation of the deformity from mild curvature, which covers curves less than Cobb's angle 25°, and enhancing the effect of bracing for moderate curvature, which covers curves ranged from Cobb's angle 25° to 45°, with low risk of progression (Negrini et al. 2005; Weiss et al. 2005); however, both physical therapy and bracing have not shown any definite evidence in reduction of risk of curve progression, existing deformity, or warrant of operation (Weinstein et al. 2008). In Hong Kong, Tui-na treatment was reported to alleviate scoliosis. Small scale clinic study was conducted by a team of Chinese medicine practitioner from the Clinical Division of the School of Chinese Medicine of Hong Kong Baptist University (According to the information provided by our collaborator Mr. Wong). However, no scientific publication has been released yet. Bracing treatment is exploited for preventing progression of the curve until skeletal maturity reaches, resulting in diminishing risk of surgery. For the adolescent patients with a primary curve greater than Cobb's angle 45°, it is generally agreed as an indication for surgery, which is involved instrumentation implantation such as posterior instrumentation, pedicle screws, and hook-wire. There are several main objectives of surgical treatment including arresting curve progression, maximizing permanent correction of the deformity in three dimensions, ameliorating appearance by balancing the trunk, and minimizing the short and long term complications (Weinstein et al. 2008). Coronal balance and sagittal balance are vital parameters for measuring outcome of surgical treatment (Figure 2.4). These balances are evaluated from posterior-anterior and lateral radiographs taken before and after surgical treatment. Coronal balance is determined by measuring distance between the cervical (C) 7 plumb line and centre sacral line; whereas, sagittal balance is determined by measuring the distance between C7 plumb line and the posterior superior corner of sacral (S) 1 (Suk et al. 2005). The coronal imbalance is defined as greater than 2 cm of thoracic (T) 1 measured from the central sacral line (He et al. 2009).

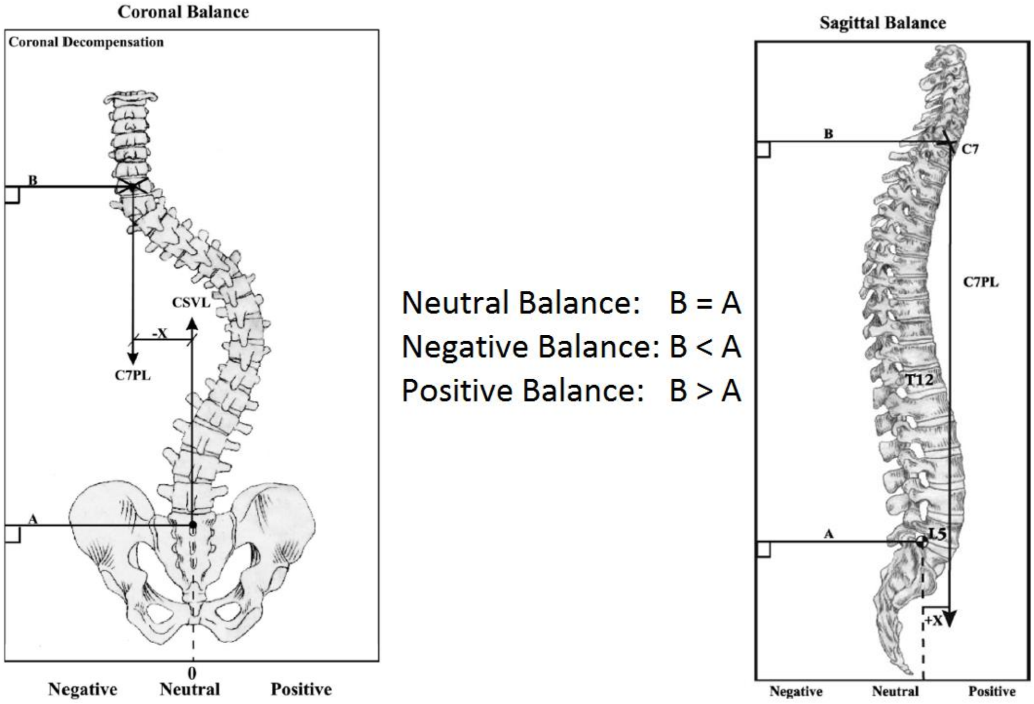

Figure 2.4. Measurement techniques for coronal and sagittal balance (Glassman et al. 2005).

In addition to the balances information, there are other geometrical parameters for determining scoliosis severity including apical vertebral translation, pelvic obliquity, and thoracic kyphosis. Apical vertebral translation for thoracic curves was determined by measuring the distance between the C7 plumb line and the center of apical vertebral body or disc. Apical vertebral translation for thoracolumbar and lumbar curves was determined by measuring the distance between the center sacral line and the center of apical vertebral body or disc. Pelvic obliquity in patients with paralytic scoliosis was determined by measuring the tilt between the horizontal line and the line that passes through top of each of ilia. Thoracic kyphosis was determined by measuring from the superior endplate of T5 to the lower endplate of T12, and lumbar lordosis from the superior endplate of T12 to the endplate of S1 by Cobb's method (Suk et al. 2005).

Apparently, any change curvature status affects the treatment option. It has been suggested that a true change in curvature status is the progression change observed with greater than 5° (Morrissy et al. 1990), and often exploits as a radiographic benchmark as their definition of treatment failure of bracing (Allington et al. 1996; Bassett et al. 1987; Emans et al. 1987; He et al. 2009; Oldafsson et al. 1995; Piazza et al. 1990). As degree of curvature is the critical parameter of diagnosis, treatment plan, and outcome measures, many methods and tools have been developed for addressing different applications.

2.2 AIS assessment tool and method

2.2.1 X-ray radiograph and other conventional methods

To identify the type of spine structure problem, clinical examinations are normally used to screen and evaluate the spine deformity before X-ray imaging. During the examinations, information such as gender, age, height, weight, leg length, onset of menarche, family history, and diseases are collected for determining a tentative prognosis; physical and spinal examination including forward bend test, neurological examination, spine side-to-side symmetry, shoulder height, iliac crest symmetry, and lateral examination are exploited to evaluate suspected AIS (Bueche 2008).

Traditionally, scoliosis screening has relied on the Adam's forward blend test (FBT) (Lonstein 1982). In FBT, the patient is requested to stand and bend forward at waist to become parallel to horizontal plane while maintaining the knees straight. The observer examines back to locate any body asymmetry such as rib hump or paralumbar prominence (Figure 2.5).

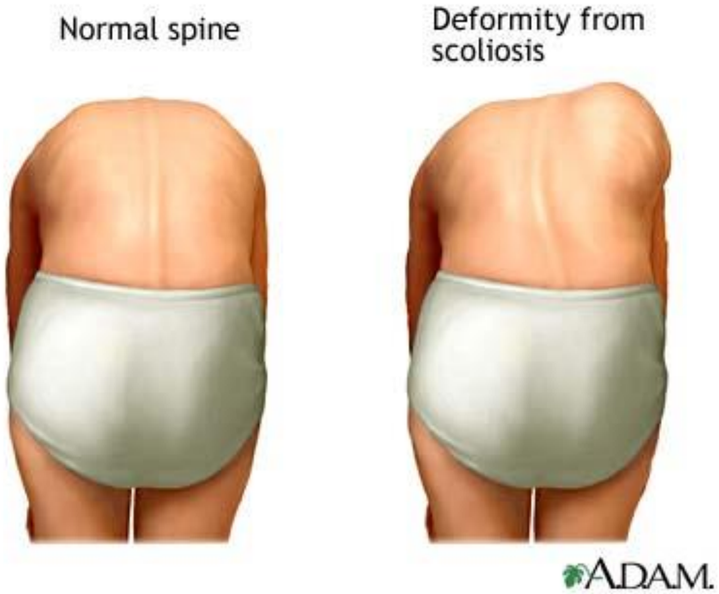

Figure 2.5. Adam's forward bend test (www.nlm.nih.gov).

FBT, however, does not provide a quantitative description of spine deformity. Therefore, different approaches have been developed aiming to achieve more accurate and objective screening results. The magnitudes of these asymmetries are measured by the inclinometer (scoliometer). Scoliometer is the simplest device developed for the purpose, which is a ruler-like handheld inclinometer to measure truck asymmetry or axial trunk rotation (ATR), also known as "rib hump deformity", by Bunnel (1984). The scoliometer does not have moving or electronics part and can quantitatively measure the degree of scoliosis (Figure 2.6a). When the hump's angle of ATR is greater than 7°, the patient is recommended for undergoing the standard radiographic (Figure 2.6b) evaluation for suspected scoliosis (Bunnell 1984). Different studies found that scoliometer measurements have high intra-rater and inter-rater variations of ATR values (Mubarak et al., 1984), high false positive rate (Huang 1988) and does not well correlate with the Cobb's method (Cobb 1948). Studies also suggested that it should not be exploited as a diagnostic tool exclusively (Amendt et al., 1990).

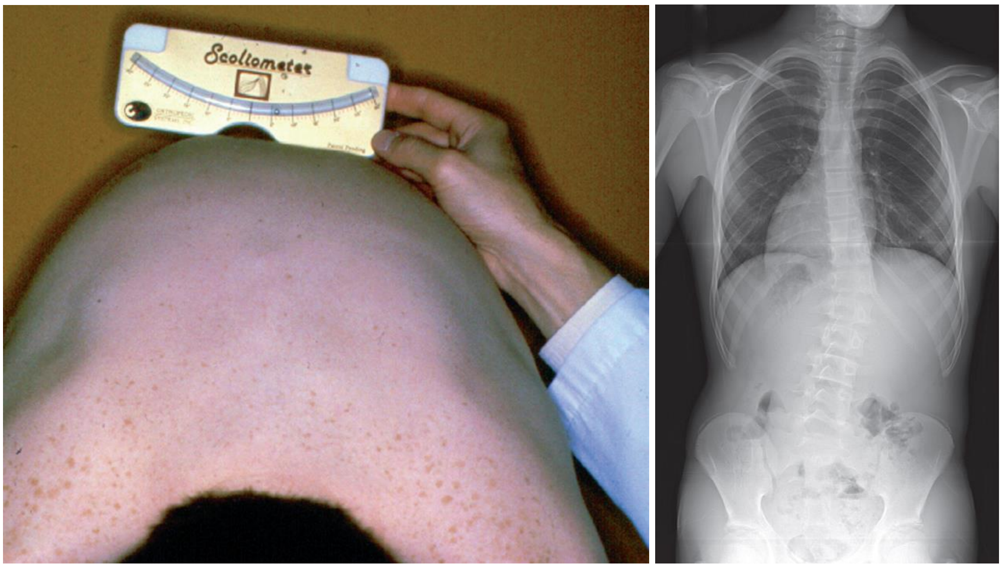

(a) (b)

Figure 2.6. Screening and diagnosis of scoliosis by scoliometer and radiography (a) Measurement of truck rotation with a scoliometer with patient in forward bend posture (b) PA radiograph (Weinstein et al. 2008).

In radiographic examination, the patients have to stand in a standard upright position in a natural and relaxed erect state, both arms hanging on either side of the torso, both feet side by side with the toes pointing forward, facing forward with eyes looking forward horizontally (He et al. 2009); while, one 36-inch standing posteroanterior (PA) radiograph and another 36-inch standing lateral (LA) radiograph are taken. In addition, four adjustable pads are exploited to stabilize the patient position if stereoradiography is undertaking (Stokes 1988). The spine deformity is revealed from its appearance on standing posteroanterior and lateral spine radiographs. In addition, it has been recommended to register the global vertical or horizontal reference on each film by Scoliosis Research Society. For PA radiograph, exploiting positioning supports to position the anterior superior iliac spine (ASIS) parallel to the X-ray film plane is recommended to align the patient’s global axis system to the X-ray film plane. For LA radiograph, the positioning procedure is similar to PA radiograph. But, the patients in relaxed standing position with arms-at-side, their arms are obscuring the LA view of spine because of the glenohumeral joint shadows blocking the visibility of the vertebral landmarks; the patients' arms have to raise and hold on the support although the arms resting position could alter the spinal shape. Equalizing differences in leg length such as by blocks under the feet should be noted (Stokes 1994). In general, the arms can forward flex to 90° and hands rest on the support (Figure 2.7).

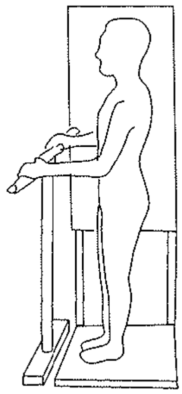

Figure 2.7. Lateral X-ray radiograph of patient positioning (adapted from Stagnara 1984).

Evaluating the scoliosis from the radiographs is undertaken by measurement of the Cobb's angle. Skeletally immature patients at risk for curve progression can be followed up with posteroanterior radiographs every 6 to 12 months (Thomsen et al. 2006). As Reamy and Slakey (2001) reported, there were about 10% of those patients with curve progression warrant intervention. This finding indicated that 90% of the patients were subject to unnecessary radiation. In addition, patients were exposed to considerable amount of radiation because of repetitiously undergoing spinal X-ray examinations over the observation, therapy, and treatment periods, and it was reported that the risk of cancer of these patients raised by 2.4/1000 (Levy et al. 1996). Even worse, the standing radiograph is often found inadequate to cover the whole spine because of the limitation of film size. Patients are warranted to undergo two radiographs or more in the same plane view, which later are stitched together (Figure 2.8) to produce whole PA or LA view of spine for assessment (Malfair et al. 2010); risk of radiation exposure is aggravated.

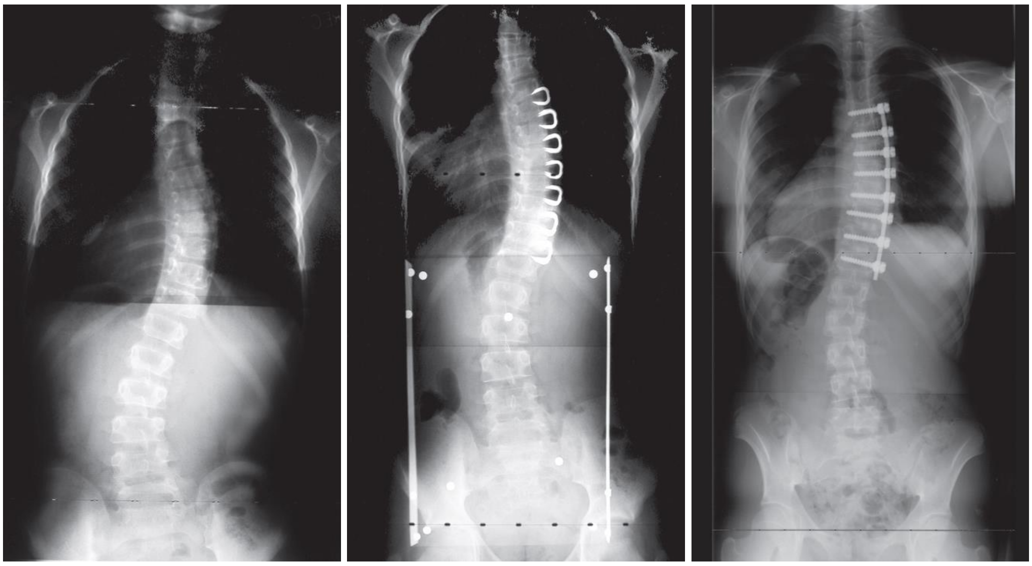

Figure 2.8. Stitching X-ray radiology (Weinstein et al. 2008).

Regardless the radiation nature of Cobb's method, intrinsic errors exist in radiograph measurement. It is sometimes difficult to identify the oblique projections of the twisting spine in X-ray images, and there is also a considerable variation in the Cobb's angle between the images obtained from different projection angles of the X-ray beam (Dickman et al. 2001). Intra-observer variation 3-5° and inter-observer variation 6-9° have been reported in the measurement of the Cobb's angle (Carmen et al. 1990; Loder et al. 1995; Morrissy et al. 1990; Pruijis et al. 1994). It is generally agreed that 5° difference has been accepted as measurement variation between assessments regardless using traditional manual drawing on film method or drawing on computer screen (Wills et al. 2007). He et al. (2009) further stated that there are two main intrinsic reasons for these variations. First, scoliotic spines often have multiple curvatures such as primary and secondary curvature. Different observers could probably select different curvature for measurement. Second, the superior and inferior end vertebrae of scoliotic spine must be identified first. Observers often select different superior and inferior vertebrae for measurement. In addition, the edges of adjacent vertebra often overlap in PA radiograph, making a difficulty in choosing correct end vertebra because of the accompanied vertebra rotation. In summary, variability of Cobb's angle has also been found affected by various factors including radiographic markers of wide diameter, selection of end vertebrate, observer bias, protractor accuracy, image acquisition techniques and time, image size, and positioning (Vrtovec et al. 2009). In addition, there are many others relevant findings on Cobb's Method. Beauchamp et al. (1993) found that 5.2° in average increases in Cobb's angle for the same patient underwent radiograph in the morning and in the afternoon. Torell et al. (1985) found that Cobb's angles reduce 9° in average when measured in supine position comparing with standing position. Pruijs (1994) reported that radiograph acquisition process may induce 2.2° error. DeSmet (1982) found that there was a 2.4° difference in posteroanterior and anteroposterior radiographs regardless the Cobb's angle magnitude. As the radiograph measurement is limited to two dimensions, it means Cobb's method does not adequately quantify to be exploited as descriptor for the three dimension spinal deformity (Chen et al. 2012).

Vrtovec et al. (2009) summarized the major problems of quantitative evaluation of spinal curvature into human capability and technical limitations, which contribute evaluation error and shelter the geometrical relationship between anatomical structures. Human evaluation is limited by non-systemic search patterns, similar characteristics of normal and pathological conditions, and by the natural biological variability of human anatomy; whereas, technical limitations are contributed by the presence of image noise, distinctive characteristics of imaging techniques, and variable positioning of the patient during image acquisition.

Indeed, positioning is a major problem. As abovementioned, during radiographs acquisition, scoliosis patient is guided to stand in a standard upright position with a nature and relaxed position, which represents the normal stance and functional balance posture. Such position, however, is limiting consistency because of variability between measurements. The deviation of lateral spinal curvature is aggravated because of rotational mal-alignment through its vertical axis and by translating the patient's lordosis or kyphosis. Previous studies reported that the sources of most inaccuracies in curvature evaluation are the postural variability of the subject and equipment positional change (Capasso et al., 1992; DeSmet et al. 1982; Pruijis et al. 1994). Postural support device, therefore, is recommended to alleviate the variability (Stoke 1994). Various devices have been development such as scoliosis chariot (Dawson et al. 1978) and throne, which is a seat with additional reference markers for sitting position spine imaging (Koreska et al. 1978). Dawson et al. (1978) reported that AP full spine scoliosis chariot view comparing with standard AP free-standing view may show a difference up to 17° and patient positioning is a main source of random error.

Bernau (1984) exploited a pair of scales, which measures the weight of both feet, to maintain the same weight on both feet during x-ray radiograph shooting to improve the reproducibility; while the optical and acoustic signal of same weight was signing the patient and clinician for adjusting balance. Kohlmaier et al. (1995) developed a balance like positioning device for standardized X-ray image of the spine for children in the upright position. The patient was standing on the balance like device when the X-ray imaging was undertaken. In this way, the patients were in a standardized posture rather than a relaxed free stand. More than two-thirds of patients in their study were found improving in reproducibility. Kohlmaier et al. (1995) also stated that the device could improve accurate prognostic aspects and fewer ionizing hazards. Recently, Dewi et al. (2010) have developed a balance device, BalancAid, comprised of a square board with a cylindrical disk attached from the bottom of the board at the centre. The device promotes the balance in the sagittal plan and frontal plan with intentional obtained the balance from all directions. The resultant balance leads to a specific upright position of the patient. Nault et al. (2002), however, reported that there exists a strong correlation between standing imbalances in scoliotic patients and the stability of specific postural alterations. Dewi et al. (2010) also claimed that BalancAid could improve the posture reproducibility of young patients with minor scoliosis and good balance only. It, therefore, is unambiguously that a body support device is principal component for assisting different imaging modalities including radiograph and ultrasound image for obtaining the longitudinal view of scoliotic patients. Apart from supporting aids, the use of an electronic balance scale may also be alleviating the problem induced by positions or misleading projection for the seemingly mild scoliosis (Mau 1985).

As evaluation of spinal curvature in the coronal plane is mainly focused on the scoliotic measurement (Vrtovec et al. 2009); publications have been focused on improvement of Cobb's method performance and evaluating its reliability (Vrtovec et al. 2009). Apart from Cobb's method, there are few other measurement methods developed including Ferguson method (Ferguson 1930), Greenspan index (Greenspan et al. 1978), Daib et al. method (Diab et al. 1995), and Centroid method (Chen YL et al. 2007), respectively.

As Cobb's method involves multiple steps and subjective procedure (He et al. 2009), its improvement has been studied by many research groups. With advancement of computer, software for measuring Cobb's angle, based on digitized X-ray images computing and analytical Cobb's method (Figure 2.9) has been commonly reported (Jeffries et al. 1980; Koreska et al. 1982; Stoke et al. 1988). Jeffries et al. (1980) exploited digital method manually identified centres of concavities at each lateral vertebral body on PA radiographs. A polygonal arc was formed using these centre points to approximate the scoliotic curve. Lines tangent to the curve were created at the apical and at the end vertebrae, at which a local inflection points were found. These points also corresponded to the first two derivatives of the polygonal arc. Stoke et al. (1988) further revealed that the polygonal arc was smoothed out using Fourier analysis with five sine waves added together for representing the scoliotic spine. The length of the spine stretched over was defined as a period of the fundamental sine wave. The inflection points and apics, subsequently, were devised mathematically. An inflection point was denoted by the zero curvature point; whereas, an apex was denoted by a point of maximal lateral deviation from the spinal axis.

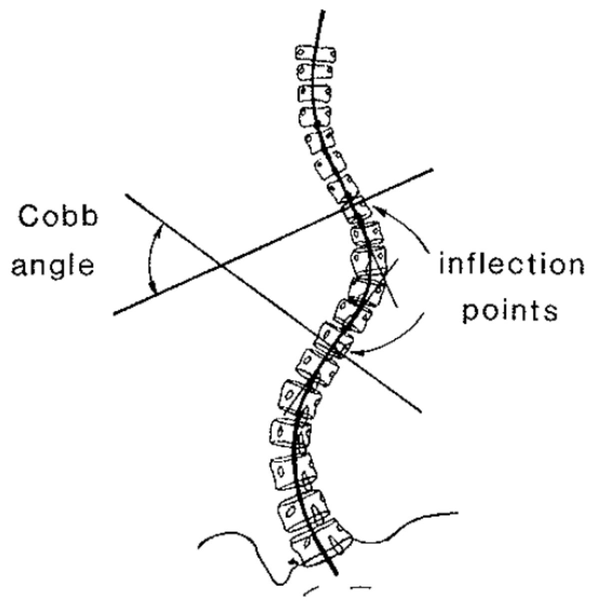

Figure 2.9. Method for determining curvature of the spine using the Cobb's method adapted to an analytic method programmed in the computer.

For each apex, an analytic Cobb's angle was defined as the angle between the normal to curves at the corresponding inflection points. Jeffries et al. (1980) reported that a positive correlation ($R^2 = 0.937$) between the computer (analytic method) and manual methods of measuring scoliosis was found with a regression equation formulated as clinical measurement = (0.88 ± 0.009) x computer method; it was also found reproducible with a standard deviation of only 1.3°. The computer method showed overestimating clinical measurement, because the inflection points did not necessarily coincide with the vertebral plate. In fact, Cobb's angle was maximized in the computer method. Reliability assessment of Cobb's angle measurements using manual and computer methods have been continuously studied by various groups. Dutton et al. (1989) reported high correlation between the two methods and showed that the computer method has a significant better reliability and repeatability. The computer method also showed the same or better in variations and reliability in other studies (Gstoettner et al. 2007; Shea et al. 1998; Wills et al. 2007).

Similar to Cobb's method, Ferguson method (Figure 2.10a) is based on manual identification of the end vertebrae, its variability and unreliability, therefore, are relatively high. Ferguson method is different from Cobb's method by including changes within the spinal curvature and translation of the apical vertebra information. It measures the angle between two lines drawn from the centre of the apical vertebra to the centres of end vertebrae. As Cobb's method (Figure 2.10b) is more reproducible, easier to use and capable to measure large curvature, Ferguson is less preferred for severe scoliosis. Instead of using angle as an index for denoting degree of spinal curvature, Greenspan et al. (1978) proposed a Greenspan index (Figure 2.10c) that measures the deformity with involving individual vertebra, allowing it particularly valuable for measuring short-segment or small spinal curvature. The index is computed from the sum of the lengths of the lines drawing from the centre point of vertebrae to the spinal line, which is formed by joining the centre of two end vertebrae and orthogonal to all others lines. For normal coronal curvature, the index is zero. Laterly, Diab et al. (1995) purposed another method (Figure 2.10d) that identifies the four vertebral body corners of the apical and end vertebrae first. The centres of end vertebrae, which lie in the intersection of lines orthogonal to the superior and inferior endplates, connect with the centre of apical vertebra to form two intersect lines that define the angle of deformity. High variability, however, has been reported (Vrtovec et al. 2009). Recently, Chen et al. (2007) purposed a Centroid method (Figure 2.10e) that formed the centres of vertebral bodies through connecting the opposite corners of two vertebral bodies from the ends for spine curve. The angle formed between the lines through the top two and bottom two vertebral centroids represents the degree of spine curvature. This angle reveals a smaller curvature with equal or less intra- and inter-observer variability.

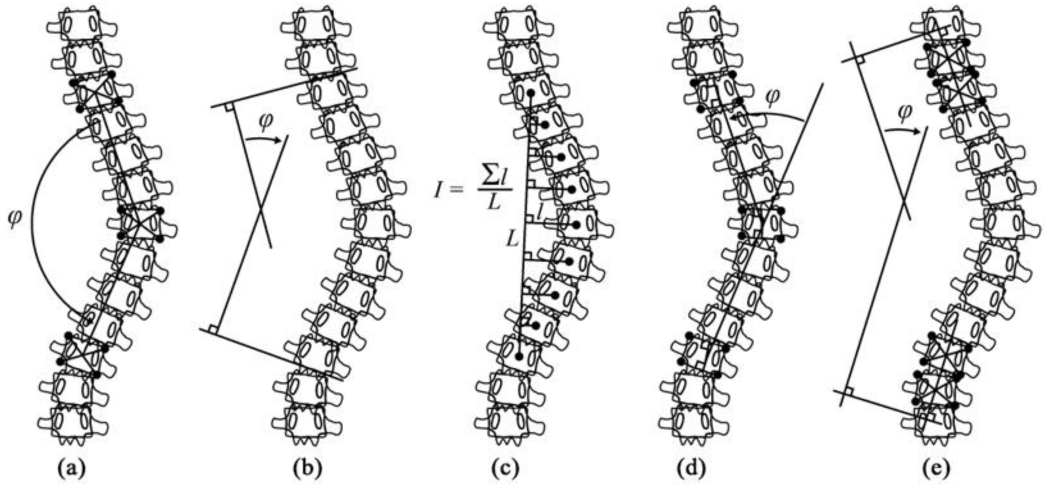

Figure 2.10. Evaluation of coronal spinal curvature in 2D images. (a) Ferguson method; (b) Cobb's method; (c) Greenspan index; (d) Diab et al. method; (e) Centroid method (Vrtovec et al. 2009).

There is alternative way using radiograph for devising spinal curvature. The location of spinous process tips are marked and used to calculate the angle. The spinous process angle was reported with very good correlation with Cobb's method (Herzenberg et al. 1990). Recently, this method is exploited for fitting brace in treatment (Li et al. 2010).

Apart from abovementioned studies searching for improvement on the problematic Cobb's method and other radiograph based methods, some non-radiograph approaches has been developed using low dose X-ray, MRI, and CT. EOS (EOS Imaging SA., Paris, France) low dose radiation bi-plane X-ray imaging system has recently introduced for assessing scoliosis. EOS exploits slot-scanning technique to obtain high-quality image while maintaining low radiation. Clinical trial has been conducted since 1993. However, its long-term health benefit from reduced radiation exposure is subtle (McKenna et al. 2012); there was also lack of evidence on other potential patient health benefits. Besides, the implications of any changes in the quality and nature of the EOS image compared with standard X-ray have yet to be assessed. Given the higher cost of an EOS machine, McKenna et al. (2012) suggested that EOS is not cost-effective with respect to the estimation of patient throughput at national level. Wessberg et al. (2006) studied Cobb's method using supine MRI image with applying axial load to the subject and compared with standing radiograph. Same Cobb's angle was found in both MRI image and radiograph with 3.4° in variation. Although it is possible to obtain high quality volumetric images of spine using MRI without the hazard of radiation, it is high cost and low accessibility. Most importantly, it has been shown that the Cobb's angle derived from the supine posture required by MRI scanning is significantly and spontaneously corrected from the standing posture (Yazici 2001). Adam et al. (2005) manually reformatted coronal CT cross-sections to perform the Cobb's method measurement in supine position. The result was found comparable to standing radiographs. However, instrument cost and cost of ownership are far more expensive in MRI and CT than in radiograph. Both imaging techniques also require longer time for imaging. CT even generates significantly more radiation during imaging. In addition, similar to radiograph, a featured room and a trained specialist are warranted to conduct examination using the imaging techniques. These factors hamper these techniques and radiograph for scoliosis treatment follow-up and screening.

Radiograph based Cobb's method, nowadays, is still considered as the gold standard for scoliosis measurement, while forward bend test or some optical techniques are exploited for scoliosis screening. For those abovementioned reasons, many innovative non-ionization and non-invasive approaches have been developed or under development by various groups such as Moire-fringe mapping, raster-based system, device that scans 360° torso profiles, stereo-photogrammetric system, and ultrasound system. None of them, however, has been commonly exploited.

2.2.2 Alterative radiation-free approach

A number of radiation-free systems have been developed for scoliosis screening, and among them, optical and surface topography techniques are most commonly used. Moire-fringe mapping is a prevalent optical technique, which is exploited to obtain the 3D shape of the patient back. Moire-fringes are generated by a grating and they are projected on subject. The images of fringe are captured by a video system. A contour line system and a sectional shape of the object are then automatically reconstructed and displayed on monitor by computer (Idesawa et al. 1977). Moire fringe mapping can produce very accurate data (resolution up to 10 microns). Surfaces at a large angle are, however, unmeasurable when the fringe density becomes too dense. In addition, the patient's position, body-build, and fat folds are the other factors causing inaccuracy to the surface topography. A poor correlation between the observed body and the underlying scoliosis has been concluded by many studies (Adair et al., 1977, Sahlstrand 1986, Pruijis 1994; Dickman et al. 2001a).

Quantec spinal image system (Quantec Image Processing, Warrington, Chesshire, UK) is one of the systems using Moire topography (Idesawa et al. 1977), raster stereo photography techniques, and is popular in UK (Thomsen et al. 2006). This system (Figure 2.11) produces a 3D surface representation image from capturing a video image of a fringe pattern that is projected onto a subject's back. The image subsequently exploits to produce a Q angle that denotes the quantitative measurement of the asymmetry reflected in a coronal plane. This system is complex and heavily relies on the surface topography, and this contributes to inaccuracy of measurement (Thometz et al. 2000). Many laser scan systems providing 360° torso profiles of patient are used to undertake scoliosis screening. Instead of utilizing laser technology, stereo photogrammetric systems, which are constructed from common digital camera systems, reconstruct a digital 3D model for measurement with fine resolution. These systems provide a fast and accurate 3D measurement of scoliotic deformities, which can be spatially recorded within a minute (Schmitz et al. 2002; Thomsen et al. 2006). The output of digital 3D model provides a resolution up to 1 mm. These optical systems provide non-invasive and non-contact measurements, however, the Cobb's angle are indirectly derived from different trunk asymmetry indices instead of bony structure or landmark; and lack of portability is also a common issue (Thomsen et al. 2006). It was also suggested that the clinical use of surface measurement technique for detection of curve progression is not recommended (Stokes et al. 1988). This is because the variation of patient position distorts the measurement; maintaining a standardized patient position is, therefore, crucial for an accurate longitudinal study. A standardized foot-plate for surface measurement technique has been developed to standardize patient positioning for reducing error and improving reproducible (Dangerfield et al. 1995).

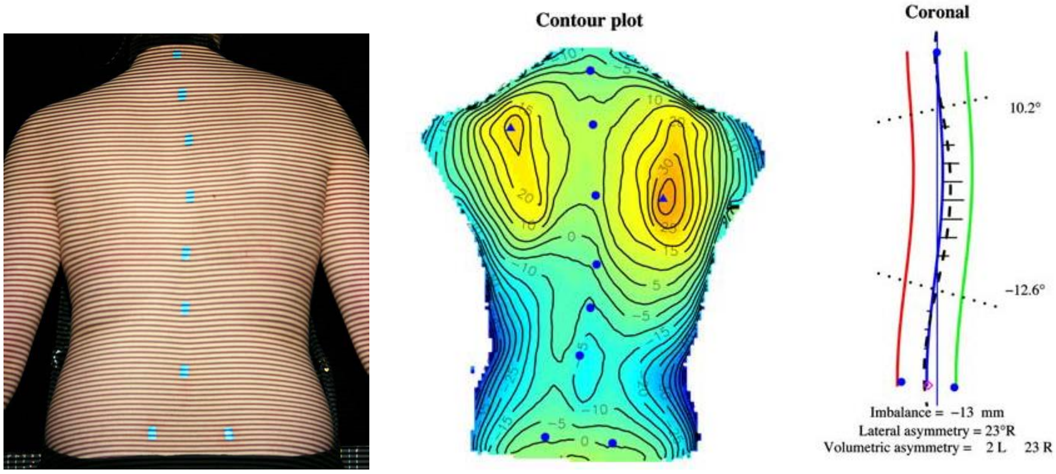

(a) (b) (c)

Figure 2.11. (a) Fringes projected onto the back, (b) contour plot, (c) estimation of spinal curvature in coronal plan (Berryman et al. 2008).

Recently, OrthoScan Technologies's Ortelius system (Orthoscan Technologies, Inc., USA), utilizing electromagnetic topographical technique, is a radiation-free system to diagnose and monitor spinal deformities by analyzing the captured spinous processes' spatial data (Dickman et al. 2001b). Whenever using Ortelius system (Figure 2.12), an examiner is to wear a spatial sensor on index finger before examination, patient's back is prudently palpated by the examiner in order to search for the tip of spinous process of each vertebra during screening (Dickman et al. 2001). The relative spatial positions of the tips of spinous processes are marked by utilizing a 3D spatial sensor attached to the examiner's finger. After all tips pinpointed, the data are exploited to reconstruct a spine representative model in computer for measuring the spinal deformation indices. The positions of spinous processes are manually palpated and determined through the examiner's finger based on body surface, which is subjective. The consecutive palpation on the patient during examination may cause certain degree of non-comfortableness and positioning issue. In addition, it has been reported with poor correlation between radiograph measure and Ortelius 800's measure under the scoliosis curve magnitude and the overall change in curve magnitude over time (Knott et al. 2006).

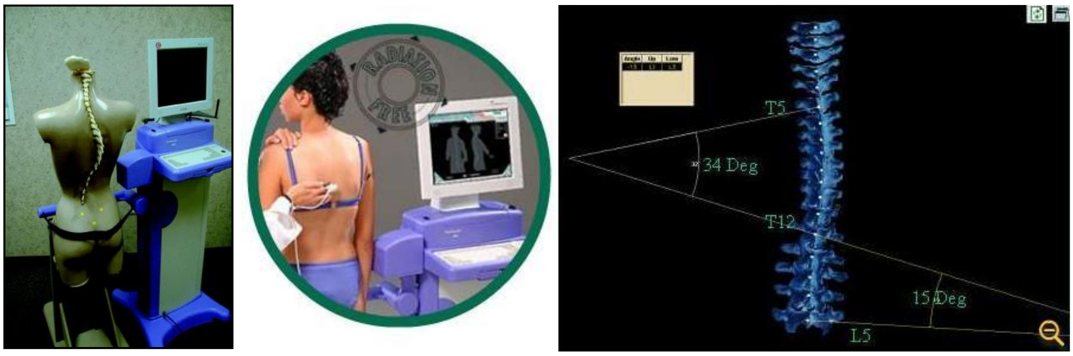

(a) (b)

Figure 2.12. (a) Evaluation of OrthoScan's Ortelious system using phantom (Knott et al. 2006), (b) OrthosScan's Ortelious system in operation and measurement (http://www.spineuniverse.com/exams-tests/novel-radiation-free-assessment-scoliosis-cobb).

2.2.3 Ultrasound imaging in spinal applications

Ultrasound imaging has been widely used for assessing fetal Spines' impairing (Nelson et al. 1993; Johnson et al. 1997). Ultrasound measurement of vertebral rotation (Suzuki et al. 1989) and intervertebral disc structure (McNally et al. 2000) has been reported in early studies. Recently, 3D ultrasound imaging for surgery application (Muratore et al. 2002) and ultrasound guide needle insertion in regional anaesthesia application (Marhofer et al. 2005) are increasingly important areas of research. These studies are targeting on small region or limited view on image. Most recently, imaging of whole spine for spinal curvature examination is an emerging area of research (Cheung CWJ et al. 2010; Dewi et al. 2009; Purnama et al. 2010; Li et al. 2010). Dewi et al. (2009) and Purmama et al. (2010) successfully reconstructed full spine volume from the images collected by a freehand 3D ultrasound system. The feasibly of using the freehand 3D ultrasound to obtain subject spine volume was demonstrated. There were considerable efforts on improving the quality of volume in their work. However, method about conducting measurement from the volume was not devised; thus no angle of curvature was obtained from the volume. Meanwhile, Cheung et al. (2010) exploited an emerging approach to successfully extract spinal curvature from raw ultrasound B-mode images with corresponding spatial information instead of using reconstructed volume. 3D Ultrasound is the primary technique in such application because it can cover the whole spine without radiation hazard. However, the major challenges remain because of the large volume data processing involved, lack of appropriate method of visualization, and unique scanning protocol needed.

2.3 3D ultrasound imaging

Over 50 years of ultrasound development, most of the advances in ultrasound technologies have been focused on 2D planar imaging. 3D ultrasound was debuted in the 1970s. The first commercial 3D ultrasound scanner, the Kretz Combison 330, which utilized mechanical volume scan transducers, was introduced in late 1980s. Since then, many research have been conducted for developing 3D ultrasound imaging system for the last two decades. The scanning speed and imaging quality have been considerably improved. 3D ultrasound application has also been extended. The standard B-mode (2D) ultrasound imaging is performed with a hand-held probe, which transmits ultrasound signal into the targeting soft tissue and receives the echoes. The timing and magnitudes of signals are exploited to generate a 2D image. 3D ultrasound is working in similar way by collecting data of a voxel array from tissues of interest. Depending on the methods of collecting data, various kinds of imaging scanning approaches, reconstruction techniques, and calibration methods are applied.

3D ultrasound reduces operator dependence in the scanning process. This is because 2D ultrasound, conventionally, requires the clinician to sweep forth and back across subject in order to mentally reconstruct 3D anatomical structure and pathology; the outcome of examination result is more subjective and considerably dependent on the skill and experience. 3D ultrasound also permits viewing of plane parallel to skin. In diagnostic and therapeutic plan, volume measure is often the principle factor for the decision. Conventional B-mode ultrasound needs to measure height, width and length in three orthogonal views for calculating the volume with assumption of ideal geometrical shape such as ellipsoidal shape, probably leading for low accuracy, high variability and operator dependency of the volume measured. Whereas, the whole view of region of interest provided by 3D ultrasound can be exploited for producing more accurate volume measure. Monitoring the therapeutic procedure or longitudinal study is considerably more difficult in B-mode ultrasound. This is because adjusting the position and orientation of the 2D ultrasound transducer for reproducing the same B-mode image plane at previous examination site is considerably difficult. In contrast, in longitudinal study, 3D ultrasound apparently excels in locating the previous examination site and setting in same orientation (Fenster el al. 2001). In order to obtain 3D ultrasound image, various techniques have been developed.

2.3.1 Scanning techniques

Over decades, scanning techniques for generating 3D ultrasound image including mechanical scanning, 2D array, and free-hand have been developed; these three kinds of technique have been used for acquisition of voxels from different tissues directly or after image reconstruction.

2.3.1.1 Mechanical scanning approach

Three types of mechanical scanning have been developed; all of them exploit a motorized mechanical apparatus, which comprises with a stepper motor and gear box, to translate (linear type), tilt (tilt type) or rotate (rotational type) a 2D ultrasound probe over the region of interest. Some of ultrasound probes encapsulate a 2D ultrasound probe and a motorized mechanical drive within an oil-filled housing (Prager et al., 2009); in contrast, in other systems, the probe is mounted onto the external driving system. The integrated probe is larger and heavier than conventional US probe but it is more convenient for use; whereas, external driving system is more bulky but it easily adapts to mount a 2D ultrasound probe for building a 3D probe system. In general, the scanning protocol of this scanning approach is predefined and precisely steered, providing an accurate relative position and orientation of each 2D image.

In the tilt or wobbling type approach (Figure 2.13a), a motorized drive mechanism, which comprises an electric motor and a frame to hold a 2D US transducer, is exploited to tilt the 2D US transducer around an axis parallel to the 2D US transducer surface. A fan shape volume formed from a pile of images, therefore, is produced because each 2D US image is acquired at regular angular interval. With the adjustably predefined angular separation, high quality volume image can be produced and provides various applications such as 3D echocardiography (Delabays et al. 1995). This type of scanning device is compact in design. Most of US manufacturers provide integrated 3D US transducers based on this design without external fixture, making it compact to allow easy manipulation. Inside the housing of these probes, the 2D transducer is wobbled or swept back and forth on a fixed trajectory. The US systems with these 3D probes are often exploited for abdominal and obstetrical imaging. Depending on US machine setting, the volume scanning rate ranges from 0.2 to 3 volume per second (Fenster et al. 2011). In general, this type of probe is better in resolution than 3D probes based on 2D array (Prager et al. 2010). However, the resolution will degrade away from the axis of rotation, because spatial distance between two consecutively acquired images increases with depth (Blake et al. 2000).

In rotational type approach (Figure 2.13b), rotational scanner exploits internal mechanism or external fixture to hold and rotate an endocavity probe about its long axis with an encoders to record the rotational data. This approach obviously allows the transducer array to rotate more than 180°. The acquired images sweep out a propeller-like fashion. Similar to tilt type, the angular interval is fixed and the resolution degrades with increasing in distance from the axis of rotation. This type of scanner has been successfully exploited to various applications such as prostate imaging (Tong et al. 1995), guided 3D US biopsy and therapy (Wei et al. 2004), and heart imaging (Roelandt et al. 1994). However, operator or subject motion particularly affects this technique because of all 2D images intersecting along the axis of rotation; any motion of axis of rotation will cause inconsistence in image alignment. The images offset or tilt from axis of rotation, therefore, must be compensated for mitigating artifacts.

With advantage of simple scan, precise in speed and spacing control, linear type mechanical scanners (Figure 2.13c) generating the acquired images are parallel to each other with equal spacing; image reconstruction of linear scanning is the simplest and fastest with simple predefined geometry. However, frame rate of the US machine and video frame grabber acquisition sampling rate are usually different so that the matching of these rates is necessary (Smith 2000). This type of scanning has been successfully implemented in various vascular imaging studies such as carotid arteries imaging (Downey et al., 1995), and tumor vascularization (Bamber et al., 1992).

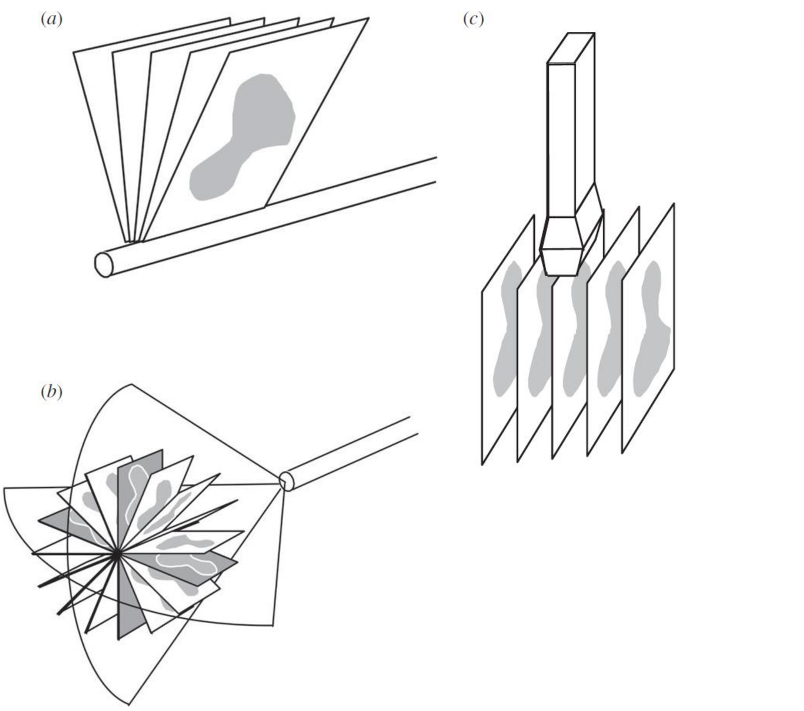

Figure 2.13. Schematic diagram of 3D ultrasound mechanical scanning methods (a) tilt or wobbling scanning mechanism (b) rotational scanning mechanism (c) linear scanning mechanism (Fenster et al. 2011).

2.3.1.2 2D arrays

A 2D phased arrays of receive and transmit elements are exploited to simultaneously produce multiple 2D B-mode US images. 1D phase array ultrasound transducers are limited to only one plane steering and focusing; whereas 2D arrays can examine in many directions on a single position (Reverdy et al. 2012). A 2D arrays transducer sweeps out a volume shaped in form of truncated pyramid (Figure 2.14).

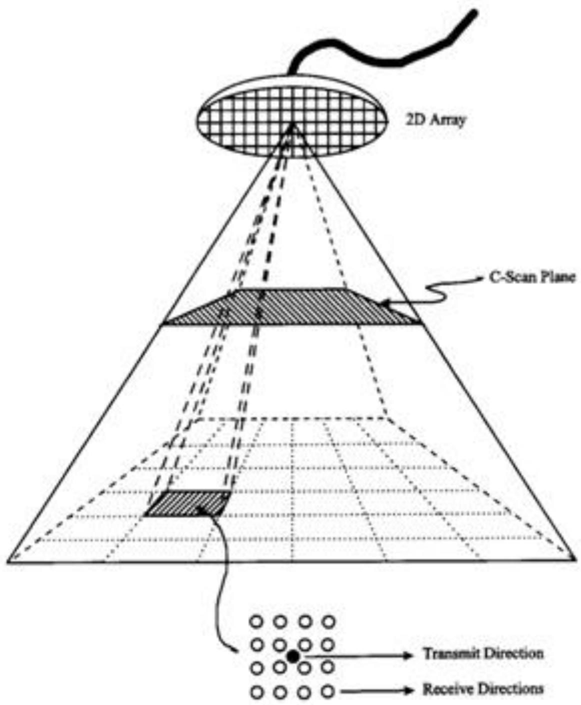

Figure 2.14, Schematic of volumetric imaging produced from 2D phase array (Shiota et al. 1998)

Multiple planes of image can be generated from the volume in real-time (Fenster et al. 2001). Typically, 128 elements are found in US linear array transducer. This suggests a 2D transducer array have 16384 elements (128X128) in form of rectangular grid. However, it will take total 2.1 second for completing a single scan if 128 ultrasound beams each take 1/60 second to complete scanning. Thus, a parallel beam former is required. Another problem is that the 16384 elements are needed individual connections. A cable diameter of probe with multi-centimeters is inevitable, causing inconvenience to use. These problems have been addressed by mounting the analogue to digital conversion and beam-former control inside the probe housing (Prager et al. 2010), but, making 2D arrays probe complex in design and high cost; few companies provide this technology. Real-time volume, which is also known as four-dimensional (4D) US imaging, can also be achieved with limited spatial resolution through reduction in elements. The geometrical dimension of the probe also confines the volume acquired (Gee et al. 2003). Although the mechanical sweeping of 2D transducers is very mature, it also was suggested that 2D array will eventually be outperformed in term of cost and performance (Light et al. 2008). The 2D array approach for 4D US imaging is successfully exploited in echocardiology for imaging heart and its valves (Prakasa et al. 2006).

2.3.1.3 Tracked free-hand scanning approach

The ultrasound probe installed with the mechanical driving assembly, in general, is heavy, bulk, limited range and inconvenient to use when compared with normal ultrasound probe, although it provides high accurate geometrical information and easy data processing. Free-hand scanning approach has been developed for overcoming these issues using various position tracking sensors, techniques and instruments for tracking a US probe's position and orientation. This spatial data and the US B-mode imaging acquired simultaneously are exploited for reconstructing 3D volume (Rohling et al. 1999). Compared free-head scanning with mechanical scanning approach, it further provides arbitrary scanning directions and covers large area for acquiring larger volume. One of the constraints of free-hand scanning is that an operator warrants steering the ultrasound probe over the targeted anatomy at an appropriate speed to minimize the gap, which considerably affects the quality of volume, because the spatial data between two consecutive B-mode US images are not predefined.

Apart from operator skill, most conventional 2D probes were not designed for 3D reconstruction purpose, resulting in poor elevational resolution and leading to anisotropic resolution in the reconstructed volume. Multiple foci feature in modern US machine mitigates the problem by focusing ultrasound beam at different depths. However, sample rate is the trade-off. Gelly et al. (1997) suggested that a 1.5D US probes (Figure 2.15) specifically fabricated for 3D imaging may provide a better answer.

Figure 2.15. 1-D array produces anisotropic elevational resolution (left), 1.5D array produces an improved beam focusing (right).

Over past decades, several tracked free-hand scanning approaches have been developed such as US with articulated arms, US with acoustic sensing, US with magnetic field sensing, US with optical sensing, US with accelerator, gyroscope and image-based sensing.

Acoustic track scanning

Acoustic tracking system (Figure 2.16a) comprises a conventional US machine, personal computer (PC), and 3D acoustic spatial locator (Model GP 8-3D, GTCO Corporation, Columbia, MD U.S.A.), which consists of microphones and sound emitting unit (King et al. 1990). The sound emitting unit is attached to the ultrasound probe. It continuously emits sound pulse while scanning. Meanwhile, the microphones continuously detect incoming sound. The position and orientation of probe can then be determined from speed and time of flight of sound pulse. The microphones must be installed over the patient, because any obstruction blocking the line of sight between emitter and the microphones causes signal interrupt. They must be placed in proximity to patient to maintain a good signal-to-noise ratio (Fenster et al. 2000). As temperature, air pressure, and humidity can significantly affect the speed of sound, the accuracy is substantially affected. King et al. (King et al. 1991) claimed that their 3D ultrasound system achieved the system error less than 0.4%. King et al. (King et al. 1991) also reported that quantitative ventriculography using freehand 3D echocardiography with an acoustic spatial locator provides highly accurate reproducible measurements of left ventricular volume, mass, and function together with 2 to 3 times better than 2D echocardiographic techniques. The acoustic spatial locator, however, is relatively bulky when compared with electromagnetic locator (King et al. 2002).

Articulated arm

This approach is considered as a partially constrained free-hand scanning approach. A

2D ultrasound probe is mounted onto a multiple-jointed mechanical arm system, which is installed with potentiometers at each joint (Figure 2.16b). The lengths of each arm segment and angles measured from the potentiometers provide the essential information for computing the relative position and orientation of the 2D ultrasound probe. B-mode images are acquired while the operator manipulates the probe with the arm system sweeping over the targeted anatomy. With this information, the 3D image volume can be reconstructed. The 3D image quality can also be improved by reducing the number of moving joint, shortening length of arm, and decreasing the scanning flexibility (Fenster et al. 2000). A mechanical arm with five degrees of freedom ultrasound imaging system has been developed for exploiting in calculating the left ventricular (LV) wall motion in vivo (Geiser et al. 1982). However, the system is limited by tracking a single object with restricted range; it is generally ponderous.

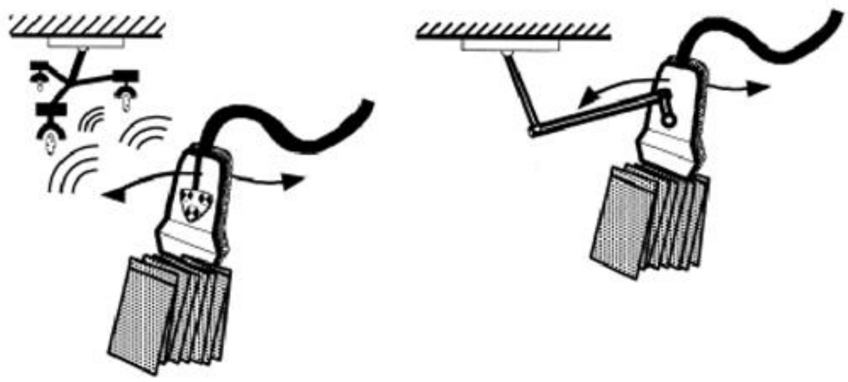

(a) (b)

Figure 2.16. Schematic diagrams showing freehand scanning approaches (a) acoustic tracking system with sound-emitter mounted above the patient and microphone mounted on the probe. (b) Articulated arms with potentiometers exploited for storing relative position information (Fenster et al. 2000).

Magnetic field based spatial position sensor

This method is the most commonly found in free-hand ultrasound scanning (Fenster et al. 2011). Several companies currently provide this kind of sensors. Northern digital incorporation (NDI) provides the Aurora sensor (Aurora, NDI, Ontario, Canada), which was designed for medical use. Polhemus provides Fastrak sensor (Fastrak, Polhemus, Colchester, VT, USA). Ascension Technology Corporation provides MiniBird sensor (MiniBird, Ascension technology corporation, Burlington, VT, USA) with reasonable price and performance; it was taken over by NDI recently. These systems make use of a transmitter to produce a spatially varying magnetic field and a sensor, which comprises with three orthogonal coils, to measure the magnet field strength for calculating the sensor's position and orientation (Figure 2.17).

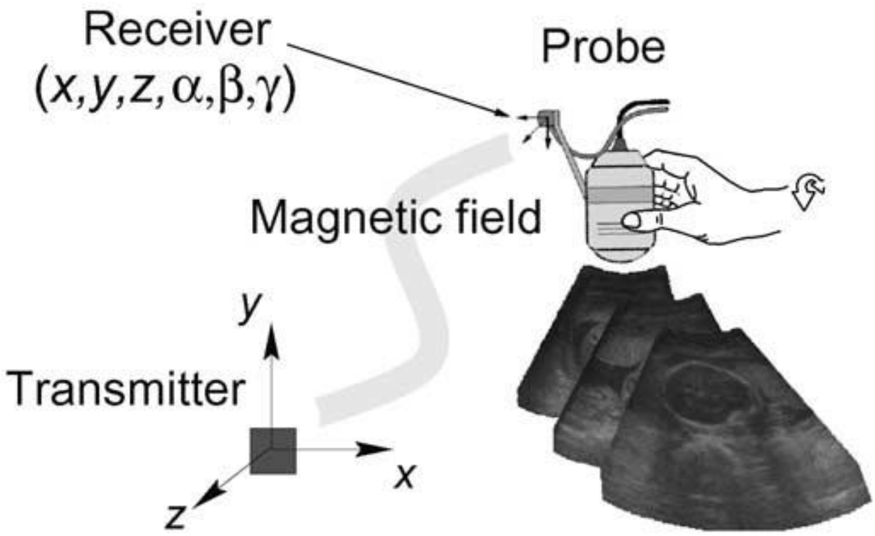

Figure 2.17, Magnetic tracking system, a sensor picks up the field strength and calculate its location (Gee et al. 2002).

These systems can provide the sample rate up to several hundred hertz. The sensor is mounted on the ultrasound probe, allowing spatial position and orientation being measured while the ultrasound B-mode image is being acquired. This information can be exploited for volume reconstruction. This approach has been successfully applied in many clinical applications such as robotic needling placement (Boctor et al. 2008), echocardiography (Delabays et al. 1995), obstetrics (Riccabona et al. 1996) and vascular imaging (Fenster et al. 1998).

Magnetic field sensors are general small and unobtrusive. 3D ultrasound system installed with the sensors does not need an external mechanical device and maintain a clean line of sight. However, they are susceptible to electromagnetic interference, which causes accuracy reduction. Cathode ray tube (CRT) monitor, alternative current (AC) power cabling, and electrical signal from ultrasound probe are common source of interference. Geometric distortion can be observed if any ferromagnetic metal presents in the detection zone. There are two common approaches for generating the magnetic field. The alternative magnetic field is implemented by Polhemus in Fastrak (Polhemus, Colchester, VT, USA) and NDI in Aurora (NDI, Ontario, Canada). However, this approach is more sensitive to eddy currents. Carefully design of metal structure in clinical environment, therefore, is warranted. The pulse magnetic field approach is an alternative and implemented by Ascension in MiniBird (Ascension technology corporation, Burlington, VT, USA). This approach is shown to be less sensitive to ferromagnetic material. In fact, non-ferromagnetic metals such as steel series 316, titanium are often recommended as the building material inside detection zone.

In addition, calibration is a major factor affecting reconstruction. The calibration is to define a relative position and orientation of an US image relative to a spatial sensor. This value is used for transforming the US image to the correct position during image registration. The detail of calibration will be discussed in later section. The quality of reconstruction also depends on the skill of operator; the sudden motions like jerk and rotation need to be totally avoided so as to maintain a good accuracy of position and orientation values. Smoothly and slowly scanning has been recommended for good quality of reconstruction (Gee et al. 2003).

Optical based spatial position sensor

In case of presenting ferromagnetic material or larger extend, optical tracking is usually replacing the magnetic field tracking. Optical tracking can use active or passive target to track the target position from the view of two (or more) calibrated cameras (Figure 2.18).

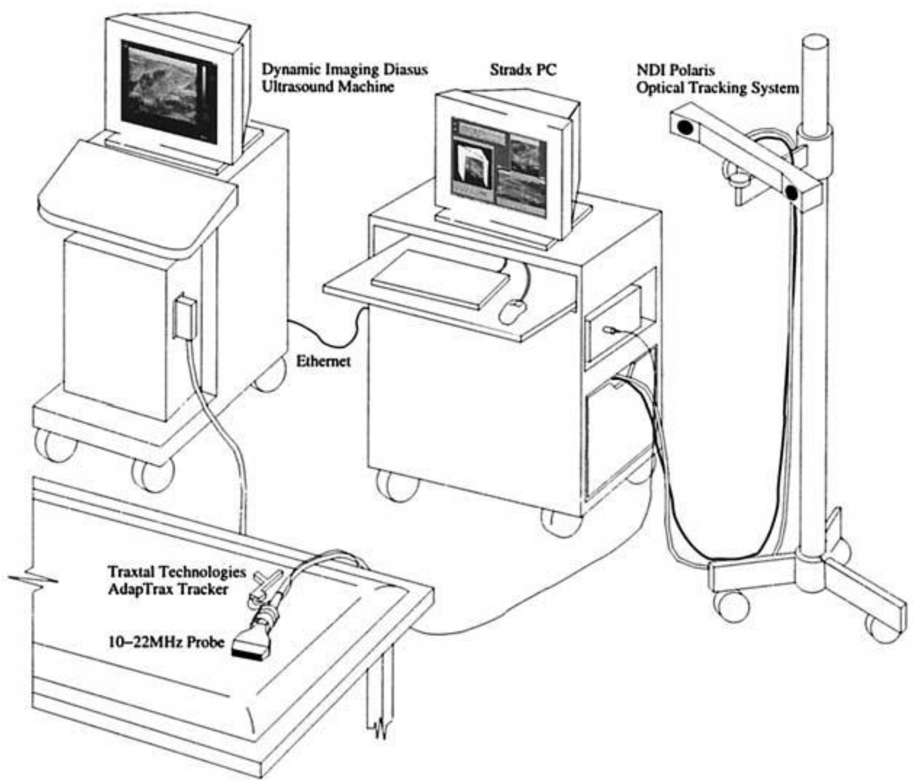

Figure 2.18. Setup of optical tracking system (Treece et al. 2003).

Passive targets, which are infrared light reflectors, with three or more matt spheres are arranged in an asymmetry order with known relative position on a small frame, allowing the tracker to infer the position and orientation of the frame (Linseth et al. 2003). Whereas, active target comprises of an array of infrared light-emitting diodes, which are excited in a known sequence and synchronized with the cameras, making the individual LED to be identified; the position and orientation, hence, can be inferred (Treece et al. 2003). In additional, these targets must be carefully maintained, making them not to stray outside the cameras' field of view. The Polaris system (Polaris, NDI, Ontario, Canada) is a one of the common optical tracker system. According to the manufacturer's product specification, it can provide the volumetric accuracy up to 0.25 mm root mean square (RMS); whereas, the Aurora magnetic field sensor system from NDI can only provide the accuracy up to 0.48 mm RMS. Optical tracker system, indeed, is more accuracy than magnetic field sensing system in measuring absolution positions and orientations in 3D space. It, however, is more expensive and less portable because of installing a few large camera systems to guarantee an uninterrupted line of sight between probe and cameras (Prager et al. 2010). Similar to magnetic position sensor, optical position needs a calibration. Optical tracker is particularly useful in MRI environment. For instance, registration of optical tracked freehand 3D ultrasound image of liver and MRI image of liver has been developed (Penny et al. 2004).

Free-hand without spatial position sensor

A freehand 3D ultrasound with spatial position sensor can provide good image for both qualitative and quantitative assessment. However, it is generally expensive, obtrusive, and requiring complicated calibration procedures. Alternatively, freehand 3D ultrasound without position sensor reconstruction approach can provide a fine scale detail, relatively unobtrusive; however, it is prone to have linear and angular tracking drift. Given that the spatial accuracy is not necessary, the 3D image can be produced without spatial sensor by assuming the ultrasound probe moving over the subject in a predefined and regular geometry during scanning. The motion of ultrasound probe must also maintain a constant linear or angular velocity moving along a subject in order to acquire the B-mode US images with a regular spacing. As the total distance travelled and total angle rotated of probe can be estimated together with the steady motion during images acquisition, a good 3D image could be reconstructed (Downey et al. 1995). However, there is no guarantee in geometrically accuracy. This approach must not be used for measurement purpose (Fenster et al. 2012). Recently, applying different algorithms and use of accelerometer or gyroscope considerably improve the quality and accuracy of this approach.

The B-mode ultrasound images can be exploited to extract their relative position information. In general, interaction between a source of coherent energy and scatters causing reflected spatial energy pattern vary because of interference; a speckle pattern is then formed in US B-mode image. Since speckle pattern embeds the scatters spatial data, the speckle patterns are same for two B-mode images acquired at same position and orientation. The degree of decorrelation of the speckles from two B-mode images is proportional to the distance between two B-mode images together with the relationship depending on the beam width in the direction of the probe motion (Tuhill et al. 1998). This phenomenon is known as speckle decorrelation. The pair of B-mode US image may not be in parallel position because of the probe titling or rotating movement; the acquired images are segmented into sub-region with similar region across these images to compute their cross-correlation. As a result, a pattern of distance vectors are generated from a pattern of decorrelation values to determine the relative position and orientation between two images (Fenster et al. 2000). The speckle decorrelation was reported to exploit for estimating the velocity of blood (Friemel et al. 1998). With speckle decorrelation, the relative positions between

B-mode ultrasound images can be estimated; 3D volume can be reconstructed accordingly. Many research groups have successfully developed ultrasound imaging system based on speckle decorrelation (Chen et al. 1997; Chang et al. 2003; Downey et al. 1995; Tuhill et al. 1998; Prager et al. 2003). However, without spatial data, the operator warrants to maintain an insignificant translational or rotational motion of the probe along an elevational direction so as to obtain the B-mode US image at regular interval. Tuihill et al. (1998) reported that the position accuracy was 87% for estimating the image spacing. This means low geometrically accuracy attained, making this approach suitable for tissue qualitative study only.

Considering two images, any in-plane motion between them can be determined from 2D imaging techniques (Bohs et al. 2000) and out of plane motion can also be determined by speckle decorrelation (Chen et al. 1997; Tuhill et al. 1998). The estimation of elevation offset, however, is difficult to eliminate from all sources of bias, resulting in cumulative drift error occurring as the inter-frame displacement are concatenated to reconstruct a 3D volume. Recently, microelectromechanical system (MEMS) device is rapidly advanced with substantial cost reduction. Miniature accelerator and gyroscope are essential component in gaming and mobile phone industrial nowadays. These sensors have been exploited for correcting angular drift in sensorless reconstructions with linear drift presented in the elevation direction with a reconstruction accuracy of around 1° (Housden et al. 2008).

2.3.1.4 Untracked free-hand scanning approach

Tracked freehand scanning approach generally needs a spatial sensor device to provide position and orientation, calibration, and additional computations on reconstruction, leading to higher cost; albeit, it permits high degree of free probe manipulated and good reconstruction result. Alternatively, with predefined scanning geometry, 3D image can also be reconstructed without using any kind of position sensor and complex decorrelation algorithm. Without geometrical information recorded during scanning, the operator must steadily move the probe at a constant linear or angular velocity in order to acquire the 2D B-mode images with a regular spacing. With known approximated total distance travelled or angle rotated and uniformly spacing, a good 3D image may possible be reconstructed. The 3D image, however, cannot be exploited for any quantities measurements because there is no guarantee on geometrically accurate (Downey t al. 1995), leading no guarantee on quality of data volume.

2.3.2 Quality of data volumes

Good quality of 3D ultrasound image is always targeted in research because of its high clinical value and facilitates new applications. Although there are many scanning techniques to acquire raw data, factors including use of the best quality image source, use of the best position measurement, carefully matching the images and positions, and adopting a good scanning technique are substantially affecting the quality of 3D imaging.

Many 3D freehand ultrasound systems are built on existing 2D ultrasound system. The video from 2D ultrasound is captured into other system for processing, leading to degrade in 2D ultrasound image quality because of analogue to digital conversion and under-sampled frame rate. In addition, the poor elevational resolution is usually found in 2D ultrasound, leading to anisotropic resolution in acquired data. Multiple foci technique alleviates the problem by narrowing the ultrasound beam between foci. The use of 1.5D probe is even considered as a better solution (Gelly et al. 1997). Good scanning technique is another important factor. For instance, data acquires in a single breath hold or using frame structure to keep the subject stationary, allowing considerably reducing in motion artifact; maintaining a constant contact pressure during scanning minimizes the pressure-induced artifacts. Choice of position measuring instrument is another major factor. Optical position system provides significantly better accuracy over magnetic sensing position system, despite its high cost and problem of line of sight. Spatial calibration between the position measuring instrument and probe is warranted for building the data relationship and requires precise working procedures. Similarly, temporal calibration is needed for matching the images and theirs positions. As the sampling rate of ultrasound 2D images output and position sensor output does not match, calibration is needed for locating the exact location where image is being captured.

2.3.3 Calibration

As noted before, calibration is the key of all tracked freehand imaging system. The most important is to determine the relative position and orientation of a spatial sensor mounted on the US probe with respect to the US B-mode scanning plane. The spatial calibration factor is including 6 constant offsets, which comprises with 3 position values and 3 orientation values. Accurate offsets are essential for reconstructing a true and good 3D image during registration. These offsets can also be roughly estimated by external measurements between the probe and the spatial sensor. As the exact location of B-mode image start corner and centre of the spatial sensor are not known, a phantom specially designed with known physical dimensions and properties is preferably used for determining the offsets (Prager et al. 1998). Apart from spatial offsets, the delay between the US B-mode image and its position tracked by spatial sensor is known as temporal offset. This is because there is unknown time delay of data delivering from US machine to PC and from spatial sensor to PC; temporal offset actually represents the relative delay between these two data streams. There also exists a problem of priority of calibration. For instance, the exact location of the object in the image is unknown during temporal calibration, which is conducted before spatial calibration. On the other hand, if spatial calibration is conducted before temporal calibration, the image's position is subject to temporal distortion (Hsu et al. 2008a). Temporal calibration must be conducted at first place before spatial calibration using continuous scanning (Prager et al. 1998). This can be overcome by holding the probe in stationary position for a short duration at each position while capturing B-mode image (Good et al. 2005; Hsu et al. 2006). Accurate calibration provides a consistent reconstructed volume, preserving a true anatomical shape. However, many calibration techniques are timely because they may take several hours for a skillful technician to conduct; they are not easy to use, and needed to undergo repetitively whenever the spatial is re-mounted (Prager et al. 1998).

2.3.3.1 Spatial calibration

Spatial calibration is an essential prerequisite for all 3D freehand ultrasound applications. It is a crucial procedure in developing a 3D freehand Ultrasound system with a spatial sensor attached on the probe because we have to accurately locate each B-mode image, which is in form of a plane, in the 3D volume coordinate system. It is also important to notice that a spatial sensing device should be mounted as close as possible to the imaging plane for maximum accuracy (Detmer et al. 1994). In simple term, spatial calibration allows a pixel in B-mode image to be registered in a 3D world coordinate system. For convenient purpose, the spatial transmitter is recognized as an origin of the world coordinate system. However, the world coordinate system may not be useful in measurement or 3D image analysis (Hsu et al. 2008b), as the clinicians concern the volume, length, and morphological information. The actual location of target anatomy structure relative to origin is less useful. However, in surgical navigation applications or registration, the 3D ultrasound image have to register with external coordinate system, allowing clinician to accurately locate the anatomical feature in 3D space; the world coordinate system needs to be involved (Gee et al. 2005).

There is a great deal of research for spatial calibration using scanning on a phantom with known geometrical properties. In general, there are four major types of phantoms. They are point phantom, stylus, plane phantom, Z-phantom and their variants respectively. The simplest and common form of phantom is a point phantom, which has been used for many research groups (Detmer et al. 1994, State et al. 1994, Barry et al. 1997; Amin et al. 2001; Gooding et al. 2005; Huang et al. 2005a; Barratt et al. 2006). Point phantom is typically formed using a pair of intersection wires strung across a water bath to create a point or using a small spherical object (Amin et al. 2001; Leotta et al. 1997). The point has to be scanned from many different directions and its location needs to be marked in each B-mode image. The collated points can then be exploited to map into world coordinate system using the position sensor readings. All points will be mapped in a same 3D location if the spatial offsets are correct. The relationship between points in the B-mode images and its 3D location are expressed in form of a series of transformation matrix, which is shown as below.

$$p^F = T_{F\leftarrow W} \bullet T_{W\leftarrow S} \bullet T_{S\leftarrow I} \bullet T_s \bullet p^{I'} \qquad (1)$$

where $T_s = \begin{pmatrix} s_\mu & 0 & 0 \\ 0 & s_v & 0 \\ 0 & 0 & 0 \end{pmatrix}$, p^F denotes a point (x,y,z) in phantom coordinate

The whole transformation process is also called probe calibration (Mercier et al. 2005). The spatial sensor S records the location relative to the stationary counterpart W, known as world coordinate (Figure 2.19). In equation (1), the reading from the spatial sensor is represented by the matrix $T_{W\leftarrow S,}$ which also notes the transformation from a sensor coordinate system to the world coordinate system. The rigid-body transformation matrix $T_{S\leftarrow I}$ consists of six parameters including the three translations along x, y, z axes, and the three rotations, azimuth, elevation, roll, on these axes, where $T_{S\leftarrow I}$ represents a rotational transformation followed by a translation from the coordinate system I (Image coordinate) to the coordinate S (Sensor coordinate). In addition, the x-axis, y-axis, and z-axis represent the probe's lateral direction, beam direction, and elevational direction, respectively. The transformational matrix $T_{F\leftarrow W}$ denotes the transformation from the world coordinate system to a phantom coordinate system, which is, in fact, not necessary unless other external device involved applications such as surgical navigation aforementioned. This matrix, therefore, is often included for convenient purpose. The resultant 3D image is unchanged even without processing it. It actually controls the position and orientation of resultant 3D image in a 3D visualization scene. The point target or the intersection of two wires is considered as the origin of the phantom coordinate system in order to reduce the complexity of mathematical expression. Apart from the coordinate system issue, the scale of B-mode image in the world coordinate system is not known. A point $p^{I'} = (\mu, \nu, 0)^t$ is represented by in a B-mode image, where μ and ν are the column and row indices respectively, with the unit in pixels instead of millimeters. For practical reasons, the top centre of the image is often recognized as the origin of image (Mercier et al. 2005). In equation (1), T_s is a scale factor matrix, where $S\mu$ and $S\nu$ represent the scales in millimeters per pixel. This matrix allows pixel unit change to metric unit. A series of B-mode images, in which the point phantom is marked in term of pixel unit, are needed for solving the calibration matrix by least squares (Arun et al. 1987) or iterative optimization techniques such as Levenberg-Marquardt algorithm (More 1977). These techniques are used for minimizing the distance between the sets of points identified in the B-mode Images, allowing the unknown calibration parameters to be found. This mathematical expression can generally be applied to all different phantom designs. Interestingly, these cumbersome mathematical procedures can be simplified by performing an external measurement of the probe casing and the spatial sensor attached for estimating the translational parameters (Hughes et al. 1996). However, without knowledge of the spatial sensor's coordinate origin, which is embedded in receiver casing, and no marker on the probe indicating the corner of B-mode image are leading to inaccurate measurement. In addition, the B-mode image is not necessarily parallel or centre to the probe casing.

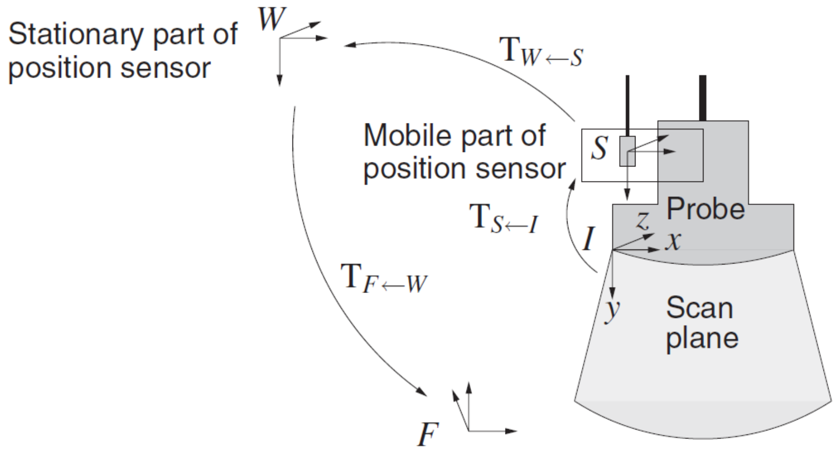

Figure 2.19. The coordinates involved in a freehand 3D Ultrasound System (Hsu et al. 2008b).

Instead of moving probe around a fixed point phantom, the probe was fixed with a tracked stylus moving around while capturing US B-mode image. In this case, stylus is recognized as a calibration phantom. A stylus is a 3D localizer for locating a point in 3D space with a spatial sensor or target attached, which has a sharpened tip with a manufacturer supplied rigid body transformation matrix (Muratore et al. 2001). Certainly, the stylus can be localization fabricated and using simple pointer calibration to compute the rigid body transformation matrix (Leotta et al. 1997). However, similar to the point phantom, the stylus's tip is difficult to align with the scan plane (Hsu et al. 2008c). Khamene et al. (2005) further improved this technique by exploiting a rod instead of the tip of stylus as an imaging target. Two ends of the rod are exploited to define the position and orientation of the rod. Some research groups have further developed multiple cross-wire techniques. For instance, Trobaugh et al. (1994) exploited three collinear points as a phantom; Peria et al. (1995) used three coplanar wires forming a triangle as a phantom; Meairs et al. (2000) exploited the triangle and a single cross wire; Kowal et al. (2003) used four coplanar 1 mm pins' tips as point targets; Leotta et al. (2004) exploited a planar array of strings and beads with a set of out of plane strings for guiding probe orientation during imaging in which the positions of string and a reference beads are known with other beads in arbitrary coplanar positions. All phantoms techniques aforementioned require scanning one or more points in the US B-mode image for ameliorating the image plane alignment issue.

There are three major disadvantages of point type phantom despite its popularity. First, the set equations could be under determined, making no unique solution to exist if the images of phantom acquired scan are not in sufficient diverse range of positions and directions (Prager et al. 1998). Second, automatic segmentation of isolated points in US B-mode is difficult. Manual or semi-automatically segmentation is usually performed, making the calibration process time consuming and wearisome. Third, ultrasound B-mode image plane, typically, has several millimeters thickness in the elevational direction, which makes the points visible even not in pointing direction, leading to difficulty in alignment between the image plane and the point. This property considerably contributes the calibration error (Hsu et al. 2008c). In addition, electromagnetic spatial sensors also are susceptible to noise with over 1 mm RMS. The calibration accuracy of the position measurements are further worsen. To mitigate the problem, a common trend is to exploit two spatial sensors instead of one. The addition spatial sensor is attached to the phantom. With the knowledge of the phantom's position, the equation set of calibration is reduced, allowing fewer images for the calibration. For instance, 2D alignment paradigm (Sato et al. 1998; Lindseth et al. 2003; Gee at al. 2005) has a particular advantage of using a single view for calibration. It, therefore, eliminates the problem of under determined equation. However, it still requires the manual alignment of the scan plane with a set coplanar phantom's features, leaving the beam thickness problem persistently unsolved. This technique is also substantially affected by the spatial sensor noise. It was reported that averaging on multiple image views can mitigate the noise (Gee et al. 2005). Gee et al. (2005) further designed a notable complicated calibration instrument with gantry, mini-water tank, and several micrometer driving stages, which requires only a single image view without veteran operator for determining the scanning directions, leading to eliminate the beam thickness problem. In addition, the spatial sensor does not participate in end-user calibration process; the spatial sensor noise, consequentially, is eliminated. However, its complicated metallic structure hampers the use of magnetic sensing spatial sensor and semi-automatic segmentation is still required.

Three-wire phantom (Carr 1996), which three wires are accurately mounted in orthogonal directions, is similar technique to the cross-wire method. The orthogonality, straightness of wires, and the degrees between the transmitter and wires determine the accuracy. The approach of finding offsets is similar to cross-wire method. Comparing with cross-wire method, it is easier to locate the cross point in US B-mode image. In addition, this technique needs not to align the scan plant with phantom. However, each wire must be separately scanned for maintaining intersects captured by the images (Hse et al. 2008b; Prager et al. 1998).

The manual alignment has been addressed by scanning of wires arranged in N or Z patterns (Comean et al. 1998; Bouchet et al. 2001; Pagoulatos et al. 2001; Lindseth et al. 2003; Chen et al. 2006; Hsu et al. 2008a). With sufficient wires, the positions of wires in B-mode image and readings from spatial sensor, the calibration spatial offsets can be devised from a single view. However, beam thickness is still an issue. Apart from aforementioned wire-based phantom, there are other similar wire phantoms in form many different arrangements such as a triangular pyramid (Liu et al. 1998), a ladder of string (Beasley et al. 1999), diagonal phantom in which a cube formed by nine orthogonal wire crossings (Lindseth et al. 2003), Hopkins US phantom (Boctor et al. 2003) in which a shape of cross formed by parallel wires.

Alternatively, wall phantom approach is exploiting a line as a target phantom, allowing the phantom easier to construct. With a simple water bath alone, the bottom of the bath can be as a target. The accuracy depends on the flatness on the floor and the degree between the flat and the spatial sensing transmitter (Prager et al. 1998). The single-wall phantom (Prager et al. 1998), a plexiglass plate (Rousseau et al. 2005), nylon membrane (Langø T. 2000) and Cambridge phantoms (Prager et al. 1998) are belonged to this approach. This approach is particularly attractive. It is still possible to locate the line even when part of the line is corrupted; the information is more redundant, allowing more reliable segmentation. Besides, automatic algorithms for line segmentation are widely available like the Hough transform and wavelet-based techniques, making this approach the quickest solution for calibration among all approaches (Mercier et al. 2005). Single-wall and membrane phantom, however, have difficult in imaging when the probe is orientated at an angle far from the normal, this is because lower intensity line or reducing in sharpness occurs. Cambridge is designed to solve this problem by locking the scanning on a thin brass bar with a clamp; the brass bar is served a virtual plane in such configuration. However, the plane warrants to be scanned in a deterministic configuration, making it difficult to inexperienced operator (Hsu et al. 2008a)

2.3.3.2 Temporal calibration

Spatial tracking device and US machine B-mode image are not synchronized in nature, leading to asynchronous signals between their data output; a computer is usually exploited for synchronized the signal data (Prager et al. 1999; Huang et al. 2005a). Temporal calibration has to be calculated for determining the temporal offset. There are two commonly used methods to transfer B-mode image to computer storage. The most common one is connecting the analog output of US machine to a frame-grabbing capture card (Detmer et al. 1994), which is installed in a desktop computer. There is also a mismatch between US machine frame rate and frame-grabber rate, leading to frame dropping or duplication. Alternatively, some US machines can send B-mode image to a computer through network cable (Lindseth et al. 2003). Either ways will introduce latency. In addition, US machine and position tracker are not generating data streams continuously. A temporal offset is essential to match the data streams (Mercier et al. 2005).

There are generally two approaches for conducting calibration. The first approach is detection of the sudden jerk in B-mode image. Initially, the US probe is held in stationary position. A sudden motion of probe is then induced, making noticeable change in B-mode image. The time of sudden motion is recorded by the attached spatial tracking device; the time of jerk occurred in B-mode image is recorded simultaneously, allowing the latency $\pm(T+t)/2$ to be determined in a single scan; where T denotes the time interval between images acquisitions, t denotes the time interval between spatial position acquisitions. The accuracy can be improved by multiple calibration scans and performing average of the latency values (Prager et al.

1998). The second is use of a constrained probe under continuous motion. Spatial calibration also needs not to be undergone prior to the temporal calibration. Several research groups exploited this approach (Borcher et al. 2001; Treece et al. 2003; Gooding et al.; Huang et al. 2005a). The position of an object like a plan surface is tracked and recorded in order to define a principle axis of motion. The position of probe are tracked and provided by the spatial position sensor as uncalibrated positions measurements. The latency can then be determined from the time offset at which the maximum correlation between the position of the object in the US B-mode image and the position of the probe happened. Interpolation can also be exploited to improve the position resolution for enhancing accuracy. Similarly, accuracy of the latency can also be ameliorated by averaging multiple measurements. In addition, both approaches have made the assumption the latency kept constant from one scan to the next (Gooding el at 2005). Gooding et al. (2005) further suggested that the temporal calibration by first approach, proposed by Prager et al. (1998), must be conducted at first. The temporal offset estimated is then exploited to use for spatial calibration. After the spatial calibration, accuracy temporal calibration is then conducted using second approach.

After spatial and temporal calibration, the exact position of pixel in 3D space can be obtained. However, the gap between images will always create void due to large separation between images. In contrast, pixels from the images could occur in same space position because of close separation between images. These problems are significantly affect the quality of image and could be addressed by reconstruction techniques.

2.3.4 Reconstruction techniques

The reconstruction techniques are exploited to build a 3D image for visualization purpose. Basically, all pixels from raw US B-mode are traversed into voxels of a 3D volume by registration using equation (1). Certainly, the size of whole 3D volume and voxel must be well-defined before the process taking place. However, without an appropriate reconstruction algorithm, the registered pixels could be formed a group of unstructured or scattered data points in 3D space only, making all anatomical information unrecognized. The true diagnostic information must be preserved along with minimized noise or artefacts (Rohling 1999). There are generally three group of reconstruction implementation methods including voxel-based methods (VBM), pixel-based methods (PBM), and function-based methods (FBM).

VBMs traverse all voxels in a target voxel grid with the value from raw US B-mode image. One or more pixels could be contributed to the value of each voxel, according to different algorithms; some far away pixels from raw image may not contribute to any voxel. Some methods just exploit one pixel from raw images to determine the value of voxel. Voxel Nearest Neighbour (VNN) is a common algorithm for implementing VBM. VNN simply assigns the value of voxel from its nearest registered image pixel. It is simple but inefficient because all nearest pixels' values must be examined. A better approach is to fill the value of a voxel lying along a line normal to the nearest US B-mode image; speed of reconstruction would, therefore, be improved (Rohling et al. 1999).

VBM problem can be ameliorated with various interpolation methods. VBM with interpolation exploits an interpolation between several registered raw images' pixels for determining a voxel value. Berg et al. (1999) exploited a 1D linear interpolation with reconstruction along in one dimension for 4D volume human heart application; the interpolation uses a weight decreasing with a distance to the scan planes. A virtual plan is introduced in middle of the scan plans if the maximum angle between the two plans is less than 20°; the linear interpolation orthogonal to the virtual plan is then used. Trobaugh et al. (1994) exploited two nearest scan images for a bilinear interpolation. The algorithm locates the two nearest image planes from each side of the voxel. Normal is computed to each plane and four surrounding pixels in each plane are bilinearly interpolated. The voxel value is determined from a distance weighted sum from two planes in orthogonal direction. Coup et al. (2005) further worked on this algorithm by estimating the probe moving trajectory to compute a virtual plane. A distance between the probe and virtual plane is estimated by interpolating the time stamp of the two nearest scan plans and four B-mode scan images are exploited together with cubic interpolation to obtain the voxel value. Thune et al. (1996) used tri-linear interpolation approach. 1D scan lines are exploited for reconstruction; the eight closest points in the scan lines are used for determining the voxel value. The main advantage of VMB with interpolation is avoiding gaps in the voxel grid or holes in a 3D volume. However, reconstruction artefacts like interpolated image mismatching its neighbours can be observed when volume is sliced. It is because the registration errors, including tissue motion and sensor errors contribute the misalignment of the B-mode scans (Rohling 1999).

Unlike VBM, PBMs traverse all pixels available in raw US B-mode image to one or several voxels. PBMs may comprise with two steps including distribution step (DS) and hole-filling step (HFS). In DS, the pixel is traversed and often stored with a weight value. In HFS, all voxels are traversed including all previous empty voxel remained after first step. However, if the raw images are too far apart or too small hole-filling-limits which define how far away from the known value to be filled, the holes could still exist in the constructed volume. Pixel Nearest Neighbor (PNN) interpolation is one of the most common PBM (Fine et al. 1991; Nelson et al. 1997; Rohling et al. 1997; Gobbi et al. 2002). Most PBMs exploited a PNN bin-filling stage as the DS. HFS may not be necessary if the raw US images are adequate close (Gobbi et al. 2002). However, dense raw images also lead to multiple pixels contribution to same voxel. The common handling method is average (Nelson et al. 1997; Gobbi et al. 2002). There are other approaches including keeping the most recent value (Ohbuchi et al. 1992), the first value (Trobaugh), and maximum value (Nelson et al. 1997). In HFS, various methods have been developed for empty voxel filling including mean of nonzero pixels from an intersecting 2D plane (McCann et al. 1988), average or maximum (Nelson et al. 1997), a median of nonzero voxels in a 3D local neighborhood (San Jose-Esterpar et al. 2003a), interpolation from the two closest voxels (Hottier et al. 1990), reduction in resolution, and use of 3X3X3 Gaussian or media filter (Nelson et al. 1997). Some methods have been further developed using a weighting to near voxel and apply the voxel value to a local neighborhood, known as kernel, around the voxel filled in DS. Kernel can be in form of spherical or ellipsoid. For instance, Barry et al. (1997) used a spherical kernel with an inverse distance weighing, also known as distance-weighted interpolation; Meairs et al. (2000) exploited an ellipsoid Gaussian kernel with exponential weighting.

Apart from VBMs and PBMs, using mathematical functions for reconstruction are also known as Function-Based Methods. For instance, Rohling et al. (1999) purposed a radical basis function interpolation to approximate with splines that exploit the underlying feature of the data for reconstruction. This approach ameliorates the discontinuities and gaps inside the volume; but, it uses more time for computing. Sanches et al. (2000) purposed a Rayleigh reconstruction with a Bayesian framework to estimate a function for the target tissue using statistical method.

2.3.5 Three-dimensional ultrasound visualization

After volume reconstruction, clinicians need powerful and efficient tool to visual the features embedded in the newly formed volume. There are generally three types of visualization approaches including multi-planar reformatting (MPR), surface rendering (SR) and volume rendering (VR).

In MPR, 2D planes are extracted from a reconstructed volume. Clinician can interact with a user interface to walk through the volume and examine the targeted anatomy. Crossed planes approach is the most common implementation method, in which single or more planes are presented in a same view; these planes are usually arranged orthogonally, but, they can also be arranged in different relative orientation (Figure 2.20). Cube-view is another approach, in which data extracted from the volume are exploited to provide texture for a polyhedron, which is texture-mapped in all faces. The orientations of each faces are determined by user-input.

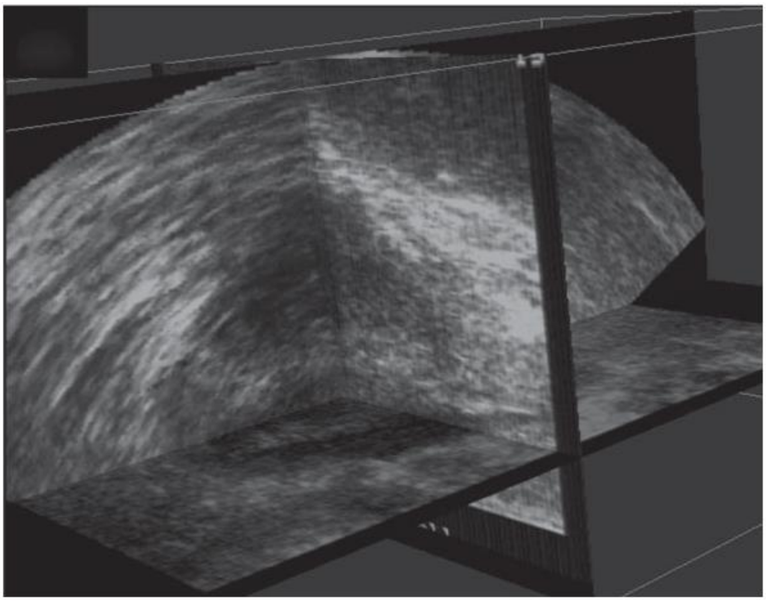

Figure 2.20. 3D Ultrasound of prostate using the mechanical rotation approach displayed by multi-planar reforming approach (Fenster et al. 2011).

In SR, anatomical surface is segmented, isolated with other tissue and displayed a view. Common boundary identification methods like snake algorithm (Kass et al. 1987), manual tracing (Gopal et al. 1997) are first applied to raw image to extract boundary information followed by methods including marching cubes, contour-connecting to generate complete surface information, which further allows calculation of enclosed volume (Figure 2.21). SR is generally fast because of less raw data exploited. However, false surface pieces or features usually affect the real anatomical structure. Small anatomical structure is particularly problematic in visualization (Nelson et al. 1998). SR technique has also been extensively used in echocardiography (Angelini et al. 2005) and obstetrics (Gee et al. 2003).

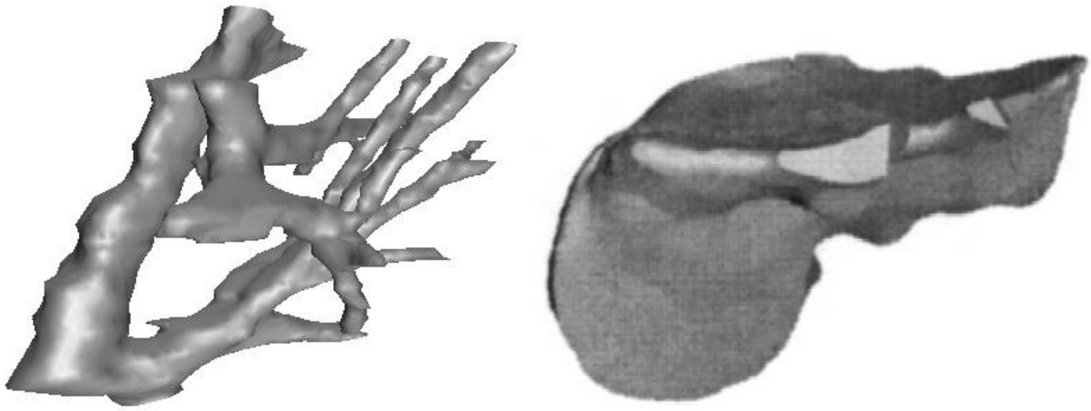

(a) (b)

Figure 2.21. Examples of surface rendering using freehand 3D ultrasound (a) in vivo hepatic system (Treece et al. 1999), (b) human liver after three sweeps (Treece et al. 2001).

Comparing with MPR and SR, VR presents all data at the same view with controlling the strength of translucent of individual voxel. As a result, examiner can look through the reconstructed volume, in which all 3-D information have been preserved with a 2D projection view. Ray-casting algorithm (Levy 1990) is a popular method for implementing the technique. Techniques like maximum intensity projection, translucency rendering and surface enhancement also are commonly exploited. US 3D volume does not have good tissue to tissue contrast, causing difficulty in segmentation in general; however, it produces an excellent contrast between tissue and fluids. VR approach for US 3D imaging, therefore, is extensively used in 3D foetal images (Lee W et al. 2003) (Figure 2.22a), power or colour Doppler 3D images (Downey et al. 1995) (Figure 2.22b), and 3D/4D US cardiac imaging (Devore GR). However, VR requires intensive computing power and does not produce good details of soft tissue.

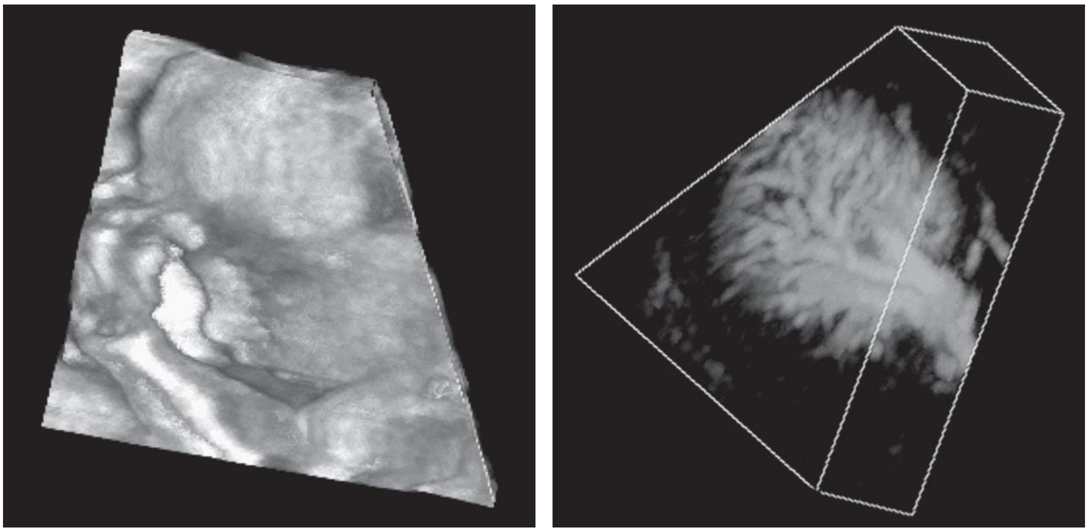

(a) (b)

Figure 2.22. Examples of volume rendering (a) foetal face, (b) vasculature in a kidney using freehand 3D ultrasound Doppler scanning (Fenster et al. 2011).

Apart from the techniques aforementioned, non-planar reslicing, narrow-band rendering (Figure 2.23a), non-planar narrow rendering (Figure 2.23b), and sequential approach are relative new approaches. In non-planar reslicing, data is extracted from a curved surface instead of a plane with predefined orientation in normal reslicing. The curve is defined by operator drawing on resliced plane. The curved surface is then unrolled into a flat plane. The curved surface also needs to preserve the distance measured similar to a flat plane. Non-planar reslicing is particularly good for foetus' unrolled spine image (Gee et al. 1999; Prager et al. 2002). Narrow-band rendering is an extension of reslicing. It is formed by combining a number of resliced planes, which is determined by the user-specified thickness. Maximum intensity compounding, minimum intensity, and simple average techniques are frequently applied to such rendering. Simple average technique can often produce X-ray style image; the others can highlight bright reflector and fluid-filled cavities (Gee et al. 2002). Non-planar narrow rendering is a combined use of non-planar reslicing and narrow band rendering techniques. Sequential approach directly registers the pixel onto the predefined plane with creating a voxel array in the first place. As any resampling process inevitably leads to corrupt the data set, sequential approach reduces the resampling from twice to only one. Full B-scan resolution US B-mode can be exploited without an overhead of a high resolution voxel array. However, the sequential approach requires significantly more computing power (Prager et al. 2002). Gee et al. (2002) combined narrow-band and non-planar approach. However, the practical implementation of narrow-band, non-planar volume is challenging (Gee et al. 2002). It defines as a compounded resultant set of non-planar adjacent unroll surface, which contains same number of rulings. With this imaging technique, resliced planes and surfaces no longer need to be accurately located; and more anatomical structure can be displayed in single view.

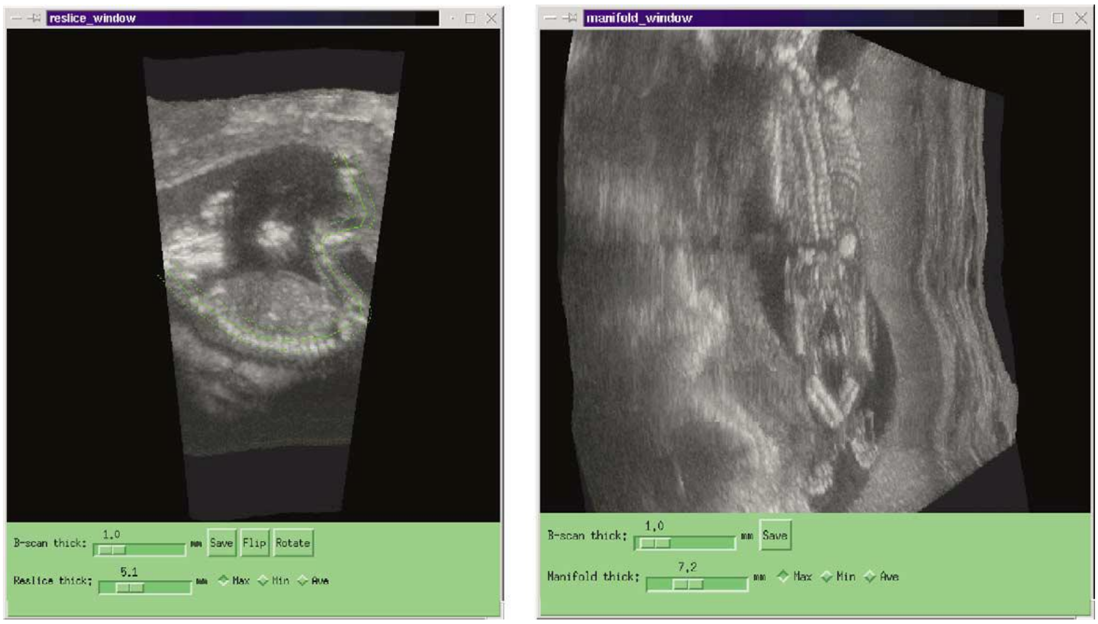

(a) (b)

Figure 2.23. (a) Narrow-band planar with planar reslice thickness set to 5.1 mm and maximum intensity compounding mode set for highlight bone, (b) Non-planar narrow rendering (compounding of non-planar reslice) with thickness set to 7.2 mm and maximum intensity compounding mode set for highlight bone.

2.3.6 Clinical applications of 3D ultrasound

3D US imaging has been playing a key role in wide range of clinical applications. In obstetrics, comparing with others modalities, 3DUS has no radiation and provides real-time examination. 3D US often has tremendous applications in prenatal diagnosis (Merz 1995) such as examining the baby's physical development and functions including breathing movements and heartbeat (Yagel et al. 2007), fetus truck and head volume measurement (Falcon et al. 2005), biomodeling (D'Urso et al. 1998), foetus spine imaging (Budorick et al. 1995), and emerging neurosonographic studies (Correa et al. 2006). In gynecology, 3D US also provides a great deal of applications such as a characterization of uterine anomalies by observing the anomalies of the uterus (Wu et al. 1997), cervix volume measurement (Hoesli et al. 1999), assessment of endometrial volume (Raga et al. 1999), and ovarian volume measurement (Schild et al. 2001). These 3D US applications evidently show its invaluable contribution to women and fetus health.

Cardiology is also a key 3D US application area. Traditionally, cardiac ultrasound provides evaluating cardiac anatomy, ventricular function, blood flow velocity, and vascular diseases. 3D echocardiography is a specific imaging technique, which provides the ability to further improve and widen the diagnostic capabilities (Hung et al. 2007) such as volume measurement (Mor-Avi et al. 2008), heart modeling (Stetten et al. 2001), imaging guidance (Smith et al. 2002), registration (Pieper et al. 1997), evaluating valve function (Kuo et al. 2005), and real-time imaging (Stetten et al. 1998)

3D US is also commonly found in breast imaging and prostate imaging. It provides evaluation of focal infiltrates, intra-cystic structure and multifocal disease (Nelson et al. 1998), better illustrating lesion margins and its topography (Chen et al. 2004), image-guided biopsy (Fenster et al. 2002), and diagnosis in breast imaging (Weismann et al. 2007). Similarly, diagnosis (Fenster et al. 1996) and imaging biopsy (Fenster et al. 2002) are also commonly exploited in prostate imaging.

Vascular imaging is another important area 3D US contributed. 3D US provides both vascular anatomy and blood-flow dynamics. There are a large number of studies on aorta imaging and carotid imaging. In aorta imaging, 3D US is exploited for segmentation (Krissian et al. 2003), intra-operative image guidance (Sjolie et al. 2001), Doppler and volume measurement study (Mehwald et al. 2002). Similar studies are also found in carotid imaging (Gill et al. 1999). The vascular imaging studies currently play an important role in preventing stroke and heart disease.

3D US imaging is also found in other soft tissue studies including eye imaging (Finger et al. 2002), kidney imaging (Zubarev et al. 2001), liver imaging (Ockenga et al. 1998), gastrointestinal imaging (Gilja et al. 2003), gall-bladder (Fine et al. 1991), and brain imaging (Lindseth et al. 2002). Aforementioned application covers only on soft tissue imaging and limited in imaging volume size. However, there are limited studies on hard tissue image in comparison. Bone imaging (Barratt et al. 2006) and spine imaging (Winter et al. 2008) are main hard tissue application area for 3D US. Application of larger organ imaging like whole spine using 3D US is even more challenging as mentioned in previous sections.

2.4 Summary

This chapter gives review on scoliosis, etiology, treatment, currently available assessment methods, and the potential of 3D ultrasound for radiation-free assessment. Human spine is relatively complex and articulated anatomical structure; with natural biological variability, an infinite range of spinal anatomies probably exists, making difficulty in defining a gold standard for spinal curvature. Cobb's method has been exploited for diagnostic purpose and monitoring curve progression. Existing problems of Cobb's method has been extensively reviewed. Apart from using radiograph, non-radiation approach using optical and magnetic techniques has been developed for mapping torso surface and locating vertebrae feature to indirectly calculate the spinal curvature. 3D ultrasound has been introduced as an emerging technique. Various scanning methods and tracking techniques for 3D ultrasound imaging have been discussed for giving an overall picture of possible setup. The outline of acquiring good quality of ultrasound volume data and the relevant calibration methods have also reviewed so as to understand the foundation of building a good 3D ultrasound system. Reconstruction techniques and visualization methods have been overviewed. The development of scanning, reconstruction, and visualization methods has led to an extensive growth in exploiting 3D ultrasound in clinical applications. This leads to the overall aim of this study, which is to develop a 3D ultrasound to accurately measure spine deformity for AIS mass screening and longitudinal follow-up during treatments without any hazard of radiation.

CHAPTER 3 METHODS

3.1 Considerations for system design

To provide a comprehensive view of the human spine using 3D ultrasound, the whole back should be scanned. Huang et al. (2005a, 2005b) had demonstrated the feasibility of 3D measurement of musculoskeletal tissue using freehand ultrasound. The system, however, had not been tested with scanning over a large area such as whole spine region. Huang's system used an ultrasound probe with an imaging width of 38mm. For large structure like lumbar vertebra, two or more B-mode images are required to cover the whole transverse cross section if such a probe is used. Therefore, a few swaps would be necessary to acquire sufficient images so as to cover the whole spine region. This will lead to two major issues for the purpose of scoliosis assessment. First, significant increase in the frame number of ultrasound image captured will make an image volume reconstruction and measurement complicated and time-consuming. Second, multi-swaps scanning involves much longer examination time. This will lead to a challenge for a patient to maintain a consistent posture during the long examination because the patient has to minimize all natural movements including breathing and body posture changing. Therefore, it is important to reduce the time required for scanning, to maintain the subject's posture during scanning, and to enhance the performance of image reconstruction and measurement.

The spatial sensor is a key component for any freehand ultrasound system. Considering cost, performance, flexibility, and accuracy, the spatial sensor using electro-magnetic field may be a suitable choice for the new system. Such a spatial sensor had also been used in the system developed by Huang et al. (2005a). Using this sensor requires non-metallic materials or non-ferromagnetic metals as the building materials for the frame structure. In addition to the performance of spatial sensing, another consideration is the quality of raw ultrasound B-mode image. Huang's system employed a portable ultrasound scanner, which only provided interleaved standard video output with relatively poor quality of image. The B-mode images output were then captured by a PC video capture card. The poor quality of captured video of images makes it difficult to correctly locate anatomical landmarks, which would be elaborated in following sub-sections. It is important to improve the quality of B-mode images for further processing.

With the collection of high quality ultrasound images and accurate spatial data under a well-controlled posture of a subject, it is then crucial to process the image with spatial data to form new images and to extract data that can represent spine deformities, including scoliosis. There are few reported systems for such purpose, thus it is a major area to explore in this study. A large set of B-mode ultrasound images would be collected for the whole spine regions, and it is a great challenge to PC for its memory requirement, computation power and display. It is also an important topic about what kind of information is useful in the huge set of images and corresponding algorithms and programs should be developed to extract such information. The bony landmarks in ultrasound images may be useful to form a profile of spine and should be first considered. However, other information in the image set may also be useful. The ultimate goal is to find an approach that can accurately describe the spine deformities and can be comparable with the current gold standard, Cobb's method.

The measurement systems described in the following sections were developed with the above considerations. It is natural that the system development has gone through a number of stages of improvements during this study. To form a complete view of the system development, the prototypes developed at different stages were introduced.

3.2 System design, improvement, and materials

3.2.1 Prototype-0 development and test

The first prototype (prototype-0) for 3D ultrasound assessment scoliosis (Figure 3.1) was comprised of a frame and three major components, which were similar to the configuration used in the system reported by Huang et al. (2005a). These components were a compact electromagnetic spatial sensing device, a portable ultrasound scanner, and a PC with customized software and installed video capture card. These components were mounted on a Polyvinyl chloride (PVC) and acrylic based frame structure (Figure 3.2a).

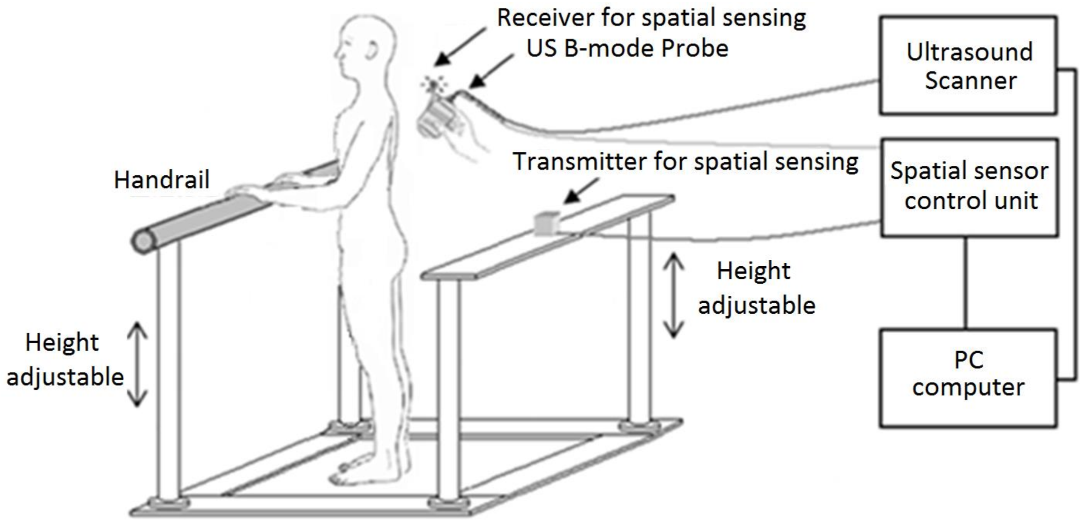

Figure 3.1. The schematic diagram of system configuration of the prototype-0 for 3D ultrasound assessment of scoliosis.

The electromagnetic spatial measurement system (MiniBird Ascension Technology Corporation, Burlington, VT, USA) was used to record the 3D position and orientation in real time (Figure 3.2b). The sampling rate for spatial data collection was up to 100 Hz. The spatial data including position and orientation being acquired by the MiniBird system were packed into a 4x4 homogenous matrix and delivered to PC via RS-232 serial port in real time during data acquisition. According to the manufacturer, positional accuracy, position resolution, angular accuracy, and angular resolution of MinBird were 1.8 mm (RMS), 0.5 mm, 0.5° (RMS), and 0.1°. The accuracy was affected by the distance between spatial sensor and electromagnetic transmitter. The highest accuracy is provided with the distance maintained within 46 cm. Therefore, sensor traveling range needed to be kept within this distance during scanning. The sensor unit (length 10 mm, width 5 mm, thickness 5 mm) was mounted onto the US probe with a custom-made mounting kit made of PVC (Figure 3.2c).

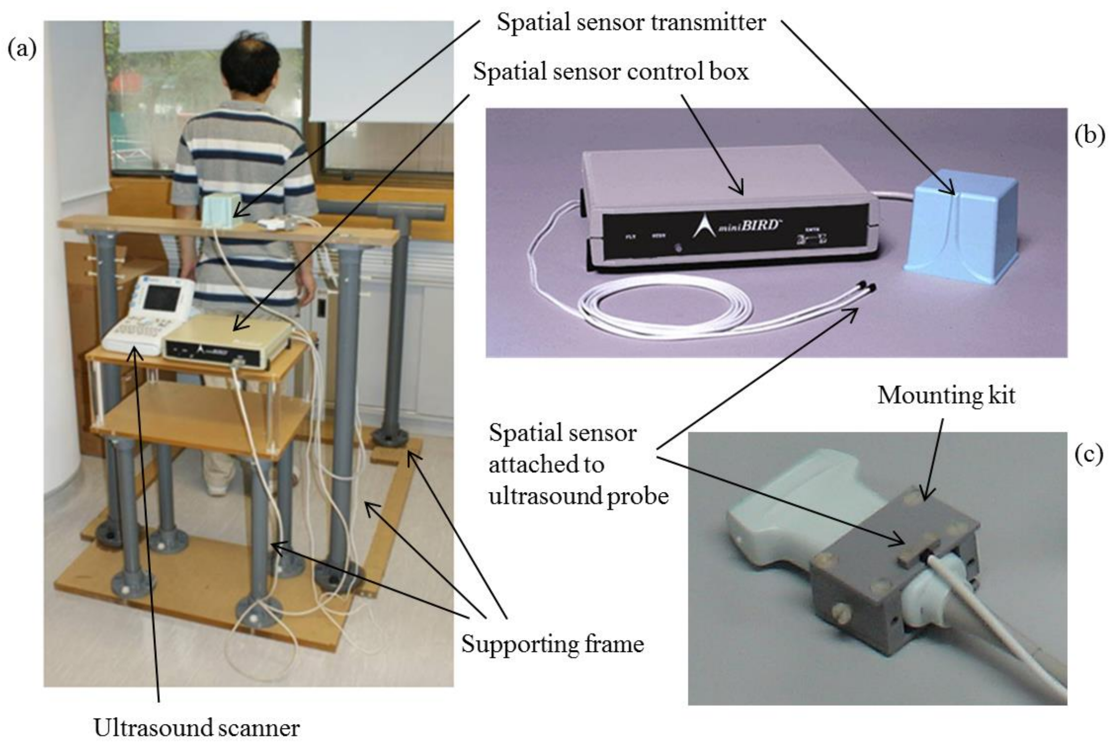

Figure 3.2. (a) The system setup of prototype-0, (b) the spatial sensing system used in prototype-0, (c) spatial senor attached to ultrasound probe with mounting kit.

Prototype-0 had been used for developing preliminary scanning protocol, optimizing ultrasound machine imaging parameters of the ultrasound scanner, and exploring new visualization methods.

A spine phantom (Figure 3.3, VB84, 3B Scientific, Germany) was scanned by prototype-0 using a water-tank scanning approach. Two visualization techniques including 3D image stack and volume reconstruction were tested (Figure 3.4). The 3D image stack technique demonstrated its advantages of retaining original image quality, simple and swift way to reveal bony features. The volume reconstruction approach provided a full 3D view of the phantom, but it was time-consuming and the image resolution was reduced after the reconstruction process.

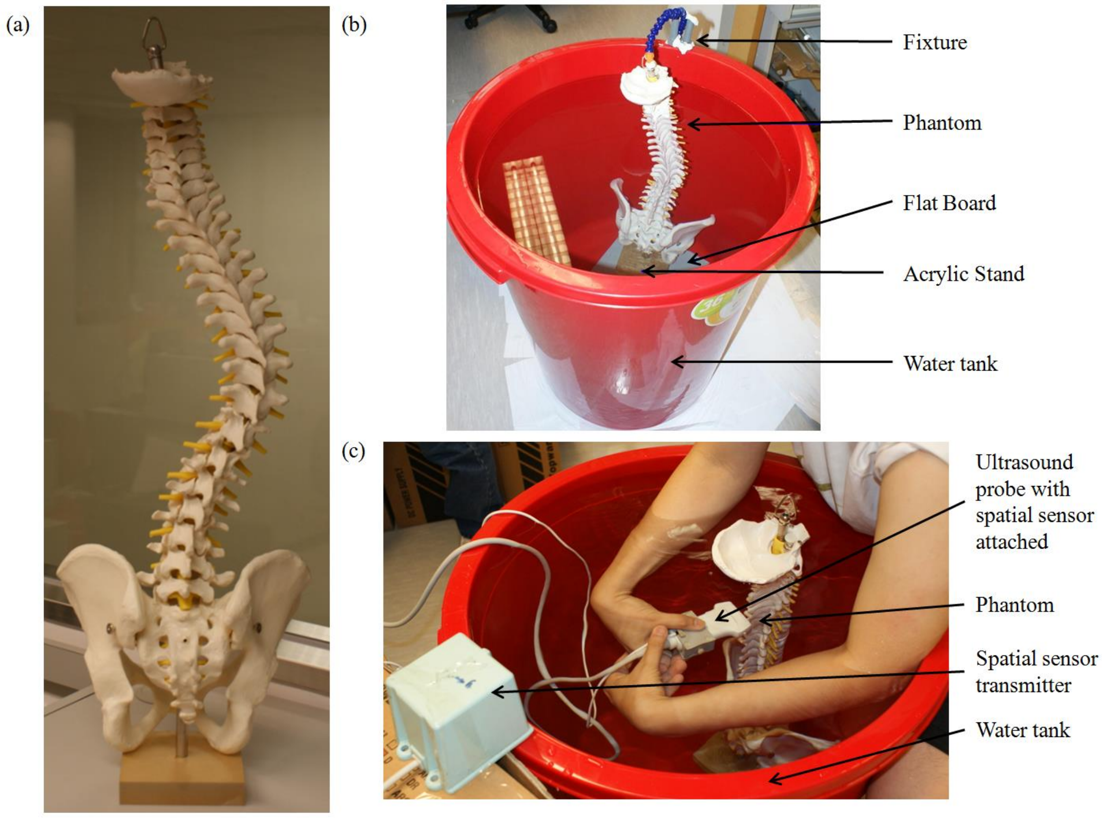

Figure 3.3. The experimental setup for spine phantom measurement. (a) Spine phantom with its deformity adjustable, (b) the spine phantom in a water tank, (c) scanning of the spine phantom in the water tank.

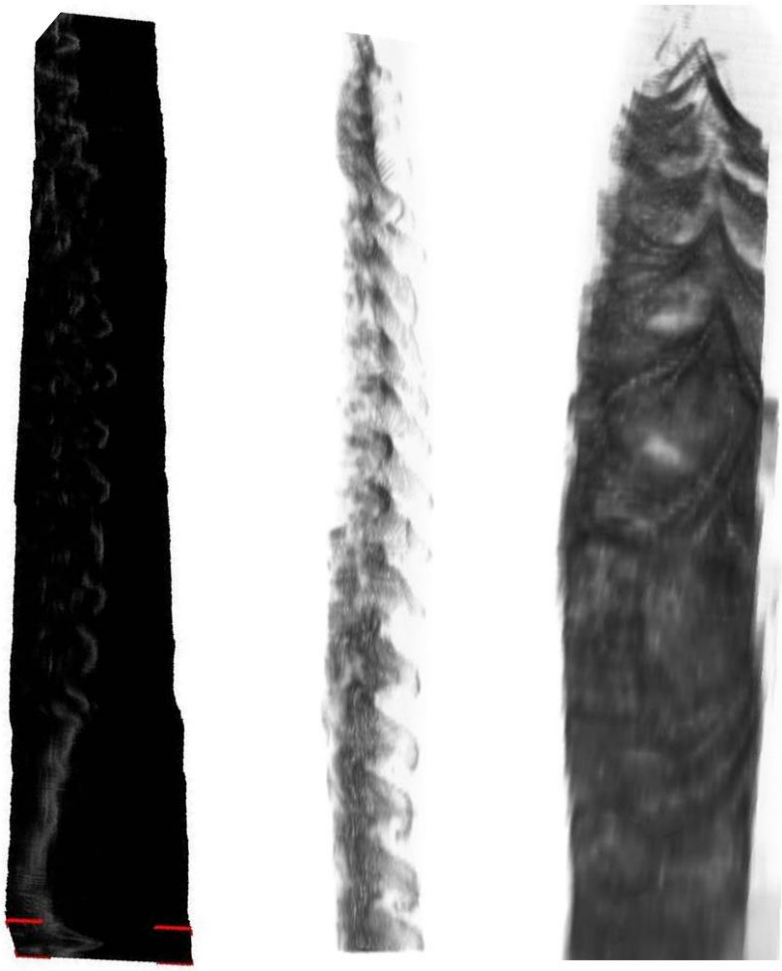

(a) (b) (c)

Figure 3.4. Typical 3D image stack obtained for the spine phantom using prototype-0. (a) LA view formed by the 3D image stack method, (b) LA view of the spine volume, (c) PA view of the spine volume

As a pilot study, a human subject was also scanned using prototype-0. Vertical scanning and horizontal scanning along with multiple swaps were explored (Figure 3.5). It was found that the multi-swap approaches were both time-consuming and difficult in aligning. After preliminary experiments, two major drawbacks of prototype-0 were identified. First, the subject could not maintain a stable standing posture during scanning. The movement of subject led to serious motion artifacts in the obtained image. Second, as the width of ultrasound probe limited the cross-sectional view of vertebra, multi-swap approach was necessary to form a full view of spine, which led to complication in image processing, and more time was required for scanning and image reconstruction.

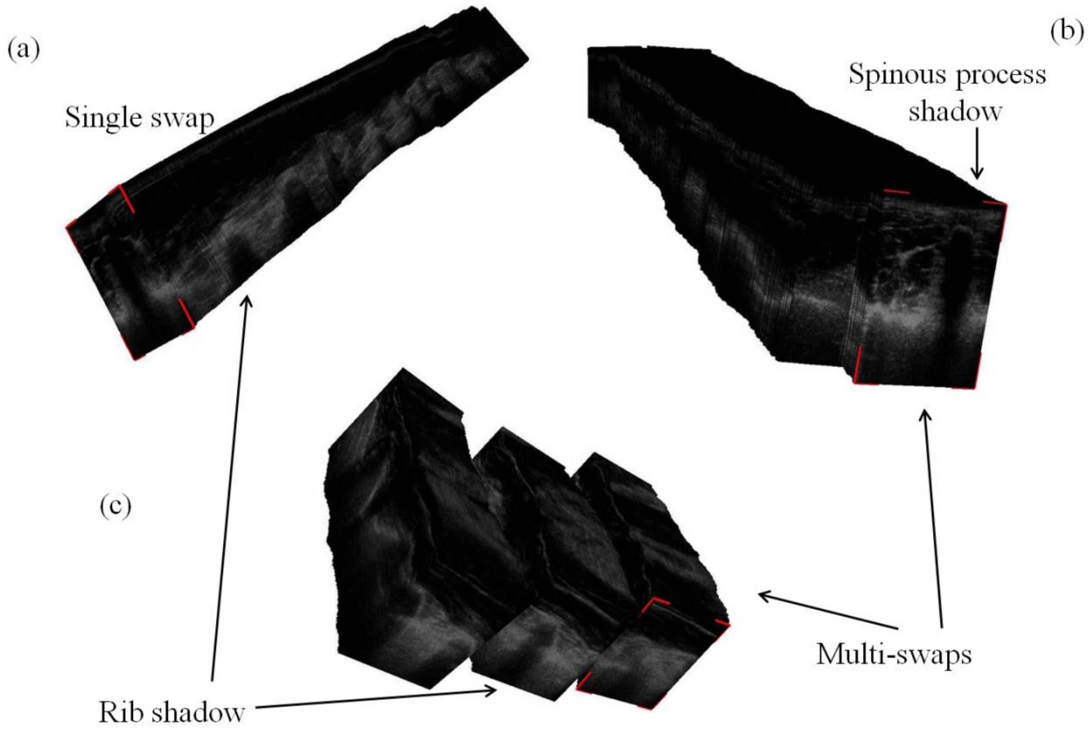

Figure 3.5. Typical results obtained by prototype-0 using 3D image stack in a human subject. (a) One swap along vertical direction, i.e. spine long axis, (b) two swaps in vertical direction, (c) three swaps in horizontal direction.

In addition, it was observed that the clear bony structure of the spine phantom scanned in the water tank could not be obtained from the human subject. Figure 3.6 shows typical ultrasound B-mode images obtained from the spine phantom and the human subject, demonstrating that human vertebral bone structure could not be seen clearly. For this reason, little effort had been made to form 3D complete vertebral bone structure in the subsequent studies.

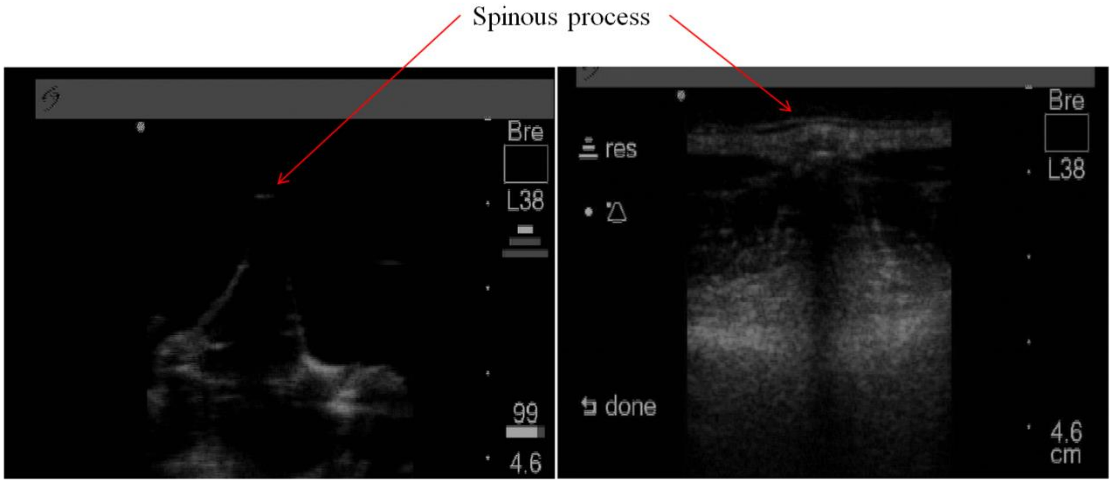

(a) (b)

Figure 3.6. Typical ultrasound B-mode images obtained from (a) the spine phantom and (b) the human subject.

3.2.2 Prototype-1 development and test

With the experiences gained from prototype-0, a new prototype (prototype-1) was an improved supporting frame to maintain subject posture and better system components to enhance the performance developed (Figure 3.7).

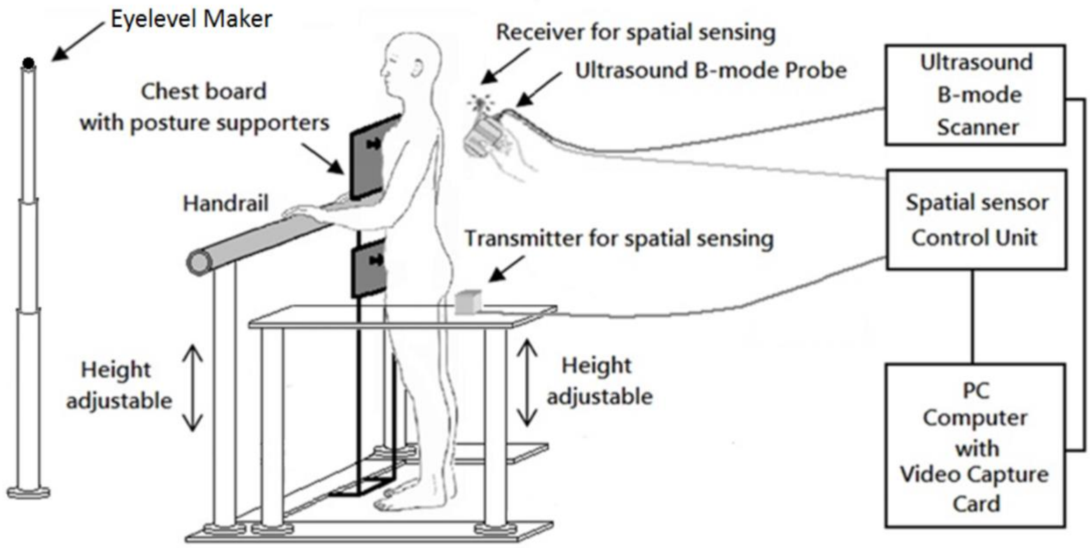

Figure 3.7. The schematic diagram of the modified 3D ultrasound system for scoliosis assessment.

The prototype-1 has been exploited to study a measurement using 3D image stack technique. The portable ultrasound scanner in prototype-0 was replaced by a high performance ultrasound scanner (EUB-8500, Hitachi Medical Corporation, Tokyo, Japan) (Figure 3.8a). A wider linear probe (L53L/10-5), from Hitachi, with 92 mm in width was used for scanning the body back. A high performance video capture card was selected to assure high quality of collected B-mode images. In addition, an upgraded spatial sensing system was used. The spatial sensor was attached on the probe using a mounting kit (Figure 3.8b).

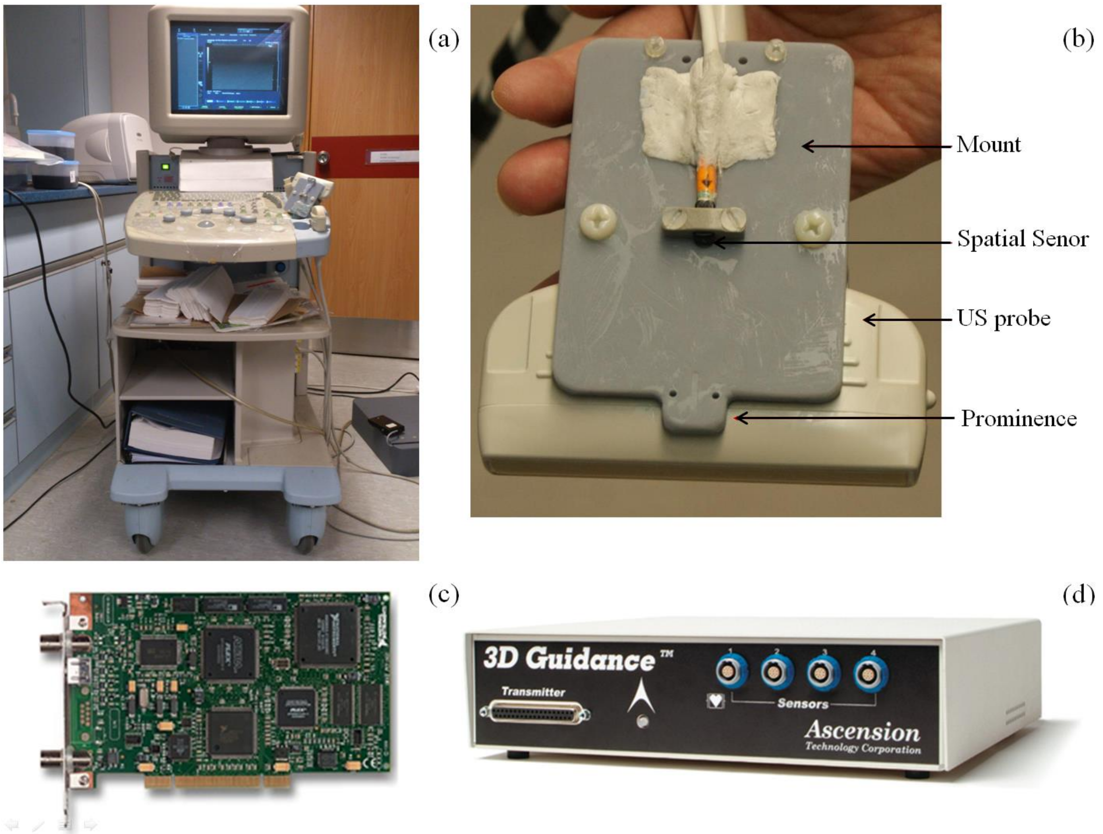

Figure 3.8. (a) Hitachi EUB-8500 ultrasound scanner, (b) Hitachi L53L/10-5 linear phase array and a spatial sensor mounted on a PVC plate with a prominence for alignment with median furrow during scanning, (c) NI-IMAQ PCI/PXI-1411 video capture card, (d) Ascension 3D Guidance magnetic tracking sensor system.

The Hitachi ultrasound system was featured with high resolution S-Video output in non-interleaved mode. A video capture card (NI-IMAQ PCI/PXI-1411, National Instruments Corporation, Austin, TX, USA) (Figure 3.8c) was installed into PC and exploited to digitalize the S-Video output into PC memory. The maximum output rate of the S-Video of the Hitachi ultrasound scanner was 25 Hz, and the PC software could capture images with a frame rate up to 23 Hz. The B-mode image and its corresponding spatial data were simultaneously stored into PC. The software was programmed using Microsoft Visual C++ Version 6.0, Visualization Toolkit Version 5.2, and Message Passing Interface Version 2.0 which provided parallel programming feature for multi-core microprocessor. The first version of the software was executed in a PC with 2.66 GHz E6750 dual core microprocessor and 4GB RAM main memory. The spatial sensor was also upgraded to 3DGuidance spatial system (MiniBird, Ascension Technology Corporation, Burlington, VT, USA). 3D Guidance (Figure 3.8d) was a DC magnetic tracking technology with significant reduction of susceptibility of presenting ferromagnetic material, allowing certain kind of metal presenting in the tracking zone including steel series 316 and brass. The highest spatial data collection rate was increased to 210 Hz.

Figure 3.9 shows typical ultrasound B-mode images collected from the spine phantom and a teenage subject using prototype-1. It was demonstrated that the new prototype could provide good image quality and the probe was wide enough to cover the processes of a whole vertebra. Thus, a single swap would be enough for scanning the spine region.

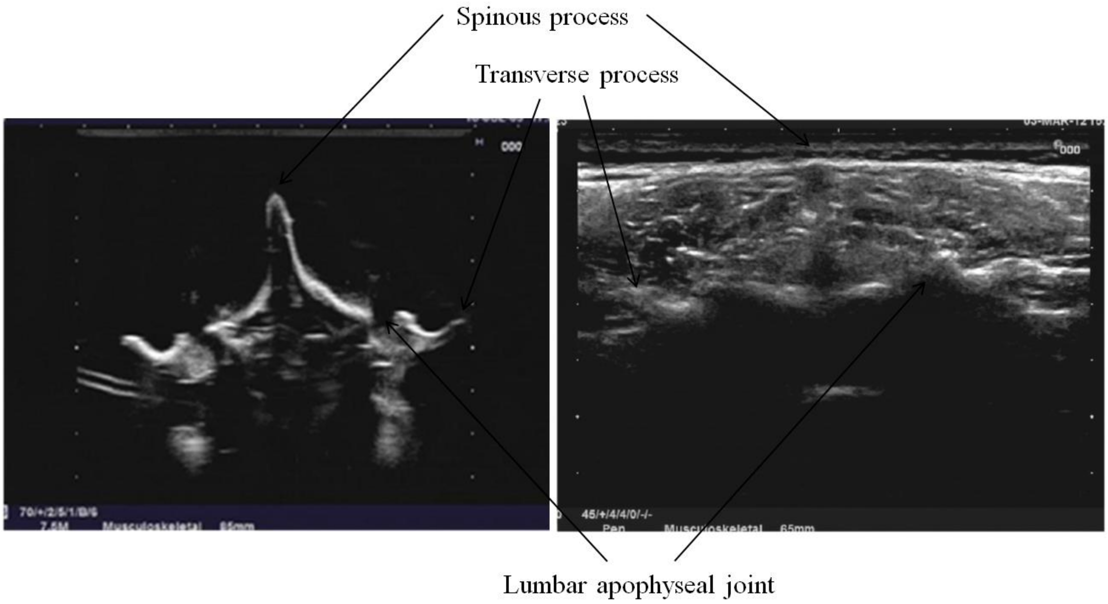

(a) (b)

Figure 3.9. Typical ultrasound B-mode images of lumbar vertebra cross-section processes (a) The spine phantom, (b) A teenage subject.

A plastic frame structure was fabricated for the phantom experiment with scoliotic measurement using 3D image stack approach (Figure 3.10). The frame was comprised of a structure for fixing the spatial sensor transmitter and phantom in order to eradicate the induced motion on phantom from operator.

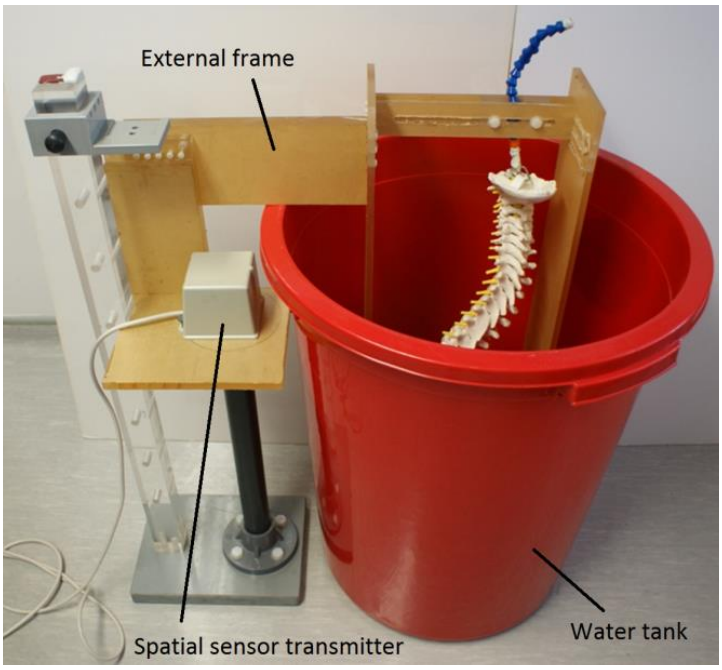

Figure 3.10. Experimental step up for the phantom test, with a water tank, spine phantom supporting frame, and a frame to support the spatial sensor transmitter.

A new supporting frame was built for prototype-1 to provide stable support to patient during scanning (Figure 3.11). A chest board, a hip board, and adjustable supporting pegs were added. In addition, an eyelevel marker with stand and steps for the operator and patient were added as assistive tools. The chest board, the hip board, the supporting pegs worked together to form a robust support for subjects. The supporting peg, which was comprised of a screw rod and cap, could be locked onto an adjustable supporting base featured with slider and clipper set for positioning in an appropriate location (Figure 3.11b). The chest and hip board further extend the range covering the adjustable supporting base. The eyelevel marker was set for making subject to focus and played an assistive role for stabilizing the upper chest and neck. The step for operator was designed for complementing the height difference between operator and subject. A foot switch was used to control the system measurement by the operator during scanning (Figure 3.11d).

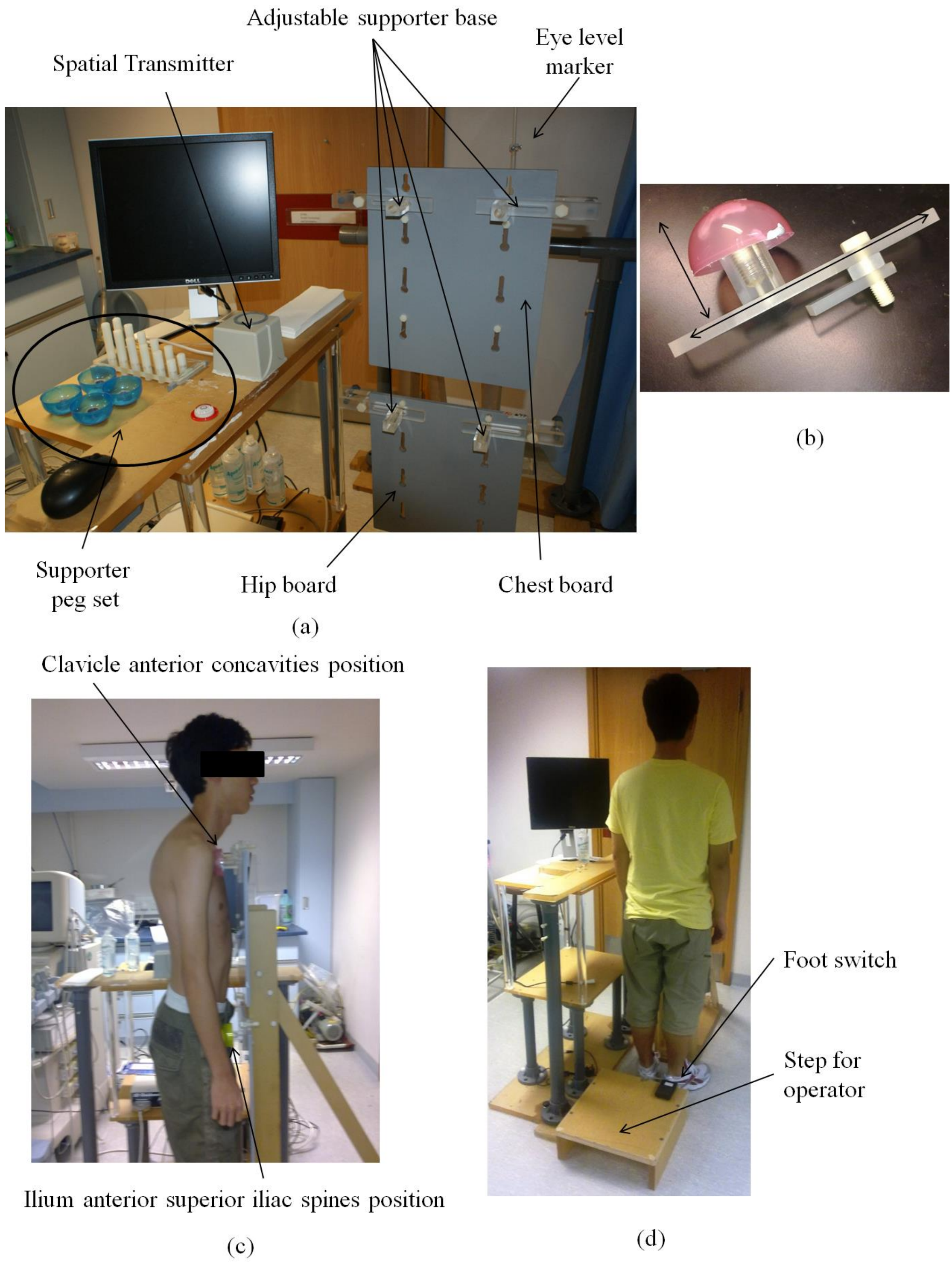

Figure 3.11. Prototype-1 of the measurement system including (a) a body supporter set including three dimensional adjustable supporting peg sets, chest and hip boards, and a eyelevel marker set, (b) pegs used in prototype-1, (c) pegs contact with clavicle anterior concavities and ilium anterior superior iliac spines, (b) a step for operator with a foot switch.

3.2.3 Prototype-2 development

With the experiences gained from prototype-1, a further improved supporting frame to maintain subject posture, a new prototype (prototype-2) was developed (Figure 3.12). The chest broad, the hip board, and supporting pigs were redesigned for better support and convenient use. A subject step was added for complementing the height between operator and short subject. A calibration reference arm was also added for verifying the spatial sensor function before scanning.

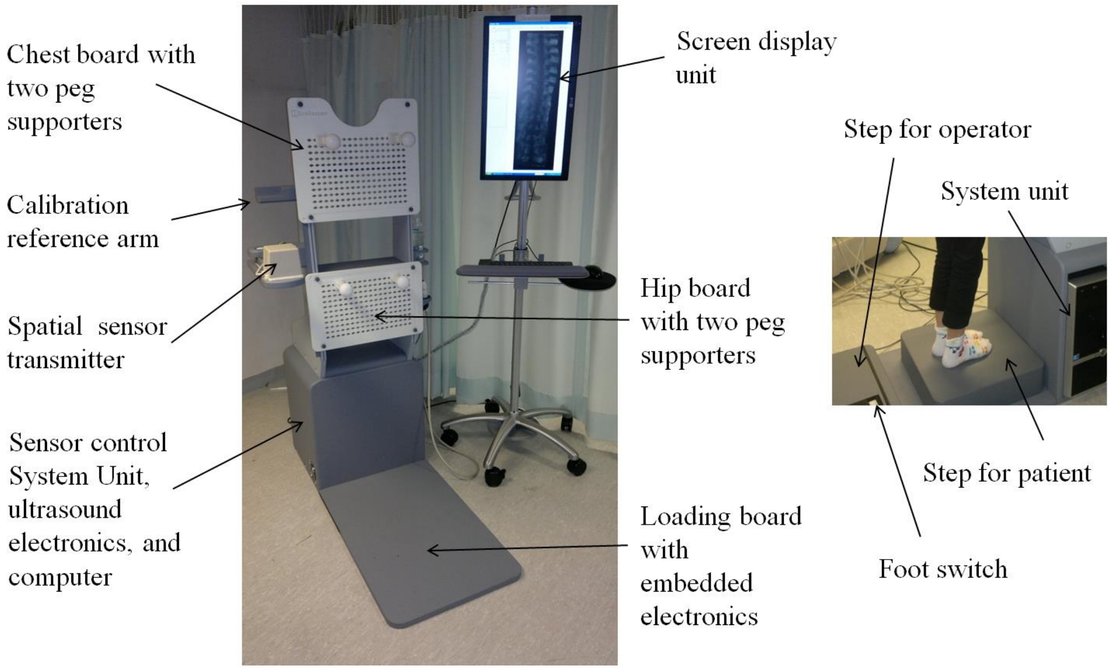

(a) (b)

Figure 3.12. Prototype-2 of clinical setup (a) body supporter set including three dimensional adjustable supporter peg sets, base chest and hip boards, eyelevel marker set, (b) a step for operator with a foot switch and a step for subject.

3.2.4 Calibrations

Before the developed system could be used to scan, the spatial calibration was conducted to determine the spatial and orientation offsets between a US probe and a spatial sensor, which represent relative position and orientation between the US probe and the spatial sensor. Ultrasound image pixel spacings were also found before calibration. In this study, the pixel spacings were found by measuring the ultrasound image dimensions acquired using Microsoft Paint program to determine the number of pixels in width and height of the image and ultrasound equipment built-in image caliber to determine the physical dimension of image. The spacings were then determined by the ratio of the measured values. The spacings were updated into a program, which has been designed for data acquisition, reconstruction, visualization, and measurement.

The offsets were determined using the cross-wire phantom (Detmer et al. 1994) spatial calibration technique. Two cotton wires were crossed and submerged into the water. The wire ends were attached onto the wall of the water tank. The US probe was steered under water to search the cross. If the cross was located, the B-mode image and its corresponding spatial data were stored into PC. In total, 60 images were captured in the calibration. The pixel positions (X-Y) of the crosses in the B-mode images were marked manually through a program tool. After all pixel positions of the crosses had been found, the position data set and its corresponding spatial data were used to update a data table inside a MatLab program. The MatLab program was implemented with a Levenberg-Marquardt non-linear algorithm (Prager et al. 1998) and exploited to calculate the spatial and orientation offset. The offsets were finally updated into the program.

For the temporal calibration, many studies did not involve or mention it during reconstruction process (State et al. 1994, Barry et al. 1997; Amin et al. 2001; Barratt et al. 2006). This probably suggested that the temporal calibration might not be an essential step in reconstruction process. Barrat et al. (2006) exploited slowly sweeping across skin scan approach with speed less than 5mm/s so as to minimize the motion artefacts and handle synchronization issue without using the temporal calibration. Therefore, it appears that it is reasonable to ignore the temporal calibration if the sweeping speed is maintained very slow while spatial sampling rate is relative high. In development of scanning protocol, the speed of probe moving on spine region was found about 4 mm/s to 5 mm/s. It is, therefore, presumed that the temporal calibration factor between the 3D guidance spatial system and the Hitachi ultrasound scanner could be ignored, if such slow scanning protocol was implemented.

3.2.5 Software development

The number of image necessary for building a spine image was considered. The images captured must cover vertebrae from T1 to L5 in order to build a whole spine image. The length of spine from the subjects recruited ranged from 40 to 50 cm. It was also reasonable to have the B-mode image with around 1 mm separation or less between consecutive frames so as to build the spine image with desirable appearance. Therefore, at least 500 frames of B-mode image in single scan were necessary to cover the full range of spinal region. For phantom scanning, the number of raw image in a single scan was around 400 to 600 images (Figure 3.13a). Considering that the ultrasound images are more complicated under the in vivo situation (Figure 3.13b), more B-mode images were necessary to be collected because some of the images were blurred and the bony features would be more difficult to be revealed.

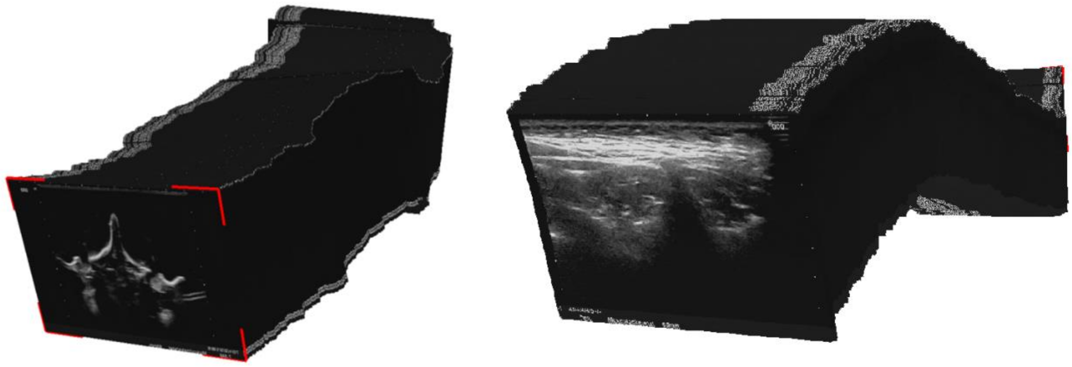

(a) (b)

Figure 3.13. (a) 3D image stack of spine phantom formed by 600 frames, (b) 3D image stack of human spine formed by 1900 frames.

For subject scanning, around 1700 to 2400 B-mode images were captured in each scan. The software was found incapable to perform volume reconstruction in term of file size, time, and quality. The software was subsequently re-developed using Microsoft Studio 2010 with Visual C++, Visualization Toolkit Version 5.8 with full 64bit architecture and multiple threading volume reconstruction feature. The new version of the software finally was executed on the PC with 2.67 GHz Intel iCore5 qual-core microprocessor and 8GB RAM main memory. The software had been used with prototype-1 and prototype-2 in subject study.

The software main functions were organized into four function panels, which were capture panel, process panel, measure panel, and render panel, respectively. Capture panel was designed to adjust and control electronic device functions (Figure 3.14). The spatial sensing system would be started first. The video capture card would then capture the screen of the ultrasound machine. Spatial data and B-mode image were displayed in real-time during scanning. The scan process would be cancelled using foot switch, if the vertebra was not displayed correctly or moved out of viewing window.

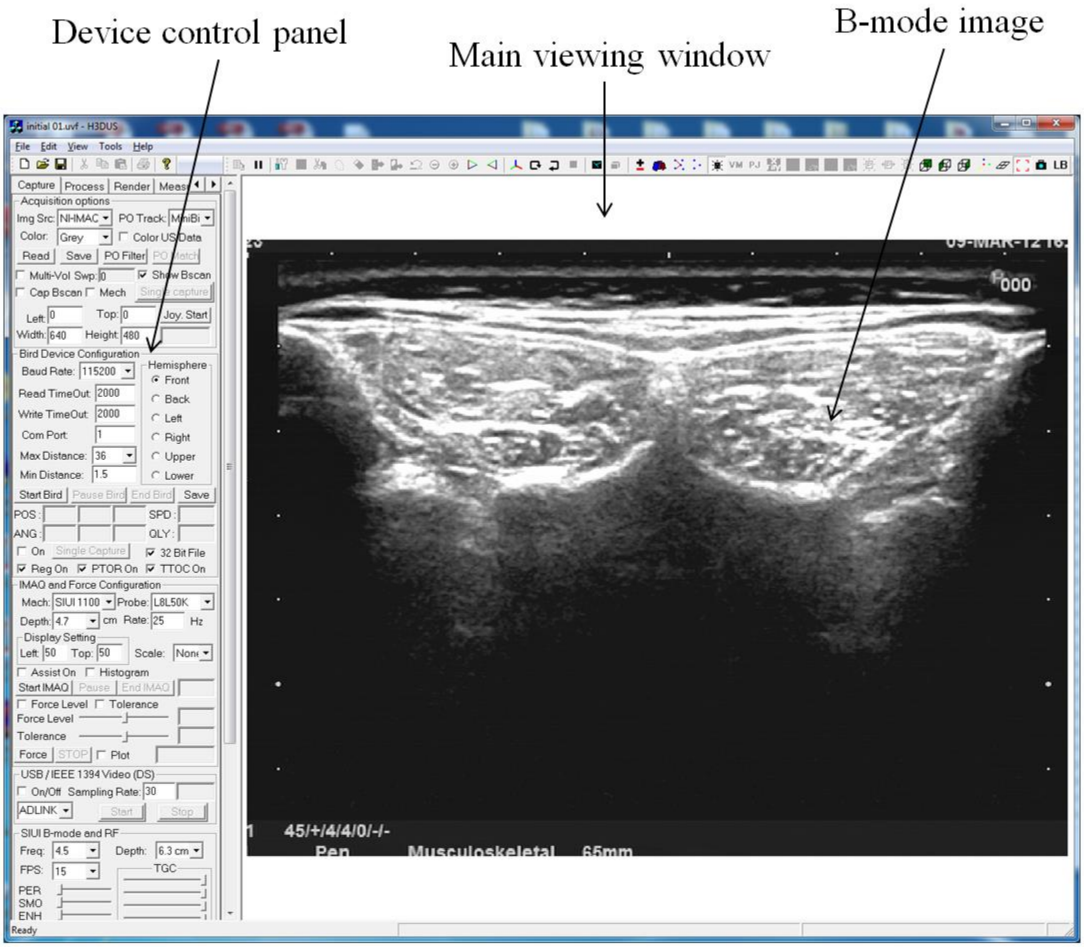

Figure 3.14. Capture panel with a B-mode image.

Process control panel was programmed to control the image processing and volume rendering (Figure 3.15). Different image processing filters could be applied to produce the best view of raw image. All image processing functions were designed to conduct off-line processing. The images captured could be processed before proceeding to conduct measurement or rendering. Volume rendering parameters could be also set from the panel. However, in my studies, raw images were maintained without further processing before measurement or volume rendering.

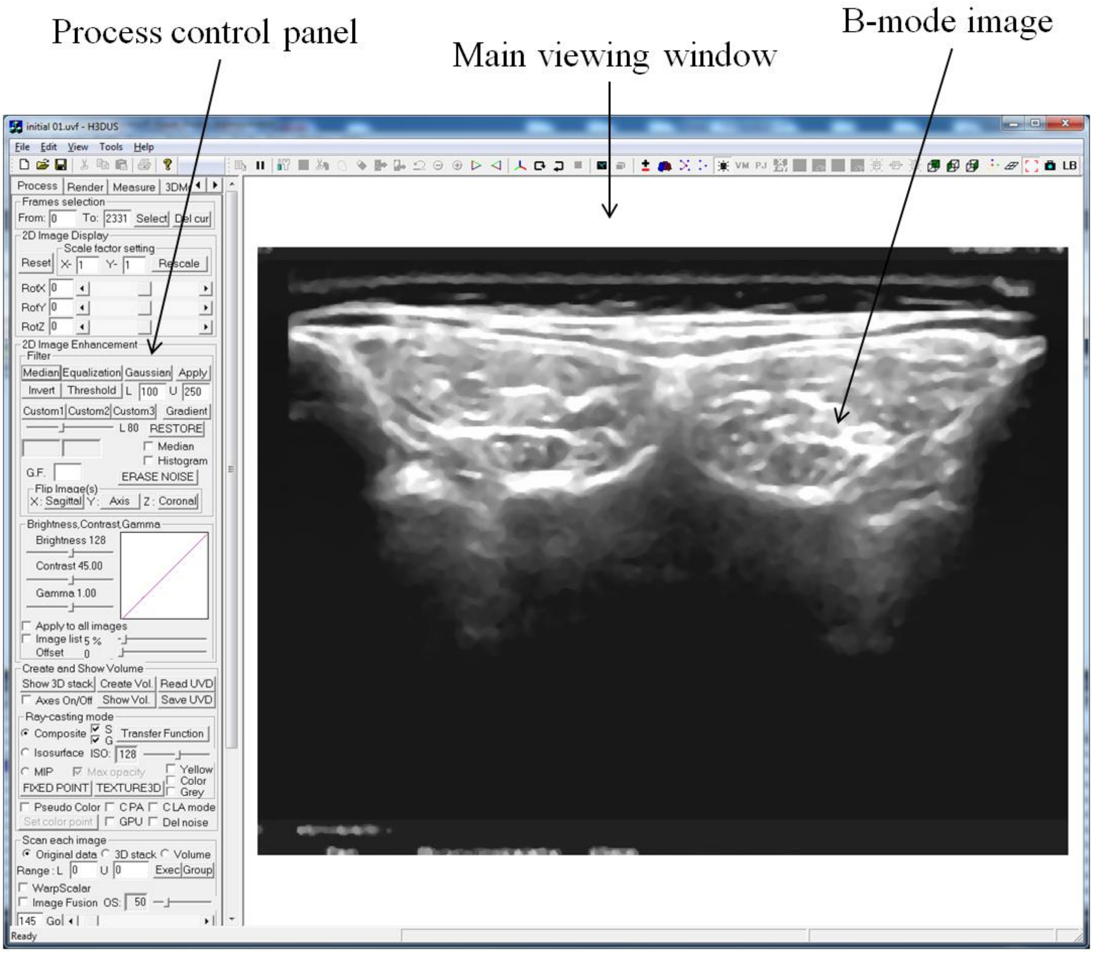

Figure 3.15. Process panel with median filtering applied to the B-mode image.

Measure control panel (Figure 3.16) was exploited to conduct 3D image stack approach, which will be described in section 3.3.1. Some functions in the panel were responsible for assisting marker placement. Marker could be labeled and changed in size and color. Other functions were designed for controlling the viewing of virtual spine model and measure the spinal curvature.

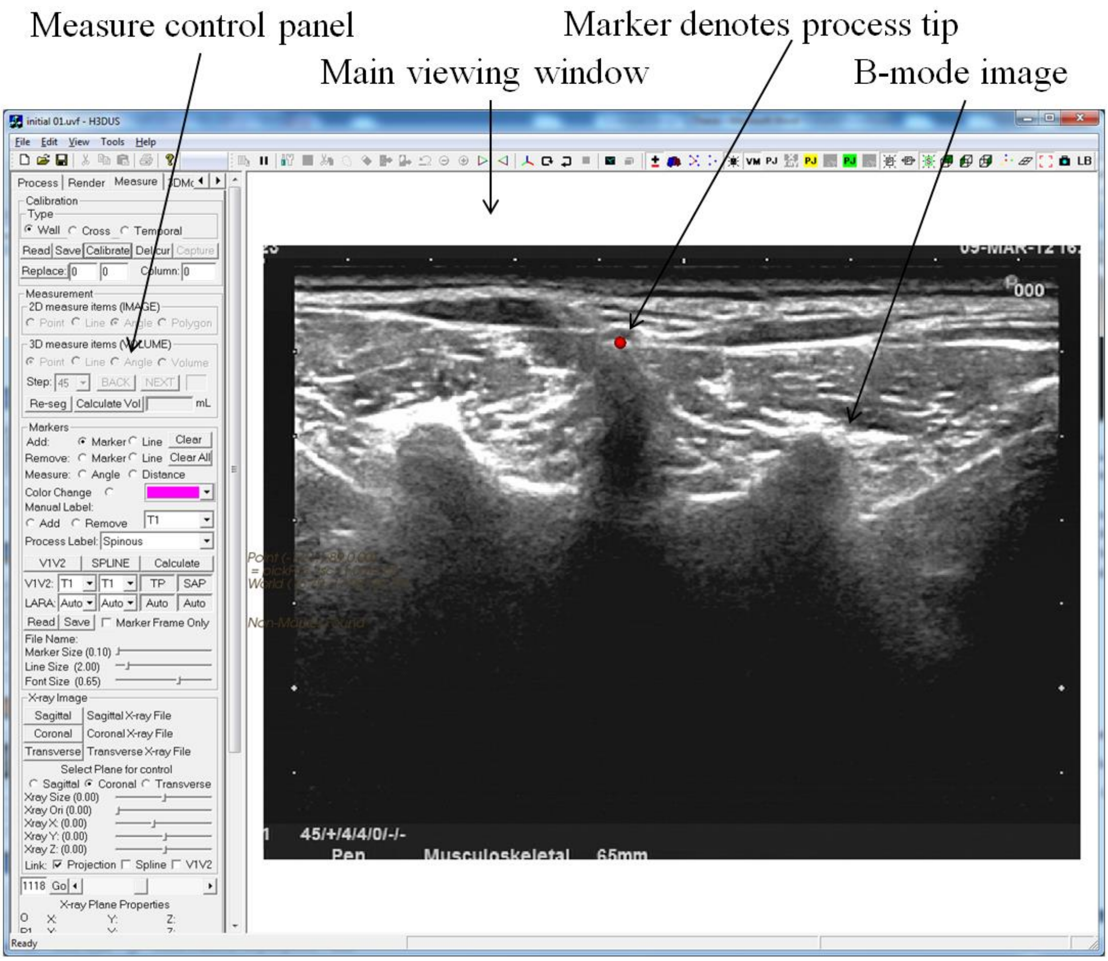

Figure 3.16. Measure panel with a marker placed on the tip of spinous process inside the B-mode image.

Render control panel (Figure 3.17) was exploited to conduct volume projection approach, which will be described in section 3.3.2. Some functions in the panel were used to draw lines for measuring spinal curvature. The other functions were designed to control the viewing of a rendered volume or a volume projection image and measure the spinal curvature.

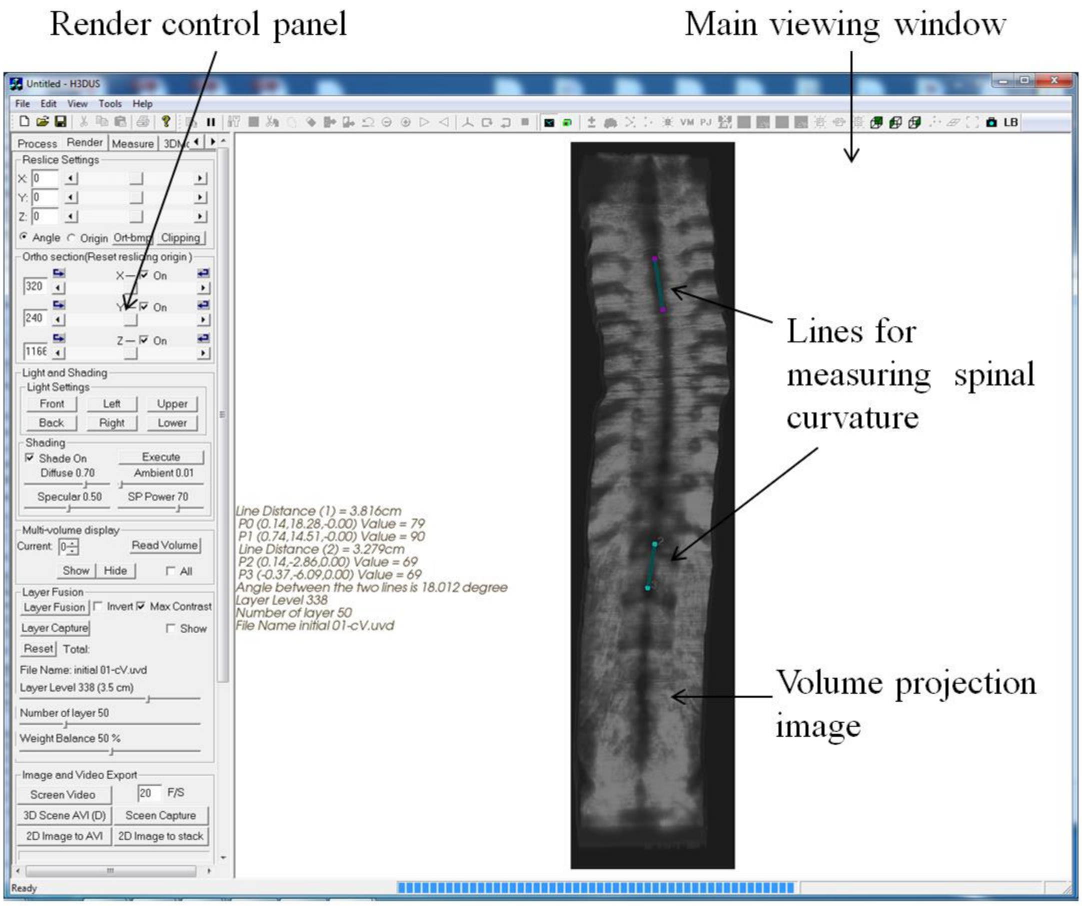

Figure 3.17. Render panel with volume project image under measurement.

3.3 Methods of data processing and measurement

The software was designed for acquisition, processing, visualization, and measurement. Two processing and measurement methods including 3D image stack approach and volume projection approach were developed. The 3D image stack approach was filed in US and PCT patent (Zheng et al. 2009). The volume projection approach was filed PRC invention patent (Zheng et al. 2012). Both approaches represent an innovative way for measuring spinal curvature.

3.3.1 3D image stack approach

The fundamental concept of 3D image stack approach exploited raw ultrasound

B-mode images for extracting key bony landmarks, which could determine the spinal curvature. Avoiding resource demanding reconstruction processing and using the best resolution preserved by raw ultrasound B-image were two key merits of this approach. The general procedure of the approach is shown in Figure 3.18.

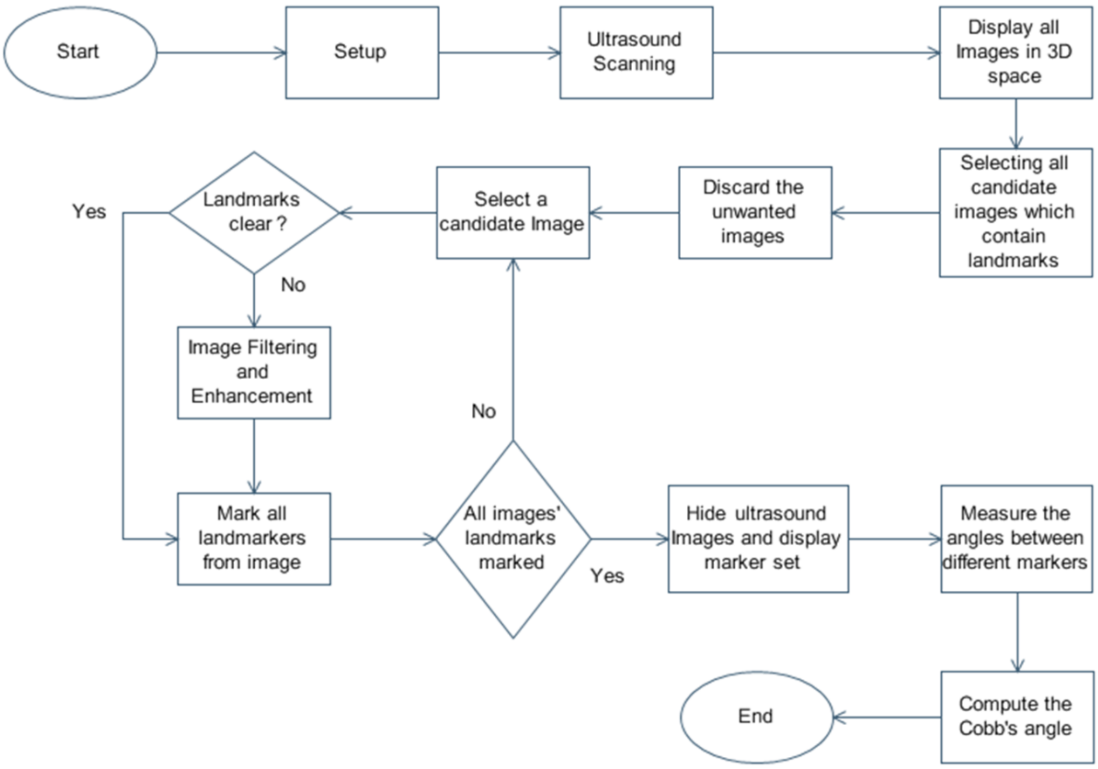

Figure 3.18. Flow chart of acquisition, visualization, processing, and measurement.

After ultrasound 3D image stack was obtained from scan, all images were displayed in 3D space to reveal a long and smooth 3D image stacks (Figure 3.19). It was carefully checked with the consistence by examination on its formation smoothness. The subject might be requested for re-scanning if there was non-smoothing region discovered. The non-smoothing region might be caused by non-steady scanning or signal interference.

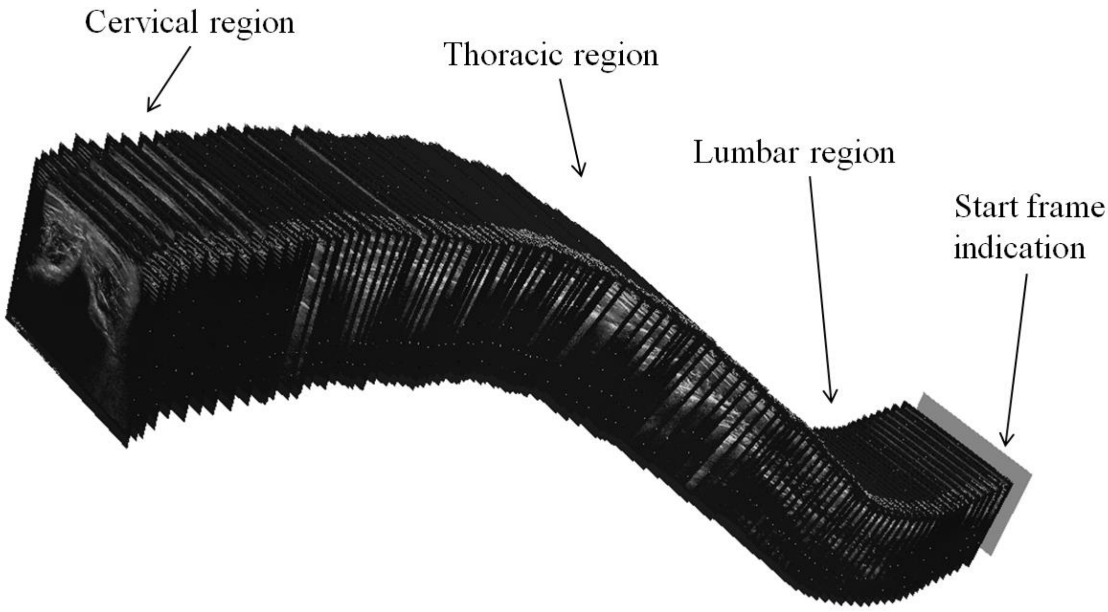

Figure 3.19. Display all images in 3D space to check the smoothness.

The next step was identification of tip of process among all frames. As around 2000 frames were captured in each scan, it would be a tedious task to examine the frame one by one to identify the tip of process. In ultrasound equipment, cinema playback is essential a feature for clinician to quickly examine a great deal of frames.

Similar cinema playback feature was implemented. Forward and backward image playbacks were controlled from keyboard; the processes were repetitively revealed and hidden during playback mode (Figure 3.20). The image would be selected when the sharpest and the smoothest tip of process in the image was observed among neighbor images; the frame image was then selected and the frame number was marked for further processing. After all images comprised with tips of processes were found, the remained images in 3D image stack would be discarded. As a result, significant reduction of data size and speeding up of system performance were achieved.

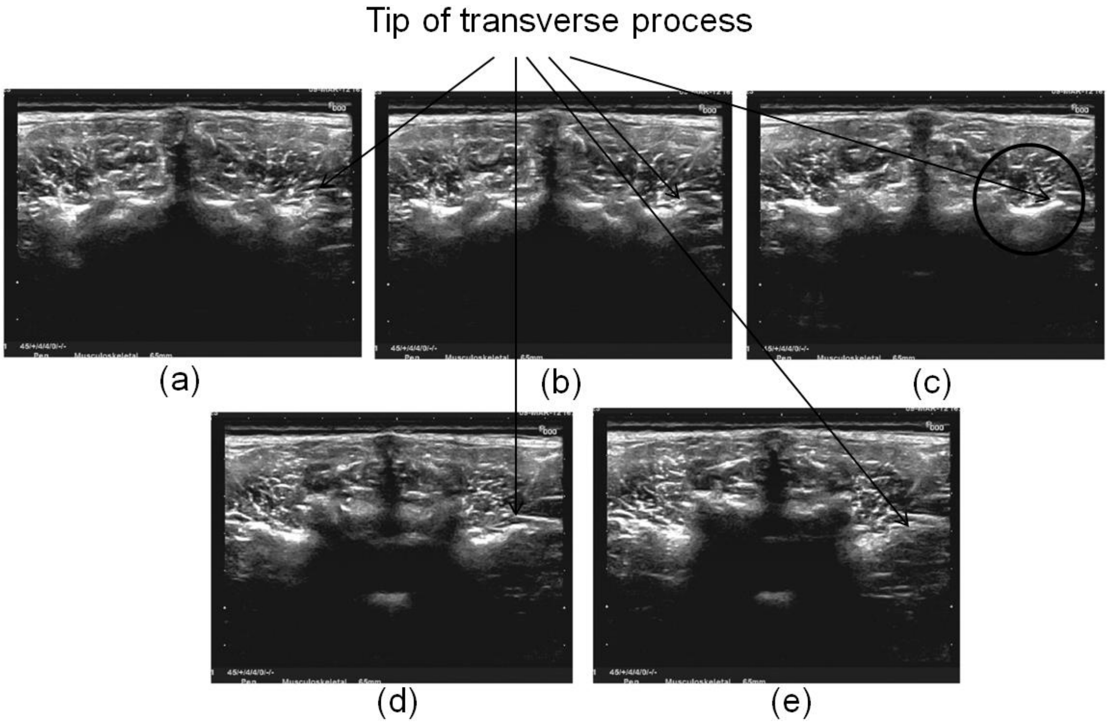

Figure 3.20. Lumbar vertebra axial views in cinema playback mode with emerging transverse process, (a) tip of transverse process hidden, (b) tip of transverse process emerging, (c) tip of transverse in the sharpest situation, (d) tip of transverse process disappearing, and (d) tip of transverse process hidden again.

The tip of transverse process is generally depicted in the image by a convex meniscus shape in various sizes and curvatures. In lumbar region, the tip appears at the edge of concave meniscus shape with a small convex meniscus shape. In contrast, in the thoracic region, the tip appears raising up from surrounding tissues with a relative larger meniscus shape (Figure 3.21). In this study, the highest point of the convex meniscus shape from the tip, which was also generally highlighted by bright ridge in the image because of the effect of hyperechoic ultrasound, was defined as the tip of process.

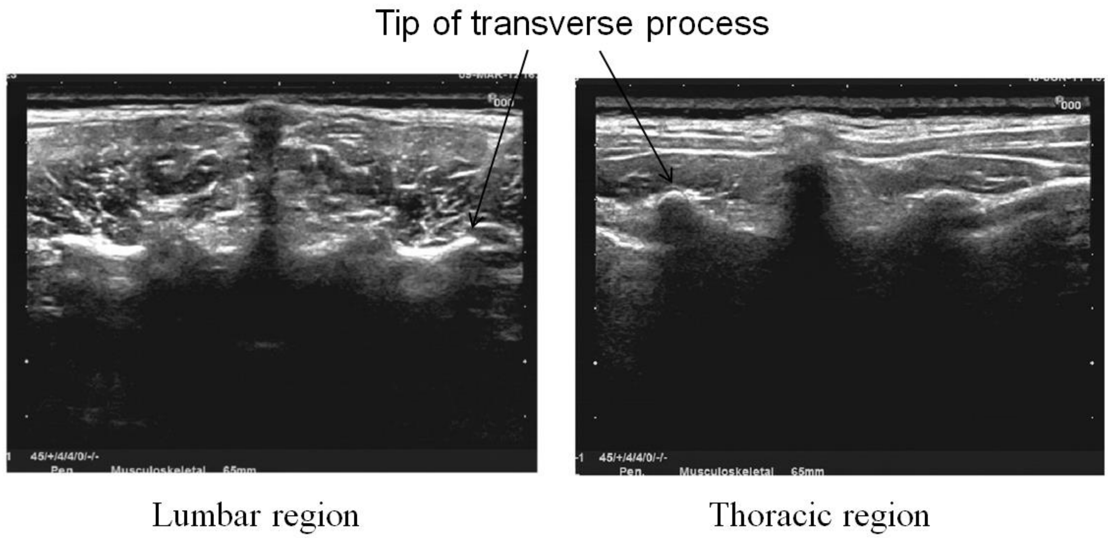

Figure 3.21. Typical example of the tip of transverse process in lumbar and thoracic region.

By clicking the tip of process in the image, a marker, which was in form of spot, was cemented onto the image. Typical examples of marker placed on the tip of process in various regions of spine are shown in Figure 3.22. In addition, the selected image might have more than one tip of process to be marked in some cases.

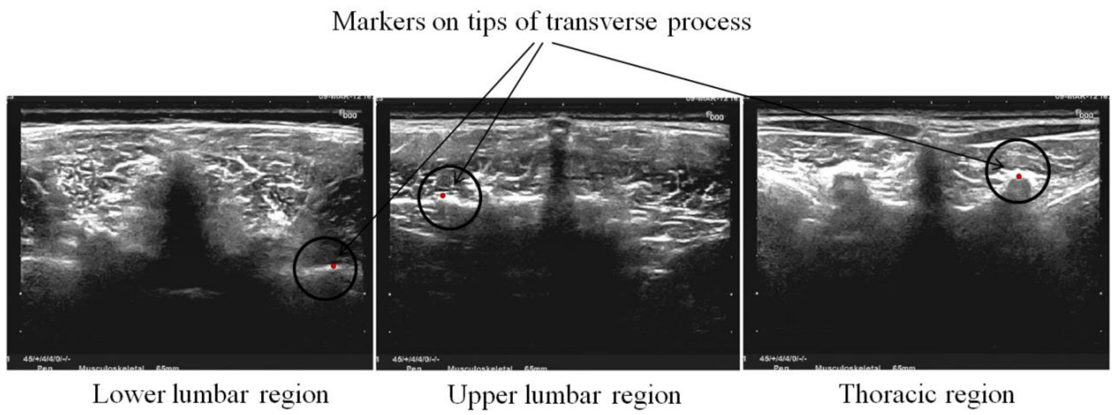

Figure 3.22. Markers on the tip of process in various regions of spine.

The size and color of marker could be altered so as to highlight the difference among different kinds of process. By dragging on the marker, the position of marker could also be fine-tuned. For assistive anatomical recognition, label could also be added beside the marker. In fact, there were three kinds of process found in the images including transverse process (TP), spinous process, and superior articular process, which could only be found in lumbar vertebra (Figure 3.23). In this study, all these processes were marked for building a spine virtual model in order to assist anatomical site identification. Otherwise, it might be difficult to confirm vertebra identity from spine. However, the spinous process and superior articular process were not involved in the curvature calculation in my study.

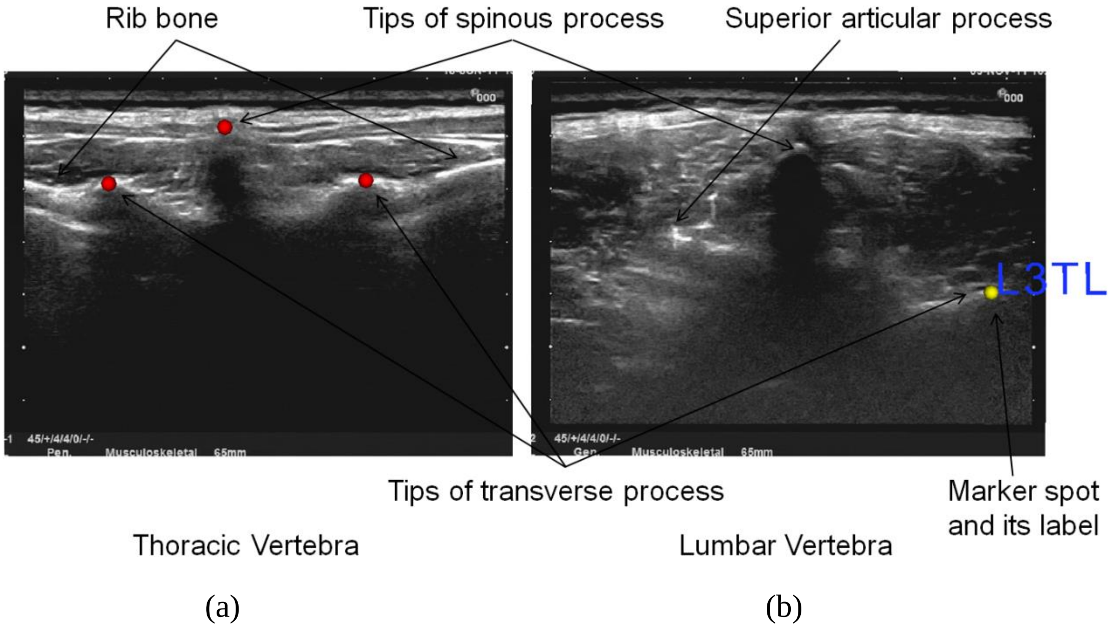

Figure 3.23. Markers on tips of process (a) spinous process and transverse processes of thoracic vertebra with markers, (b) transverse processes of lumbar vertebra marked and labeled; L3TL denotes the left transverse process of third lumbar vertebra.

The image identification and marker placing procedures were reiterated until all tips of process in all thoracic and lumbar vertebrae were identified. Although the marker was placed on the 2D image, the centre point of the marker on the image in term of image pixel X-Y coordinate could be used to calculate the three dimensional coordination of the tip through a series of rigid body transformation.

After all tips were found, the 3D positions of the markers were devised from the tips. The markers would be displayed on screen for checking any missing markers and inconsistency (Figure 3.24).

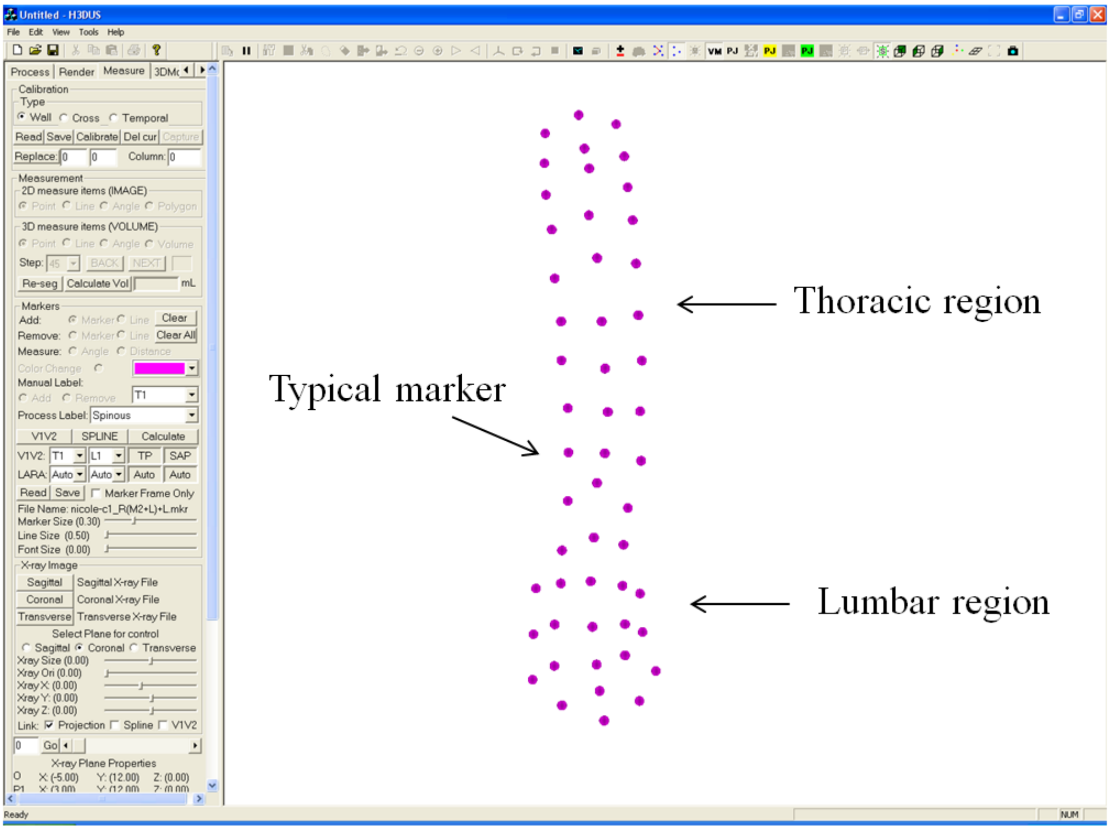

Figure 3.24. Virtual spine model with markers in 3D.

However, a cluster of points could reduce the details of spine model and increase the difficulty in analysis. Lines were manually added between different markers to enhance the anatomical structure recognition. In fact, during process of line connection, the markers would be identified with the vertebra belonged. The markers from the same vertebra were connected. In thoracic region, the markers denoting transverse process were connected to spinous process to form a “V” shape; whereas, in lumbar region, the markers denoting transverse process were connected to its near neighbor markers denoting superior articular process, which were connected to the marker denoting spinous process to form “W” shape. A typical line connected virtual spine model is shown in Figure 3.25.

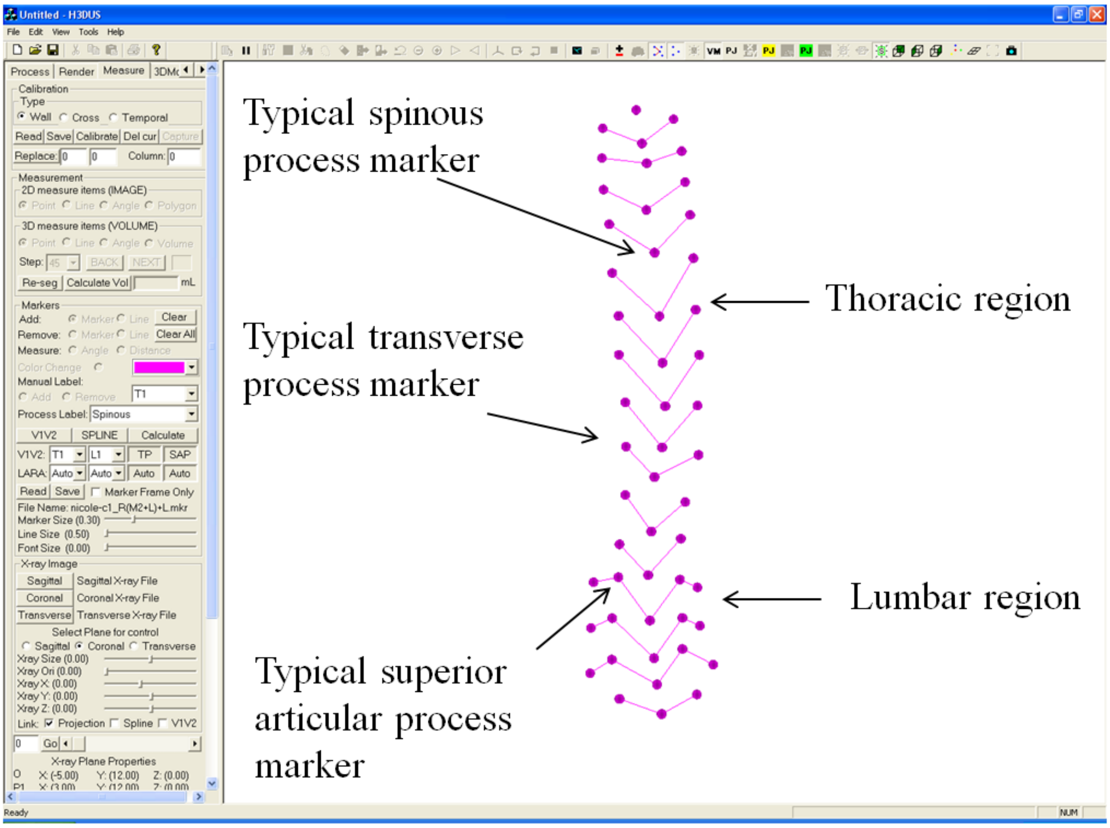

Figure 3.25. Virtual spine model with lines connected between tips of processes of the same vertebra.

Before measuring spinal curvature, two most titled vertebrae must be selected. In order to select pair of vertebra correctly, the processes were labeled. For examples, a left side and a right side transverse process from thoracic vertebra T7 were labeled as T7TL and T7TR. The first two characters denoted the vertebra. The third character denoted the transverse process. The last character denoted the side. Other processes could be labeled in the similar way. A labeled virtual spine model is shown in Figure 3.26.

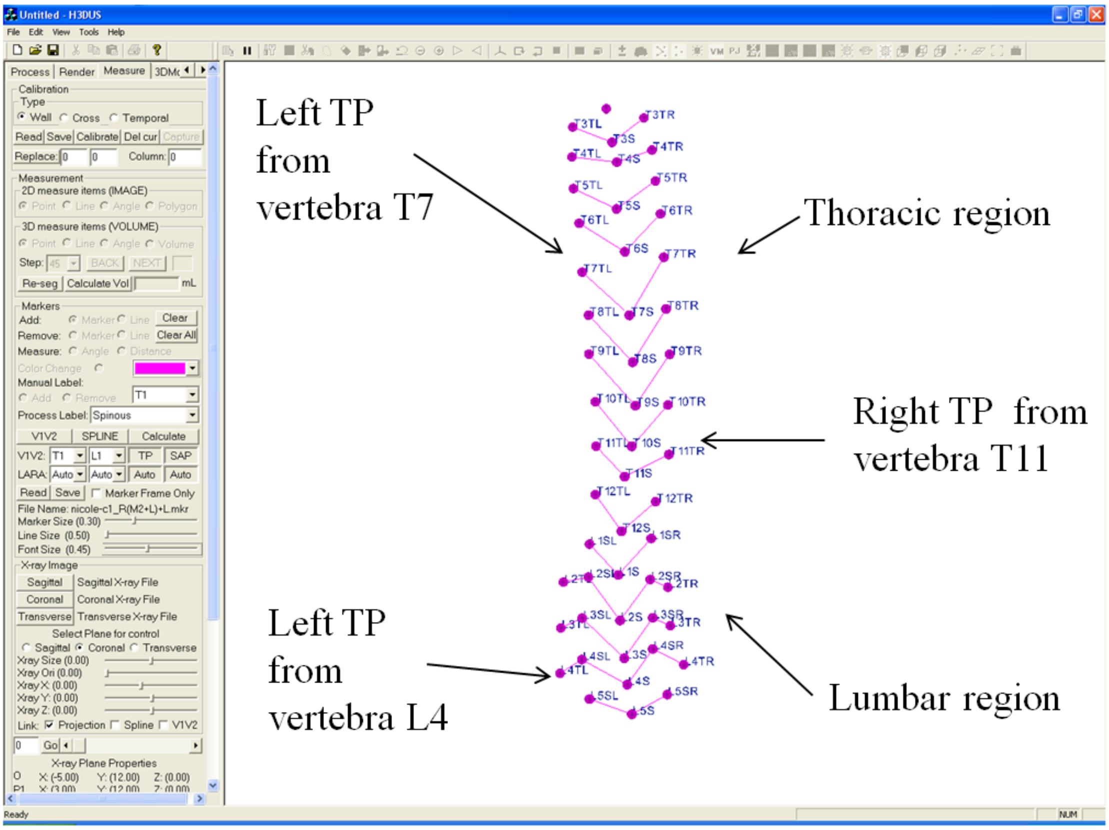

Figure 3.26. A completely labeled virtual spine model.

Two most tilted vertebrae could be observed from the virtual spinal model in a typical PA view and was called a pair vertebra. In this model, two TP markers from the same vertebra could be used to form a line to denote unique geometrical information of the vertebra. Using the 3D positions of TP makers from the pair vertebrae, two line equations would be devised using two points form. However, the line pair was typically skew lines, which means no intersection between the lines. This also means that there was no meaningful angle existed between the line pair. Using the concept of projection similar to X-ray radiograph, the TP markers were projected on a plane with plane normal to PA direction for producing a pair of line with an intersection point. As a result, an angle between two lines on the plane could be calculated (Figure 3.27).

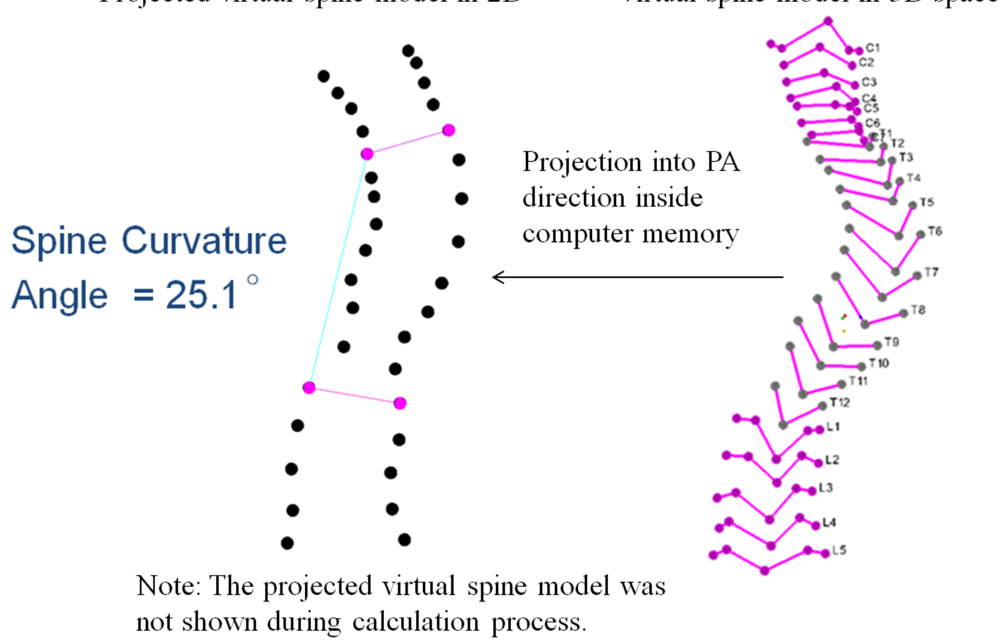

Figure 3.27. Illustration of angle devised from the selected vertebra pair.

In order to devise the angle from the selected vertebra pair, operator would use the Combo boxes from the measure control panel to select the most tilted vertebra pair or any pair of vertebra interested. The angle of spinal curvature was then shown in the Text field from measure control panel (Figure 3.28).

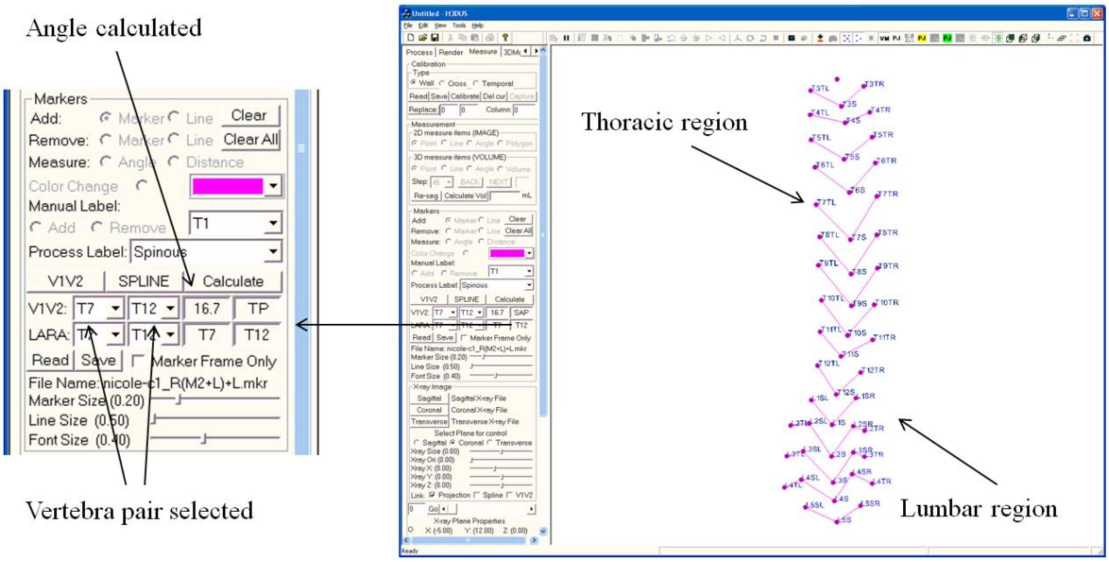

Figure 3.28. Angle calculated after selection the vertebra pair from the Combo boxes.

Certainly, it might not be necessary to obtain the spinal curvature using the full virtual spine model. In some cases, selecting the most tilted groups of B-mode image observed from the 3D image stack for marking could substantially reduce the time for performing measurement.

3.3.2 Volume projection approach

3D image stack approach allows spinal curvature devised from raw B-mode data. However, full automatic measurement of the approach was definitely challenging to be achieved because of the complexity of spine anatomical structure. With the advent of 64bit version of the developed software, volume reconstruction of a whole spine became viable. Therefore, in later stage of development, volume projection construction has been developed as an alternative to the 3D image projection approach.

Huang et al. (2005a) used freehand 3D ultrasound to scan of small object like finger from 258 B-mode images to produce a typical volume comprised by 126x103x103 = 1336734 voxels. Aforementioned, a typical spine scan produces around 2000 B-mode images. For improving the cross-sectional coverage and maintaining best resolution, the B-mode image resolution was fixed to 640x480. Thus, a typical volume size of spine was 640x480x2000 = 614400000 voxels; it was roughly ~460 times increased in data size. In order to ensure a good quality of volume reconstructed, distance weight reconstruction algorithm was applied in reconstruction algorithm. For mitigating the problem of memory resource and rendering time, scan images were divided into several groups. Each group was formed as a small volume representing a portion of spine. The hidden bony feature inside the volume would be revealed using composite ray-casting method (Figure 3.29).

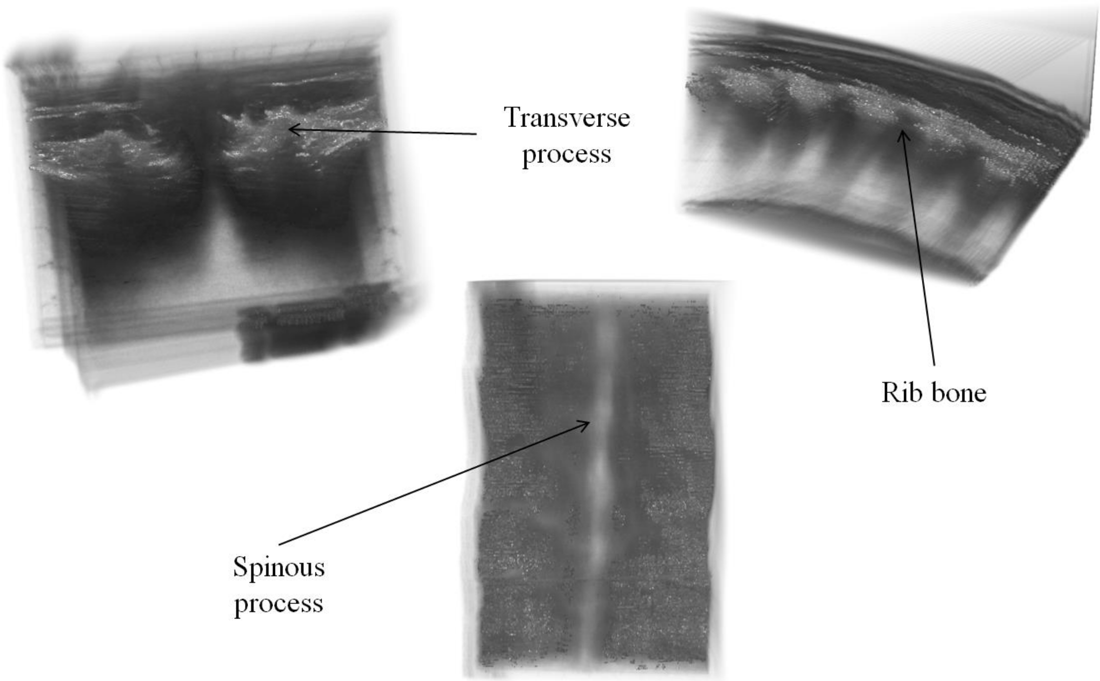

Figure 3.29. Single volume of a patient spine viewed from three directions using composite ray-casting method.

For a typical spine scan, the B-mode images were evenly divided into 8 to 10 groups to render volumes. After generating all individual portion of volumes, these volumes were joined together to form a whole spine volume (Figure 3.30). Inter-volume segment lines were formed in volume rendering view as an artifact of the ray-casting method. However, these lines were not affecting further processing. This is because these lines were not logically existed in memory array. The full spine would then be studied in any directions. However, the bony features were embedded deep inside the volume and difficult to measure directly.

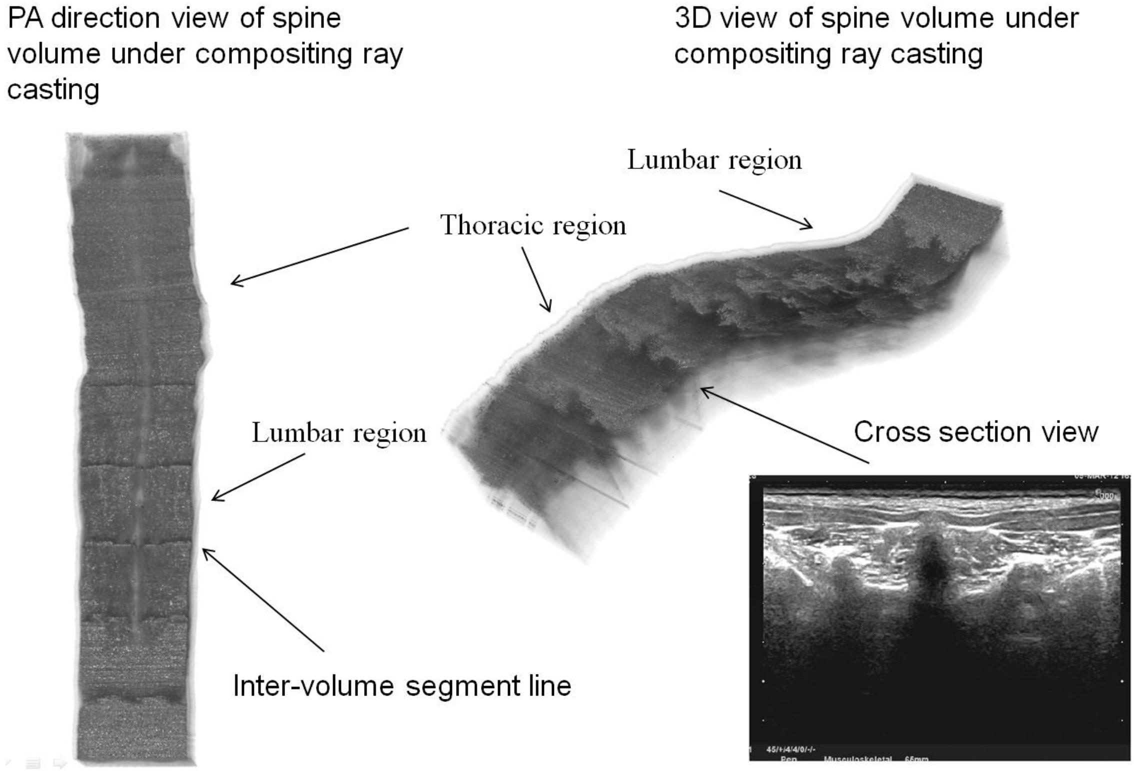

Figure 3.30. Full spine volume from a typical scoliotic patient in PA and 3D view.

Applying a general volume re-slicing technique, three cross sectional orthogonal planes with position respected to axis directions of the world coordinates of the spatial senor system produced from the spine volume were obtained (Figure 3.31).

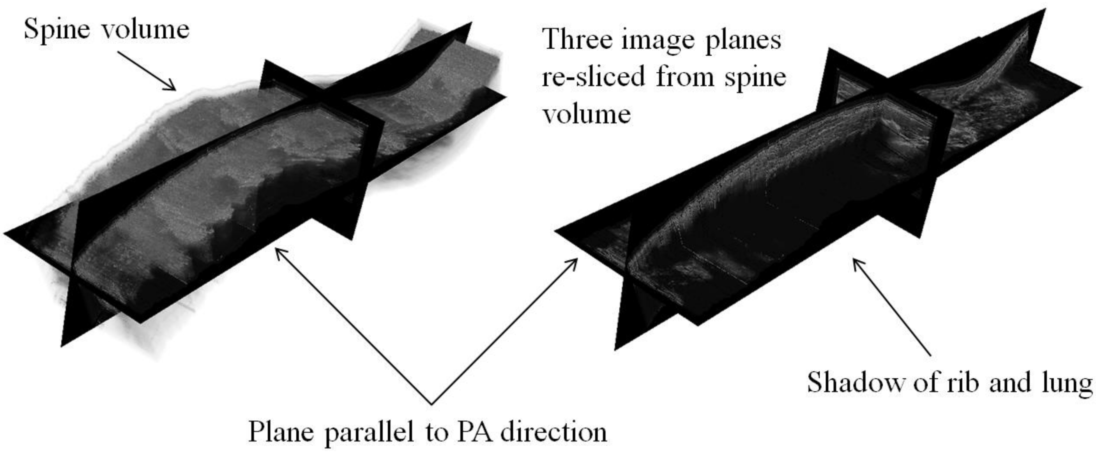

Figure 3.31.Full spine volume from a typical scoliotic patient in PA and 3D view with re-sliced plane cut at middle of volume.

The position of re-slicing planes could be adjusted to obtain the best view. The hidden information at different depth of the spine would be revealed. In order to obtain the scoliotic curvature information, the cross sectional orthogonal plane parallel to the PA direction was further investigated.

In most of the position along the PA direction where the cross sectional orthogonal plane was re-sliced, there was a no data region observed (Figure 3.32). Apparently, completed spine information could not be revealed in a single re-sliced image. As a result, operator warranted observing the cross sectional plane in different positions and mentally reconstructing the anatomical information.

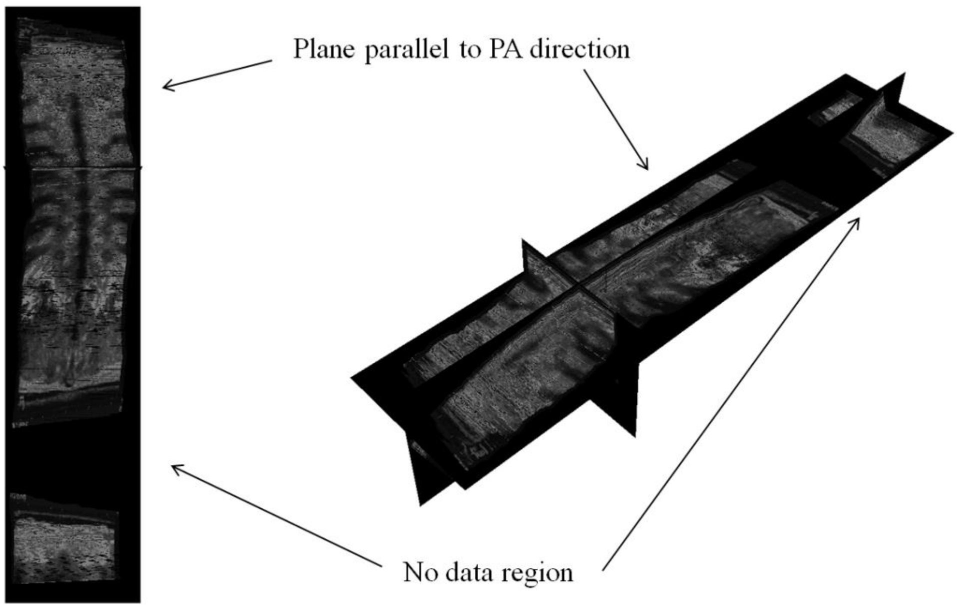

Figure 3.32. A re-sliced spine volume from a typical scoliotic patient in PA and 3D view with re-sliced plane cut near the skin surface of volume.

In order to eradicate the no data region, non-planar re-slicing technique was developed. Instead of cutting according to the world coordinates position, skin surface was used as a reference. Position of a non-planar cut-plane was according to the distance from the skin surface in the B-mode image (Figure 3.33).

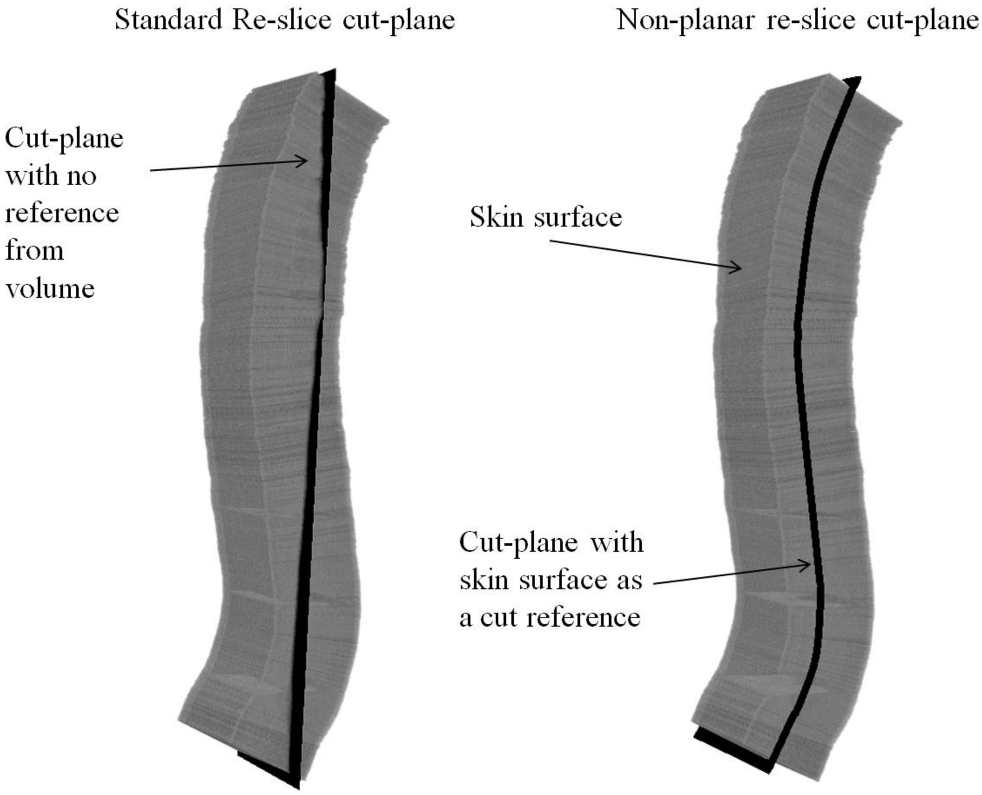

Figure 3.33. Illustration of non-planar re-slicing technique using skin surface as a cut reference.

However, the data of non-planar cut-plane was in form of 3D coordinate. It was not feasible to measure angle of spinal curvature directly. With the inspiration from X-ray radiograph, the data of non-planar cut-plane were projected to PA direction similar to radiograph. To achieve the proposed approach, the voxels from the spine tissue of the rectangular reconstructed volume were relocated according to their coordinate along the posterior to anterior direction while other two spatial coordinates were unchanged. The voxels of body tissue with the most posterior coordinate, which denoted the skin layer voxel and theirs posterior to anterior coordinate closest to the posterior edge of the volume, were relocated at the most posterior coordinate of volume in posterior to anterior direction, resulting in all the tissue voxels with the most posterior coordinate at various positions projected to a rectangular plane with its plane normal parallel to the PA direction. After all most posterior coordinate voxels were relocated; this process was repeated to a new set of tissue voxels with its posterior-anterior coordinate becoming the most posterior coordinate until all voxels of spine tissue were relocated. Each layer of the tissue voxels was formed a rectangular plane with its plane normal parallel to the PA direction. As a result, a set of rectangular planes denoted a set of non-planar cut-planes at different depths of the tissue were obtained. The pseudo codes of the volume projection image formation process were shown as following:

Volume Projection plane formation Algorithm

```
begin VPA;
// Threshold is a value to distinguish the tissue and void voxel;
obtain the threshold value and the dimensions reconstructed volume data including
height, width, depth in term of number of voxel;
define variables (new_position) and boolean (bfirst_encounter);
for all rows (i) in the reconstructed volume data; /* Height */
      for all column (k) in the reconstructed volume data    /* Width */
        /* new position denotes new position to store voxel value */
        set posterior position in the reconstructed volume data in PA direction to
        (new_position);
        set boolean variable (threshold value encounter) to false;
        for all voxels (j) /* Depth, reading from surface (posterior position) toward deep
inside the tissue (anterior position) */
            if voxel value is greater than threshold value
                if the value is first encounter /* tissue or target surface is first encountered
                */
                        set first encourter position = j;
                        set (bfirst_encounter) to true;
                        /* Move to the most posterior position (new_position) of the volume
                        along the line of posterior-anterior direction */
```

```
            set the voxel value from j to (new_position) in the reconstructed
            volume data;
            set the current voxel value to zero; /* erase the current location value
            */
            set position of (new_position) toward anterior direction by one voxel;
        else
            /* Move to the next most posterior position (new_position) of the
            volume along the line of posterior-anterior direction */
            set the voxel value to (new_position) in the reconstructed volume data;
            set the current voxel value to zero;
            set position of (new_position) toward anterior direction by one voxel;
        end-if;
      end-if;
    end-for
   end-for;
end-for;
end VPA;
```

The resultant data, however, was noise. Therefore, projections of 50 non-planar cut-plane data, which was covered around one centimeter thickness of nearby tissue according to B-mode image, were exploited for further processing using averaging. As a result, a new form of ultrasound spine imaging technique was developed. This approach is known as volume projection approach (Figure 3.34). In addition, volume rendering techniques including averaging, maximum intensity projection could also be used to process voxels data from different layers of non-planar cut-plane.

.

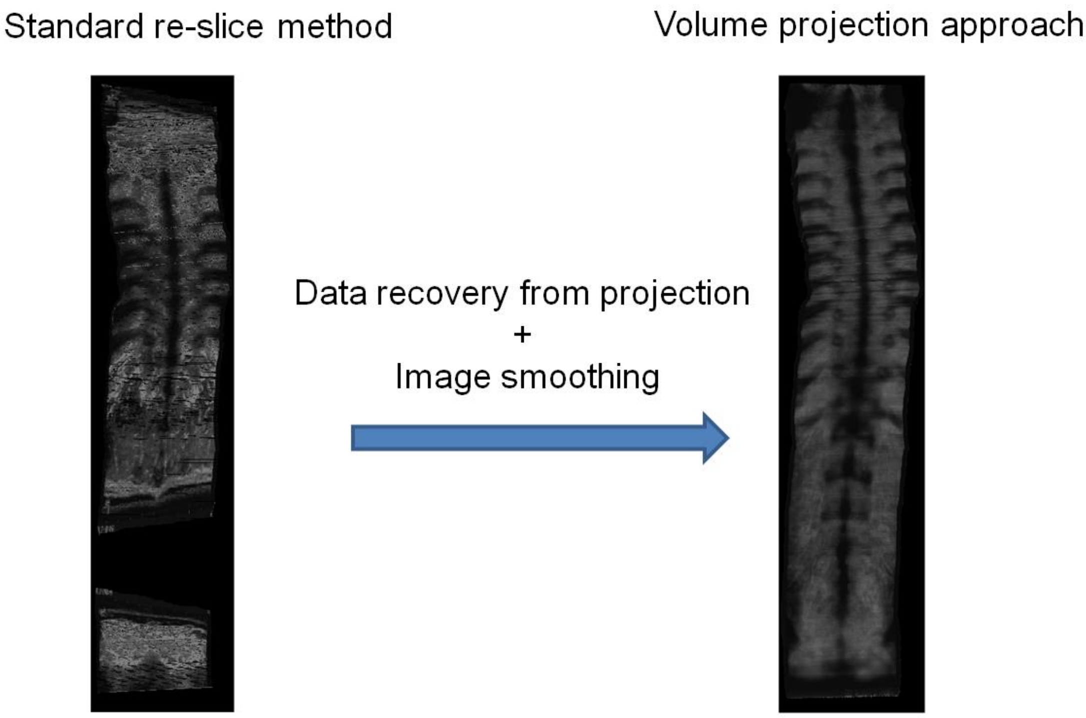

Figure 3.34. Use of non-planar cut-plane image with averaging imaging processing technique to produce volume projection image from a spine volume.

Similar to normal re-slice technique, the volume projection image could be used to reveal the spine features at different depth measured from the patient skin surface. As a result, many bony features were remarkably manifested (Figure 3.35). The number of cut-plane data could be increased or decreased according to the feature under investigation. In my study, 50 non-planar cut-plane data was fixed for the investigation.

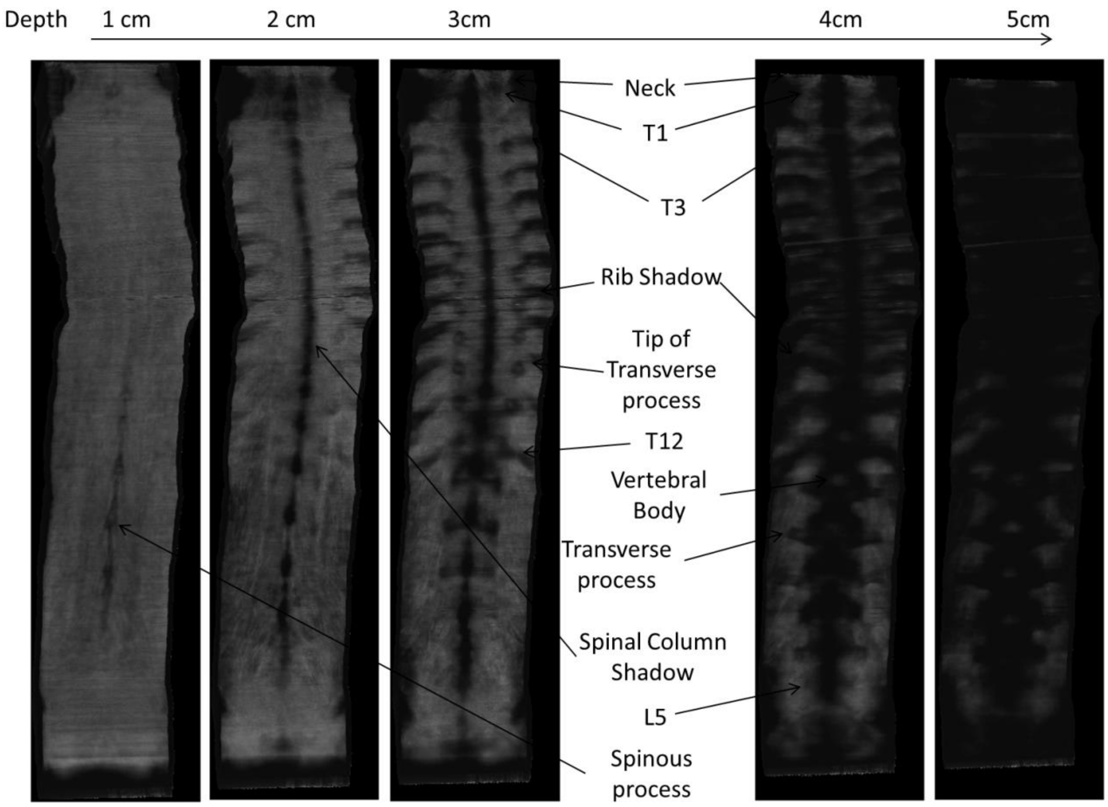

Figure 3.35. Bony features of spine revealed at different depth of non-planar re-slice projection image plane.

Two measurement methods using different references were implemented for fulfilling the purpose of spinal curvature measurement. Using the shadow curve formed by spinous processes and nearby tissues, which could be found in mid-line of the volume projection image, the two most turning portions of the curve could be found and treated as the most tilted vertebrae for measurement. Two short lines were manually drawn from the middle of the shadow curve on the image plane for denoting the local turning of curve. The angle of spinal curvature would be automatically devised according to the line geometrical information after the lines drawn. The angle formed by two lines was analog to analytic Cobb’s method. This drawing method was known as volume projection approach using the spine column profile as a reference (Figure 3.36).

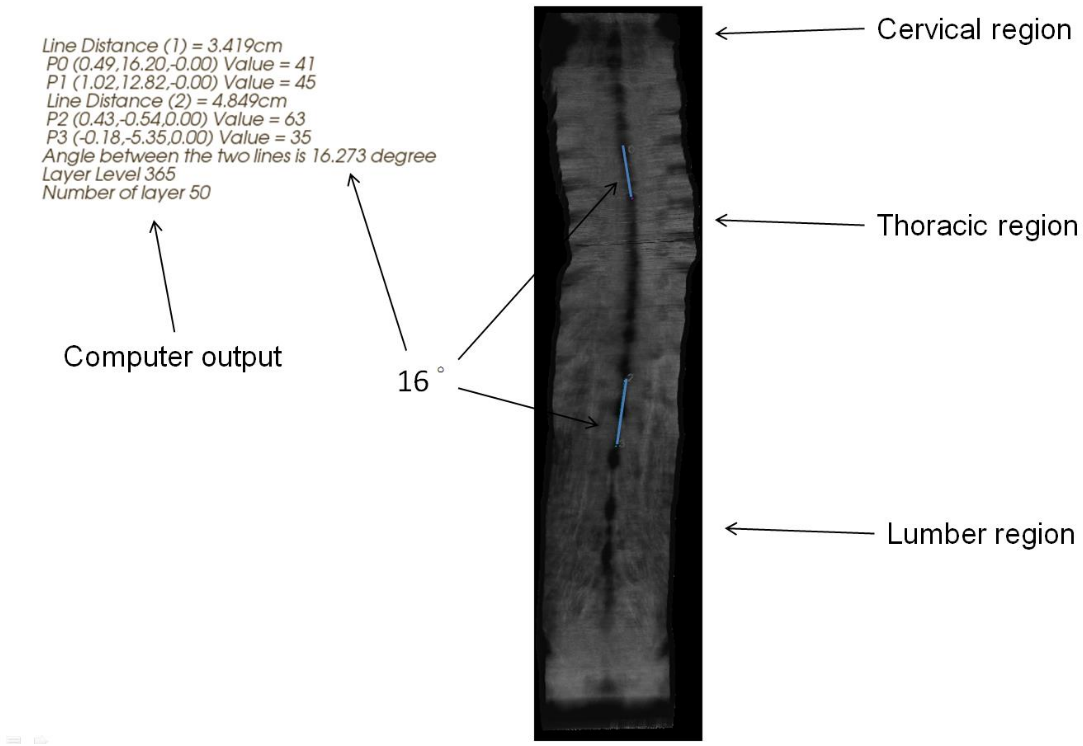

Figure 3.36. Spinal curvature manual measurement using the spine column profile as a reference,

Alternatively, transverse process was used as a reference. In order to draw the two lines correctly, the operator examined the image at various depths for identification of the tips of transverse processes from various vertebrae (Figure 3.37). This is because the depth of transverse process located are various among different vertebrae. In a few cases, tips of transverse processes in vertebra could not be identified because of reduction in resolution or tips moved beyond the imaging range particularly in lower lumbar region. The ends of transverse process were used in the case of tips of transverse process unidentified in my study. This drawing method was known as volume projection approach using TP as a reference. In addition, in part of my study, the preselected vertebrae according to the Cobb's method were used to define where the lines to be drawn using the spine column profile and TP as reference. Thus, the observer had to identify the preselected vertebrae from the image before conducting drawing.

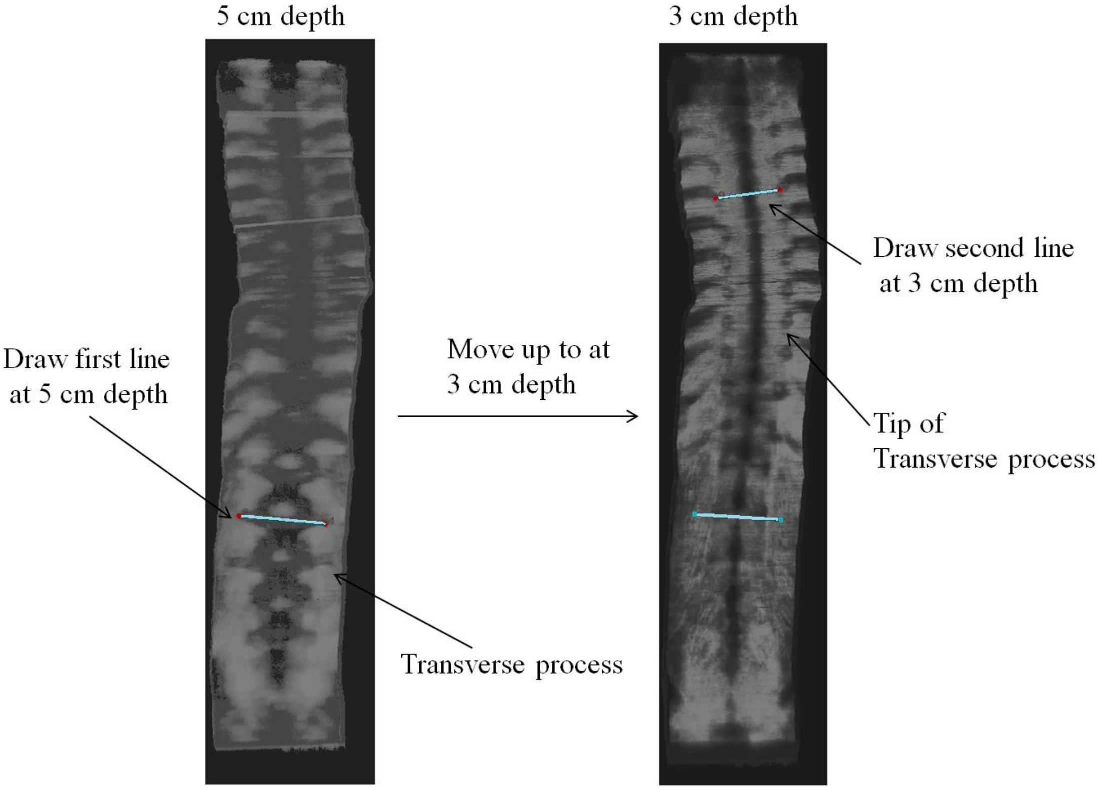

Figure 3.37. Spinal curvature measurement using TP as a reference.

The volume projection approach using 3D ultrasound technique provides a new way to measure the spine curvature notably similar to radiograph. The methods of validation of these two approaches introduced are described in next section.

3.3.3 Cobb's angle measurement.

The patients' radiographies were collected from the patients' clinician and digitalized in DICOM format. Sante Dicom Viewer (SDV) free edition version 1.3 (Santesoft Ltd, Athens, Greece) were exploited for converting DICOM formatted digital radiograph into computer BMP format file for further analysis and measuring the subjects' and phantoms' Cobb's angle. According to the Cobb's method, the Cobb's angle was measured according to the most titled pair of vertebrae in the posterior-anterior X-ray image. In SDV main screen (Figure 3.38), a pair of lines was drawn from the vertebra bodies of the most titled vertebrae on the radiograph. The perpendicular lines were then drawn from the ends of these two lines to form an angle, which was then measured by the angle tool using another pair of lines drawn on the angle being measured.

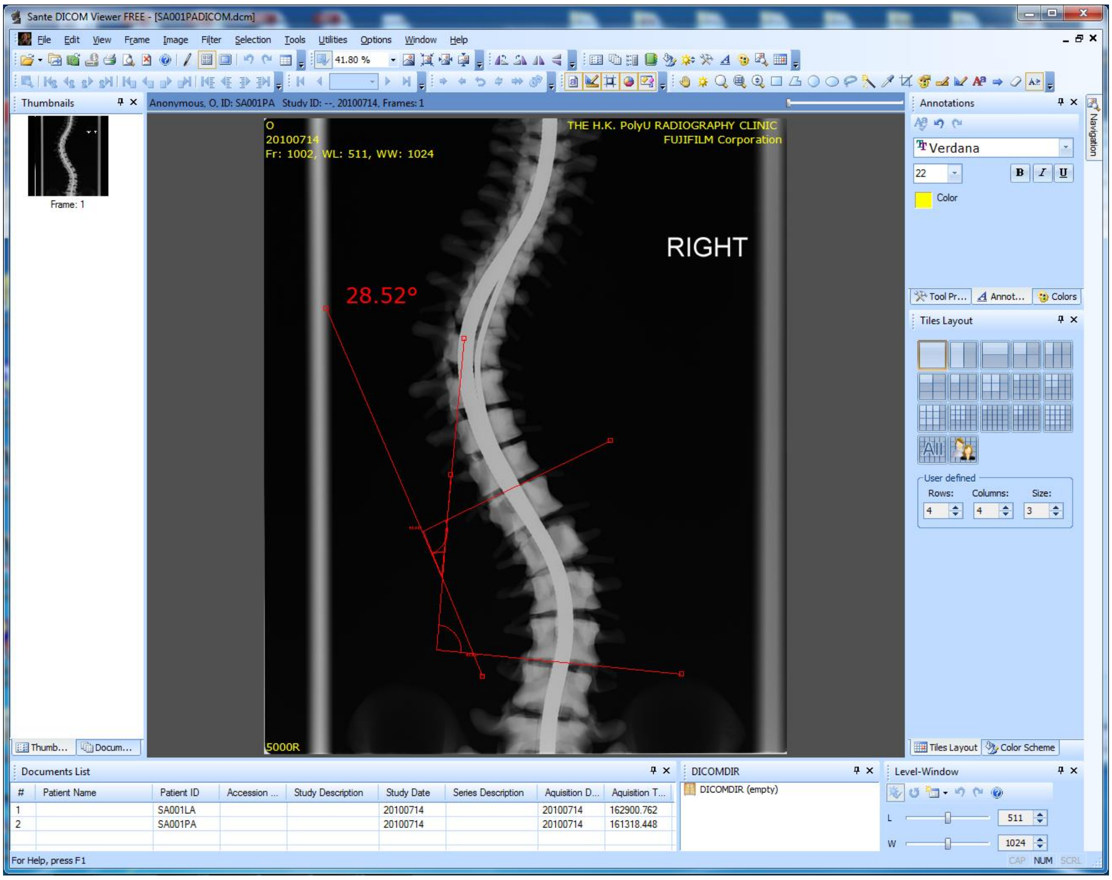

Figure 3.38. Radiograph measurement of a phantom using SDV.

In spine phantom test, the Cobb's angle measurement from phantoms' radiographs using SDV was performed twice by the same operator and the mean value was used for comparing with the result of 3D ultrasound measurement. A typical measurement on the spine phantom's radiograph using SDV is shown in Figure 3.38. In clinical study, the Cobb's method was also exploited to measure the Cobb's angle from the subjects' PA radiographs using SDV (Figure 3.39). Similar to spine phantom test, the

Cobb's angle measurement from subject's radiograph using SDV was performed twice by the same operator and the mean value was used for comparing with the results of 3D ultrasound measurement in human subject test.

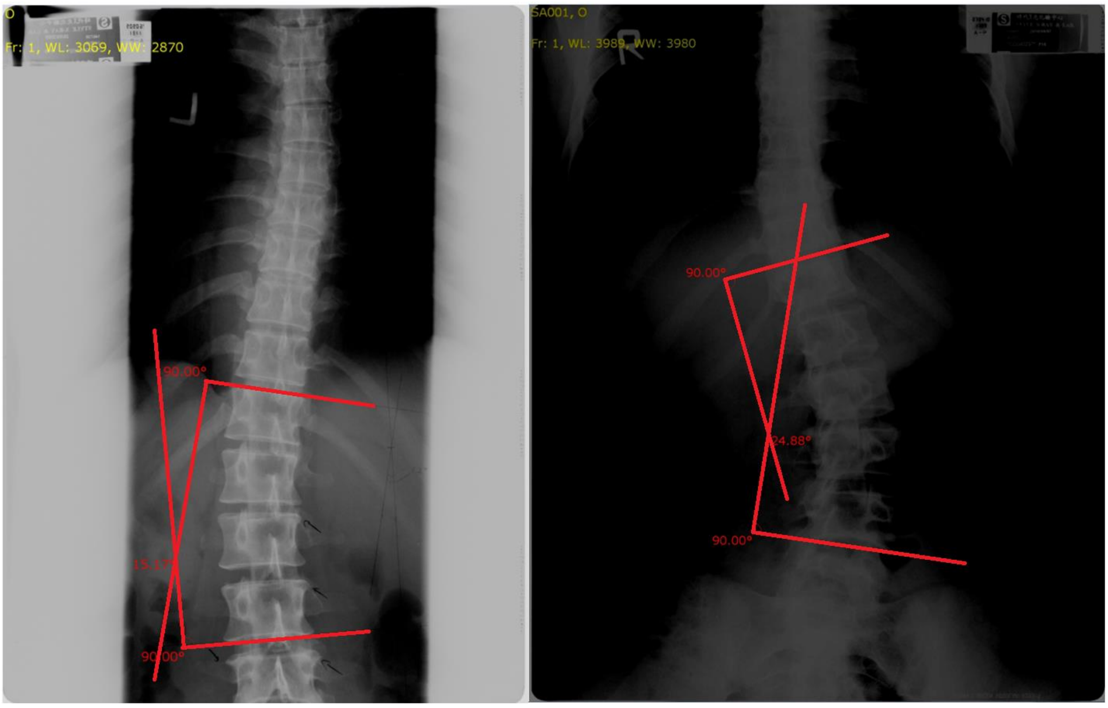

(a) (b)

Figure 3.39. Typical examples of subject's radiograph measurement, (a) an example with high image quality, and (b) an example with poor image quality.

3.4 Spine phantom test

3.4.1 Spine phantoms

Four flexible spinal column phantoms featured with soft intervertebral discs allowing deformation (VB84, 3B Scientific, Germany) were used in the phantom tests. These spine phantoms were 105 cm in height without any deformity. Each of them was deformed into four different curvatures to simulate different scoliotic conditions. Therefore, in total, 16 phantoms were examined with different degrees of simulated scoliotic curvatures (Figure 3.40).

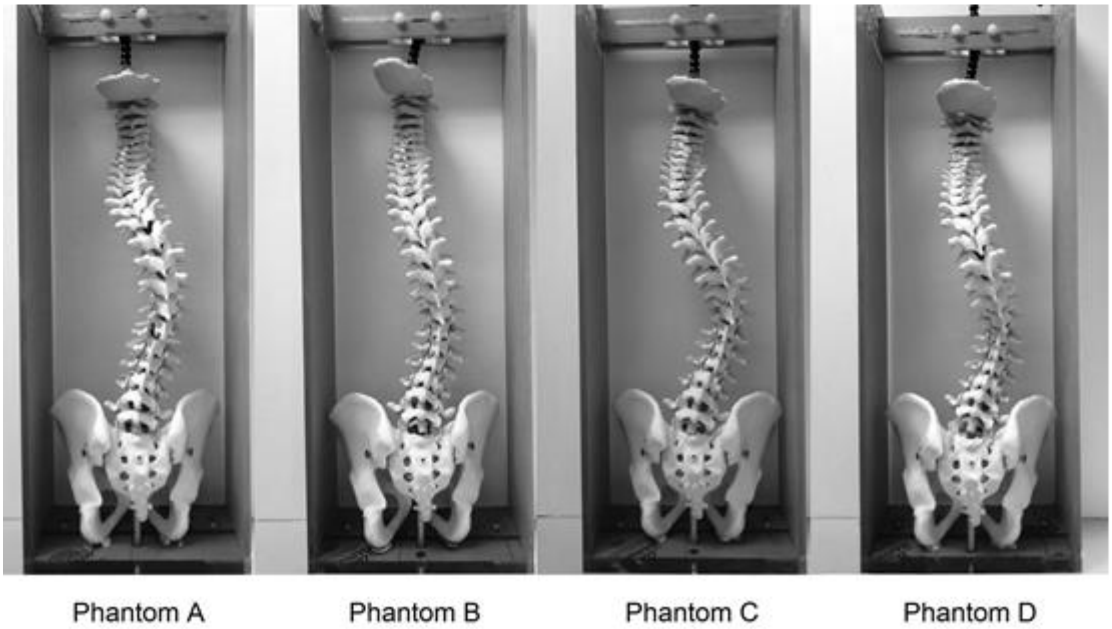

Figure 3.40. Four flexible spinal column phantoms with different simulated scoliotic curvatures.

3.4.2 Experimental protocol

A rigid frame (Figure 3.40) made of acrylic plates and nylon screws was exploited to mount the deformed phantom to avoid the change of its shape during transportation and scanning. Each of these spine phantoms underwent X-ray chest radiography in both posterior-anterior and lateral positions. The X-ray images were digitized and stored in DICOM format for further processing. The Cobb's angle was measured using SDV free edition version 1.3 (Santesoft Ltd, Athens, Greece). The mounted phantoms were then submerged into a water tank filled with water until all vertebrae covering from T1 to L5 were under water. The prototype-1 electronics equipment setup was exploited in the tests. Before data acquisition, the observer needed to submerge the probe at the level of L5 and captured the position, and raised the probe to the level of T1 and captured the position. This procedure was exploited for defining the 3D images stack and volume coordinates. During image acquisition, the observer drove the probe slowly and steadily rising from L5 to T1 vertebra. While the probe was moved upward, the probe's middle line position, which was denoted by the mounting kit's prominence (Figure 3.8b), was being continuously adjusted and aligned with spinous process to ensure that the traverse processes were imaged in the ultrasound images. The scanning time was approximately 2 minutes for the probe driven from L5 to T1 vertebra position. During each scan, 500 to 700 frames of B-mode image were captured with image capturing rate of 6 to 8 frames per second.

Considering the intraobserver variation, each deformed phantom was scanned three times before it was raised up above water level for repositioning. After the phantom was raised above the water level, it was immediately submerged into water again for setting new position and scanning for another three times. After the second round of scanning was accomplished, the phantom was raised above the water level for preparing the third round scan, and so on. For the first and second rounds of experiments, each phantom configuration underwent a total of 9 scans in each round of scanning. Experiments for testing interobserver variation were also conducted. In contrast to the first and second rounds of experiment, in the third and fourth rounds of experiment, another observer was introduced after 9 scans were conducted by the first observer. After an additional phantom repositioning, the second observer conducted additional three scans. There were a total of 12 scans conducted for each phantom configuration in the third and fourth rounds. After all the four phantoms were scanned, they were deformed into other curvatures. The phantoms with new configurations would be scanned again using the above protocol. This procedure was repeated for four times. Therefore, there were a total of 16 sets of data captured representing different severity of spine deformity.

3.4.3 Statistical analysis

Four deformable spine phantoms randomly deformed were underwent X-ray radiograph. The deformed phantoms were then scanned underwater using the developed 3D ultrasound system. The procedure was repeated for four times until four PA radiographs and corresponding 3D ultrasound images were produced from the same phantom. In total, 16 PA view radiographs and its corresponding ultrasound images were obtained. Cobb's method was conducted on digitized radiograph. Two measurements were conducted to produce a mean value. The selected pair of most tilted vertebrae was exploited for locating the same vertebra pair in ultrasound image for marking. All 9 scanned images from the same deformed spine phantom were exploited to calculate a mean value of the angle formed by the vertebra pair. Three scanned images without reposition from the same deformed spine phantom were exploited for producing the mean value in intra-observer and inter-observer study. 3D image stack approach was performed to measure the curvature for phantom test only because there was no skin surface for reference in the phantom. Thus, volume projection could not be used.

The intra-observer reproducibility between the results of the repeated sets of 3D ultrasound scanning was tested using intra-class coefficient (ICC) and linear correlation. Linear correlation and Bland-Altman plot were used to test the agreement between the Cobb's angles obtained using radiograph and the angle from 3D ultrasound measurement. For calculating the correlation, the mean of two repeated measurements using X-ray images and the mean of the nine repeated measurements using 3D ultrasound imaging were used.

Statistical analysis software SPSS (Version 16, SPSS Inc., Chicago, IL, USA) and BMedCalc (Version 12.4, MedCalc Software, Ostend, Belgium) were exploited to undertake intra-class reliability test and Bland-Altman analysis for the data analysis. The intra-class correlation coefficent (ICC) was exploited to test the repeatability of the intra-observer (ICC, Model 3) and inter-observer (ICC, Model 2) measurements (Rankin and Stokes 1998). A statistical level of $p<0.05$ was chosen to indicate a significant correlation or difference.

3.5 Human subjects tests

3.5.1 Subjects

Number of subjects recruited in different studies was slightly different. In total, 36 subjects were recruited for 3D ultrasound examination. 7 subjects had not submitted their radiographs. Thus, 29 subjects were involved in the clinical test for studying the relationship between the Cobb's angle obtained by X-ray radiographs and the result obtained using the 3D ultrasound image approaches. All the 36 subjects (age: 31.1 ± 14.7), which included eleven teenagers, were involved in first intra-observer and inter-observer study of the volume projection approach. Another 11 subjects were recruited or re-recruited for second intra- and inter-observer test of scanning and the volume projection approach by different observers. Three subjects were newly recruited among the subjects. Human ethical approval was obtained from the Human Subjects Ethics Sub-Committee of The Hong Kong Polytechnic University. All the subjects were requested to read the information sheet (Appendix B) and signed the informed consent form (Appendix B) before scanning. Informed consent form was signed by his/her parent if the subject was under legal age.

3.5.2 Human subject test experimental protocol

The subjects' radiographs were supplied by their clinician. Similar to phantom test protocol, The X-ray radiographs were digitized and stored in DICOM format for further processing. The Cobb's angle was measured using SDV free edition version 1.3 (Santesoft Ltd, Athens, Greece). As non-uniform tissue properties presents along the scanning direction of spine, it is ideal to continuously adjust the ultrasound machine settings including depth of focus and frequency during scanning. The ultrasound machine settings were determined by the operator after examinations on various positions in the spine region. The operator had to make the best judgment on the balance of settings for meeting the need of good imaging on different regions for each subject. The program was limited to maximum B-mode image captured in a single scan of 2480 frames because of the limitation on the program architecture and computer memory. In order to maintain good quality of volume reconstruction, re-scan was warranted if the images acquired in a single was less 1500 – 2000 frames depending on the height of subject. With improved equipment, frame acquisition rate was upgraded to 23 frames per second. The scanning time was around 90 to 120 seconds with slow and steady moving speed. The flowchart of scanning procedure is shown in Figure 3.41.

Subject changes dress

Adjust chest board and hip board position

Move and extend the peg supporters to the most suitable position

Observe the subject in sagittal plane and adjust the eye level spot

Place the tissue paper onto the underpants

Paint gel onto subject, fill the spinal furrow

Active spatial sensor and ultrasound probe

View position around T1,T12, L5 to adjust the best B-mode by fine tuning

Position the probe at below L5 spinous process before start

Scan from L5 until over T1 spinous process

Preview the result and determine the necessity of repeating scan

Save raw images

Clean up subject and probe

Subject changes dress

Figure 3.41. Scanning procedure workflow.

Subject was requested for undressing upper garments and wore only a dressing gown with opening on the back, and removing all metallic wears, electronics goods, and any suspected ferromagnetic material made items. The subject then stood on flat platform or step for preparing pegs adjustment. The chest board and the hip board were repositioned at different heights by operator. Two pegs on the chest board were relocated to align with clavicle anterior concavities and the length of peg's shafts was adjusted until contacted with subject; similarly, another two pegs on the hip board were relocated to align with ilium anterior superior iliac spines and the length of peg's shafts was adjusted until contacted with subject; while, subject preserved his/her natural standing posture (Figure 3.42).

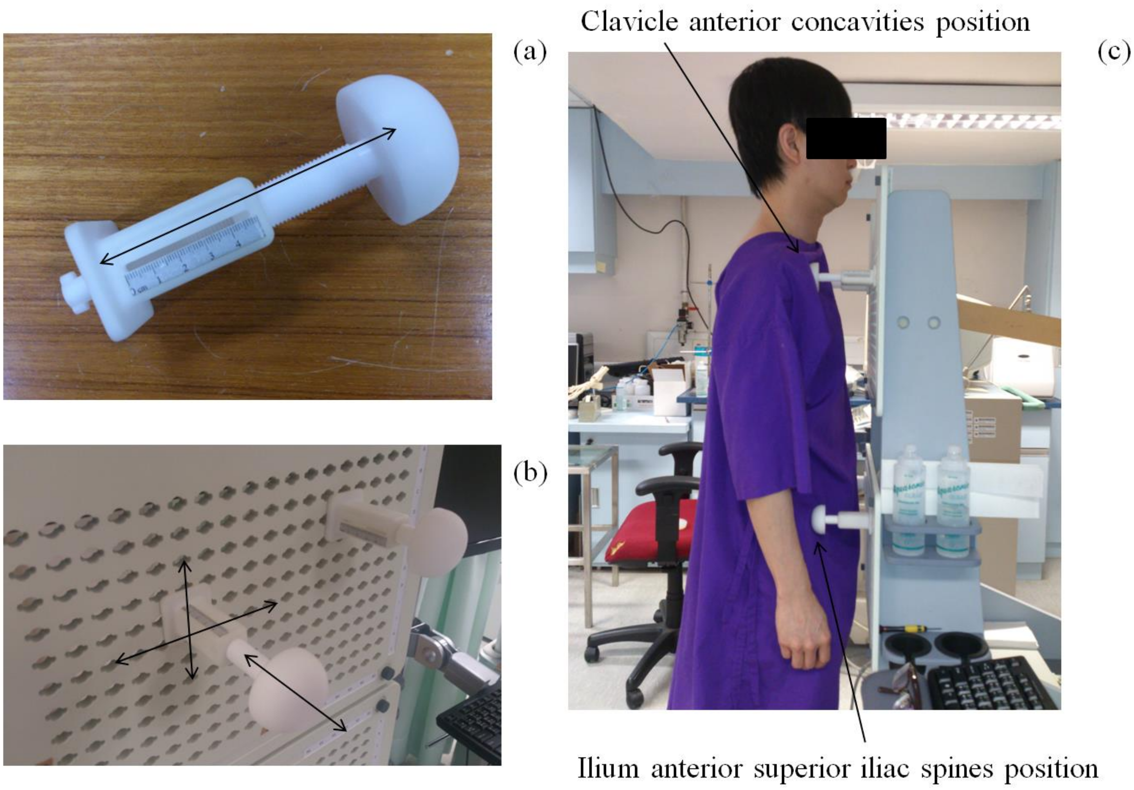

Figure 3.42. Pegs in (a) prototype-2, (b) pegs on chest broad in prototype-2 (c) pegs contact with clavicle anterior concavities and ilium anterior superior iliac spines.

Operator moved the eye marker stand parallel to subject's coronal plane until it was aligned with the subject's sagittal plane and then the eye level marker spot (Figure 3.43) was raised to the subject's eye level. Subject was instructed to stare at eye level marker spot while scanning in progress.

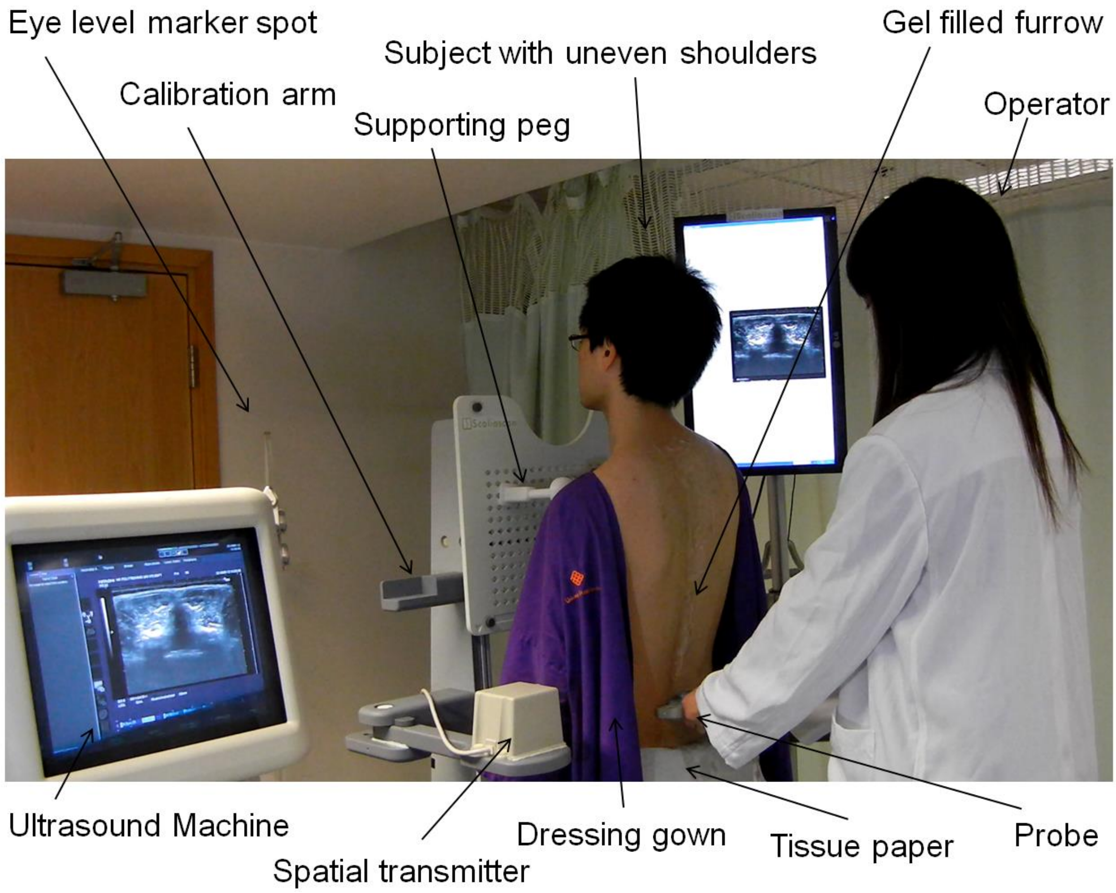

Figure 3.43. System, subject, and operator at the moment before scanning.

After completion of frame adjustment, a few large sheets of tissue paper were slotted into the subject's underpants in half and left out another half outside for preventing the gel falling onto the lower garments. Aqueous gel, which was warmed up by a hot water bath or gel warmer before use, was painted onto the subject by the operator to fill the spinal furrow and covered all the extent where the probe would sweep across in order to avoid unnecessary blocking out of ultrasound signal. The operator started to activate spatial sensor transmitter after gel painting, and used calibration arm

(Figure 3.43) to check the accuracy of the spatial sensor. Re-calibration would be needed to be conducted if operator failed to restore reference values by adjusting the position of the probe mounting kit. By viewing B-mode image from the positions around T1, T12, and L5, operator adjusted gain and dynamic contrast settings of the ultrasound machine to obtain the best overall B-mode image. All other features for imaging enhancement including compound imaging were maintained in the same settings for all subjects. Frequency mode and focus depth were set at penetration mode and 65 mm respectively. After setting adjustment was completed, the operator placed the probe at below L5 spinous process before start (Figure 3.43), and the subject was instructed to stand still and breathed shallowly during scanning.

By stepping on the foot switch, the scanning was commenced. The operator drove the probe up from below L5 vertebra position to over T1 vertebra position while the probe was moved along the spinal column with the probe's mounting kit prominence aligned to the middle of furrow and spinous process (Figure 3.44).

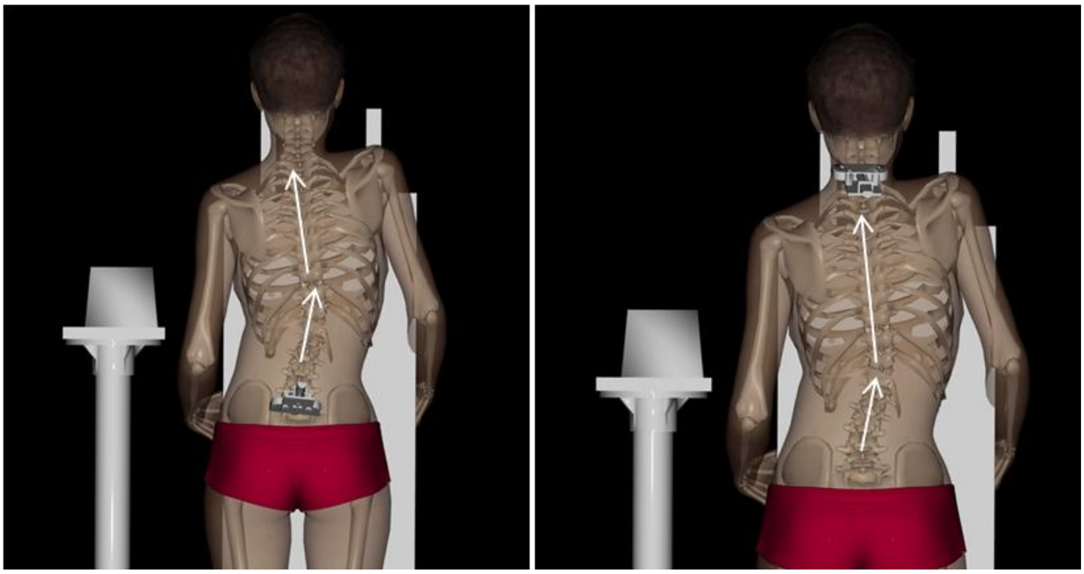

(a) (b)

Figure 3.44. Illustration of scanning along with curved spine. (a) Scanning start position below L5 vertebra position, and (b) scanning stop above T1 vertebra position.

Concerning the probe capable of covering all vertebra cross section in a single B-mode image, multiple-sweeps were not conducted for all subjects. The B-mode images and theirs spatial data captured were saved into a single file. The file was then reviewed by viewing the raw B-mode images to determine the necessity of repeating scan. After scanning, the operator cleaned up the subject and the probe with tissue paper for removing the gel. The subject was then allowed to change dress.

In the examinations, three patients were not feeling well and required clinician caring. After 30 minutes rest, all patients continued their examinations. Clinician reported that these patients had a history of cardiopulmonary function weakness, which is a topical scoliotic symptom. Winged scapula was encountered in two patients (Figure 3.45). The operators found that the probe was blocked by the sticking out bladebones of scapula. The subjects were instructed to cross their arms so as to widen the pathway between the bladebones.

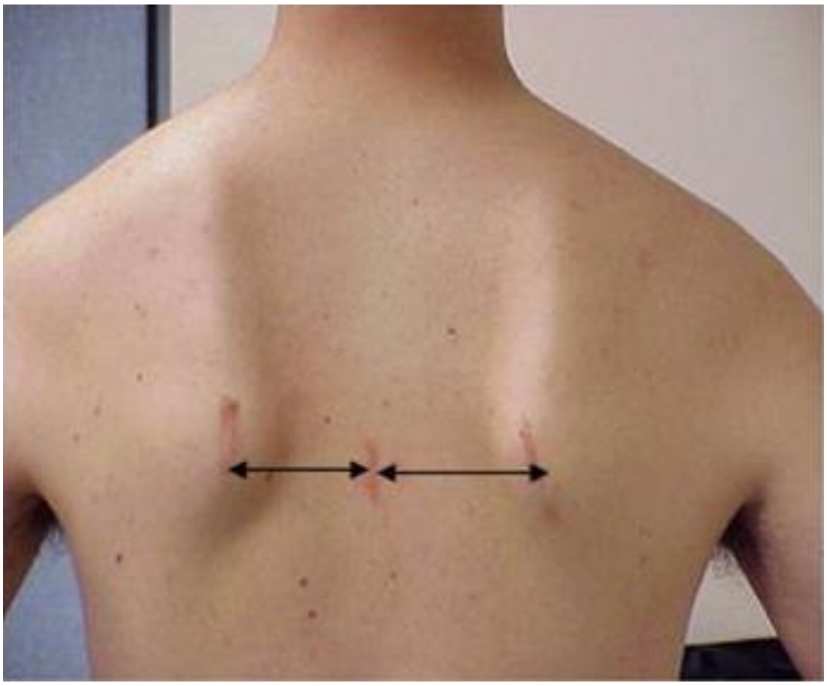

Figure 3.45. Winged scapula (http://forum.bodybuilding.com/showthread.php?t=731648&page=1).

Two sets of ultrasound B-mode images captured in video card's black and white mode at 23 frames per second and one sets of ultrasound B-mode image captured in video card's color mode at 8 frames per second were captured from the subject. In 3D image stack approach, two good quality image sets from the three image sets were selected for assessment. In volume projection approach, two image sets with higher frames rate were exploited for assessment. The 3D ultrasound scans were performed in the Hong Kong Polytechnic University.

In the first intra- and inter-observers studies, three scans in one single examination were conducted by a single observer. The measurements were conducted by two observers with the information of pre-selected vertebra. The results were used to study the correlation between the purposed approaches and X-ray Cobb's method (Table 3.1). Second intra- and inter-observers studies were conducted by two observers for scanning and conducting measurement independently without the information of pre-selected vertebrae, allowing investigation on the effect of scanning and measurement using the volume projection approach with the spine column profile as a reference. Each observer scanned twice on the same subject. A third observer also conducted the measurement on observer 1 and observer 2 scan data without the information of pre-selected vertebrae (Table 3.2).

Table 3.1. Scan and measurement arrangements on first intra- and inter-observer test with the information of pre-selected vertebra.

Observer	Scan	Measure on observer 1 scan data
Observer 1	Yes	Yes
Observer 2	No	Yes

Table 3.2. Scan and measurement arrangements on second intra- and inter-observer test without the information of pre-selected vertebra.

Observers	Scan	Measure on observer 1 scan data	Measure on observer 2 scan data
Observer 1	Yes	Yes	Yes
Observer 2	Yes	Yes	Yes
Observer 3	No	Yes	Yes

3.5.3 Statistical analysis

3.5.3.1 3D Image stack approach

Two scan data were selected and two virtual spine models were built for each subject. The most tilted vertebrae were determined from X-ray radiograph during Cobb's method measurement. Same pair of vertebra employed in radiograph was selected in the two virtual spine models from the same subject to determine the spine curvature by averaging the angle measured from the models. Random selections of subjects's scan data set were used to build two new virtual spine models for intraobserver test. Similarly, another group of randomly selected subjects's scan data set was used to build two new virtual spine models for inter-observer study by another observer.

The intra-observer and inter-observer reproducibility between the results of the repeated sets of angle measured using 3D ultrasound image were tested using intra-class coefficient (ICC) and linear correlation. Linear correlation and Bland-Altman plot were used to test the agreement between the Cobb's angles obtained using X-ray Cobb's method and the 3D ultrasound measure. For the correlation test, the mean of two repeated measurements using X-ray radiograph and the mean of the two repeated measurements using 3D ultrasound measure were used.

3.5.3.2 Volume projection approach

Two sets of volume projection images were reconstructed from each subject's raw B-mode ultrasound images. As volume projection images could provide various depth of view, freedom of choice on depth in measure was allowed for maximizing the operator perception and quality on the volume projection image. Following the same pattern in 3D image stack approach, the pre-selected vertebrae were exploited as the reference for locating the same vertebrae pair in the volume projection image. Volume projection approach using different references aforementioned were conducted in measurement on each selected volume projection image. Two measurements were conducted in the same image for producing the mean value in volume projection approach using the spine column profile and TP as reference. Similar to 3D image stack approach, the intra-observer and inter-observer reproducibility between the results of the repeated sets of 3D ultrasound measures were tested using intra-class coefficient (ICC) and linear correlation. Linear correlation and Bland-Altman plot were used to test the agreement between the Cobb's angles obtained using X-ray Cobb's method and the 3D ultrasound measure. For the correlation test, the mean of two repeated measurements using X-ray images and the mean of the two repeated measurements using 3D ultrasound measure were used. The same set of X-ray Cobb's method results from subject was exploited in studying both 3D image stack approach and volume projection approach for evaluating the purposed methods.

For further assessing the volume projection approach, scanning and measuring by another intra-observer and inter-observer tests were conducted. Three observers were involved. Observer 1 and observer 2 were responsible for scan and measure. Observer 3 was responsible for measure only. Observer 1 and observer 2 scanned a subject twice in haphazard order during a single examination, and measured the images twice to determine the mean value using volume projection approach using the spine column profile as a reference from their own scan data. Each of the two observers also measured the images twice to determine the mean value using volume projection approach using the spine column profile as a reference from the other observer's scan data. Observer 3 measured the images twice for producing the mean value using volume projection approach using the spine column profile as a reference from the observer 1's and 2's scan data. Intra-observer tests of observer 1's and 2's results were conducted. The inter-observer test between observer 1's measure using her scan data and observer 2's measure using own scan data was conducted. The inter-observer test between observer 1's measure using own scan data and observer 3's measure using observer 2's scan data were conducted. The inter-observer test between observer 2's measure using own scan data and observer 3's measure using observer 1's scan data were conducted. The inter-observer test between observer 3's measure using observer 1's scan data and observer 3's measure using observer 2's scan data were conducted. The intra-observer and inter-observer reproducibility between the results of the repeated sets of 3D ultrasound measures among three operators were tested using intra-class coefficient (ICC).

The statistical analysis software and model exploited were the same as phantom test. The detail is shown on section 3.4.3.

CHAPTER 4 RESULTS

4.1 Results of phantom using 3D image stack approach

The spine phantom curvatures measured by the Cobb's method ranged 10.0° to 54.0°, using the mean of the two measures. The curvatures obtained by the 3D image stack approach with TP as the reference markers ranged from 16.6° to 50.1° (Please refer to Table A.1 for details). The regression equation between the two sets of data was y=0.967x (Figure 4.1), with x representing the X-ray radiograph result and y representing 3D ultrasound image result. The slope of this regression line closely approached to 1.0 and crossed the origin, indicating a very good linear relationship. There was a significant linear correlation between the results obtained by the two methods (R^2=0.7586, p<0.001), indicating that there was a good agreement between two methods. The Bland-Altman plot showed a low mean difference (d = 0.5°), limits of agreement (±1.96 SD = 10.1°), all data points located inside ±1.96 SD from the mean, and the differences symmetrically distributed around zero (Figure 4.2). It indicated that there was a good agreement between two methods without consistent bias. The results demonstrated that the developed system could measure the spine curvature and reliably collect images with feature landmarks from the spine phantoms. The intra-observer and inter-observer repeatability tests showed that the proposed measurement using 3D image stack approach with transverse processes formed lines as a reference were highly repeatable with ICC value of 0.99 (p<0.001) (Figure 4.3) and 0.89 (p<0.001) (Figure 4.4), respectively. This indicated that the 3D US measurement using 3D image stack approach with TP as the reference markers was operator independent in phantom study.

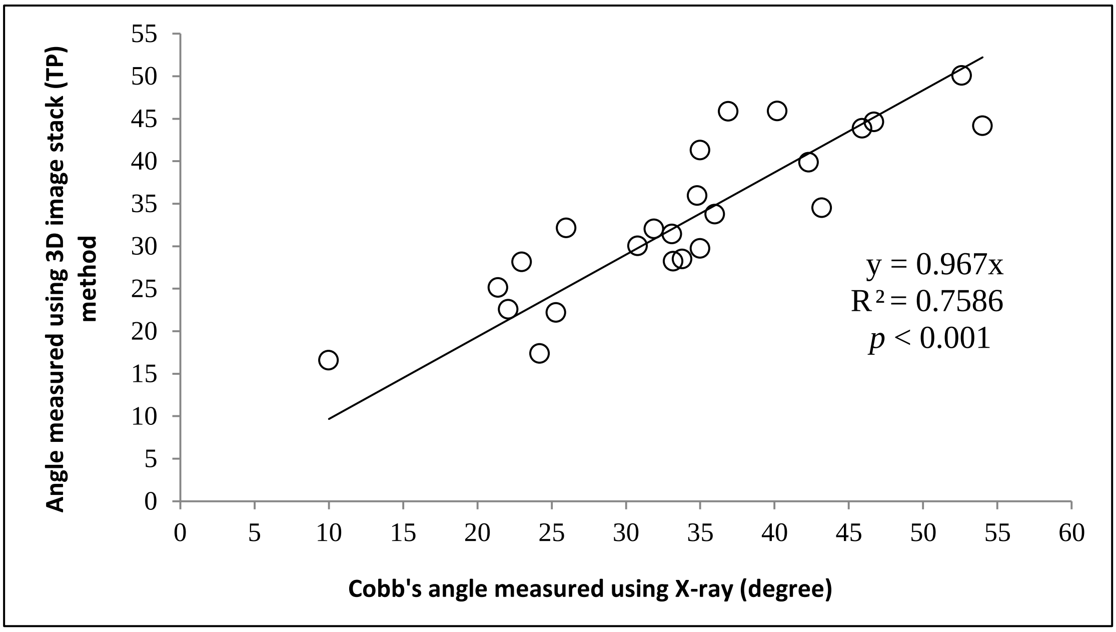

Figure 4.1. The correlation between the Cobb's angle measured using X-ray radiograph and angle measured by the 3D ultrasound image stack approach with transverse processes forming lines as references. The vertebrae for ultrasound measurement were selected according to what used in X-ray image measured. Each data point of X-ray was the mean of two measurements, and that of ultrasound was the mean of nine measurements.

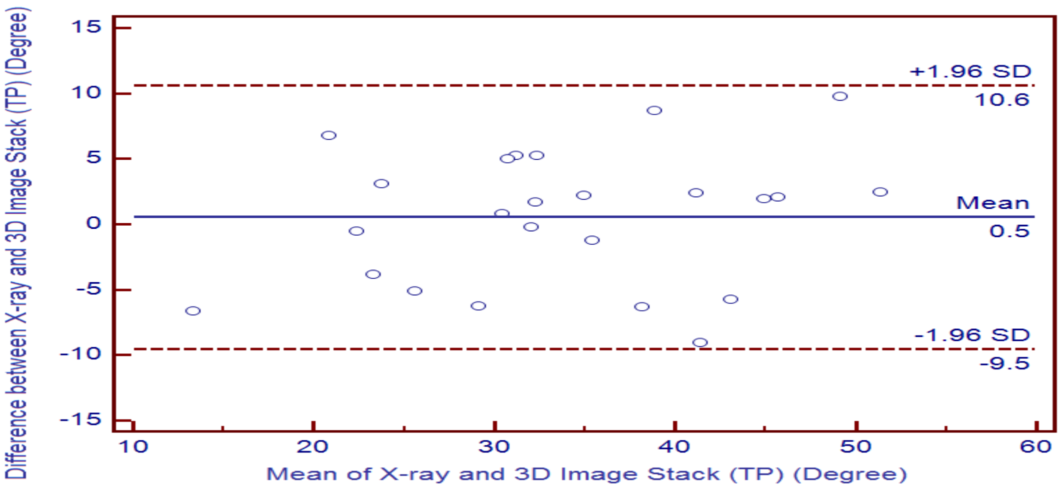

Figure 4.2. Bland-Altman plot between the Cobb's angle measured using X-ray radiograph and angle measured by the ultrasound 3D image stack approach with transverse processes forming lines as the reference. The vertebrae for ultrasound measurement were selected according to what used in X-ray image measured. Each data point of X-ray was the mean of two measurements and that of ultrasound was the mean of nine measurements.

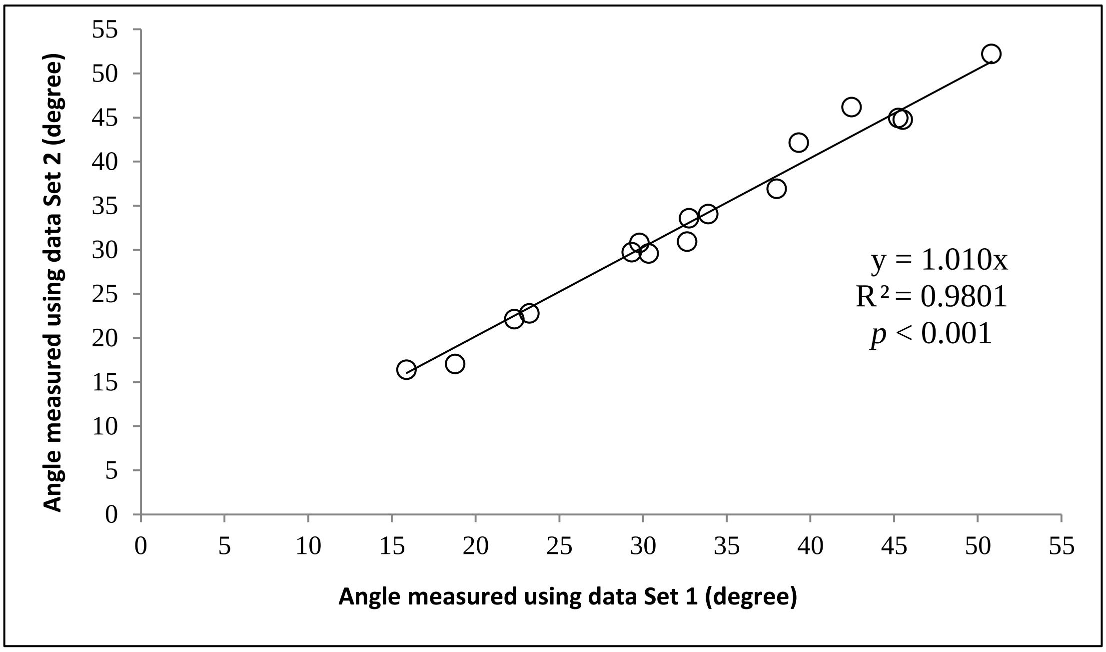

Figure 4.3. The correlation between the angles measured by the same observer using 3D image stack approach with transverse processes forming lines as references. The vertebrae for ultrasound measurement were selected according to what used in X-ray image measured. Each data point of ultrasound was the mean of three measurements.

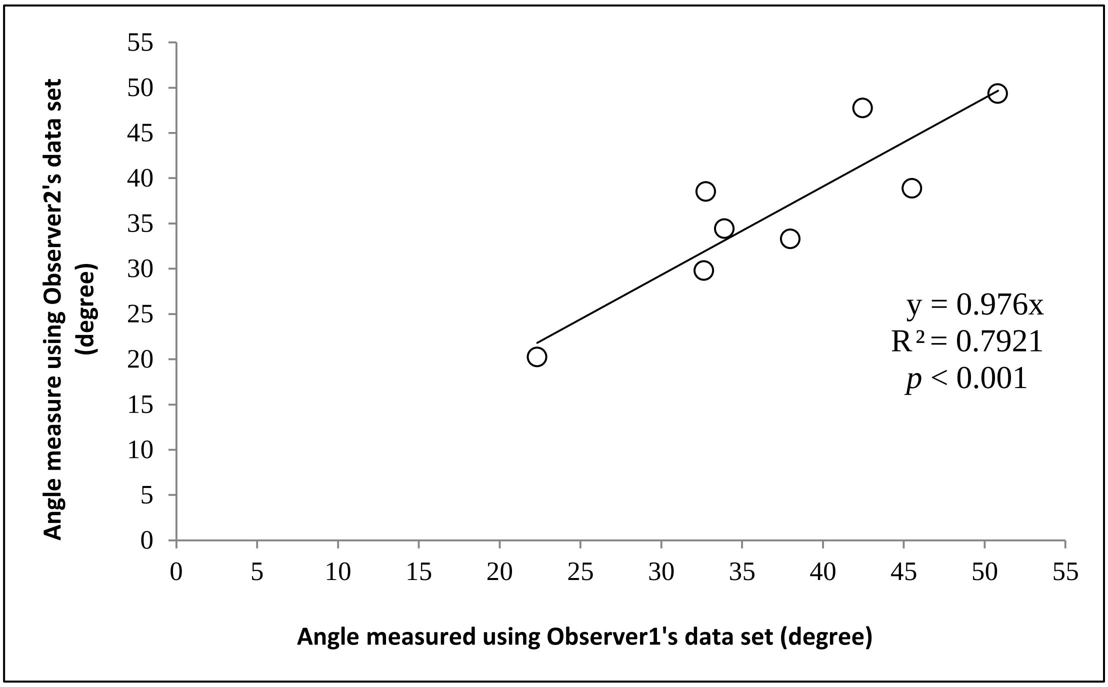

Figure 4.4. The correlation between the angles measured by the two observers using 3D image stack approach with transverse processes forming lines as references. The vertebrae for ultrasound measurement were selected according to what used in X-ray image measured. Each data point of ultrasound was the mean of three measurements.

4.2 Results of human subject using 3D image stack approach

In total, 28 subjects and 37 angles measured were included in the human subject test to compare the results obtained by radiograph and 3D image stack approach with transverse processes as the reference markers. The subject spine curvatures obtained using the 3D ultrasound 3D image stack approach ranged from 0.4° to 20.7°, while that obtained by the Cobb's method ranged from 1.9° to 29.9° (Table A.4). The regression equation of the two sets of data was y=0.643x (Figure 4.5), with x representing the results of X-ray radiograph measurement and y representing the result of 3D image stack approach. The slope of this regression line was not so close to 1.0, though a significant linear correlation between two methods (R^2=0.6806, p<0.001) was demonstrated. The Bland-Altman plot (Figure 4.6) showed a low mean difference (d = 4.3°), limits of agreement (±1.96 SD = 7.5°), 94.6% data points located inside ±1.96 SD from the mean, and the differences symmetrically distributed around zero. It indicated that there was no consistent bias and moderate agreement between two methods.

US B-mode image in subject was generally more ambiguous and noisy. However, the findings suggested that 3D image stack approach persistently maintained a good correlation. The results demonstrated that the developed system with 3D image stack approach could measure the spine curvature and reliably collect images with feature landmarks from human subject. The findings probably suggested that the virtual spine model of individual subject successfully constructed could represent the subject spine deformity in PA view. However, if the results obtained by the ultrasound have to be compared with the Cobb's method result, a proper scaling should be used for the human's subject results.

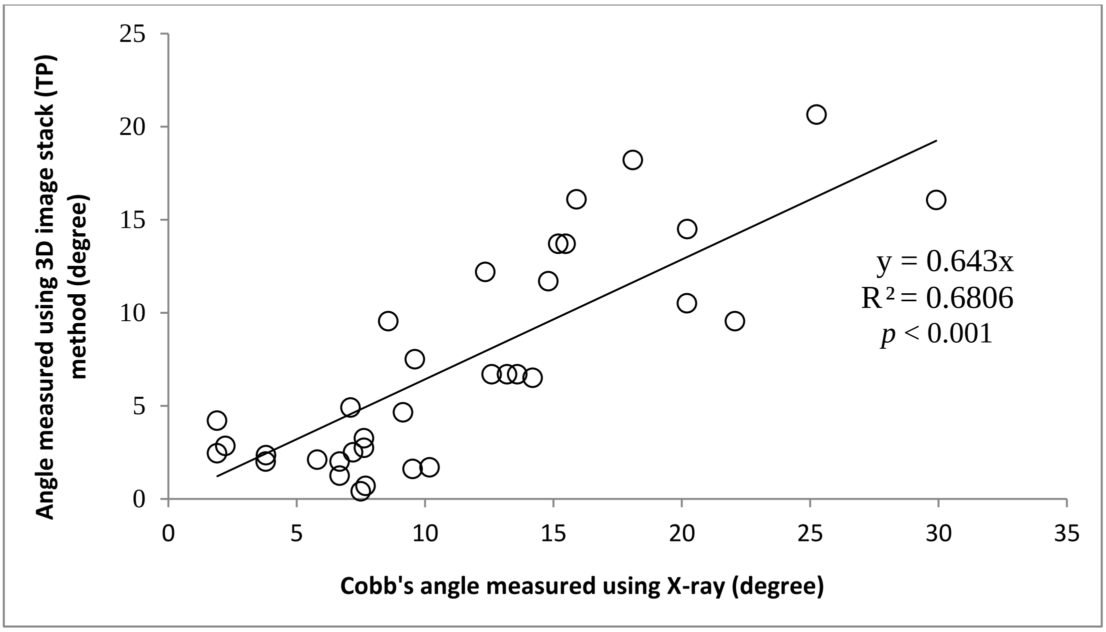

Figure 4.5. The correlation between the Cobb's angle measured using X-ray radiograph and angle measured by the 3D ultrasound image stack approach with transverse processes forming lines as references. The vertebrae for ultrasound measurement were selected according to what used in X-ray image measured. Each data point of X-ray was the mean of two measurements, and that of ultrasound was the mean of two measurements.

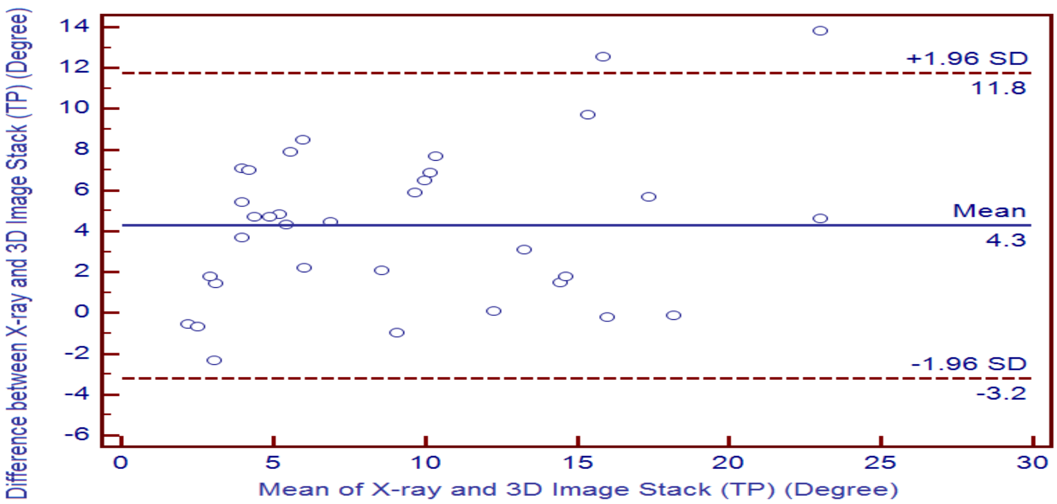

Figure 4.6. Bland-Altman plot between the Cobb's angle measured using X-ray radiograph and angle measured by the ultrasound 3D image stack approach with transverse processes forming lines as the reference. The vertebrae for ultrasound measurement were selected according to what used in X-ray image measured. Each data point of X-ray was the mean of two measurements and that of ultrasound was the mean of two measurements.

The intra-observer and inter-observer repeatability test showed that the proposed measurement using 3D image stack approach with preselected vertebra following X-ray radiograph and TP as the reference markers were satisfactory with ICC value of 0.565 (p=0.0045) (Figure 4.7) and 0.75 (p<0.001) (Figure 4.8), respectively. The results moderately indicated that the 3D ultrasound using 3D image stack approach with TP as the reference markers was operator independent.

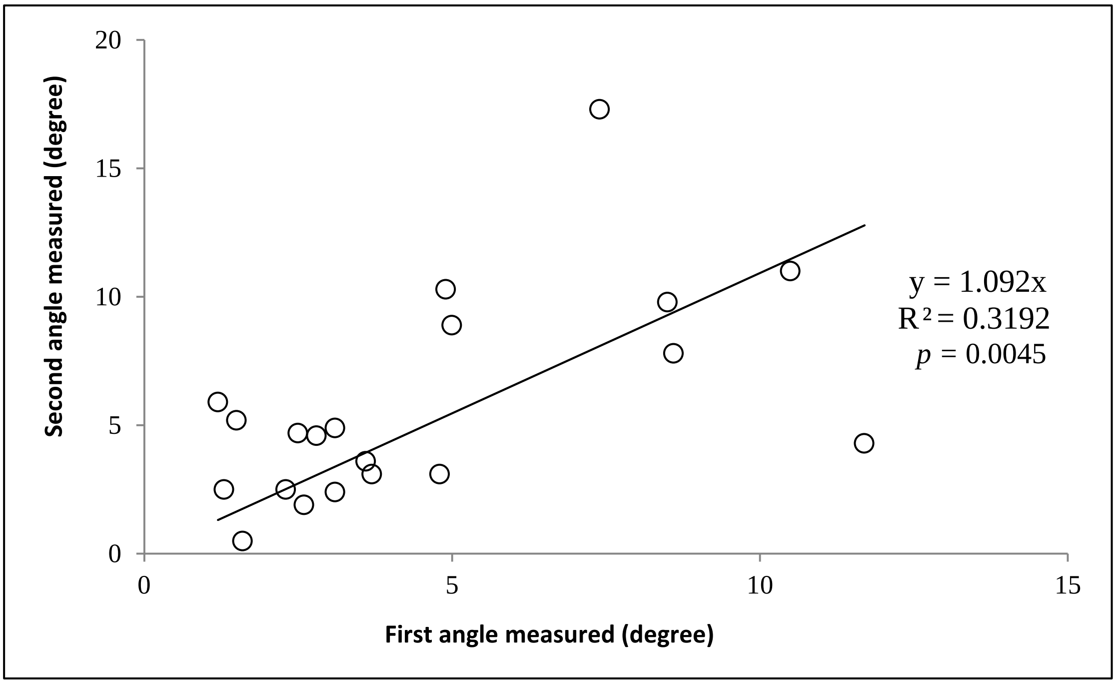

Figure 4.7. The correlation between the angles measured by the same observer using 3D image stack approach with transverse processes forming lines as references. The vertebrae for ultrasound measurement were selected according to what used in X-ray image measured. Each data point of ultrasound was the mean of two measurements.

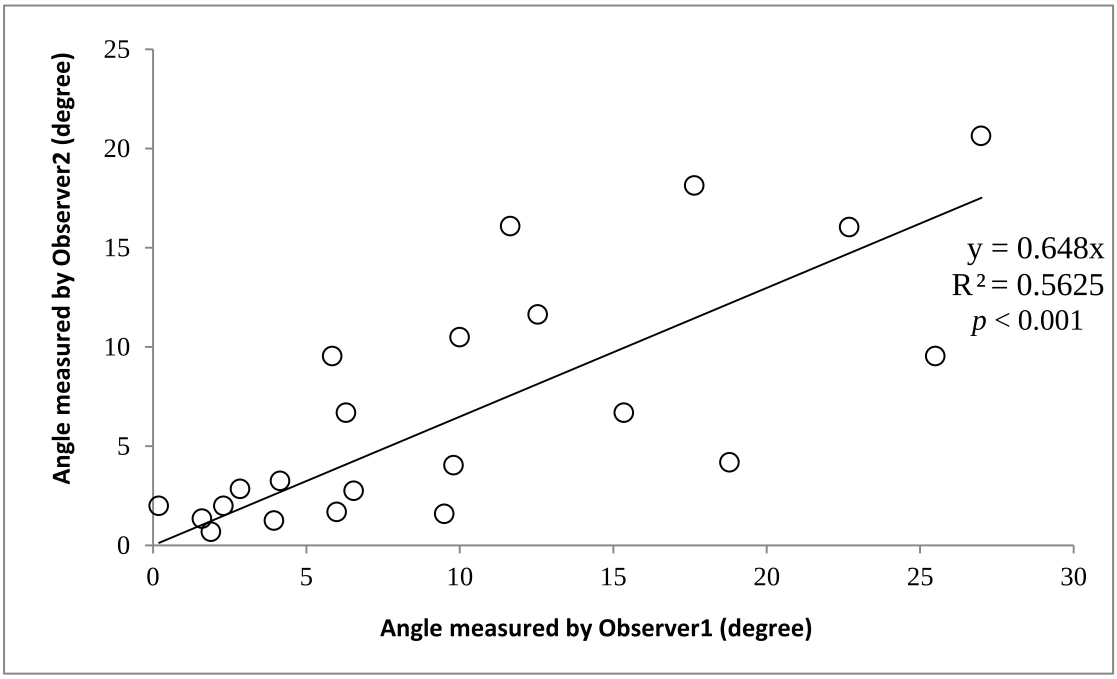

Figure 4.8. The correlation between the angles measured by the two observers using 3D image stack approach with transverse processes forming lines as references. The vertebrae for ultrasound measurement were selected according to what used in X-ray image measured. Each data point of ultrasound was the mean of two measurements.

4.3 Results of human subject using volume projection approach

One subject with high body mass index (BMI) was excluded in measurement using 3D image stack approach. As volume projection approach was less affected by high BMI. The subject was included in the measurements using volume projection approach study. In total, 29 subjects and 38 angles measured were included in the study to compare the results obtained using X-ray radiograph and the 3D ultrasound volume projection approach. The subject spine curvatures obtained using the volume projection approach with the spine column profile as a reference ranged from 4.3° to 30.2° (Table A.7). The range was 3.9° to 31.8° when TP was used as a reference (Table A.7). The subject spine curvatures measured using Cobb's method ranged from 1.9° to 29.9° (Table A.7).

The regression equation was y=1.074x when the spinal column profile was used to as the reference for measurement (Figure 4.9), with x representing X-ray radiograph result and y representing the 3D US measurement result using volume projection approach. The slope of this regression line approached to 1.0 and crossed the origin, indicating a good linear relationship. There was also a significant linear correlation between two methods (R^2=0.7903, p<0.001). The Bland-Altman plot (Figure 4.10) showed a low mean difference (d = -1.9°), limits of agreement (±1.96 SD = 7.3°), all data points located inside ±1.96 SD from the mean, and the differences symmetrically distributed around zero. It evidently indicated that there was a good agreement between two methods without consistent bias.

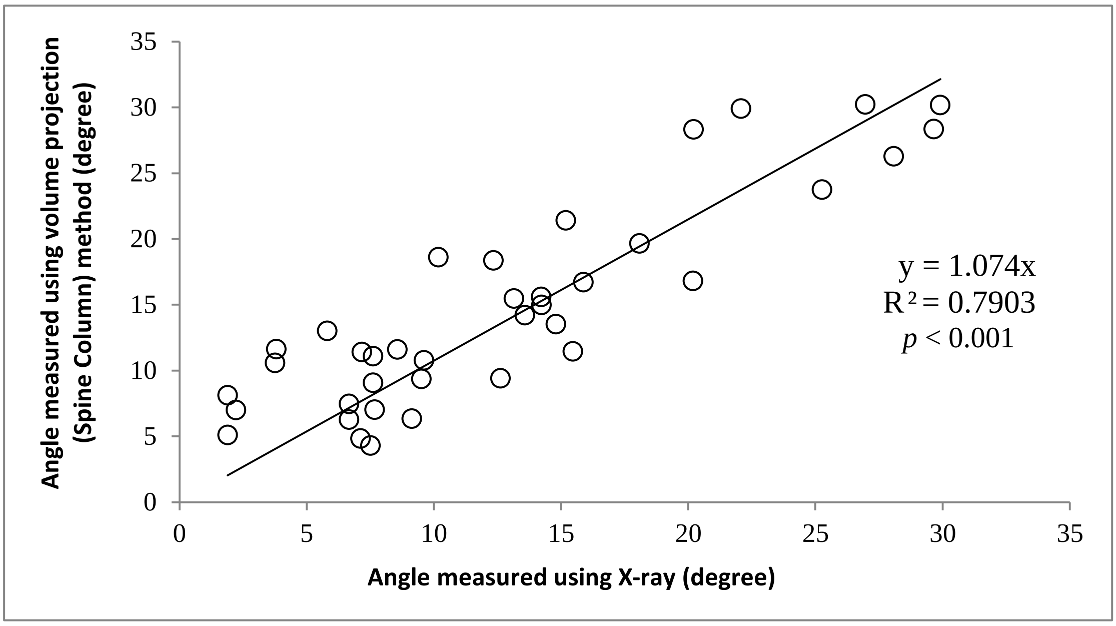

Figure 4.9. The correlation between the Cobb's angle measured using X-ray radiograph and angle measured by the 3D ultrasound volume projection approach with spine column profile as the reference. The vertebrae for ultrasound measurement were selected according to what used in X-ray image measured. Each data point of X-ray was the mean of two measurements, and that of ultrasound was the mean of two measurements.

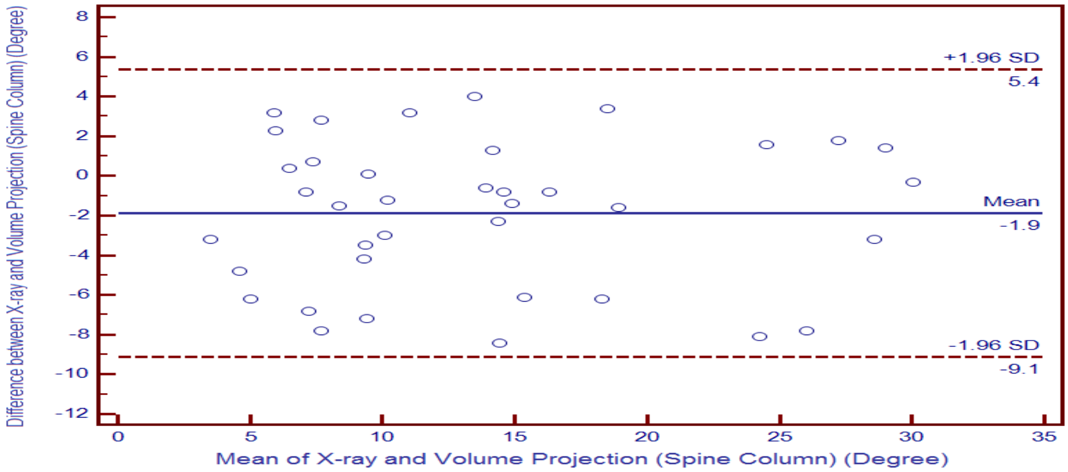

Figure 4.10. Bland-Altman plot between the Cobb's angle measured using X-ray radiograph and angle measured by the 3D ultrasound volume projection approach with spine column profile as the reference. The vertebrae for ultrasound measurement were selected according to what used in X-ray image measured. Each data point of X-ray was the mean of two measurements and that of ultrasound was the mean of two measurements.

When TP was used as the reference for measurement, the regression equation was y=0.994x (Figure 4.11), with x representing the mean of X-ray radiograph measurement and y representing the mean of 3D ultrasound measurement using volume projection approach measurement. The slope of this regression line approached to 1.0 and crossed the origin, indicating a good linear relationship. There was also a significant linear correlation between two methods (R^2=0.7779, p<0.001). The Bland-Altman plot (Figure 4.12) showed a low mean difference (d = -0.7°), limits of agreement (±1.96 SD = 7.4°), all data points located inside ±1.96 SD from the mean, and the differences symmetrically distributed around zero. It clearly indicated that there was a good agreement and no consistent bias between two methods.

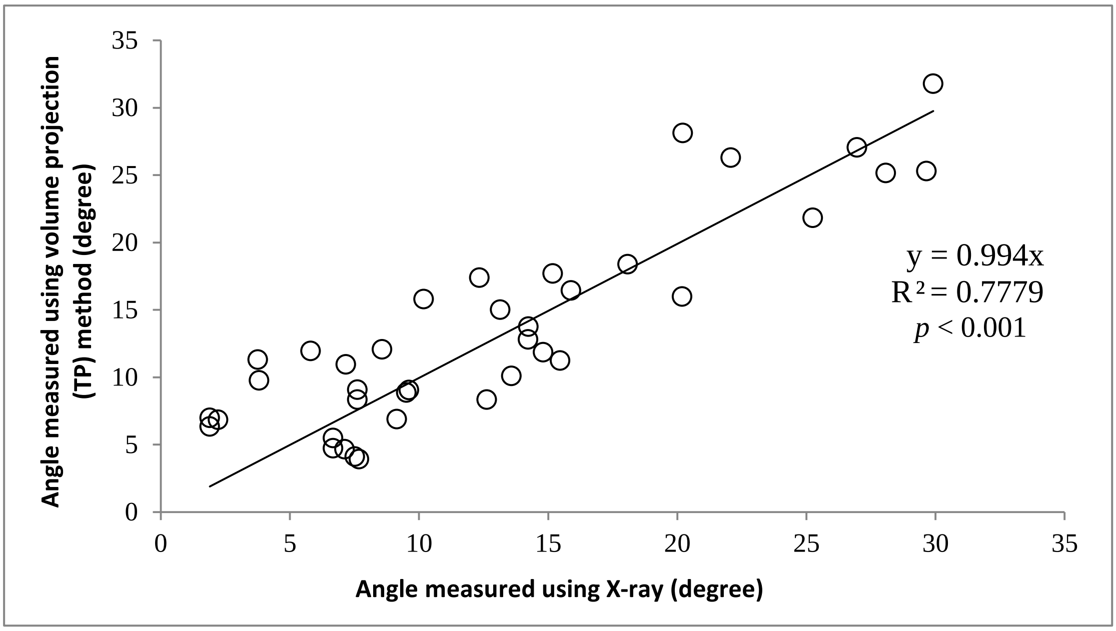

Figure 4.11. The correlation between the Cobb's angle measured using X-ray radiograph and angle measured by the 3D ultrasound volume projection approach with transverse processes forming lines as references. The vertebrae for ultrasound measurement were selected according to what used in X-ray image measured. Each data point of X-ray was the mean of two measurements, and that of ultrasound was the mean of two measurements.

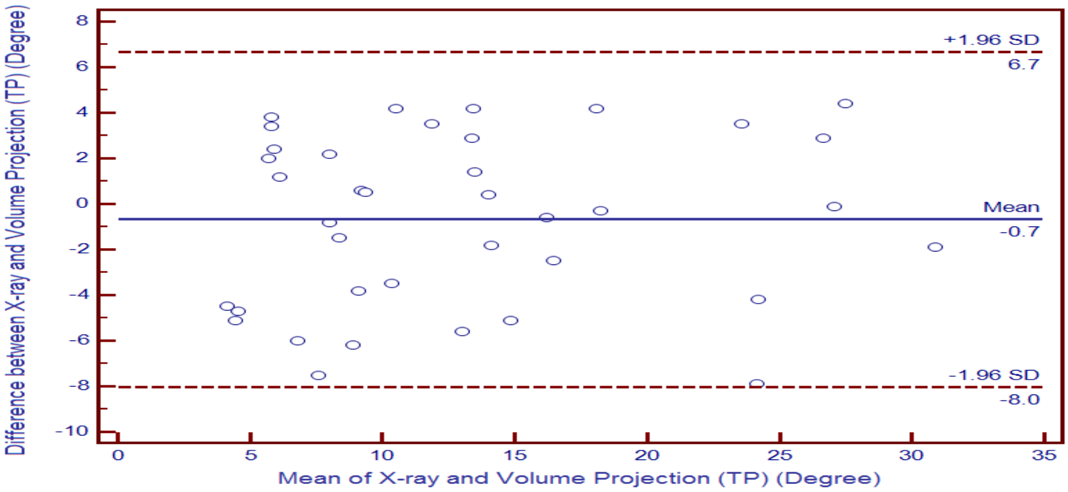

Figure 4.12. Bland-Altman plot between the Cobb's angle measured using X-ray radiograph and angle measured by the 3D ultrasound volume projection approach with transverse processes forming lines as references. The vertebrae for ultrasound measurement were selected according to what used in X-ray image measured. Each data point of X-ray was the mean of two measurements and that of ultrasound was the mean of two measurements.

It was observed that the volume projection approach could still be used to extract important bony feature for measurement even the quality of ultrasound B-mode image was relatively poor. The volume projection approach performed well for most of the cases with a good correlation, good agreement and no consistent bias. The results suggested that the 3D ultrasound imaging system with volume projection approach could be used to measure the spine curvature in human subjects.

The intra-observer repeatability tests on human subjects using the volume projection approach with the spine column profile as the reference and with TP as the reference showed that the proposed measurements were highly repeatable with ICC values of 0.99 (p<0.001) (Figure 4.13) and 0.98 (p<0.001) (Figure 4.14) respectively. The inter-observer repeatability between the two observers was also high with ICC values of 0.919 (p<0.001) (Figure 4.15) and 0.961 (p<0.001) (Figure 4.16), for the measurements using the spine column profile and TP as references, respectively. The results indicated that the 3D ultrasound measurements using the volume projection approach were operator independent.

In the repeatability tests introduced above, the data were collected by a single operator and the obtained images were processed by two observers. When two observers independently conducted scanning and measurement for 11 subjects twice, the intra-observer repeatability test of the measurement using the volume projection approach with the spine column profile as the reference was high with an ICC value of 0.975 (p<0.001) for the observer 1 (Figure 4.17). The ICC value was 0.946 (p<0.001) for the observer 2 (Figure 4.18).

The inter-observer repeatability tests of the measurement was high with an ICC values of 0.92 (p<0.001) (Figure 4.19), when the two observers conducted scan and analyzed their own data. When the data obtained by the two observers were analyzed by the third observer, the ICC value was 0.916 (p<0.001). For the data collected by observer 1, the ICC value was 0.958 (p<0.001) when the results obtained by the observer 1 and the third observer were compared. The ICC value was 0.954 (p<0.001) when the data obtained by observer 2 were analyzed by observer 2 and the third observer. The results showed that the measurements using 3D ultrasound volume projection with the spine column profile as the reference were very repeatable for the scanning as well as image analysis for measurement.

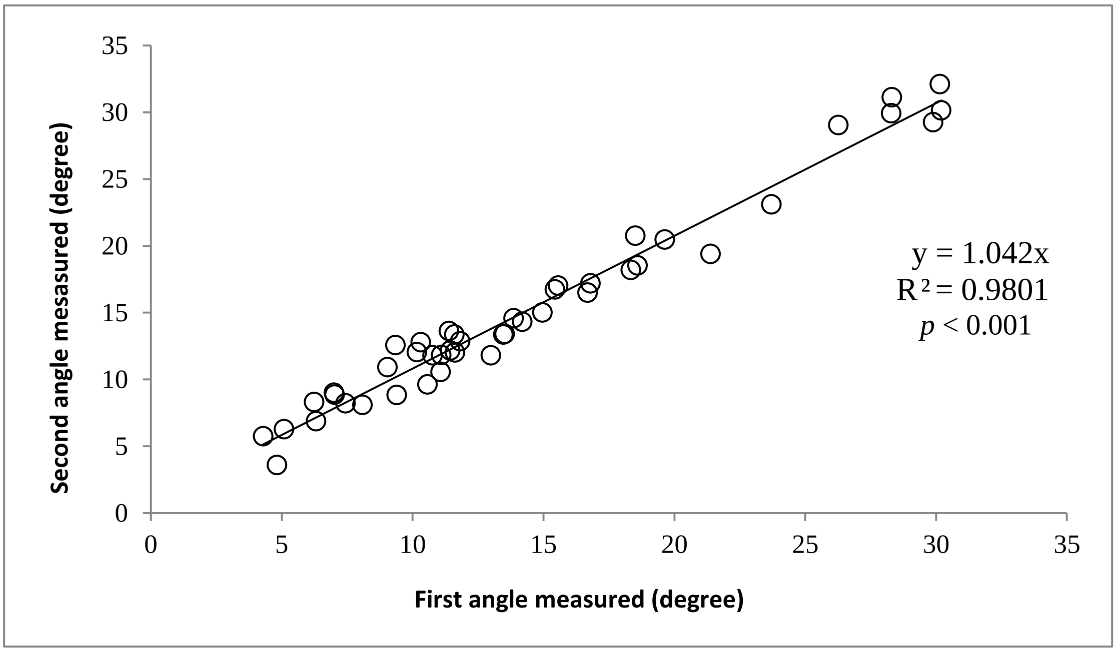

Figure 4.13. The correlation between the angles measured by the same observer using 3D ultrasound volume projection approach with spine column profile as the reference. The vertebrae for ultrasound measurement were selected according to what used in X-ray image measured. Each data point of ultrasound was the mean of two measurements.

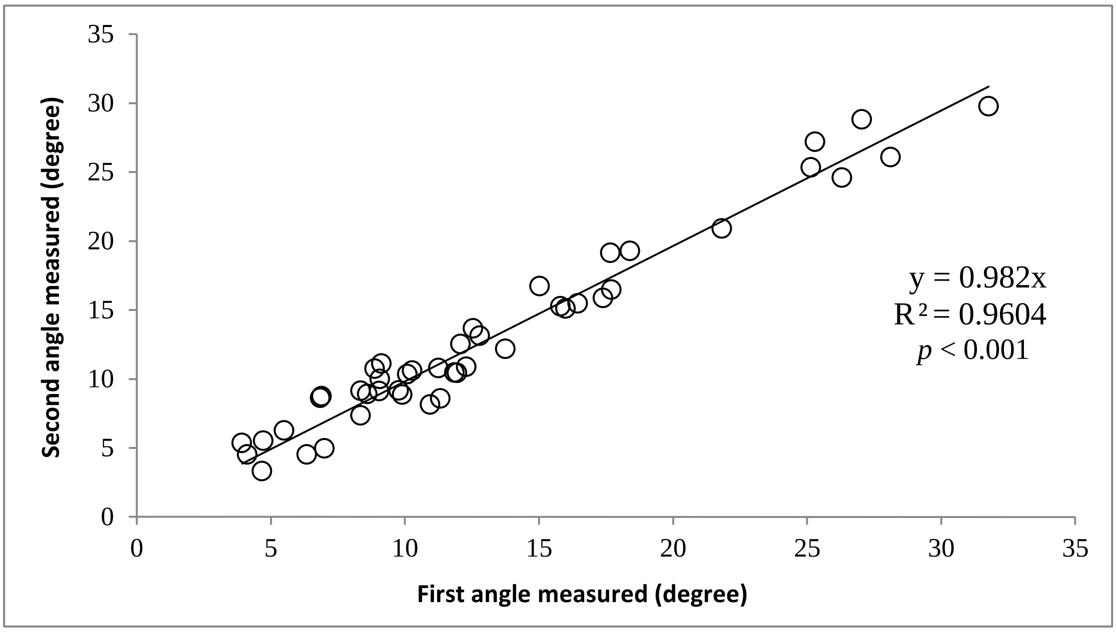

Figure 4.14. The correlation between the angles measured by the same observer using 3D ultrasound volume projection approach with transverse processes forming lines as references. The vertebrae for ultrasound measurement were selected according to what used in X-ray image measured. Each data point of ultrasound was the mean of two measurements.

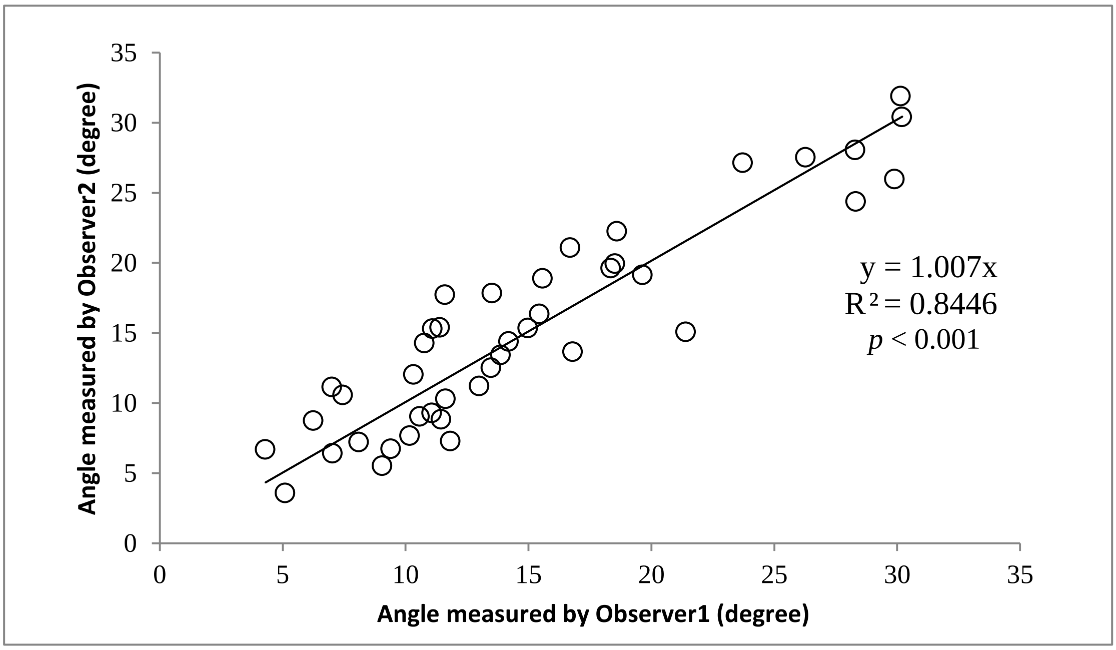

Figure 4.15. The correlation between the angles measured by the same observer using 3D ultrasound volume projection approach with spine column profile as the reference. The vertebrae for ultrasound measurement were selected according to what used in X-ray image measured for observer 1, observer 2 had no such information. Each data point of ultrasound was the mean of two measurements.

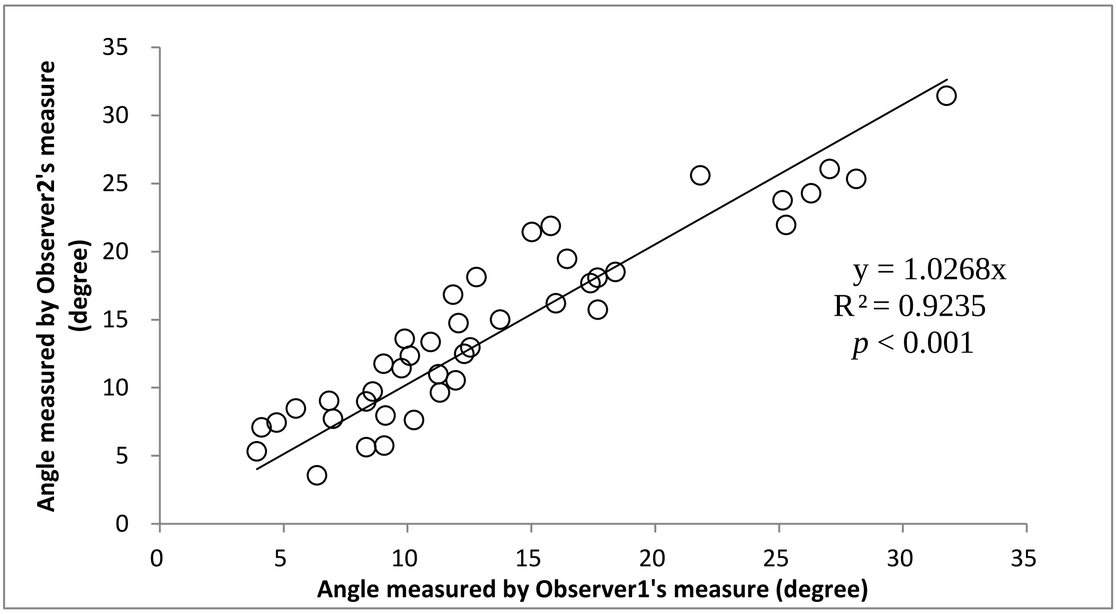

Figure 4.16. The correlation between the angles measured by the same observer using 3D ultrasound volume projection approach with transverse processes forming lines as references. The vertebrae for ultrasound measurement were selected according to what used in X-ray image measured for observer 1, observer 2 had no such information. Each data point of ultrasound was the mean of two measurements.

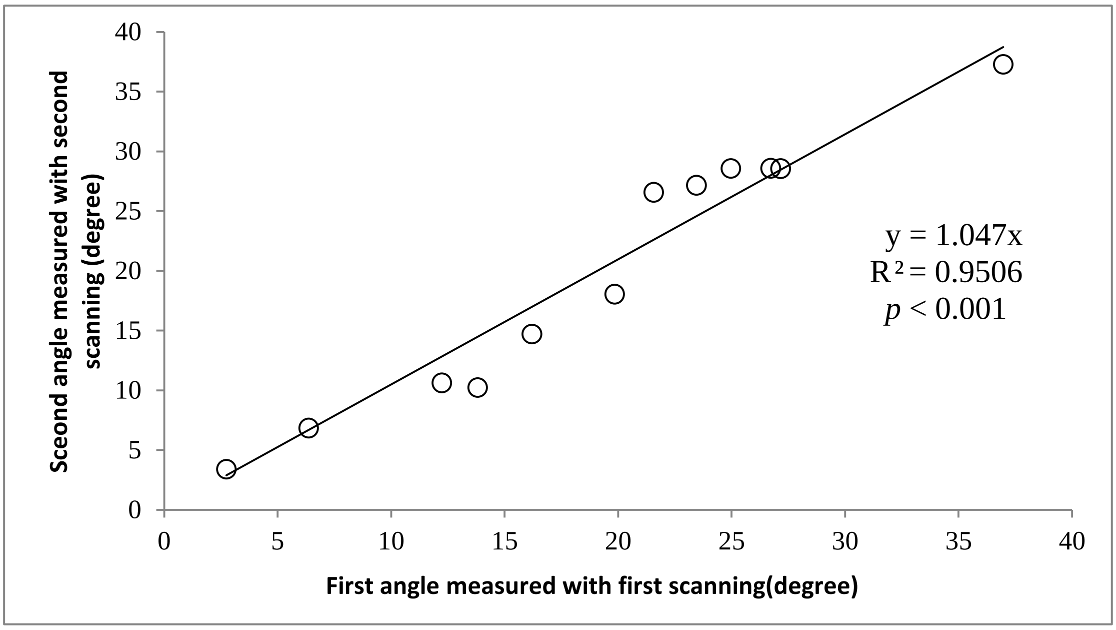

Figure 4.17. The correlation between the angles measured by the observer 1 using the 3D ultrasound volume projection approach with the spine column profile as the reference. The observer 1 conducted scan and analyzed using own data.

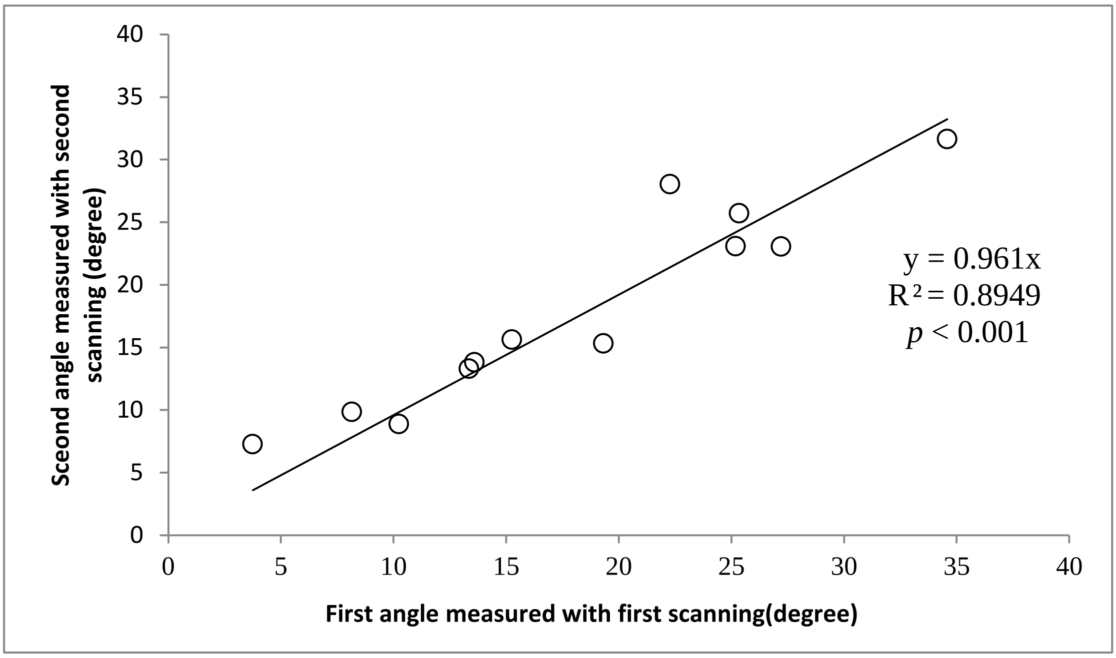

Figure 4.18. The correlation between the angles measured by the observer 2 using the 3D ultrasound volume projection approach with the spine column profile as the reference. The observer 2 conducted scan and analyzed using own data.

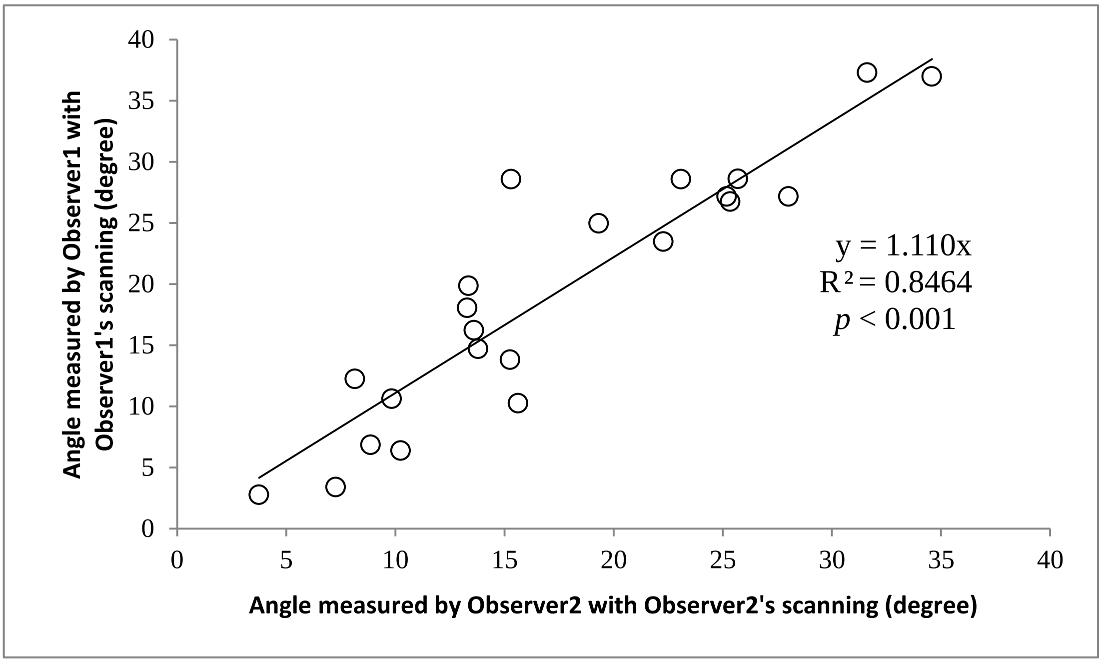

Figure 4.19. The correlation between the angles measured by the two observers using the 3D ultrasound volume projection approach with the spine column profile as the reference. The observers conducted scan and analyzed their own data independently.

CHAPTER 5 DISCUSSION

In this study, a freehand 3D ultrasound imaging method for the radiation-free assessment of scoliosis has been successfully developed together with preliminary tests on subjects with scoliosis. This chapter discusses the methods used, results of system evaluation, limitations, possible causes of errors, and potential improvements. The comparison between this new system and other available radiation-free methods for the measurement of spine curvature is also discussed. Finally, various potential applications are discussed.

5.1 3D image stack approach and choice of landmark

In the 3D image stack approach developed in this study, transverse processes were used as references for the measurement of spine curvature for scoliosis. In the initial stage of development, measurements using different sets of processes were tested, and finally the transverse process was selected as a reference because of its superior performance in comparison with others. It is worthwhile to have a systematic understanding about this selection by reviewing related findings reported previously in the literature.

Given that spine is a relatively complex and articulated structure with natural biological variability, there are many possible way to use of the bony structures as geometrical landmarks to devise the spine curvature. The question is which set of spinal landmarks is most suitable for the 3D ultrasound measurement. Some landmarks may appear ambiguous in 3D images even with well-defined shapes in 2D images (Vrtovec et al. 2009). Spine US scanning can be performed in the transverse (axial scan) or longitudinal (sagittal scan) plane. In our preliminary trials, it was found that the transverse scan was more convenient to be conducted in standing posture and it was particularly useful for covering the whole spine in a single swap. It was found that US B-mode images obtained in the transverse plane covered majority of posterior column of spine and part of middle column of spine according to Denis classification (Denis 1983). Vertebra processes were found to be more easily identified in comparison with other spinal landmarks because of its sharp delineation in the US B-mode images. The processes, therefore, were chosen as candidates of the geometrical landmarks for the spine curvature measurement.

A typical vertebra consists of four articular processes, two transverse processes, and one spinous process. The spinous process has been previously used as a landmark for devising spinal curvature. Herzenberg et al. (1990) purposed a spinous process angle for measuring spinal curvature using spinous process tip as the landmark. However, the authors reported that the spinous process angle was found to underestimate the degree of spinal curvature in comparison with the Cobb's method, particularly where appreciable axial rotation presented. In fact, vertebral axial rotation with vertebral lateral deviation is one of the abnormalities observed in idiopathic scoliosis deformity. It was also suggested that the magnitude of vertebral axial rotation correlated with the lateral deviation of vertebrae from the spinal axis, and the rotation maximal was found near the curve apex (Stokes et al. 1991). As scoliotic deformity is characterized by both lateral curvature and vertebral rotation, the vertebrae and spinous processes in the area of major curve rotate toward the concavity of the curve while the disease is progressing. On the concave side of the curve, the ribs are closed together; in contrast, the ribs are widely separated on the convex side. When the vertebral bodies rotate, the spinous processes increasingly deviate to the concave side and the ribs also follow the rotation of the vertebrae (Middleditch et al. 2005). In fact, vertebral rotation is one of the spinous process deviations. Van Schaik et al. (1989) reported that the spinous process deviation could lead to a number of consequences, including the developmental asymmetries of the neural arch, rotation of entire vertebra, and isolated deviation. It may cause confusion in interpretation of the PA radiographs of spine and may imitate vertebral body malalignment (Mellado et al. 2011a; 2011b). These consequences may possibly hinder spinous process as a good landmark.

On the other hand, deviations of transverse process similar to spinous process have not been widely reported. It was reported that transverse process features with enlarged or elongated anterior tubercles, which is commonly found in cervical vertebra C7 (Brewin et al. 2009). Transverse process elongated in lumbar vertebrae has also been reported (Eom et al. 2010; Thawait et al. 2012). Denis (1983) reported that minor spinal injuries occurred in both transverse process and spinous process. However, transverse process elongation and injury are not frequently occurred. These findings suggested that transverse process may be a suitable candidate as a geometrical landmark. Therefore, the 3D image stack approach based on transverse process as a reference was developed.

In this study, the virtual 3D model of phantom spine (from L5 to T1) was established based on the landmarks obtained from US images. The system could provide the deformity information of the spine phantom in any view plane. As X-ray radiograph for scoliosis examination is conducted in posterior-anterior plane, the landmarks projected on the coronal plane were measured in this study. The results of the spine phantom test demonstrated that the relationship between Cobb's angle (x) and the angle (y_u) measured using the 3D image stack approach with a pair of transverse processes as the reference was $y_u = 0.9671*x$, with a good correlation ($R^2 = 0.7586$, $p<0.001$). Very good intra-operator (ICC=0.99, $p<0.001$) and inter-operator (ICC=0.89, $p<0.001$) repeatability were also demonstrated. The findings suggested that transverse process could be a suitable landmark for measuring the spinal curvature for scoliosis using the 3D image stack method.

In spite of the encouraging results demonstrated in the phantom study, some limitations of the current system were identified. The procedure of manual placing markers on the tips of process was time-consuming, and the results might strongly depend on the quality of US images and the subjective interpretation from the operators. As ribs and muscle were absent in the phantom, the flexible phantom allowed great number of possible forms of deformation. Although the phantoms were mounted on the frame, the relative moment could be induced during transportation between the X-ray radiography clinic and the ultrasound laboratory. Another possible source of error in the phantom study was a problem of steering the ultrasound probe under water. It was because the buoyancy effect constantly drove the probe up. The operator needed to undertake training before scanning so as to maintain a steady speed and correct moving direction as good as possible. However, the operator was found inevitable to swiftly alter the moving path and create motion artifact, particularly in the severely curved phantoms. As a result, the ultrasound images were blurred because of the unsteady motion. The ultrasound reflection from the wall of water tank was further aggravating the image quality. In addition, viewing of operator was hampered by the opening of the water tank; moving direction of operator was impeded because of the arm movement restricted by the water tank. Under these conditions, the high quality of image acquisition was difficult to be maintained.

In the human subject test, some subjects were found with thick subcutaneous fat. It was reported that image quality of ultrasound would be degraded under thick subcutaneous fat tissue (Carpenter et al. 1995). Studies also reported that obesity and adiposity were associated with poor US B-mode image at different anatomical locations (Almeida et al. 2008; Magnussen et al. 2011; Shmulewitz et al. 1993). As the 3D image stack approach considerably depends on the quality of US B-mode image, locating the tip of transverse process from the image was more challenging, particularly for those subjects with high BMI. One subject with the highest BMI among the subjects was excluded from the analysis using the 3D image stack approach. This is because observers reported that some tips of transverse process in lumbar region of this subject were unable to be identified. Finally, 28 human subjects were included for the subject test. For the subjects tested, the relationship between the Cobb's angle (x) and the angle measured using the 3D image stack approach (y_u) was $y_u = 0.6434*x$, with moderate correlation ($R^2 = 0.6806$, $p<0.001$). The results also showed moderate intra-operator (ICC=0.565, $p=0.0045$) and inter-operator (ICC=0.75, $p<0.001$) repeatability. Concerning that relative poor quality of US B-mode images were found in the subjects comparing with the phantoms, the subjective manual marking procedure could be substantially affected. Reduction in repeatability and correlation could be probably inevitable. In addition, significant drifting away from 1.0 in the linear relationship suggested that some systematic error could probably exist. Use of tissue harmonic imaging could be considered as a solution to the problem. As ultrasound signals with the second harmonic frequency are generated beyond the body wall structure, the effect of presence of thick subcutaneous fat is mitigated. Because of the higher frequency, the axial and lateral resolutions are also significantly improved. It was reported that tissue harmonic imaging provided a greater lesion visibility and more concrete diagnosis in patients with abdominal disease and BMI index over 30 (Choudhry et al. 2000).

As transverse processes vary in sizes and lengths, it was difficult to identify the best position of tip on the large transverse processes, particularly in the lumbar region. In addition, lower lumbar vertebrae locate deeply under thick muscle groups. One reason for the systematic error was that the tips of transverse processes in the lumbar region could be confused with other muscle interfaces, which made more difficult for identification. This could also be the leading cause for undetected transverse processes and missing data points in Table A.4 and A.6. Vertebral rotation could also cause tips of processes relocated deeper and out of the preset range of ultrasound viewing depth in some cases. This may also contribute to the missing tips of transverse process. Some problems may be solved by lowering down the ultrasound frequency to 3 MHz and using persistence imaging technique to reduce noise.

It is reasonable to believe that improving in ultrasound B-mode imaging technique could lead to a better result in the 3D image stack approach. However, better image quality often requires high cost ultrasound machine. Building a virtual spine model for subject is also a time consuming and tedious task. In practice, building a comprehensive virtual model could be avoided if the most tilted vertebrae were determined by PA standard radiograph in the first place. It may be unnecessary to build a whole virtual spine model to monitor change of spinal curvature, which could be determined by the landmarks on the preselected vertebrae. In a complete flow of spine treatment, only before treatment radiograph and after treatment radiograph would still be necessary for diagnosis and treatment outcome measurement. Significant numbers of radiograph examination could be avoided by using the 3D US for monitoring the change during treatment. The findings of studies abovementioned suggested that derivation spine curvature from the 3D image stack approach may be a practical and viable option.

Blurred B-mode image in lumbar region may possibly be the main error of the 3D image stack approach. It is necessary to develop new technique to overcome the problem of quality of image. Regarding reconstruction an image from multiple B-mode images for reducing noise using image processing technique such as averaging, volume reconstruction may be considered as one of the solutions. Identification of transverse process from spine volume was not performed at the initial stage of this study because of the limitation of desktop computer internal memory size, rendering time, parameters adjustment of transfer function, possible interpolation errors, and tedious work warranted for adjusting process of reslicing volume to locate the processes. In fact, the concept of the 3D image stack approach and system utilized in the earlier study was conceived to evade the problem of volume rendering using those raw B-mode ultrasound images with processes to build a virtual spine model for conducting measurement.

5.2 Volume projection approach

With regard to the weakness of the abovementioned 3D image stack approach and advancement of desktop computer, volume projection approach has been developed for surmounting the problems. Volume projection approach exploited all ultrasound images and different visualization techniques to create a representative image for denoting spine. The central idea of this technique is to highlight the shadow created from the strong ultrasound echo reflected from bone surface. As a result, bony landmark would not be required to identify in individual B-mode images. Therefore, the quality requirement for single image was considerably reduced. The effect of high BMI problem caused low quality of B-mode image would also be greatly lessened. As the spinal image formed also allowed direct curvature measurement on the image resemble to the measurement conducted on radiograph, tedious manual marking of landmark was eradicated. The volume projection approach was substantially explored for devising a better measurement protocol and comparing with Cobb's method. With the advantage of this new approach, the scan data of the subject excluded in the 3D image stack approach was also included in the analysis, making total 29 subjects involved.

The results of the subject test demonstrated that the volume projection approach using transverse process as a reference was reliable with good correlation (R^2 = 0.7779, p<0.001) between the Cobb's angle (x) and the 3D US measurement (y_u), y_u = 0.9943*x. The intra-operator repeatability of the measurement was very high (ICC=0.98, p<0.001). A similar result was achieved when the spine column profile was used, with y_u = 1.0744*x (R^2 = 0.7903, p<0.001) and very good intra-operator (ICC=0.99, p<0.001) and inter-operator (ICC=0.919, p<0.001) repeatability. The findings suggested that systematic error observed for the 3D image stack approach was eliminated, as the liner regression coefficients were very close to 1.0 for the two volume project methods. The maximum SD in the 3D image stack approach was 7.1°. In contrast, it was 2.0° and 2.5° for the volume projection approach using the spine column profile and TP as references, respectively. The findings suggested that the volume projection approach demonstrated a significant smaller variance. Instead of using the tip of TP as the reference in the 3D image stack approach, the location of TP was much easier to be located in the volume project approach. It was the main reason why the volume projection approach was outperformed 3D image stack approach in the subject test. Overall, the repeatability, linear coefficient and correlation were significantly improved when comparing with the 3D image stack approach. Comparing the two references used for the volume projection approach, using the spine column profile as the reference was slightly better in the correlation with the Cobb's angle. In addition, two images had to be selected to measure the spine curvature when TP was used as the reference, as the TPs of different vertebrae might not all clearly observed in a single projection image. In contrast, a single image was enough using the spine column profile as the reference. As a result, the variance of angle measurement was shown reduced using spine column as the reference. It was also more convenient and time-saving to use a single image to measure the spine curvature resemble to the measurement of Cobb's angle using X-ray radiograph.

With such an advantage, the subsequent study was focused on further proof of repeatability of the volume projection approach using the spine column profile as a reference with measurement and scanning. Eleven subjects were recruited for purpose the systematic investigation of measurement repeatability. Observer 1 and observer 2 were instructed to conduct scan and analysis using the spine column profile as a reference for these subjects. Observer 3 was instructed to conduct the measurement on both observers' scans. The ICC values for intra-observer repeatability of observer 1 and observer 2 for the scan-analysis were 0.975 (p<0.001) and 0.946 (p<0.001), respectively. The inter-observer repeatability of analysis conducted by observers 1, 2 and 3 using the scan data collected by either observers 1 or 2, all the ICC values were all larger than 0.92 (p<0.001) . The results of intra-observer and inter-observer tests strongly suggested that the volume projection approach using the spine column profile as a reference was repeatable. These studies also demonstrated that the 3D US methods were considerably compatible with X-ray Cobb's method. With implementation of the volume projection approach, scanning, image formation and image analysis could be completed in several minutes. It evidently suggested that volume projection approach using the spine column profile as a reference could be a good candidate for spinal curvature measurement.

5.3 Limitations, sources of error, and potential improvements

The basic clinical protocol of acquisition 3D US images of spine has been developed, and subjects with different degrees of spine curvatures were successfully evaluated by the newly developed system. However, there were several limitations of the data in the subject test. The range of spine curvature was limited to lower range because of scoliosis patient availability. Patients with larger degree of spine curvature were found to be more difficult to be recruited. It may be due to the fact that the patients with larger degree of spine curvature trends to be treated properly. All the subjects recruited in this study had undergone coronal X-ray radiograph, the range of spine curvature measured using Cobb's method was from 2° to 30°, indicating that the data set was adequate for mass screening. This is because scoliosis diagnostic uses 10° and

20° as criteria for categorizing the subjects into normal, under monitoring, and brace treatment warranted. However, the results might not indicate that patient with larger degree of curvature could be accurately measured, as the data range in the study was not covered well above 30°. Indeed, the surgery is warranted with the curvature reached 40° or above. In future large scale clinical trials, extended in curvature range would be clearly needed. However, severe spinal curvatures may lead to difficulty in scanning and image formation. Scanning procedure and volume projection image formation algorithm may have to be revised. New assistive tools for maintaining the posture of patient with severe curvature need to be developed.

The time difference between the 3D US scanning and the radiograph produced might introduce the inaccuracy. As some subjects were teenager youngsters with skeletal immaturity, rapidly change in scoliotic curvature could possibly occur within a short period. The position of subject and position of radiographic tube, when radiograph was taken, might also affect the results (Morrissy et al. 1990). As the subjects were undergone radiograph in different laboratories, some inconsistency might exist. X-ray radiograph for subjects should be better conducted in the same radiography clinic in future study.

As the cinema playback mode in 3D image stack approach mitigates the operator workload to locate the best US B-mode image with transverse process, the operator didn't examine all frames one by one. To find a transverse process, it was first coarsely located by the cinema playback mode using keyboard's arrow keys for navigation; when the transverse process was located, the operator had to examine the nearby a few US B-mode images one by one and selected the best one with a transverse process tip to manually place the marker. It is possible to select an image which might not be the image best representing the bony landmark. In fact, locating the tip of transverse process depends on the operator skill, experience, and quality of US B-mode image. As 2000 or more US B-mode images were collected for each scan and the length of scan was less than 50cm in most of the cases, the average distance between two consecutive US B-mode images was less than 0.25mm; the second or third image next to the best US B-mode image selected from nearby US B-mode images for marking may not significantly affect the curvature measured. Using Cobb's method, 5° difference in measurement has been generally accepted (Wills et al. 2007). It is possible for the operator to incorrectly select a feature not representing the process. With the availability of corresponding volume projection image, the location of transverse process could be first located in a 2D volume projection image and automatically select the closest raw B-mode image for the operator to mark the transverse process, making the possibility of incorrect selection of process minimized.

Full automatic detection of tip of transverse process is highly possible in thoracic region. This is because these transverse processes have more regular size and shape; image recognition will be more effective. For instance, a specific meniscus temple could be exploited to detect the tip of transverse in raw US B-mode; while an O-ring or a spot temple could be exploited to detect the corresponding transverse process in volume projection image. With successful detection of the transverse process from these images, its complete spatial information could be devised. These automatic detections could also be used to refine the spatial information in manual marking and vice versa. Whereas, spinous process and transverse process in lumbar region are not in well-defined shape and size, making the temple based recognition approach less effective. Spinous process deviation and vertebra rotation in lumbar region might be further aggravating the possibility of correctly locating these processes. New approach should be investigated.

The volume projection approach required a smooth surface as a reference for performing the non-planar cutting for image projection. Since the B-mode images of the spine phantoms could not provide a smooth surface for the reference, the data obtained from the phantoms could not be used for generating volume projection image. This is the reason why no result was reported for the phantoms using the volume projection method. In future studies, phantoms with simulated curvatures should be covered by silicone or other materials to better mimic the human body. With the new phantoms, operators could be trained to handle scanning spines with in different curvatures and produce qualified images before conducting examination on subject.

The electromagnetic spatial sensor used in this study was sensitive to metal nearby. In our study, the metallic parts and structure inside US probe and attached wires possibly created some distortion in the electromagnetic field leading to a system offset or transient jitter generated in the spatial data. Concerning the processes located at different depths, the developed system was preset with a set of optimal parameters. This could affect the identification of process more seriously when greater difference in tissue thickness and properties from different region observed in the subject. As the vertebra position could be estimated from the spatial sensor, the vertebra could be identified. Preset US imaging parameters could be dynamically changed according to the identified vertebra. Given that the US control parameters including beam focus, beam direction, time gain control, dynamic contrast, and frequency could be adjustable according to the different spatial position in real time. Quality of images could be further improved with a mechanism of automatic adjustment of these imaging parameters.

Noises in ultrasound image and errors of calibration could affect the quality of image reconstruction and measurement. Thus, ultrasound compound imaging was used in our studies so as to minimize the noise; over-sampled data were captured in the calibration procedures to reduce the variation. These measures were introduced to improve the overall measurement accuracy.

Image quality and data size are other issues. In the subject test, compounding images and reduction in dynamic contrast in US equipment were used to enhance the bony edge and structure for improving image quality of the ultrasound. However, these features may vary among different ultrasound scanners. Obtaining raw RF images for processing could allow more viable image processing. A large set of US images could cause long data processing time and storage problem. Given that the most tilted vertebrae are known from radiograph, these vertebrae should be scanned alone instead of whole spine scan. This would reduce the raw data size considerably. Such an approach would be suitable for follow-up monitoring. Alternatively, image pattern recognition techniques could also be designed to reduce the selection time for identifying image with tip of process, mitigating subjective identification of process. Dedicated ultrasound image enhancement methods should be developed to facilitate the identification of the process tip and enhance bone delineation. Automatic or semi-automatic methods, therefore, could be developed to reduce the manual efforts in identifying tip of process in 3D image stack approach. As the transverse process and spinous process on thoracic vertebrae are prominent in ultrasound image, developing an automatic marker tip location module of these processes could probably be implemented. In contrast, the identification of processes on lumbar vertebrae could probably be more challenging; semi-automatic process identification procedures and assisting tools could ameliorate the problem. The automatic and semi-automatic methods in volume projection approach should be developed. A curve, which denotes the curve of spinal column, could be devised from the volume projection image. The inflection points from the curve could be exploited for measuring the spine curvature.

5.4 Comparison with other spinal curvature measurement systems and methods

The validations of other radiation-free assessment systems for scoliosis have previously been reported. Quantec system, based on a surface topographical technology, and Ortelius 800, based on electromagnetic spatial sensing, are commercially available in UK and US. It was reported that the spine curvature measured by the Quantec system (y_q) had a linear correlation with the X-ray Cobb's angle (x) with $R^2 = 0.66$ and $y_q = 2.91+0.52*x$ (Goldberg et al. 2001). For Ortelius 800 system, it was reported that the correlation between the results of the Ortelius 800's measurement and the Cobb's method was poor ($R^2 = 0.42$ for thoracic curvature data, and $R^2 = 0.017$ for lumbar curvature data) (Knott et al. 2006). In our 3D ultrasound volume projection approach using the spine column profile as a reference, a very good correlation was found between the 3D ultrasound measurement (y_u) and Cobb's angle (x) ($R^2 = 0.79$, $y_u = 1.0744*x$). Comparing Quantec system and

Orthoscan Ortelius 800, the findings in our study suggested that the 3D ultrasound system was notably outperformed. It should also be noted that the data reported for the two commercial systems were from human subjects with larger range of spinal curves than current studies. Therefore, further comparison in wider range of curvature is necessary.

Spinous process angle (y_s) also demonstrated a very good correlation with Cobb's angle (x) ($R^2 = 0.903$, $y_s = -1.0404+0.74813x$) (Herzenberg et al. 1990). The spinous process angle was performed slightly better in correlation comparing with the 3D US volume projection approach. A possible explanation for the outperformance is that spinous processes actually reflect the pure geometric relationship between same modality because it devises the angle from the same radiograph image for producing Cobb's angle. The subject needed not to undergo to two examinations. In contrast, the correlation between the 3D US volume projection approach and radiograph represented the correlation between different imaging modalities. The subjects underwent radiograph examination and the 3D US scanning at different time and places, resulting in a greater variance. However, the 3D US volume projection approach outperformed the spinous process angle with approximated same angle as Cobb's method produced. The spinous process angle significantly underestimated Cobb's angle, as spinous process angle was produced from the tips of the spinous processes, which is more deviated with vertebral rotation. In contrast, images produced from the 3D US volume projection approach involved a layer of tissue with 1 cm in thickness for projection. The starting layer was below the tip of spinous process. The resultant shadow involved not only the tips of spinous processes, but also involved whole spinous processes, ridges and laminas. The vertebral rotation might cause the widening of the spinal column shadow in the image. Effect of small spinous process deviation or vertebral rotation could be embedded inside shadow. As the midline of shadow column was selected as the reference line, the effect from larger spinous process deviation or vertebral rotation could also be lessened. This is because the shift in shadow column midline was always less than shift in tips perpendicular to the axis of rotation. This unique feature made the 3D US volume projection with the spine column as a reference has an advantage over other methods.

5.5 Potential applications

Scoliosis has been increasingly recognized as a 3D spine deformation problem with substantial researches being conducted for characterizing and measuring the spine in 3D (Herzenberg 1990). Yazici et al. (2001) suggested that AIS should be evaluated on coronal, sagittal, and traverse plane with standing posture. The vertebral rotation of spine is also important for predicting prognosis and monitoring the progression; however, no rotation information can be directly acquired by a standard chest radiograph, accurate measurement of degree of rotation cannot be undertaken (Yazici et al. 2001). It was report that the degree of vertebral rotation could be measured using computed tomography (CT) (Aaro et al. 1981). Recently, Kouwenhoven et al. (2006) conducted a study of preexistent vertebral rotation in whole normal spine; however, problems of locating landmarks and neutral reference still persisted. Although CT and MRI provide high quality images in 3D, almost all these equipment require the patients being imaged in supine position. This is because limited availability of standing posture 3D imaging equipment such as recently released Upright multi-position MRI (Fonar Corporation, Melville, NY, USA).

It has been reported that the spinal deformity indices, such as vertebral rotation can be derived by ultrasound B-mode image (Suzuki et al. 1989). It was reported that there was a linear relationship between the Cobb's angle and the rotation of the thoracic and the lumbar spine in brace untreated patient. The rotation of spine was measured by recording the probe's inclination through an attached inclinometer when the transverse processes and the laminae from both sides of same vertebra displayed on B-mode image becomes the same level on the screen through manual inclination adjustment (Suzuki et al. 1989). Despite simplicity of the approach, the Cobb's angle could not be accurately measured. As 3D image approach uses transverse process as the reference, this might suggest that vertebral rotation angle of an individual vertebra could be devised from the virtual spine models using the position information of transverse processes from the vertebra. This also indicates that the developed system might be potential to further develop useful rotational parameter for clinical usage. Vertebral rotation measurement development, however, was excluded in this study because neither CT nor MRI data were available from the subjects for comparison. Further studies should be considered along this direction. With no significant correlation between the amount of scoliosis and the amount of kyphosis (Stokes et al. 1987), development was focused on coronal plan. With the 3D virtual spine model, the measurement of other forms of spine deformation such as kyphosis and lordosis could also possibly be developed. Lateral view curvature assessment methods using processes and volume projection have still been conceived. Comparing with spinal curvature in PA view, it is more difficult to measure the angle of individual vertebra, because there is no simple reference line devised using transverse processes. One possible solution could be developed using all landmarks to produce a tendency line with suitable curve fitting algorithm; with the tendency line, the inflection points and its respected angle could possibly be measured. Similarly, the data recovery technique in volume projection was inadequate to produce an image for directly measuring curvature because skin could not be the reference for reslicing in LA view. A new imaging approach has been speculated using vertebra column shadow as a non-planar curve reference to produce a lateral view image and applying techniques including TRAILL method (Chernukha et al. 1998) and posterior tangents (Harrison et al. 1996) for measurement.

As the developed system provides unlimited usage, change of spinal curvature could be assessed intermediately with different stimulated situations. School-age children are always carrying books and personal belongings; it has been considered as a constant load bringing problem (Chow et al. 2005; 2006). Abnormal external loading has been speculated as one of the possible reasons, leading to exacerbate spinal deformity. Thus, children are frequently recommended to carry balanced load over the shoulders. Cheng et al. (2013) exploited the developed system to reveal the change of spinal curvatures using different weights over one side of shoulder. As asymmetric and side-shift exercises have been suggested as effective therapeutic exercises for scoliosis management, the developed system could be useful for monitoring the effect of different loads and adjusting the weight for providing an effective therapy.

Li et al. (2010) exploited a 3D freehand ultrasound system for assisting the fitting procedure of spinal orthosis using spinous process angle to devise spine curvature. However, it was time consuming to locate the spinous processes. The developed system could provide much quick assessment with volume projection approach for facilitating usage.

McLeod et al. (2008) suggests that ultrasound imaging may have a potential role to facilitate insertion of epidural catheters in scoliotic patients. Anaesthesia in spine could be further benefited from the developed system with a better viewing of spinal deformation and possibly mitigating location target sit.

5.6 Future studies

As elaborated in the last section, the newly developed system may have many potential applications. As spine is a musculoskeletal system, the paraspinal muscles problem has been concerned. The paraspinal muscles size asymmetry in AIS patient was report by Kennelly et al. (1993). The muscle size could be devised using the newly developed system. It is useful for providing information on the role of the musculature in the pathogenesis of AIS. In addition, the skeletal muscle abnormality is a factor of AIS (Tang et al. 2003), paraspinal muscle stiffness could potentially be a useful parameter for further study. It is also possible to integrate the stiffness information into the developed system to provide more detail diagnosis.

Scoliosis patent is usually undergone radiograph in PA and LA view. It is obvious that the developed system should be capable to measure the spinal curvature in LA view. DeSmet et al. (1984) reported that there was no significant correlation between degree of curvature in scoliosis and degree for curvature in kyphosis. The development effort was mainly used in PA view in order to fit the time allowed for the thesis. In fact, the volume projection approach could be applied in LA view. With the information in PA view, a new algorithm is being developed for devising new volume projection approach in LA. A study has also been planned for investigating the relationship between degree of spinal curvature using radiograph Cobb's method in LA view and degree of spinal curvature using the new volume projection approach. In addition, automatic spinal curvature measurements algorithm in both LA and PA view will further underpin the clinical application and possibly eradicate subjective factor in measurements. These automatic measurements also needed to be validated. Other form of spinal deformities including flatback and spondylolisthesis could also be included in future clinical studies.

Similarly, the vertebral rotation should be provided by the developed system using new 3D image stack approach; validation and clinical study have also yet to be conducted. CT and MRI information should be obtained for providing adequate information to study spinal deformation in three-dimension for comparison. Future studies are required to validate the measurement of the spine curvatures in all PA view, LA view as well as the rotational deformity using same subject data. However, analysis from these views is rather traditional. New parameters dedicated for 3D data analysis should be explored.

Certainly, it might not be possible to explore all potential anatomical landmarks for measuring spinal deformation in this PhD study; two approaches for measurement methods were investigated. Recently, Chen et al. (2012) investigated scoliotic curvature using the centre of lamina as a landmark using 3D ultrasound. The future investigation on other possible bony landmark including vertebra body, superior articular process, spinous process and lamina, have to be conducted.

In order to facilities further studies and development, spine phantom have to be continuously improved. Scoliosis mimicking spine phantoms could be embedded inside a thick silicone and molded into body torso shape for providing more realistic condition for spinal curvature evaluation.

One of the key factors hindering the developed system usage is cost. Substantial cost reduction should be considered. Prior to the PhD study, the author and co-workers developed a technique using web-camera to perform same function of spatial position sensor (Zheng et al. 2011). Thus, electromagnetic sensor used in the developed system could be possibly replaced by a low cost web-camera. Given that accelerometers and gyroscopes from MEMS device and a web-camera are integrated into the ultrasound probe, a reliability low cost freehand 3D ultrasound imaging system could be probably created. Video capture card, which is limiting the frame rate, image size, and quality of image, has been an important component for the developed system. In facts, it could be eliminated using special functions provided by some ultrasound manufacturers. Some ultrasound equipment have already provided the raw B-mode image over local area network (LAN) or saving into local storage. Small number of manufacturers further provide software library to be called by any custom-made program for capturing raw ultrasound image directly. With removal of the spatial sensor and video capture card, the cost of the developed could be further reduced.

It was reported that 3D image stack approach may be considerably affected by the quality of raw image. 3D image stack approach with volume projection image as a guiding could be a potential solution. Instead of marking on the raw B-mode image, the markers could be placed on the processes shown on the volume projection image. However, the markers on the volume projection image could not provide an accurate depth of the tip of process, because multiple layers of vowels are used to form the image. A new algorithm should be developed to determine the corresponding raw B-mode image containing the markers from the volume projection image; the algorithm should also be capable to determine the depth of the tip of process from the B-mode image. The speed and accuracy of marking could be dramatically improved. Mixture B-mode with volume projected image in same scene for manual marking could probably improve the new approach performance. Some ultrasound equipment also provides tissue harmonics imaging, which could further improve the quality. This imaging technology should be included into the developed system to enhance the performance of the approach.

For facilitating the practical usage of the developed system, operator and subject usage experience should be considered. In preparing scanning, gel painting and filling consumes considerable time. Prolonged use of probe by operator could cause fatigue and develop possible long term health problem. These factors may hinder the practical use of the developed system. It is important to develop a probe with a water bag and an ergonomic design handle for improving usage experience. With the state of art ultrasound equipment, higher frame rate B-mode imaging could be used in the developed system. As a result, the scanning time could be substantially reduced. Volume projection image usually consumes a few minutes in each scan. The subject and operator have to wait for the outcome and decide the necessity of re-scan. It is possible to undermine the developed system usage. With the state of art computer processing unit, volume generation speed could significantly be ameliorated using vector instructions in graphic processing unit. The volume projection algorithm should be modified using the vector instructions for providing real-time volume reconstruction and projection to eradicate the problem. As the higher computer main memory capacity in desktop PC is more popular, the developed system could allow over 10000 frames acquired in each scanning. With sufficient frames, the gap filling time during image reconstruction could be substantially reduced. It is also possible to scan the whole torso back with multiple swaps. However, there is a glaring problem; the file size also exponentially increases. In a clinic, thousands of file have to be stored and used up tremendous memory storage space. Thus, it is important to develop a file management system for handling the raw data and the image produced in future development.

There are many other important factors, which allow better management of patients with scoliosis, including coronal balance, sagittal balance and Risser grading. Glass et al. (2005) also stated that sagittal balance is the most important and reliable radiographic predictor of clinical health status. Nault et al. (2002) and Dewi et al. (2010) reported the importance of studying balance and possible improvement on the posture reproducibility. It is obvious that a balance board system should be integrated into the developed system. Risser (Risser 1948) grade is the one of the most frequently used method to determine skeletal maturity and essentially manage the patients with scoliosis. Thaler et al. (2008) suggested that ultrasound imaging could be exploited as an alternative method to X-ray radiograph evaluation on Risser grading. Risser grading evaluation software should be implemented into the developed system for enhancing the developed system feature.

It is evidently suggested that the developed system has provided a good platform for studying spinal deformity. There are many possible features and applications to be developed. However, the real challenges are still ahead to perfect the system for real clinical applications.

CHAPTER 6 CONCLUSIONS

In this study, a non-radiation free-hand 3D ultrasound imaging system for assessing scoliosis has been developed. In addition to the hardware system, a program was developed together with two approaches of scoliotic angle measurement and an assessment protocol. Phantom and subject tests were conducted to investigate the relationship between the X-ray Cobb's angle and the spine deformity obtained by the 3D image stack approach with transverse process as a reference. The results showed there was a systemic error in using the 3D image stack approach because of the inaccuracy caused by the marker identification in B-mode US images and other possible reasons discussed. The volume projection approach was subsequently developed, which provided an X-ray like image showing the spine column profile and transverse processes. The results of subject test revealed that the results obtained by the volume projection approach well agreed with the Cobb's angle. The volume projection approach using the spine column profile as a reference was further investigated with additional subjects to study the reliability of the scanning and image analysis. The results indicated that the volume projection approach using the spine column profile as a reference could be a potential clinical tool for assessing scoliosis.

Spinal curvature is the most important parameters for the evaluation of spinal deformities (Stoke et al. 1994). Radiological evaluation is important for scoliosis management in three ways including confirmation of scoliotic condition presence, assisting identification of etiology and flexibility of the deformity, and quantification of initial degree of curvature and subsequent change (Jeffries et al. 1980). Some or all these conditions should be satisfied for any imaging modality. The newly developed system has shown its potential to achieve these conditions.

In the light of this study, it can be concluded that the newly developed system provides a new way to assess AIS without radiation hazard; the ultrasound B-mode image with corresponding spatial data collected could also potentially provide measurement for spine rotation, kyphosis, and monitoring spine curvature change under load bearing condition. It could be considerably valuable for other spinal deformation study. With a portable ultrasound machine and movable supporting framework, the system developed in this study could be developed into a fully portable system to facilitate mass screening and prognosis monitor. The portable ultrasound assessment system could be relocated to small clinic or school classroom to provide mass-screening to students. The developed system has also been evidently shown its clinical potential as a mass screening and complementary equipment of radiograph Cobb's method without concerning on frequent use and time interval for progression monitoring.

The major achievements of this study are summarized as follows:

- A free-hand 3D ultrasound imaging system for scoliosis assessment was successfully developed, with a novel body supporting framework
- Two novel approaches of measuring scoliotic angles were developed, including the 3D image stack approach with transverse processes as reference marks and the volume projection using the spine column profile or transverse processes as references
- Flexible spine phantoms with different degrees of simulated scoliosis were tested to investigate the relationship between the Cobb's angle and the scoliotic angle obtained by the 3D ultrasound method.

- Subject tests were conducted to investigate the reliability of the newly developed system. It was demonstrated that the volume projection approach using the spine column profile could achieve measurement results well correlated with Cobb's method and very good repeatability.
- An assessment protocol for scoliosis subject using the 3D ultrasound imaging system was established.

APPENDIX

A. Data table

Table A.1 Comparing Cobb's Method with 3D Ultrasound Method using 3D image stack approach with TPs forming lines as references, their means and SDs in phantom study are shown below. There are two angles measured in same phantom under same round of simulated spine deformation; they are labeled as angle 1 and 2.

Phantom	Angle Number	Round Number	Cobb's Method		3D Image Stack (TP)	
			Mean	SD	Mean	SD
A	1	1	36.9°	2.5°	45.9°	2.5°
A	1	2	24.2°	1.7°	17.4°	2.9°
A	1	3	35.0°	2.6°	29.7°	1.5°
A	1	4	33.8°	1.6°	28.5°	2.2°
B	1	1	35.0°	0.1°	41.3°	2.6°
B	1	2	10.0°	2.0°	16.6°	1.9°
B	1	3	33.2°	2.6°	28.2°	4.4°
B	1	4	22.1°	1.3°	22.6°	2.6°
B	2	2	21.4°	3.0°	25.2°	3.3°
B	2	4	30.8°	0.0°	30°	2.4°
C	1	1	40.2°	1.3°	45.9°	2.3°
C	1	2	34.8°	0.4°	36.0°	3.9°
C	1	3	33.1°	0.0°	31.4°	2.0°
C	1	4	25.3°	0.1°	22.2°	1.1°
C	2	3	45.9°	1.7°	43.9°	2.0°
C	2	4	43.2°	0.5°	34.5°	2.4°
D	1	1	36.0°	1.3°	33.8°	3.9°
D	1	2	52.6°	1.3°	50.1°	3.1°
D	1	3	31.9°	0.9°	32.1°	4.4°
D	1	4	54.0°	0.1°	44.2°	3.1°
D	2	1	26.0°	1.6°	32.2°	3.5°
D	2	2	42.3°	2.1°	39.9°	3.0°
D	2	3	23.0°	0.0°	28.1°	4.9°
D	2	4	46.7°	1.9°	44.6°	2.5°

Table A.2. Results of intra-observer study of 3D Ultrasound Method using 3D image stack approach with TPs forming lines as references in two measures, their means and SDs in phantom study are shown below. There are two angles measured in same phantom under same round of simulated spine deformation; they are labeled as angle 1 and 2.

Phantom	Angle Number	Round Number	3D Image Stack (TP) Data Set 1		3D Image Stack (TP) Data Set 2	
			Mean	SD	Mean	SD
A	1	1	45.3°	3.4°	44.9°	2.5°
A	1	2	18.8°	4.5°	17.0°	1.8°
A	1	3	30.4°	0.6°	29.6°	1.3°
A	1	4	29.3°	1.8°	29.7°	2.5°
B	1	1	39.3°	3.0°	42.2°	1.5°
B	1	2	15.9°	2.0°	16.4°	2.4°
B	1	3	29.8°	3.1°	30.8°	4.7°
B	1	4	23.2°	3.2°	22.8°	2.5°
C	1	1	45.5°	0.5°	44.7°	2.4°
C	1	2	38.0°	3.2°	36.9°	3.9°
C	1	3	32.6°	1.2°	30.9°	2.9°
C	1	4	22.3°	0.8°	22.1°	1.6°
D	1	1	32.8°	8.0°	33.6°	4.3°
D	1	2	50.8°	1.8°	52.2°	1.9°
D	1	3	33.9°	2.9°	34.0°	5.2°
D	1	4	42.5°	2.8°	46.2°	3.1°

Table A.3. Results of inter-observer study of 3D Ultrasound Method using 3D image stack approach with TPs forming lines as the references for the two observers, their means and SDs in phantom study are shown below. There are two angles measured in same phantom under same round of simulated spine deformation; they are labeled as angle 1 and 2.

Phantom	Angle Number	Round Number	3D Image Stack (TP) Observer 1 Data Set		3D Image Stack (TP) Observer 2 Data Set	
			Mean	SD	Mean	SD
A	**1**	**3**	45.5°	0.5°	38.9°	2.7°
B	**1**	**3**	38.0°	3.2°	33.3°	3.8°
C	**1**	**3**	32.6°	1.2°	29.8°	0.9°
D	**1**	**3**	22.3°	0.8°	20.2°	0.1°
A	**1**	**4**	32.8°	8.0°	38.5°	2.2°
B	**1**	**4**	50.8°	1.8°	49.3°	3.1°
C	**1**	**4**	33.9°	2.9°	34.4°	5.9°
D	**1**	**4**	42.5°	2.8°	47.7°	1.4°

Table A.4. Comparing Cobb's Method with 3D Ultrasound Method using 3D image stack approach with TPs forming lines as references; their means and SDs in clinical study are shown below. There are two angles measured in same subject under same scanning; these angles are labeled as angle 1 and 2.

Subject	Angle Number	Cobb's Method		3DUS Image Stack (TP)	
		Mean	SD	Mean	SD
1	1	12.3°	1.3°	12.2°	2.4°
2	1	22.1°	4.0°	9.6°	3.0°
3	1	15.2°	0.0°	13.7°	0.3°
3	2	20.2°	1.3°	14.5°	6.6°
4	1	1.9°	0.0°	4.2°	0.8°
5	1	1.9°	0.0°	2.5°	2.6°
6	1	3.8°	0.0°	2.4°	1.1°
7	1	6.7°	1.4°	2.0°	0.7°
8	1	13.6°	0.4°	6.7°	2.5°
9	1	7.5°	0.2°	0.4°	Note 1
10	1	7.1°	0.7°	4.9°	1.3°
10	2	5.8°	0.0°	2.1°	1.7°
11	1	7.6°	0.0°	2.8°	1.3°
11	2	9.5°	0.0°	1.6°	1.6°
12	1	7.7°	0.1°	0.7°	Note 1
13	1	7.6°	0.0°	3.3°	0.6°
13	2	6.7°	1.4°	1.3°	0.1°
14	1	10.2°	1.7°	1.7°	0.3°
15	1	2.2°	0.5°	2.9°	0.4°
16	1	3.8°	0.1°	2.0°	2.1°
17	1	8.6°	1.3°	9.6°	1.3°
18	1	15.5°	0.4°	13.7°	0.6°
18	2	9.1°	1.4°	4.7°	3.0°
19	1	25.3°	0.0°	20.7°	0.6°
19	2	29.9°	1.3°	16.1°	5.4°
20	1	13.2°	0.2°	6.7°	7.1°
21	1	14.8°	0.5°	11.7°	1.1°
21	2	20.2°	1.4°	10.5°	Note 1
22	1	15.9°	0.0°	16.1°	0.6°
23	1	12.6°	1.0°	6.7°	3.3°
24	1	7.2°	0.4°	2.5°	0.8°

25	**1**	18.1°	0.3°	18.2°	3.3°
25	**2**	27.0°	0.4°	Note 2	Note 1
26	**1**	14.2°	1.3°	6.5°	0.4°
27	**1**	9.6°	0.1°	7.5°	3.5°
28	**1**	28.1°	2.4°	Note 2	Note 1
28	**2**	29.7°	2.1°	Note 2	Note 1

Note 1: Only one angle was measured from select vertebra pair. This made no SD value produced

Note2: No angel was measured from select vertebra pair. Because tip of TP could be identified in one of select vertebra pair.

Table A.5 Results of intra-observer study of 3D Ultrasound Method using 3D image stack approach with TPs forming line as references, their data sets in clinical study are shown below. There are two angles measured in same subject under same scanning; these angles are labeled as angle 1 and 2.

Subject	**Angle Number**	**3D Image Stack (TP) Data Set 1**	**3D Image Stack (TP) Data Set 2**
1	**1**	11.7°	4.3°
1	**1**	7.4°	17.3°
2	**1**	4.8°	3.1°
2	**1**	3.6°	3.6°
3	**1**	5.0°	8.9°
3	**2**	2.3°	2.5°
3	**1**	3.1°	4.9°
3	**2**	1.6°	0.5°
4	**1**	1.5°	5.2°
4	**2**	2.5°	4.7°
5	**1**	8.5°	9.8°
5	**1**	4.9°	10.3°
6	**1**	3.7°	3.1°
6	**1**	1.3°	2.5°
6	**2**	2.8°	4.6°
6	**2**	1.2°	5.9°
7	**1**	3.1°	2.4°
7	**1**	2.6°	1.9°
8	**1**	8.6°	7.8°
8	**1**	10.5°	11.0°

Table A.6. Results of inter-observer study of 3D Ultrasound Method using 3D image stack approach with TPs forming lines as references, their means and SDs in clinical study are shown below. There are two angles measured in same subject under same scanning; these angles are labeled as angle 1 and 2.

Subject	**Angle Number**	**3D Image Stack (TP) Observer 1 Data Set**		**3DUS Image Stack (TP) Observer 2 Data Set**	
		Mean	**SD**	**Mean**	**SD**
1	**1**	25.5°	Note	9.6°	3.0°
2	**1**	18.8°	Note	4.2°	0.8°
3	**1**	9.8°	2.0°	4.1°	1.3°
	2	1.6°	2.0°	1.4°	0.4°
4	**1**	2.3°	1.7°	2.0°	0.7°
5	**1**	6.3°	3.5°	6.7°	2.5°
6	**1**	6.6°	3.9°	2.8°	1.3°
	2	9.5°	Note	1.6°	1.6°
7	**1**	1.9°	Note	0.7°	Note
8	**1**	4.2°	2.5°	3.3°	0.6°
	2	4.0°	2.1°	1.3°	0.1°
9	**1**	6.0°	Note	1.7°	0.3°
10	**1**	2.9°	2.5°	2.9°	0.4°
11	**1**	0.2°	Note	2.0°	2.1°
12	**1**	5.9°	3.5	9.6°	1.3°
13	**1**	27.0°	6.2°	20.7°	0.6°
	2	22.7°	Note	16.7°	5.4°
14	**1**	15.4°	1.1°	6.7°	7.1°
15	**1**	12.6°	0.2°	11.7°	1.1°
	2	10.0°	7.1°	10.5°	Note
16	**1**	11.7°	1.6°	16.1°	0.6°
17	**1**	17.7°	8.1°	18.2°	3.3°
	2	14.7°	2.8°	Note	Note

Note: only one angle was measured. This made no SD value produced

Table A.7. Comparing Cobb's Method with 3D Ultrasound Method using volume projection approach with spine column profile as the reference, TP forming lines as references; their means and SDs in clinical study are shown below. There are two angles measured in same subject under same scanning; these angles are labeled as angle 1 and 2.

Subject	**Angle Number**	**Cobb's Method**		**Volume Projection Spine Column Profile as Reference**		**Volume Projection TP forming lines as References**	
		Mean	**SD**	**Mean**	**SD**	**Mean**	**SD**
1	**1**	12.3°	1.3°	18.4°	0.2°	17.4°	1.3°
2	**1**	22.1°	4.0°	29.9°	0.1°	26.3°	0.2°
3	**1**	15.2°	0.0°	21.4°	0.2°	17.7°	2.5°
3	**2**	20.2°	1.3°	28.3°	0.2°	28.1°	1.6°
4	**1**	1.9°	0.0°	8.1°	0.2°	7.0°	1.0°
5	**1**	1.9°	0.0°	5.1°	0.3°	6.4°	0.2°
6	**1**	3.8°	0.0°	11.6°	0.7°	9.8°	0.3°
7	**1**	6.7°	1.4°	7.5°	0.7°	4.7°	0.1°
8	**1**	13.6°	0.4°	14.2°	0.0°	10.1°	0.2°
9	**1**	7.5°	0.2°	4.3°	0.3°	4.1°	0.1°
10	**1**	7.1°	0.7°	4.8°	0.7°	4.7°	0.4°
10	**2**	5.8°	0.0°	13.0°	0.1°	12.0°	0.2°
11	**1**	7.6°	0.0°	9.1°	0.4°	9.1°	0.6°
11	**2**	9.5°	0.0°	9.4°	0.1°	8.9°	1.3°
12	**1**	7.7°	0.1°	7.0°	0.1°	3.9°	0.6°
13	**1**	7.6°	0.0°	11.1°	0.1°	8.4°	0.0°
13	**2**	6.7°	1.4°	6.3°	0.1°	5.5°	0.5°
14	**1**	10.2°	1.7°	18.6°	2.0°	15.8°	0.5°
15	**1**	2.2°	0.5°	7.0°	0.4°	6.9°	0.4°
16	**1**	3.8°	0.1°	10.6°	0.1°	11.3°	0.8°
17	**1**	8.6°	1.3°	11.6°	0.1°	12.1°	0.6°
18	**1**	15.5°	0.4°	11.5°	0.3°	11.3°	0.2°
18	**2**	9.1°	1.4°	6.3°	0.1°	6.9°	0.3°
19	**1**	25.3°	0.0°	23.7°	0.8°	21.8°	0.4°
19	**2**	29.9°	1.3°	30.2°	0.2°	31.8°	0.5°
20	**1**	14.2°	1.3°	15.6°	0.1°	12.8°	0.0°
21	**1**	13.2°	0.2°	15.5°	0.5°	15.0°	1.3°

22	**1**	14.8°	0.5°	13.5°	0.3°	11.9°	0.0°
22	**2**	20.2°	1.4°	16.8°	0.3°	16.0°	0.9°
23	**1**	15.9°	0.0°	16.7°	0.2°	16.5°	0.0°
24	**1**	12.6°	1.0°	9.4°	0.8°	8.4°	0.3°
25	**1**	7.2°	0.4°	11.4°	0.1°	11.0°	0.6°
26	**1**	18.1°	0.3°	19.7°	0.1°	18.4°	0.1°
26	**2**	27.0°	0.4°	30.2°	0.2°	27.1°	0.9°
27	**1**	14.2°	1.3°	15.0°	0.8°	13.8°	0.3°
28	**1**	9.6°	0.1°	10.8°	0.4°	9.1°	0.8°
29	**1**	28.1°	2.4°	26.3°	0.7°	25.2°	0.1°
29	**2**	29.7°	2.1°	28.3°	0.4°	25.3°	0.4°

Table A.8. Results of intra-observer of 3D Ultrasound Method using volume projection approach with spine column profile as reference and TP forming lines as references; their means and SD in clinical study are shown below. There are two angles measured in same subject under same scanning; these angles are labeled as angle 1 and 2.

Subject	Angle Number	Volume Projection Spine Column Profile As Reference				Volume Projection TPs Forming Lines As References			
		Data Set 1		Data Set 2		Data Set 1		Data Set 2	
		Mean	SD	Mean	SD	Mean	SD	Mean	SD
1	**1**	18.4°	0.6°	18.2°	1.1°	17.4°	1.2°	15.9°	0.5°
2	**1**	29.9°	0.2°	29.3°	1.0°	26.3°	0.4°	24.6°	0.3°
3	**1**	21.4°	1.4°	19.4°	2.3°	17.7°	0.1°	16.5°	0.8°
3	**2**	28.3°	3.1°	30.0°	0.6°	28.1°	0.8°	26.1°	1.2°
4	**1**	8.1°	0.1°	8.1°	1.1°	7.0°	1.2°	5.0°	0.1°
5	**1**	5.1°	1.1°	6.3°	0.2°	6.4°	2.0°	4.5°	1.9°
6	**1**	11.6°	1.2°	12.0°	0.7°	9.8°	0.1°	9.2°	0.4°
7	**1**	7.5°	1.8°	8.2°	1.1°	4.7°	0.5°	5.5°	1.2°
8	**1**	14.2°	1.0°	14.3°	0.0°	10.1°	0.1°	10.4°	0.3°
9	**1**	4.3°	1.1°	5.8°	1.1°	4.1°	0.6°	4.5°	0.5°
10	**1**	4.8°	0.7°	3.6°	1.1°	4.7°	1.0°	3.3°	1.7°
10	**2**	13.0°	3.2°	11.8°	1.5°	12.0°	0.8°	10.5°	0.0°
11	**1**	9.1°	2.5°	10.9°	0.7°	9.1°	0.4°	10.0°	0.5°
11	**2**	9.4°	2.6°	12.6°	1.7°	8.9°	0.0°	10.8°	1.3°
12	**1**	7.0°	0.9°	8.9°	1.3°	3.9°	0.8°	5.4°	0.1°
13	**1**	11.1°	0.9°	10.6°	0.3°	8.4°	0.6°	7.4°	0.1°
13	**2**	6.3°	2.1°	8.3°	0.7°	5.5°	1.3°	6.3°	1.2°
14	**1**	18.6°	0.6°	18.6°	0.3°	15.8°	0.4°	15.3°	0.0°
15	**1**	7.0°	1.3°	9.0°	0.5°	6.9°	1.6°	8.6°	1.0°
16	**1**	10.6°	0.7°	9.6°	0.2°	11.3°	0.5°	8.6°	0.4°
17	**1**	11.6°	0.9°	13.4°	0.2°	12.1°	1.0°	12.5°	0.0°
18	**1**	11.5°	0.8°	12.2°	2.4°	11.3°	0.6°	10.8°	0.6°
18	**2**	6.3°	0.7°	6.9°	1.3°	6.9°	0.1°	8.8°	1.9°
19	**1**	23.7°	1.4°	23.1°	2.1°	21.8°	0.3°	20.9°	1.1°
19	**2**	30.2°	1.1°	32.1°	1.2°	31.8°	1.0°	29.8°	3.5°
20	**1**	15.6°	3.1°	17.0°	1.1°	12.8°	2.8°	13.1°	1.0°
21	**1**	15.5°	0.5°	16.8°	1.3°	15.0°	1.0°	16.7°	0.2°
22	**1**	13.5°	0.6°	13.4°	0.6°	11.9°	0.4°	10.5°	0.5°

22	**2**	16.8°	1.3°	17.2°	2.5°	16.0°	1.5°	15.1°	1.4°
23	**1**	16.7°	0.2°	16.5°	0.2°	16.5°	1.1°	15.5°	0.3°
24	**1**	9.4°	3.5°	8.9°	1.3°	8.4°	3.8°	9.2°	2.8°
25	**1**	13.5°	0.4°	13.4°	0.8°	12.6°	0.2°	13.7°	0.3°
26	**1**	11.4°	2.8°	13.6°	0.0°	11.0°	1.1°	8.2°	0.4°
27	**1**	10.2°	0.2°	12.1°	0.8°	9.1°	1.6°	11.1°	1.5°
28	**1**	19.7°	2.6°	20.5°	3.4°	18.4°	1.5°	19.3°	3.1°
28	**2**	30.2°	2.4°	30.2°	2.5°	27.1°	0.0°	28.8°	2.7°
29	**1**	15.0°	0.1°	15.0°	1.7°	13.8°	0.5°	12.2°	0.6°
30	**1**	11.8°	0.5°	12.9°	1.5°	10.3°	0.5°	10.6°	0.6°
31	**1**	10.8°	0.6°	11.8°	0.7°	9.1°	1.5°	9.1°	0.2°
32	**1**	26.3°	2.1°	29.1°	1.0°	25.2°	1.6°	25.4°	2.1°
32	**2**	28.3°	0.3°	31.1°	2.2°	25.3°	0.0°	27.2°	2.4°
33	**1**	13.9°	1.1°	14.6°	2.6°	12.3°	2.0°	10.9°	1.2°
34	**1**	18.5°	1.2°	20.8°	0.9°	17.7°	0.2°	19.2°	0.7°
35	**1**	11.1°	0.6°	11.9°	0.8°	9.9°	1.2°	8.9°	1.4°
36	**1**	10.3°	1.1°	12.8°	0.4°	8.6°	0.2°	8.9°	0.1°

Table A.9. Results of inter-observer of 3D Ultrasound Method using volume projection approach with spine column profile as the reference, observer1 with preselected vertebrae information, observer2 without non-preselected vertebrae information; their means in clinical study are shown below. There are two angles measured in same subject under same scanning; these angles are labeled as angle 1 and 2.

Subject	Angle Number	Volume Projection Spine Column Profile as Reference Preselected Observer1		Volume Projection Spine Column Profile as Reference Non-Preselected Observer2	
		Mean	SD	Mean	SD
1	**1**	18.4°	0.6°	19.6°	0.1°
2	**1**	29.9°	0.2°	26.0°	0.3°
3	**1**	21.4°	1.4°	15.1°	0.6°
3	**2**	28.3°	3.1°	28.1°	0.5°
4	**1**	8.1°	0.1°	7.2°	0.9°
5	**1**	5.1°	1.1°	3.6°	0.2°
6	**1**	11.6°	1.2°	10.3°	1.0°
7	**1**	7.5°	1.8°	10.6°	1.5°
8	**1**	14.2°	1.0°	14.4°	0.0°
9	**1**	4.3°	1.1°	6.7°	1.4°
10	**1**	4.8°	0.7°	Note	Note
10	**2**	13.0°	3.2°	11.2°	0.3°
11	**1**	9.1°	2.5°	5.5°	1.4°
11	**2**	9.4°	2.6°	Note	Note
12	**1**	7.0°	0.9°	6.4°	0.7°
13	**1**	11.1°	0.9°	9.3°	2.6°
13	**2**	6.3°	2.1°	8.8°	1.0°
14	**1**	18.6°	0.6°	22.3°	0.3°
15	**1**	7.0°	1.3°	11.1°	1.1°
16	**1**	10.6°	0.7°	9.1°	1.3°
17	**1**	11.6°	0.9°	17.7°	0.3°
18	**1**	11.5°	0.8°	8.8°	0.0°
18	**2**	6.3°	0.7°	Note	Note
19	**1**	23.7°	1.4°	27.2°	0.5°
19	**2**	30.2°	1.1°	31.9°	0.1°
20	**1**	15.6°	3.1°	18.9°	0.3°

21	**1**	15.5°	0.5°	16.4°	2.0°
22	**1**	13.5°	0.6°	17.9°	0.8°
22	**2**	16.8°	1.3°	13.7°	0.6°
23	**1**	16.7°	0.2°	21.1°	0.3°
24	**1**	9.4°	3.5°	6.8°	0.3°
25	**1**	13.5°	0.4°	12.5°	0.2°
26	**1**	11.4°	2.8°	15.4°	1.0°
27	**1**	10.2°	0.2°	7.7°	0.2°
28	**1**	19.7°	2.6°	19.1°	1.3°
28	**2**	30.2°	2.4°	30.4°	6.0°
29	**1**	15.0°	0.1°	15.4°	1.4°
30	**1**	11.8°	0.5°	7.3°	0.2°
31	**1**	10.8°	0.6°	14.3°	0.5°
32	**1**	26.3°	2.1°	27.5°	0.7°
32	**2**	28.3°	0.3°	24.4°	0.3°
33	**1**	13.9°	1.1°	13.4°	3.4°
34	**1**	18.5°	1.2°	20.0°	0.5°
35	**1**	11.1°	0.6°	15.3°	0.9°
36	**1**	10.3°	1.1°	12.1°	0.5°

Note: Observer2 unrecognized two angles exist.

Table A.10. Results of inter-observer of 3D Ultrasound Method using volume projection approach with TPs forming lines as references, observer1 with preselected vertebrae information, observer2 without non-preselected vertebrae information; their means in clinical study are shown below. There are two angles measured in same subject under same scanning; these angles are labeled as angle 1 and 2.

Subject	**Angle Number**	**Volume Projection TP forming lines as the References Preselected Observer1**		**Volume Projection TP forming lines as a Reference Non-Preselected Observer2**	
		Mean	**SD**	**Mean**	**SD**
1	**1**	17.4°	1.3°	17.7°	0.0°
2	**1**	26.3°	0.2°	24.3°	1.8°
3	**1**	17.7°	2.5°	15.7°	2.1°
3	**2**	28.1°	1.6°	25.3°	2.8°
4	**1**	7.0°	1.0°	7.7°	0.6°
5	**1**	6.4°	0.2°	3.6°	1.1°
6	**1**	9.8°	0.4°	11.4°	1.7°
7	**1**	4.7°	0.2°	7.4°	0.5°
8	**1**	10.1°	0.2°	12.4°	4.0°
9	**1**	4.1°	0.1°	7.1°	1.6°
10	**1**	4.7°	0.3°	Note	Note
10	**2**	12.0°	0.2°	10.6°	0.2°
11	**1**	9.1°	0.6°	5.7°	0.4°
11	**2**	8.9°	1.3°	Note	Note
12	**1**	3.9°	0.6°	5.3°	0.6°
13	**1**	8.4°	0.0°	9.0°	1.7°
13	**2**	5.5°	0.5°	8.5°	0.9°
14	**1**	15.8°	0.5°	21.9°	0.8°
15	**1**	6.9°	0.4°	9.0°	1.7°
16	**1**	11.3°	0.9°	9.6°	0.0°
17	**1**	12.1°	0.7°	14.7°	1.3°
18	**1**	11.3°	0.2°	11.0°	0.5°
18	**2**	6.9°	0.3°	Note	Note
19	**1**	21.8°	0.4°	25.6°	1.8°
19	**2**	31.8°	0.5°	31.4°	0.6°
20	**1**	12.8°	0.0°	18.1°	0.6°

21	**1**	15.0°	1.4°	21.4°	1.7°
22	**1**	11.9°	0.0°	16.8°	2.1°
22	**2**	16.0°	0.9°	16.2°	0.4°
23	**1**	16.5°	0.0°	19.5°	0.7°
24	**1**	8.4°	0.3°	5.6°	2.2°
25	**1**	12.6°	0.2°	13.0°	0.8°
26	**1**	11.0°	0.6°	13.3°	2.0°
27	**1**	9.1°	0.1°	8.0°	0.3°
28	**1**	18.4°	0.1°	18.5°	0.1°
28	**2**	27.1°	0.9°	26.0°	2.5°
29	**1**	13.8°	0.3°	15.0°	1.4°
30	**1**	10.3°	0.3°	7.6°	1.0°
31	**1**	9.1°	0.8°	11.8°	0.5°
32	**1**	25.2°	0.1°	23.8°	0.3°
32	**2**	25.3°	0.4°	21.9°	0.4°
33	**1**	12.3°	0.5°	12.5°	1.2°
34	**1**	17.7°	0.7°	18.1°	2.0°
35	**1**	9.9°	0.1°	13.6°	0.2°
36	**1**	8.6°	0.4°	9.7°	0.7°

Note: Observer2 unrecognized two angles existed.

Table A.11. Results of intra-observer study of 3D Ultrasound Method using volume projection approach with spine column profile as the reference; data and scanned by same observer, their means and SDs in clinical study are shown below. There are two angles measured in same subject under same scanning; these angles are labeled as angle 1 and 2.

Subject	**Angle Number**	**Observer 1 Data Set 1**		**Observer 1 Data Set 2**	
		Mean	**SD**	**Mean**	**SD**
1	**1**	2.7°	0.0°	3.4°	0.6°
2	**1**	25.0°	0.1°	28.6°	0.2°
3	**1**	6.4°	0.1°	6.8°	0.8°
4	**1**	23.5°	0.4°	27.2°	0.3°
5	**1**	26.7°	0.0°	28.6°	0.0°
6	**1**	37.0°	1.4°	37.3°	0.3°
7	**1**	12.2°	1.2°	10.6°	0.6°
8	**1**	13.8°	0.8°	10.2°	1.1°
9	**1**	27.2°	0.9°	28.6°	0.5°
10	**1**	18.9°	1.3°	18.0°	0.7°
11	**1**	16.2°	0.7°	14.7°	0.1°

Table A.12. Results of intra-observer study of 3D Ultrasound Method using volume projection approach with spine column profile as the reference; data and scanned by same observer, their means and SDs in clinical study are shown below. There are two angles measured in same subject under same scanning; these angles are labeled as angle 1 and 2.

Subject	**Angle Number**	**Observer 2 Data Set 1**		**Observer 2 Data Set 2**	
		Mean	**SD**	**Mean**	**SD**
1	**1**	3.8°	1.3°	7.3°	0.5°
2	**1**	19.3°	0.8°	15.3°	0.3°
3	**1**	10.2°	0.6°	8.9°	0.7°
4	**1**	22.3°	0.9°	28.0°	0.8°
5	**1**	25.3°	1.0°	25.7°	0.5°
5	**2**	27.2°	0.3°	23.0°	0.6°
6	**1**	34.6°	0.9°	31.6°	0.2°
7	**1**	8.2°	0.9°	9.8°	0.8°
8	**1**	15.3°	1.1°	15.6°	0.9°
9	**1**	25.2°	0.0°	23.1°	0.5°
10	**1**	13.4°	0.0°	13.3°	0.7°
11	**1**	13.6°	0.5°	13.8°	0.9°

Table A.13. Results of inter-observer of 3D Ultrasound Method using volume projection approach with spine column profile as the reference; their means in clinical study are shown below. There are two angles measured in same subject under same scanning; these angles are labeled as angle 1 and 2.

Subject	**Scan Order No.**	**Angle No.**	**Observer 1 Scan**		**Observer 1 Scan**		**Observer 2 Scan**		**Observer 2 Scan**	
			Observer1 Measure		**Observer3 Measure**		**Observer3 Measure**		**Observer2 Measure**	
			Mean	**SD**	**`Mean**	**SD**	**Mean**	**SD**	**Mean**	**SD**
1	**1**	**1**	2.7°	0.0°	5.7°	1.1°	3.2°	0.6°	3.8°	1.3°
	2	**1**	3.4°	0.6°	5.0°	0.3°	2.2°	0.9°	7.3°	0.5°
2	**1**	**1**	25.0°	0.1°	20.7°	1.1°	17.3°	0.0°	19.3°	0.8°
	2	**1**	28.6°	0.2°	22.6°	1.2°	15.3°	0.1°	15.3°	0.3°
3	**1**	**1**	6.4°	0.1°	8.8°	0.7°	9.7°	0.1°	10.2°	0.6°
	2	**1**	6.8°	0.8°	8.0°	0.5°	11.2°	0.7°	8.9°	0.7°
4	**1**	**1**	23.5°	0.4°	31.7°	0.3°	29.7°	0.8°	22.3°	0.9°
	2	**1**	27.2°	0.3°	30.5°	2.2°	33.6°	0.6°	28.0°	0.8°
5	**1**	**1**	26.7°	0.0°	28.1°	1.3°	26.8°	0.4°	25.3°	1.0°
	2	**1**	28.6°	0.0°	29.9°	1.5°	27.9°	0.5°	25.7°	0.5°
5	**1**	**2**	Note		26.2°	0.8°	29.6°	0.9°	27.2°	0.3°
	2	**2**	Note		32.5°	0.4°	28.0°	1.4°	23.0°	0.6°
6	**1**	**1**	37.0°	1.4°	39.7°	0.1°	33.6°	0.9°	34.6°	0.9°
	2	**1**	37.3°	0.3°	43.1°	1.0°	28.3°	1.1°	31.6°	0.2°
7	**1**	**1**	12.2°	1.2°	11.9°	0.8°	10.6°	0.3°	8.2°	0.9°
	2	**1**	10.6°	0.6°	12.7°	0.6°	13.8°	0.6°	9.8°	0.8°
8	**1**	**1**	13.8°	0.8°	12.8°	0.1°	15.2°	1.4°	15.3°	1.1°
	2	**1**	10.2°	1.1°	10.4°	0.1°	14.3°	1.4°	15.6°	0.9°
9	**1**	**1**	27.2°	0.9°	26.1°	0.1°	27.3°	0.8°	25.2°	0.0°
	2	**1**	28.6°	0.5°	26.7°	0.5°	25.7°	1.3°	23.1°	0.5°
10	**1**	**1**	19.8°	1.3°	19.5°	0.2°	12.2°	0.2°	13.4°	0.0°
	2	**1**	18.0°	0.7°	15.6°	0.4°	13.7°	0.2°	13.3°	0.7°
11	**1**	**1**	16.2°	0.7°	16.3°	0.3°	15.4°	1.2°	13.6°	0.5°
	2	**1**	14.7°	0.1°	13.4°	0.4°	16.2°	0.1°	13.8°	0.9°

Note: Observer1 unrecognized the second angle existed.

B. Information sheet

THE HONG KONG
POLYTECHNIC UNIVERSITY
香港理工大學

Information Sheet

Project Title: Scolioscan: Radiation-Free Scoliosis Assessment System using 3D Ultrasound Imaging

You are invited to participate on a study conducted by Mr. James Cheung, a PhD student of Prof. Yongping Zheng, who is an Acting Head and Professor of the Interdisciplinary division of Biomedical Engineering in The Hong Kong Polytechnic University.

You will be required to sign the Consent form before any test of this study. The aim of this study is to develop a 3D ultrasound system for the assessment of scoliosis. If successful, this system will provide a low-cost and convenient approach for the assessment.

You will first be asked to stand steadily with the help of a frame structure. Operator will then apply ultrasound gel on the spinal region and ultrasound images will be taken from this region. The test may last for half an hour. You may also be invited to have further assessment for the back muscle stiffness. Operator will record ultrasound images at 6-8 positions from the back, varying from cases to cases.

The testing should not result in any undue discomfort. All information related to you will remain confidential, and will be identifiable by codes only known to the researcher.

You have every right to withdrawn from the study before or during the measurement without penalty of any kind.

If you have any complaints about the conduct of this research study, please do not hesitate to contact Mr Eric Chan, Secretary of the Human Subjects Ethics Sub-Committee of The Hong Kong Polytechnic University in person or in writing (c/o Human Resources Office of the University).

If you would like more information about this study, please contact Prof. Yongping Zheng at 27667664.

Thank you for your interest in participating in this study.

THE HONG KONG
POLYTECHNIC UNIVERSITY
香港理工大學

Information Sheet

Project Title: Scolioscan: Radiation-Free Scoliosis Assessment System using 3D Ultrasound Imaging

Your child is invited to participate on a study conducted by Mr. James Cheung, a PhD student of Prof. Yongping Zheng, who is an Acting Head and Professor of the Interdisciplinary division of Biomedical Engineering in The Hong Kong Polytechnic University.

You will be required to sign the Consent form before any test of this study. The aim of this study is to develop a 3D ultrasound system for the assessment of scoliosis. If successful, this system will provide a low-cost and convenient approach for the assessment.

Your child will first be asked to stand steadily with the help of a frame structure. Operator will then apply ultrasound gel on the spinal region and ultrasound images will be taken from this region. The test may last for half an hour. Your child may also be invited to have further assessment for the back muscle stiffness. Operator will record ultrasound images at 6-8 positions from the back, varying from cases to cases.

The testing should not result in any undue discomfort. All information related to your child will remain confidential, and will be identifiable by codes only known to the researcher.

You and your child have every right to withdrawn from the study before or during the measurement without penalty of any kind.

If you or your child has any complaints about the conduct of this research study, please do not hesitate to contact Mr Eric Chan, Secretary of the Human Subjects Ethics Sub-Committee of The Hong Kong Polytechnic University in person or in writing (c/o Human Resources Office of the University).

If you would like more information about this study, please contact Prof. Yongping Zheng at 27667664.

Thank you and your child for your interest in participating in this study.

C. Consent form

THE HONG KONG
POLYTECHNIC UNIVERSITY
香港理工大學

CONSENT FORM

Project Title: Scolioscan: Radiation-Free Scoliosis Assessment System using 3D Ultrasound Imaging

I, __________________ (name of subject), hereby consent to participate as a subject for the captioned project above.

- I have understood the experimental procedures presented to me.
- I have understood the information presented in the information sheet.
- I have given an opportunity to ask questions about the experiment, and these have been answered to my satisfaction.
- I understand that I can discontinue the experiment with no reasons given and no penalty received during the experiment.
- I realize that the results of this experiment may be published, but that my own results will be kept confidential.
- I understand that information obtained from this research may be used in future research and published.
- I also understand that my personal information will not be disclosed to people who are not related to this study.
- I realize that the results of this experiment are the properties of The Hong Kong Polytechnic University.

Subject name: ______________________ Signature:____________________

Witness name: _____________________ Signature:____________________

Investigator name:___________________ Signature:____________________

Date: __________________________

THE HONG KONG POLYTECHNIC UNIVERSITY
香港理工大學

CONSENT FORM

Project Title: Scolioscan: Radiation-Free Scoliosis Assessment System using 3D Ultrasound Imaging

I, __________________ (name of subject' parent), hereby consent to allow my child __________________ (name of subject) to participate as a subject for the captioned project above.

- I have understood the experimental procedures presented to me and my child.
- I have understood the information presented in the information sheet.
- I and my child have given an opportunity to ask questions about the experiment, and these have been answered to my satisfaction.
- I understand that I and my child can discontinue the experiment with no reasons given and no penalty received during the experiment.
- I realize that the results of this experiment may be published, but that my child's information will be kept confidential.
- I understand that information obtained from this research may be used in future research and published.
- I also understand that my child's personal information will not be disclosed to people who are not related to this study.
- I realize that the results of this experiment are the properties of The Hong Kong Polytechnic University.

Subject' parent name: _____________________ Signature:____________________

Witness name: _____________________ Signature:____________________

Investigator name:___________________ Signature:____________________

Date: __________________________

REFERENCES

Aaro S, Dahlborn M. Estimation of vertebral rotation and the spinal and rib cage deformity in scoliosis by computer tomography. Spine, 1981;6(5):460-467.

Adair IV, Van Wijk MC. Armstrong GW. Moire topography in scoliosis screening, Clin Orthop, 1977;129:165-171.

Adam C, Izatt M, Harvey J, Askin G. Variability in Cobb angle measurements using reformatted computerized tomography scans. Spine, 2005;30:1664-1669.

Ahn UM, Ahn NU, Nallamshetty L, Buchowski JM, Rose PS, Miller NH, Kostuik JP, Sponseller PD. The etiology of adolescent idiopathic scoliosis. Am J Orthop, 2002;31:387–395.

Almeida ADM, Alves E, Athayde LGMD, Barbosa DBV, Bitencourt AGV, Cotrim HP, Freitas ALRD, Rios A, Santos AS. Fatty liver disease in severe obese patients: Diagnostic value of abdominal ultrasound. World J Gastroenterol, 2008;14(9):1415–1418.

Allington NJ, Bowen JR. Adolescent idiopathic scoliosis: treatment with the Wilmington brace. A comparison of full-time and part-time use. J Bone Joint Surg, 1996;78(A): 1056–62.

Amendt LE, Ause-Ellias KL, Eybers JL, Wadsworth CT, Nielsen DH, Weinstein SL, Validity and reliability testing of the scoliometer, Physical Therapy, 1990:70(2):108-117.

Angelini ED, Homma S, Pearson G, Holmes JW, Lain AF. Segmentation of real-time three-dimension ultrasound for quantification of ventricular function: A clinical study on right and left ventricles. Ultrasound Med Biol, 2005;31(9):1143-1158.

Arun KS, Huang TS, Blostein SD. Least-squares fitting of two 3D point sets. IEEE

Trans Pattern Analys Mach Intel, 1987;9:698-700.

Amin DV, Kanade T, Jaramaz B, DiGioia AM III, Nikou C, LaBarca RS, Moody JE Jr. Calibration Method for determining the physical location of the ultrasound image plane. In:Niessen WJ, Viergever MA (eds.), Proceedings of Medical Image Computing and Computer-Assisted Intervention (MICCAI) 2001. Lecture Notes in Computer Science. Utrecht, The Netherlands, 2001;2208:940-47.

Azeddine B, Letellier K, Wang da S, Moldovan F, Moreau A. Molecular determinants of melatonin signaling dysfunction in adolescent idiopathic scoliosis. Clin Orthop Relat Res, 2007;462:45–52.

Bamber JC, Eckersley RJ, Hubregtse P, Bush NL, Bell DS, Crawford DC. Data processing for 3D ultrasound visualization of tumor anatomy and blood flow. Proc. SPIE, 1992;1808:651-63.

Barry CD, Allot CP, John NW, Mellor PM, Arundel PA, Thomson DS, Waterton JC. Three-dimensional freehand ultrasound: Image reconstruction and volume analysis. Ultrasound Med Biol, 1997;23(8):1209-24.

Barratt DC, Penny GP, Chan CSK, Slomczykowski M, Carter TJ, Edwards PJ, Hawkes DJ. Self-calibrating 3D ultrasound based bone registration for minimally invasive orthopedic surgery. IEEE Trans Med Imaging, 2006;25:312-323.

Bassett GS, Bunnell WP. Influence of the Wilmington brace on spinal decompensation in adolescent idiopathic scoliosis. Clin Orthop Rel Res, 1987;223:164-69.

Beasley RA, Stefansic JD, Herline AJ, Guttierez L, Galloway RL Jr. Registration of ultrasound images. SPIE Proc, 1999;3658:125-132.

Beauchamp M, Labelle H, Grimard G, Stanciu C, Poitras B, Dansereau J. Diurnal variation of Cobb angle measurement in adolescent idiopathic scoliosis. Spine, 1993;18:1581-1583.

Berg S, Torp H, Martens D, Steen E., Samstad S, Hoivik I, Olstad. Dynamic three-dimensional freehand echocardiography using raw digital ultrasound data. Ultrasound Med Biol, 1999;25:745-753.

Bernau A., Zur Frage der Reproduzierbarkeit von Rontgenaufnahmen der Wirbelsaule im Stehen (On the Problem of the Reproducibility of X-rays of the Spinal Column Standing), Z Ortho, 1984:122:150-151.

Berryman F, Pynsent P, Fairbank J, Disney S. A new system for measuring three-dimensional back shape in scoliosis. Eur Spine J, 2008;17:663-672.

Blake C, Elliot T, Slomka P, Downey D, Fenster A. Variability and accuracy of measurements of prostate brachytherapy seed position in vitro using three dimensional ultrasound: an intra- and inter-observer study. Med Phys, 2000;27: 2788-95.

Boctor EM, Jain A, Choti MA, RH Taylor, G Fichtinger. A rapid calibration method for registration and 3D tracking of ultrasound images using spatial localizer. SPIE Proc, 2003;5033:521-532.

Boctor EM, Choti MA, Burdette EC, Webster RJ III. Three-dimensional ultrasound-guided robotic needle placement: an experimental evaluation. Int J Med Robot, 2008;4:180-191.

Bohs LN, Geiman BJ, Anderson ME, Gebhart SC, Trahey GE. Speckle tracking for multi-dimensional flow estimation. Ultrasonics, 2000;38(I-8):369-375.

Bouchet LG, Meeks SL, Goodchild G, Bova FJ, Buatti JM, Firedman WA. Calibration of three-dimensional ultrasound images for image-guided radiation therapy. Phys Med Biol, 2001;46:559-577.

Brewin J, Hill M, Ellis H; The prevalence of cervical ribs in a London population. Clin Anat, 2009;22(3):331-6.

Budorick NE, Pretorius DH, Nelson TR. Sonography of the fetal spine. Technique, Imaging findings, and clinical Implications. Am J Roentgenol, 1995;164:421-428.

Bueche MJ. Scoliosis and Kyphosis. In: Neinstein LS, ed. Adolescent Healthcare: A Practical Guide, Philadelphia:Lippincott, 2008;235-242.

Bunnell WP. An objective criterion for scoliosis screening. J Bone Joint Surg Am, 1984;66:1381-1387.

Bunnell WP. The natural history of idiopathic scoliosis before skeletal maturity. Spine, 1986;11:773.

Bunnell WP. The natural history of idiopathic scoliosis. Clin Orthop, 1988;229:20-25.

Burcher MR, Han L, Noble JA. Deformation correction in ultrasound images using contact force measurement. In Proc. Workshop Math. Methods Biomed. Image Analysis, 2001;63-70.

Carman DL, Browne RH, Birch JG. Measurement of scoliosis and kyphosis radiographs. Intraobserver and interobserver variation. J Bone Joint Surg Am, 1990;72:328-333.

Carr J. Surface reconstruction in 3D medical imaging. PhD. Thesis, University of Canterbury. Christchurch. New Zealand, 1996.

Carpenter DA, Kossoff G, Griffiths KA. Correction of distortion in US images caused by subcutaneous tissues: Results in tissue phantoms and human subjects. Radiology, 1995;195:563-567.

Capasso G, Maffulli N, Testa V, The validity and reliability of measurements in spinal deformities: a critical appraisal. Acta Orthop Belg, 1992;58:126-135.

Castelein RM, van Dieën JH, Smit TH. The role of dorsal shear forces in the pathogenesis of adolescent idiopathic scoliosis--a hypothesis. Med Hypotheses, 2005;65(3):501-8.

Chang RF, Wu WJ, Chen DR, Chen WM, Shu W, Lee JH, Jeng LB. 3-D US frame positioning using speckle decorrelation and image registration. Ultrasound Med Biol, 2003;29(6):801-12.

Chen DR, Chang RF, Chen C, Chang CC, Jeng LB. Three-dimensional ultrasound in margin evaluation for breast tumor excision using Mammotome ®. Ultrasound Med Biol, 2004;30(2):169-179.

Chen JF, Fowlkes JB, Carson PL, Rubin JM. Determination of scan plane motion using speckle decorrelation: theoretical considerations and initial test. Int J Imaging Sys Tech, 1997;8:38-44.

Chen TK, Abolmaesumi P, Thurston AD, Ellis RE Automated 3D freehand ultrasound calibration with real-time accuracy control. In: Med Image Comput Comput Asist Interv int Conf Med Image Comput Comput Assist Interv. Lecture Notes in Computer Science. Springer, 2006;9(Pt 1):899-906.

Chen W, Le LH, Lou EHM. Ultrasound imaging of spinal vertebrae to study scoliosis. Open Journal of Acoustics, 2012;2:95-103.

Chen YL, Chen WJ, Chiou WK. An alternative method for measuring scoliosis curvature. Orthopedics, 2007:30:828-831.

Cheng LK, Sands GB, French RL, Withy SJ, Wong SP, Legget ME, Smith WM, Pullan AJ. Rapid construction of a patient specific torso model from 3D ultrasound for non-invasive imaging of cardiac electrophysiology. Med. Biol.

Engng Comput, 2005;43(3):325-330.

Cheng HHY, Huang ZW, Cheung JCC, Zheng YP, Chow DHK. The application of asymmetric loading for spine curvature correction in subjects with adolescent idiopathic scoliosis. In: Proceedings of the 14th ISPO 2013, Hyderabad, India, Feb 2013. In Press.

Chernukha K, Daffner R, Reigel D. Lumbar lordosis measurement: a new method versus Cobb technique. Spine, 1998;23:74-79.

Cheung CWJ, Zheng YP. Development of 3-D Ultrasound System for Assessment of Adolescent Idiopathic Scoliosis. In: Lim CT, Goh JCH, ed. WCB 2010, IFMBE Proceedings 31, 2010:584-587.

Cheung KM, Wang T, Poon AM, Carl A, Tranmer B, Hu Y, Luk KD, Leong JC. The effect of pinealectomy on scoliosis development in young nonhuman primates. Spine, 2005;30:2009-2013.

Choudhry S, Gorman B, Charboneau JW, Tradup DJ, Beck RJ, Kofler JM, Groth DS. Comparison of tissue harmonic imaging with conventional US in abdominal disease. Radiographics, 2000;20(4):1127-35.

Chow DHK, Kwok MLY, Au-Yang ACK, Holmes AD, Cheng JCY, Yao FYD, Wong MS. The effect of backpack load on the gait of normal adolescent girls. Ergonomics, 2005;48(6):642-65.

Chow DHK, Kwok MLY, Cheng JCY, Lao MLM, Holmes AD, Au-Yang ACK, Yao FYD, Wong MS. The effect of backpack weight on the standing posture and balance of schoolgirls with adolescent idiopathic scoliosis and normal controls. Gait & Posture, 2006;24(2):173-181.

Cobb JR, Outline for the study of scoliosis, In American Academy of Orthopedic Surgeons, Instructional Course Lectures. St Louis, CV Mosby, 1948;261-275.

Comean RM, Fenster A, Peters TM, Integrated MR and ultrasound imaging for improved image guidance in neurosurgery. In: Proceedings of SPIE 1998, 1998;3338:747-754.

Correa FF, Lara C, Bellver J, Remohi J, Pellicer A, Serra V. Examination of the fetal brain by transabdominal three-dimensional ultrasound: potential for routine neurosonographic studies. Ultrasound Obstet Gynecol, 2006;27:503-508.

Coup P, Hellier P, Azzabou N, Barillot C. 3D freehand ultrasound reconstruction based on probe trajectory. Proceedings of Medical Image Computing and Computer-Assisted intervention (MICCAI), Palm Springs, CA, USA:Springer, 2005;3749:587-604.

Dangerfield PH, Pearson JD, Dorgan JC, Hobson CA, Scutt D, Giakas G, Clinical Experience of Employing Computerised Back Shape Analysis to measure the 3D Deformity of Scoliosis, In:D'Amico M, Merolli A, Santambrogio GC, ed. Three Dimensional Analysis of Spinal Deformities, IOS Press, 1995:231-238.

Dawson EG, Smith RK, McNiece GM, Radiographic evaluation of scoliosis: a reassessment and introduction of the scoliosis Chariot, Clin Orthop Relat Res, 1978;131:151-155.

Delabays A, Pandian NG, Cao QL, Sugeng L, Marx G, Ludomirski A, Schwartz SL. Transthoracic real-time three-dimensional echocardiography using a fan-like scanning approach for data acquisition: methods, strengths, problems, and initial clinical experience. Echocardiography, 1995;12:49-59.

Denis F. The three column spine and its significance in the classification of acute thoracolumbar spinal injuries. Spine, 1983;8(8):817-31.

DeSmet AA, Goin JE, Asher MA, Scheuch HG, A clinical study of the differences between the scoliotic angles measured on posteroanterior and anteroposterior radiographs, J Bone Joint Surg, 1982,64:489-493.

DeSmet AA, Asher MA, Cook LT, Goin JE, Scheuch H, Orrick JM. Three dimensional analysis of right thoracic idiopathic scoliosis. Spine, 1984;9:377-381.

Detmer PR, Bashein G, Hodges T, Beach KW, Strandness DE Jr. 3D ultrasonic image feature location based on magnetic scan head tracking: In vitro calibration and validation. Ultrasound Med Biol, 1994;20:923-36.

Devore GR. Three-dimensional and four-dimensional fetal echocardiography: a new frontier. Curr Opin Pediatr, 2005;17:592-604.

Dewi DE, Wilkinson MH , Mengko TL , Purnama IK, 3D Ultrasound Reconstruction of Spinal Images using an Improved Olympic Hole-Filling Method. In International Conference on Instrumentation, Communication, Information Technology and Biomedical Engineering (ICICI-BME), 2009;1-5

Dewi DE, Veldhuizen AG, Burgerhof JG, Purnama IK, van Ooijen PM, Wilkinson MH, Mengko TL, Verkerke GJ, Reproducibility of standing posture for X-ray radiography: a feasibility study of the BalancAid with healthy young subjects, Annals of Biomedical Engineering, 2010, 38(10):3237-3245.

Diab K, Sevastik J, Hedlund R, Suliman I. Accuracy and applicability of measurement of the scoliotic angle at the frontal plane by Cobb's method, by Ferguson's method and by a new method. Eur Spine J, 1995;4:291-295.

Dickman D, Caspi O. Assessment of scoliosis with ortelius 800 – preliminary results. Clin Appl Notes 2001a;April:1-7.

Downey DB, Fenster A. Vascular imaging with a three-dimensional power Doppler system. Am J Roentgenol, 1995;165:665-668.

Dutton K, Jones T, Slinger B, Scull E, O'Connor J. Reliability of the Cobb angle index derived by traditional and computer assisted methods. Australas Phys Eng

Sci Med, 1989;12:16-23.

D'Urso PS, Thompson RG. Fetal biomodelling. Aust. N.Z.J. Obstet. Gynaecol. 1998;38(2):1182-1186.

Emans J, Kaelin A, Bancel P, Hall JE. The Boston bracing system for idiopathic scoliosis. Follow-up results in 295 patients. Spine, 1986;11:792–801.

Eom KS, Kim TY, Moon SK. Extreme elongation of the transverse process of the fifth limber vertebra: An unusual variant. Turk Neurosurg, 2011;21(4):648-650.

Falcon O, Peralta CFA, Cavoretto P, Faiola S, Nicolaides KH. Fetal truck and head volume measured by three-dimensional ultrasound at 11+0 to 13+6 weeks of gestation in chromosomally normal pregnancies. Ultrasound Obstet Gynecol, 2005;26:263-266.

Fenster A, Tong S, Cardinal HN, Blake C, Downey DB. Three-dimensional ultrasound imaging system for prostate cancer diagnosis and treatment. IEEE Instrum. Meas. Mag. 1996;1(4),32-35.

Fenster A, Lee D, Sherebrin S, Rankin R, Downey D. Three-dimensional ultrasound imaging of the vasculature. Ultrasonics, 1998;36:629-633.

Fenster A, Downey DB. Three-dimensional ultrasound imaging. Annu Rev Biomed Eng, 2000;2:457-475.

Fenster A, Downey DB, Cardinal HN. Three-dimensional ultrasound imaging. Phys Med Biol, 2001;46:R67-99.

Fenster A, Surry K, Smith W, Gill J, Downey D. 3D ultrasound imaging: applications in image-guided therapy and biopsy. Comput. Graphics, 2002;26:557-568.

Fenster A, Parraga G, Bax J. Three-dimensional ultrasound scanning. Interface Focus, 2011;1:503-519.

Ferguson A. The study and treatment of scoliosis. South Med J, 1930;23:116-120.

Fine D, Perring S, Herbetko J, Hacking CN, Fleming JS, Dewbury KC. Three-dimensional (3D) ultrasound imaging of the gallbladder and dilated biliary tree: reconstruction from real-time B-scans. Brit J Radiol, 1991;64:1056-1057.

Finger PT, Khoobehi A, Ponce-Contreras MR, Rocca DD, Garcia Jr PS. Three dimensional ultrasound of retinoblastoma: initial experience. Br. J Opthalmol, 2002; 86(10):1136-1138.

Friemel BH, Bohs LN, Nightinggale KR, Trahey GE. Speckle decorrelation due to two-dimensional flow gradients. IEEE trans, Ultrason. Ferroelectr. Frequency Control, 1998;45:317-327.

Geiser EA, Christie LG Jr, Conetta DA, Conti CR, Gossman GS. A mechanical arm for spatial registration of two-dimensional echocardiographic sections. Cathet. Cardiovasc. Diagn., 1982;8:89-101.

Gee AH, Prager RW, Berman L. Non-planar reslicing for freehand 3D ultrasound. In: Medical Image Computing and Computer-assisted Intervention-MICCAI'99, INCS, Cambridge, UK: Springer, 1999;1679:716-725.

Gee AH, Prager RW, Treece GM, Berman L. Narrow-band volume rendering for freehand 3D ultrasound. Computers and Graphics, 2002:26(3):463-476.

Gee AH, Prager RW, Treece GM, Berman L. Engineering a freehand 3D ultrasound system. Pattern Recognition Lett, 2003;24(12):757-777.

Gee AH, Houghton NE, Treee GM, Prager RW. A mechanical Instrument for 3D ultrasound probe calibration. Ultrasound Med. Biol., 2005;31(4):505-518.

Gelly JF,.Tournois P, Bureau JM, Nguyen T, Maurel P, Steichen W. Curved-linear 128 X 7 two-dimensional array for 1.5D ultrasound medical imaging. In: Shung KK(eds.) Medical imaging 1997: ultrasonic transducer engineering. SPIE, Bellingham, 1997;71-80.

Gill JD, Ladak HM, Steinman DA, Fenster A. Development and evaluation of a semiautomatic 3D segmentation technique of the carotid arteries from 3D ultrasound images. In Medical imaging 1999: image processing, Proceedings of the SPIE, 1999;3661;214-221.

Gilja OH, Hausken T, Odegaard, S, Berstad A. Three-dimensional ultrasonography of the gastric antrum in patients with functional dyspepsia. Scand. J. Gastroenterol., 1996;31(9):847-855.

Glassman SD, Berven S, Bridwell K, Horton W, Dimar JR. Correlation of radiographic parameters and clinical symptoms in adult scoliosis. Spine, 2005;30:682-688.

Gobbi DG, Peters TM (2002). Interactive intraoperative 3D ultrasound reconstruction and visualization, Lect Notes Comput Sc, 2002;2488:156-163.

Goldberg C, Kaliszer M, Moore DP, Fogarty EE, Dowling FE. Surface topography, Cobb angles, and cosmetic change in scoliosis. Spine, 2001;26(4):E55 - E63

Good CR. The genetic basis of adolescent idiopathic scoliosis. J Spinal Res Found, 2009;4(1):13-17.

Gooding MJ, Kennedy SH, Noble JA (2005) Temporal calibration of freehand three-dimensional ultrasound using image alignment. Ultrasound Med. Biol. 2005;31(7):919-927.

Gopa AS, Schnellbaecher MJ, Shen ZQ, Akinboboye OO, Spain PM, King DL. Freehand three-dimensional echocardiography for measurement of left ventricular mass: in vivo anatomic validation using explanted human hearts. J Am Coll Cardiol., 1997;30(3):802-810.

Greenspan A, Pugh J, Norman A, Norman R. Scoliotic index: a comparative evaluation of methods for the measurement of scoliosis. B Hosp Jt Dis Ort, 1978;39:117-125.

Gstoetter M, Sekyra K, Walochnik N, Winter P, Wachter R, Bach C. Inter- and intra-observer reliability assessment of the Cobb angle: manual versus digital measurement tools. Eur Spine J, 2007;16:1587-1592

Harrison DD, Janik T, Troyanovich S, Holland B. Comparisons of lordotic cervical spine curvatures to a theoretical ideal model of the static sagittal cervical spine. Spine, 1996;21:667–675.

He JW, Yan ZH, Liu J, Yu ZK, Wang XY, Bai GH, Ye XJ, Zhang X. Accuracy and repeatability of a new method for measuring scoliosis curvature. Spine, 2009;34:E323-E329.

Herzenberg JE, Waanders NA, Closkey RF, Schultz AB, Hensinger RN. Cobb angle versus spinous process angle in adolescent idiopathic scoliosis. The relationship of the anterior and posterior deformities. Spine, 1990;15(9):874-879.

Hoseli IM, Survek DV, Tercanli S, Holzgreve W. Three dimensional volume measurement of the cervix during pregnancy compared to conventional 2D-sonography. Int. J. Gynecol. Obstet., 1999;64:115-119.

Hottier F, Billon AC, 3D echography: Status and perspective. In: Hohne KH, Fuchs H, Pizer SM, eds. imaging in medicine. Berlin Heidelberg: Springer-Verlag, 1990;F60:21-41.

Housden R, Treece G, Gee A, Prager R. Calibration of an orientation sensor for freehand 3D ultrasound and its use in a hybrid acquisition system. Biomed Eng

Online, 2008;7:5.

Hsu PW, Prager RW, Gee AH, Treece GM. Rapid, easy and reliable calibration for freehand 3D ultrasound. Ultrasound Med. Biol., 2006;32(6):823-835.

Hsu PW, Prager RW, Gee AH, Treece GM Real-time freehand 3D ultrasound calibration. Ultrasound Med. Biol., 2008a;34(2):239-251.

Hsu PW, Prager RW, Gee AH, Treece GM. Freehand 3D ultrasound calibration: a review. In: Sensen CW, Hallgrimsson B. (eds.) Advanced imaging in biology and medicine, Berlin: Springer-Verlag, 2008b;ch3.:47-84.

Hsu PW, Prager RW, Gee AH, Treece GM. Comparison of freehand 3D ultrasound calibration techniques using a stylus. Ultrasound Med Biol, 2008c;34(10):1610-1621.

Huang QH, Zheng YP, Lu MH, Chi ZR. Development of a portable 3D ultrasound imaging system for musculoskeletal tissues. Ultrasonics, 2005a;43:153-163.

Huang QH, Zheng YP, and Lee R. 3D measurement of body tissues based on ultrasound images with 3D spatial information. Ultrasound Med Biol, 2005b; 31(12):1607-1615.

Huang QH and Zheng YP. A new scanning approach using a film container filled with water in freehand 3D ultrasound. Ultrasound Med. Biol., 2005c; 31: 575-583.

Hughes SW, D'Arcy TJ, Maxwell DJ, Chiu WSC, Milner A, Saunders JE, Sheppard RJ. Volume estimation from multiplanar 2D ultrasound images using a remote electromagnetic position and orientation sensor. Ultrasound Med. Biol., 1996;22:561-572.

Hung J, Lang R, Flachskampf F, Shernan SK, McCulloch ML, Adams DB Thomas J, Vannan M, Ryan T. 3D echocardiography: a review of the current status and future directions. J Am Soc Echocardiogr, 2007;20:213–233.

Huang SC, Effectiveness of scoliometer in school screening of scoliosis. Taiwan I Hsueh Hui Tsa Chih, 1988;87:955-959.

Idesawa M, Yatagai T, Soma T. Scanning moiré method and automatic measurement of 3-D shapes. Appl. Opt., 1977;16:2152-2162.

Jeffries BF, Tarlton M, DeSmet AA, Dwyer SJ, Brower AC. Computerized measurement and analysis of scoliosis. Radiology. 1980;134:381-385.

Johnson DD, Pretorius DH, Riccabona M, Budorick NA, Nelson TR. Three-dimensional ultrasound of the fetal spine. Obstet Gynecol, 1997;89:434-438.

Kafer ER. Respiratory and cardiovascular functions in scoliosis. Bull Eur de Physiopathol Respir, 1977;13:299–321.

Kass M, Witkin A, Terzopoulos D. Snakes – active contour models. Int J Comput Vision, 1997;1(4):321-331.

Kearon C, Viviani GR, Kirkley A, Killian KJ. Factors determining pulmonary function in adolescent idiopathic thoracic scoliosis. Am Rev Respir Dis, 1993;148: 288–294.

Kennelly KP, Stokes MJ. Pattern of asymmetry of paraspinal muscle size in adolescent idiopathic scoliosis examined by real-time ultrasound imaging. Spine, 1993;18:913-917.

Khamene A, Sauer F. A novel phantom-less spatial and temporal ultrasound calibration method. In: Med Iamge Comput Comput Assist Interv Int Conf Med Image Comput Comput Assist Interv, Lecture Notes in Computer Science. Springer-Verlag, 2005;3750:65-72.

Kindsfater K, Lowe T, Lawellin D, Weinstein D, Akmakjian J. Levels of platelet calmodulin for the prediction of progression and severity of adolescent idiopathic scoliosis. J Bone Joint Surg Am, 1994;76:1186 –1192.

Kim H, Kim HS, Moon ES, Yoon CS, Chung TS, Song HT, Suh FS, Lee YH, Kim SJ. Scoliosis imaging: what radiologists should know. RadioGraphics, 2010; 30:1823–1842

King DL, King DJ, Shao MY. Three-dimensonal spatial registration and interactive display of position and orientation of real-time ultrasound images. J. Ultrasound Med. 1990;9:525-532.

King DL, King DLS, Shao MY. Evaluation of in vitro measurement accuracy of a three-dimensional ultrasound scanner, J. Ultrasound Med., 1991;10(2):77-82.

King DL. Errors as a result of metal in the near environment when using an electromagnetic locator with freehand three-dimensional echocardiography. J Am Soc Echocardiogr, 2002;15:731-735.

Knott P, Mardjetko S, Nance D, Dunn Megan. Electromagnetic topographical technique of curve evaluation for adolescent idiopathic scoliosis. Spine, 2006;31(24):E911-E915.

Kohlmaier W., K. Lercher K., Tschauner C. Einsatz, einer dynamischen wippe zur standardisierten aufnahmetechnik von roentgengesamtaufnahmen der wirbelsaule im stehen bei kindern (Balance-like positioning device for taking standardized X-rays of the spine when the patient is standing). Radiologe, 1995;35:60–66.

Koreska J, Schwentker EP, Albisser AM, Gibson DA, Mills RH, A simple approach to standardized spinal radiographs, Med Instrum, 1978;12(1):59-63.

Koreska J, Smith JM. Portable desktop computer-aided digitizer system for the analysis of spinal deformities. Med Biol Eng Comput, 1982;20:715-726.

Kouwenhoven JW, Vincken KL, Bartels LW, Castelein RM. Analysis of preexistent vertebral rotation in the normal spine. Spine, 2006;31(13):1467-1472.

Kouwenhoven JW, Castelein RM. The pathogenesis of adolescent idiopathic scoliosis: review of the literature. Spine (Phila Pa 1976). 2008;33:2898–2908.

Kowal J, Amstutz CA, Caversaccio M, Nolte LP. On the development and comparative evaluation of an ultrasound B-mode probe calibration method. Comput Aided Surg, 2003;8:107-119.

Krissian K, Ellsmere J, Vosburgh K, Kikinis R, Westin CF. Multiscale segmentation of the aorta in 3D ultrasound images. In proceedings of the 25th Annual International Conference of the IEEE Engineering in Medicine and Biology Society, Cancun, Mexico, 2003:638-641 (IEEE, New York).

Kuo J, Atkins BZ, Hutcheson KA, von Ramm OT. Left ventricle wall motion analysis using real-time three dimensional. Ultrasound Med Biol, 2005;31(2):203-211.

Langø T. Ultrasound guided surgery: image processing and navigation. Ph.D. thesis, Norwegian University of Science and Technology, Trondheim, Norway, 2000.

Lee W. 3D fetal ultrasonography. Clin. Obstet. Gynecol., 2003;46:850-867.

Leotta DF, Demter PR, Marin RW. Performance of a miniature magnetic position sensor for three-dimensional ultrasound aiming. Ultrasound Med. Biol. 1997; 23(4):597-609.

Leotta DF, An efficient calibration method for freehand 3-D ultrasound imaging systems. Ultrasound Med. Biol., 2004:30:999-1008.

Levoy M. Efficient ray tracking of volume data. ACM Transactions on Graphics, 1990;9(3):245-261.

Levy AR, Goldberg MS, Mayo NE, Hanley JA, Poitras B. Reducing the lifetime risk of cancer from spinal radiographs among people with adolescent idiopathic scoliosis. Spine, 1996;21(13):1540-1548.

Li M, Cheng J, Ying M, Ng B, Zheng YP, Lam TP, Wong WY, Wong MS. Application of 3D ultrasound in assisting the fitting procedure of spinal orthosis to patients with adolescent idiopathic scoliosis. Stud Health Technol Inform, 2010;158:34–37.

Light ED, Angle JF, Smith SW. Real-time 3D ultrasound guidance of interventional devices. IEEE Trans. Ultrasonics, Ferroelectrics, Frequency Control, 2008;55(9):2066-2078.

Lin MC, Liaw MY, Chen WJ, Cheng PT, Wong AM, Chiou WK. Pulmonary function and spinal characteristics: their relationships in persons with idiopathic and postpoliomyelitic scoliosis. Arch Phys Med Rehabil, 2001;82:335–341.

Lindseth F, Langø T, Bang J, Hernes TAN. Accuracy evaluation of a 3D ultrasound-based neuronavigation system. Comput. Aided Surg., 2002:7:197-222.

Lindseth F, Tangen GA, Langø T. Probe calibration for freehand 3D ultrasound. Ultrasound Med. Biol., 2003;29(11):1607-1623.

Liu J, Gao X, Zhang Z, Gao S, Zhou J. A new calibration method for freehand 3-D ultrasonic imaging system. 20th Annual Conference. IEEE Eng Med Biol, 1998;20:839-841

Loder RT, Urquhart A, Steen H, Graziano G, Hensinger RN, Schlesinger A, Schork MA, Shyr Y. Variability in Cobb angle measurements in children with congenital scoliosis. J Bone Joint Surg Br, 1995;77:768-770.

Loder RT, Spiegel D, Gutknecht S, Kleist K, Ly T, Mehbod A. The assessment of intraobserver and interobserver error in the measurement of noncongenital scoliosis in children ≤ 10 years of age. Spine, 2004;29:2548-2553.

Lonstein JE, Bjorklund S, Wanninger MH, Nelson RP. Voluntary school screening for scoliosis in Minnesota. J Bone Surg(Am), 1982;64:481-488.

Lonstein JE, Carlson JM. The prediction of curve progression in untreated idiopathic scoliosis during growth. J Bone Joint Surg, 1984;66-A: 1061-1071.

Lowe TG, Edgar M, Margulies JY, Miller NH, Raso VJ, Reinker KA, Rivard CH. Etiology of idiopathic scoliosis: current trends in research. J Bone Joint Surg, 2000;82a:1157-1168.

Machida M, Dubousset J, Yamada T, Kimura J. Serum melatonin levels in adolescent idiopathic scoliosis prediction and prevention for curve progression - a prospective study. J Pineal Res, 2009;46:344-348.

Magnussen CG, Thomson R, Juonala M, Viikari JS, Dwyer T, Raitakari OT, Venn A. Use of B-mode ultrasound to examine preclinical markers of atherosclerosis: image quality may bias associations between adiposity and measures of vascular structure and function. J Ultrasound Med, 2011;30(3):363-369.

Malfair D, Flemming AK, Dvorak MF, Munk PL, Vertinsky AT, Heran MK, Graeb DA. Radiograph evaluation of scoliosis: Review. American Journal of Roentgenology, 2010; 194(3): S8-S22.

Marhofer P, Greher M, Kapral S: Ultrasound guidance in regional anesthesia. Br J Anaesth, 2005;94:7-17.

Mau H. Scoliosis screening in West Germany and its pitfalls with Scheuermann’s disease. Arch Orthop Trauma Surg, 1985, 104:201-206.

McCann HA, Sharp JC, Kinter TM, McEwan CN, Barillot C, Greenleaf JF. Multidimensional ultrasonic imaging for cardiology. Proc. IEEE, 1988;76:1063-1072.

McKenna C, Wade R, Faria R, Yang H, Stirk L, Gummerson N, Sculpher M, Woolacott N. EOS 2D/3D X-ray imaging system: a systematic review and economic evaluation. Health Technol Assess, 2012;16(14):1-188.

McLeod A, Roche A, Fennelly M. Case series: ultrasonography may assist epidural insertion in scoliosis patients. Can J Anaesth, 2005;52(7):717-720.

McNally DS, Naish C, Halliwell M. Intervertebral disc structure: observation by a novel use of ultrasound imaging. Ultrasound Med Biol, 2000;26(5):751-758.

Meairs S, Beyer J, Hennerici M. Reconstruction and visualization of irregularly sampled three- and four-dimensional ultrasound data for cerebrovascular applications. Ultrasound Med Biol, 2000;26:263-272.

Mehwald PS, Rusk RA, Mori Y, Li XN, Zetts AD, Jones M, Sahn DJ. A validation study of aortic stroke volume using dynamic 4-dimensional color Doppler: an in vivo study. J. Am. Soc. Echocardiogr., 2002;15(10):1045-1050.

Mellado JM, Larrosa R, Martin J, Yanguas N, Solanas S, Cozcolluela R. MDCT of variations and anomalies of the neural arch and its processes: part 1— pedicles, pars interarticularis, laminae, and spinous process. AJR, 2011a;197:W104–W113.

Mellado JM, Larrosa R, Martin J, Yanguas N, Solanas S, Cozcolluela R. MDCT of variations and anomalies of the neural arch and its processes: part 2— articular processes, transverse processes, and high cervical spine. AJR, 2011b;197:W114–W121.

Mercier L, Langø T, Lindseth F, Collins LD. A review of calibration techniques for freehand 3D ultrasound system. Ultrasound Med Biol, 2005;31(2):143-165.

Merz E. Use of 3D ultrasound in prenatal diagnosis. Ultraschall Med., 1995;16(4):154-161.

Middleditch A, Oliver J. Functional anatomy of the spine. 2e. Elsevier, 2005;1-62.

Miller NH. Genetics of familial idiopathic scoliosis. Clin Orthop Relat Res, 2007;462:6–10.

Mor-Avi V, Sugeng L, Lang RM, Three-dimensional adult echocardiography: where the hidden dimension helps. Current Cardiol. Rep., 2008;10(3):218-225.

More JJ. The Levenberg-Marquardt algorithm: implementation and theory. In Watson Ga (eds.) Numerical analysis. Lecture Notes in Mathematics 630. Berlin: Springer-Verlag, 1977;105-116.

Moreau A, Wang DS, Forget S, Azeddine B, Angeloni D, Fraschini F, Labelle H, Poitras B, Rivard CH, Grimard G. Melatonin signaling dysfunction in adolescent idiopathic scoliosis. Spine, 2004;29:1772–1781.

Morrissy RT, Goldsmith GS, Hall EC, Kehl D, Cowie GH. Measurement of the Cobb angle on radiographs of patients who have scoliosis. J Bone Joint Surg, 1990; 72:320-327.

Mubarak SJ, Wyatt MP, Leach J, Evaluation of the intra-examiner reliability of the scoliometer in measuring trunk rotation, Orthop Trans, 1984;9:113.

Muratore DM, Galloway RL. Beam calibration without a phantom for creating a 3D freehand ultrasound system. Ultrasound Med Biol, 2001;27:1557-1566.

Muratore DM, Russ JH, Dawant BM, Galloway RL Jr. Three-dimensional image registration of phantom vertebrae for image-guided surgery: a preliminary study.

Comp Aid Surg, 2002;7:342-352

Nash C, Moe JH. A study of vertebral rotation. J Bone Joint Surg, 1969;51:223-229

Nault ML, Allard P, Hinse S, Le Balanc R, Caron O, Labelle H, Sadeghi H, Relations between standing stability and body posture parameters in adolescent idiopathic scoliosis, Spine, 2002, 27:1911-1917.

Negrini S, Aulisa L, Ferraro C, Fraschini P, Masiero S, Simonazzi P, Tedeschi C, Venturin A. Italian guidelines on rehabilitation treatment of adolescents with scoliosis or other spinal deformities. Eura Medicophys, 2005;41:183-201.

Nelson TR, Elvins TT. Visualization of 3D ultrasound data. IEEE Comput. Graphics Appl., 1993;13(6):50-57.

Nelson TR, Pretorius DH. Interactive acquisition, analysis and visualization of sonographic volume data. Int J Imag Systems Technol, 1997;8:26-37.

Nelson TR, Pretorius DH. Three-dimensional ultrasound imaging. Ultrasound Med. Biol. 1998;24(9):1243-1270.

Ockenga J, Gebel M, Caselitz M, Topalidis T, Boozari B, Bleck J, Manns MP. 3D ultrasound in imaging diagnosis and follow-up of an atypical hydatid cyst. Z. Gastroenterol., 1998;36(7):599-603.

Ohbuchi R, Chen D, Fuchs H. Incremental volume reconstruction and rendering for 3-D ultrasound imaging. Proceedings of Visualization in Biomedical Computing ’92, Capel Hill, NC, USA: SPIE, 1992;1808:312-323.

Olafsson Y, Saraste H, Soderlund V, Hoff sten M. Boston brace in the treatment of idiopathic scoliosis. J Pediatr Orthop, 1995;15:524–527.

Pagoulatos N, Haynor DR, Kim Y. A fast calibration method for 3-D tracking of ultrasound images using a spatial localizer, Ultrasound Med. Biol., 2001;27(9):1219-1229.

Pehrsson K, Larsson S, Oden A, Nachemson A. Long-term follow up of patients with untreated scoliosis: a study of mortality, causes of death, and symptoms. Spine, 1992;17:1091-1096.

Penney GP, Blackall JM, Hamady MS, Sabharwal T, Adam A, Hawkes DJ. Registration of freehand 3D ultrasound and magnetic resonance liver images. Med. Image Analysis, 2004;8(1):81-91.

Peria O, Chevalier L, Francois-Joubert A, Caravel JP, Dalsoglio S, Lavallee S, Cinquin P, Using a 3D position sensor for registration of SPECT and US images of the kidney, Lecture Notes Comput Sci, 1995;903:23-29.

Peterson LE, Nachemson AL. Prediction of progression of the curve in girls who have adolescent idiopathic scoliosis of moderate severity. Logistic regression analysis based on data from The Brace Study of the Scoliosis Research Society. J Bone Joint Surg, 1995;77-A:823–827.

Piazza MR, Bassett GS. Curve progression after treatment with the Wilmington brace for idiopathic scoliosis. J Pediatr Orthop, 1990;10:39-43.

Pieper S, Weidenbach M, Berlage T, Registration of 3D ultrasound images to surface models of the heart. In Proceedings of the Conference on Interfaces to real and virtual worlds, Montpellier, France, 1997;211-213.

Prager RW, Rohling RN, Gee AH, Berman L. Rapid calibration for 3D freehand ultrasound, Ultrasound Med. Biol., 1998;24(6):855-869.

Prager RW, Gee AH, Berman L. Stradx: real-time acquisition and visualization of freehand three-dimensional ultrasound, Med Image Anal, 1999;3(2):129-140.

Prager RW, Gee AH, Treece GM, Berman L. Freehand 3D ultrasound without voxels: volume measurement and visualization using the Stradx system, Ultrasonics, 2002;40(1-8):109-115.

Prager RW, Gee AH, Treece GM, Cash CJC, Berman L. Sensorless freehand 3-D ultrasound using regression of the echo intensity. Ultrasound Med Biol, 2003;29(3):437-446.

Prager RW, Ijaz UZ, Gee AH, Treece GM. Three-dimensional ultrasound imaging. Proc InstMech EngH 2010;224:193–223.

Prakasa KR, Dalal D, Wang J, Bomma C, Tandri H, Dong J, James C, Tichnell C, Russell SD, Spevak P, Corretti M, Bluemke DA, Calkins H, Abraham TP. Feasibility and Variability of Three Dimensional Echocardiography in Arrhythmogenic Right Ventricular Dysplasia/Cardiomyopathy. Am. J. Cardiol, 2006;97(5):703-709.

Pruijis JEH, Hageman MAPE, Kessen W, van der Meer R, van Wieringen JC. Variation in Cobb angle measurements in scoliosis. Skeletal Radiol, 1994;23:517-520.

Purnama KE, Wilkinson MH, Veldhuizen AG, van Ooijen PM, Lubbers J, Burgerhof JG, Sardjono TA, Verkerke GJ. A framework for human spine imaging using a freehand 3D ultrasound system. Technol Health Care, 2010;18(1):1-17.

Raga F, Bonilla-Musoles F, Casan EM, Klein O, Bonilla F. Assessment of endometrial volume by three-dimensional ultrasound prior to embryo transfer: clues to endometrial receptivity. Human Reproduction, 1999;14(11):2851-2854.

Rankin G, Stokees M. Reliability of assessment tools in rehabilitation: An illustration of appropriate statistical analyses. Clin Rehabil, 1998;12:187–199.

Reamy BV, Slakey JB. Adolescent idiopathic scoliosis: review and current concepts.

Am Fam Physician, 2001;64:111–116.

Reverdy F., Ithurralde G, Dominguez N. Advanced Ultrasonic 2D Phased-Array Probes. In: Proc. of the 18th Conf. on Non- Destructive Testing. Online publication at http://www.ndi.net. 2012.

Riccabona M, Nelson TR, Pretorius DH, Davidson TE. Three dimensional ultrasound: display modalities in the fetal spine and thorax Eur. J Radiol, 1996;22:141-145.

Risser JC. Important practical facts in the treatment of scoliosis. Instr Course Lect, 1948;5:248-260.

Rizzatto G. Evolution of ultrasound transducers:1.5 and 2D arrays. Eur Radiol, 1999;9(3):304-306.

Roelandt JRTC, Ten Cate FJ, Vletter WB, Taams MA. Ultrasonic dynamic three-dimensional visualization of the heart with a multiplane transesophageal imaging transducer. J Am Soc Echocardiogr, 2004;7:217-229.

Rohling RN, Gee AH, L Berman. Three-dimensional spatial compounding of ultrasound images. Med Image Anal, 1997;1(3):177-193.

Rohling RN, Gee AH, L Berman. A comparison of freehand three-dimensional ultrasound reconstruction techniques. Med Image Anal, 1999;3(4):339-359.

Rousseau F, Hellier P, Barillot C. Confhusius: A robust and fully automatic calibration method for 3D freehand ultrasound. Med Image Analyst, 2005;9:25-38.

Sahlstrand T., The clinical value of Moire topography in the management of scoliosis, Spine, 1986;11(5):409-417.

San Jose-Estepar R, Martin-Fernandez M, Caballero-Martinez PP, Alberola-Lopez C, Ruiz-Alzola J. Freehand ultrasound reconstruction based on ROI prior modeling and normalized convolution. Processing of Medical Image Computing and Computer-Assisted Intervention (MICCAI), Montreal, Canada: Springer, 2003;2879:382-390.

Sanches JM, Marques JS. A Rayleigh reconstruction/interpolation algorithm for 3D ultrasound. Pattern Recog Lett, 2000;21:917-926.

Sato Y, Nakamoto M, Tamaki Y, Sasama T, Sakita I, Nakajima Y, Monden M, Tamura S. Image guidance of breast cancer surgery using 3-D ultrasound images and augmented reality visualization. IEEE Trans Med Imaging, 1998;17(5):681-693.

Schild RL, Knobloch C, Dorn C, Fimmers R, van der Ven H, Hansmann M. The role of ovarian volume in an in vitro fertilization programme as assessed by 3D ultrasound. Arch. Gynecol. Obstet., 2001;265:67-72.

Schmitz A, Gabel H, Weiss HR, Schmitt O., Anthropometric 3D-body scanning in idiopathic scoliosis, Z Orthop Ihre Grenzgeb, 2002;140(6):632-636.

Shea KG, Stevens PM, Nelson M, Smith JT, Masters KS, Yandow S. A comparison of manual versus computer-assisted radiographic measurement. Intraobserver measurement variability for Cobb angles. Spine, 1998;23:551–555.

Sherebrin S, Fenster A, Rankin RN, Spence D. Freehand three-dimensional ultrasound: Implementation and applications. Proceedings of Medical Imaging 1996: Physics of Medical Imaging, Newport Beach, CA, USA: SPIE, 1996;2708:296-303.

Shiota T, Jones M, Chikada M, Fleishman C, Castellucci JB, Cotter B, DeMaria AN, von Ramm OT, Kisslo J, Ryan T, Sahn D. Real-time three-dimensional echocardiography for determining right ventricular stroke volume in an animal model of chronic right ventricular volume overload. Circulation, 1998;97:1897-1900.

Shmulewitz A, Teefey SA, Robinson BS. Factors affecting image quality and diagnostic efficacy in abdominal sonography: a prospective study of 140 patients, J Clin Ultrasound, 1993;21:623-630.

Sjolie E, Kaspersen JH, Wesche J, Lindseth F, Hernes TAN. Minimal invasive abdominal surgery based on ultrasound vision, possible? In CARS 2001: computer assisted radiology and surgery, International Congress Series, 2001;1230:38-43 (Elsevier, Amsterdam).

Smith SW, Booi RC, Light ED, Merdes CL, Wolf PD. Guidance of cardiac pacemaker leads using real time 3D ultrasound: feasibility studies. Ultrasonic imaging, 2002;24(2):119-128.

Smith WL, Fenster A (2000). Optimum scan spacing for three-dimensional ultrasound by speckle statistics. Ultrasound Med Biol, 2000;26:551-562.

Stagnara P., Spinal Deformity (Trans Dove J.), London:Butterworths, 1988;16-23.

State A, Chen DT, Techor C, Brandt A, Chen H, Ohbuchi R, Bajura M, Fuchs H, Case study: Observing a volume rendered fetus within a pregnant patient. In: Proceedings of the Conference on Visualization ’94, IEEE Visualization. IEEE Computer Society Press California, 1994;364-368.

Stetten GD, Ota T, Ohazama CJ, Fleishman C, Castellucci J, Oxaal J, Ryan T, Kisslo J, von Ramm OT. Real-time 3D ultrasound: a new look at the heart. J. Cardiovascular Diagnosis Procedures, 1998, 15(2):73-84.

Stetten GD, Drezek R. Active Fourier contour applied to real time 3D ultrasound of the heart. Int. J. Image Graphics, 2001;1(4):647-658.

Stokes IAF, Bigalow LC, Moreland MS. Three-dimensional spinal curvature in idiopathic scoliosis. J Orthop Res, 1987;5:102-113.

Stokes IAF, Shuma-Hartwick D, Moreland MS: Spine and back-shape changes in

Scoliosis, Acta Orthop Scand, 1988;59:128-133.

Stokes IAF, Gardner-Morse M. Analysis of the interaction between vertebral lateral deviation and axial rotation in rotation in scoliosis. J. Biomechanics, 1991;24:753-759.

Stokes IAF, Three-dimensional terminology of spinal deformity: a report presented to the Scoliosis Research Society by the Scoliosis Research Society Working Group on 3-D terminology of spinal deformity, Spine, 1994;19:236-248.

Suk SI, Chung ER, Kim JH, Kim SS, Lee JS, Choi WK. Posterior vertebral column resection for severe rigid scoliosis. Spine, 2005;30:1682-1687.

Suzuki S., Yamamuro T, Shikata J, Shimizu K., Iida H. Ultrasound measurement of vertebral rotation in idiopathic scoliosis. J Bone Joint Surg, 1989:78(B):252-255.

Tang SP, Cheng JCY, Ng BKW, Lam TP. Adolescent idiopathic scoliosis (AIS): An overview of the etiology and basic management principles. HK J Paediatr, 2003;8:299-306.

Thaler M, Kaufmann G, Steingruber I, Mayr E, Liebensteiner M, Bach C. Radiographic versus ultrasound evaluation of the Risser grade in adolescent idiopathic scoliosis: a prospective study of 46 patients. Eur Spine J, 2008;17(9):1251-1255.

Thawait GK, Chhabra A, Carrino JA. Spine segmentation and enumeration and normal variants. Radiol Clin North Am, 2012;50(4):587-598.

Thometz JG, Lamdany R, Liu XC, Lyon RJ. Relationship between Quantec measurement and Cobb angle in patients with idiopathic scoliosis. Pediatr Orthop, 2000;20(4):512-516.

Thomsen M., Abel R. Imaging in scoliosis from the orthopedic surgeon's point of view. Eur J Radiol, 2006;58:41-47.

Thune N, Gilja OH, Hausken T, Matre K. A practical method for estimating enclosed volumes using 3D ultrasound. Eur J Ultrasound, 1996;3:83-92.

Treece GM, Preager RW, Gee AH, Berman L. Fast surface and volume estimation from non-parallel cross-sections for freehand three-dimensional ultrasound. Med. Image Anal, 1999;3(2):141-173.

Treece GM, Preager RW, Gee AH, Berman L. 3D ultrasound measurement of large organ volume. Med. Image Anal, 2001;5(2):41-54.

Treece GM, Gee AH, Prager RW, Cash CJC, Berman LH. High-definition freehand 3D ultrasound. Ultrasound Med. Biol, 2003;29(4):529-546.

Tong S, Downney DB, Cardinal HN, Fenster A. A three-dimensional ultrasound prostate imaging system. Ultrasound Med. Bio, 1996;22:735-746

Torell G, Nachemson A, Haderspeck-Grib K, Schultz A. Standing and supine Cobb measures in girls with idiopathic scoliosis. Spine, 1985;10:425-427.

Trobaugh JW, Trobaugh DJ, Richard WD. Three-dimensional imaging with stereotactic ultrasonography. Comput Med Imaging Graph, 1994;18:315-323.

Tuthill TA, Krucker JF, Fowlkes JB, Carson PL. Automated three-dimensional US frame positioning computed from elevational speckle decorrelation. Radiology, 1998;209:575-582.

Van Schaik JP, Verbiest H, Van Schaik FD, Isolated spinous process deviation: a pitfall in the interpretation of AP radiographs of the lumbar spine. Spine, 1989;14:970-976.

Vrtovec T, Pernus F, Likar B. A review of methods for quantitative evaluation of spinal curvature. Eur Spine J, 2009;18(5):1-15.

Wei Z, Wan G, Gardi L, Mills G, Downey D, Fenster A Robot-assisted 3D-TRUS guided prostate brachytherapy: system integration and validation. Med Phys, 2004;31:539-548.

Weismann CF, Datz L. Diagnostic algorithm: how to make use of new 2D, 3D, 4D ultrasound technologies in breast imaging. Eur J Radiol, 2007;64(2):250-257.

Weinstein SL, Zavala DC, Ponseti IV. Idiopathic scoliosis: long-term follow-up and prognosis in untreated patients. J. Bone Joint Surg. Am, 1981;63:702-712.

Weinstein SL, Ponseti IV. Curve progression in idiopathic scoliosis. J. Bone Joint Surg. Am, 1983;65:447-455.

Weintstein SL, Dolan LA, Spratt KF, Peterson KK, Spoonamore MJ, Ponseti IV. Health and function of patients with untreated idiopathic scoliosis – a 50-year natural history study. JAMA, 2003;289(5):559-567.

Weinstein SL, Dolan LA, Cheng JC, Danielsson A, Morcuende JA. Adolescent idiopathic scoliosis. Lancet, 2008;371:1527–1537.

Weiss HR, Negrini S, Rigo M, Kotwicki T, Hawes MC, Grivas TB, Maruyama T, Landauer F. Indications for conservative management of scoliosis (guidelines). Scoliosis, 2006;1:5.

Wessberg P, Danielson B, Willen J. Comparison of Cobb angles in idiopathic scoliosis on standing radiographs and supine axially loaded MRI. Spine, 2006;31:3039-3044.

Wills BP, Auerbach JD, Zhu X. Caird MS, Horn BD, Fynn JM, Drummond DS, Dormans JP, Ecker ML. Comparison of Cobb angle measurement of scoliosis radiographs with preselected end vertebrae: traditional versus digital acquisition.

Spine, 2007;32:98–105.

Winter S, Brendel B, Pechlivanis I, Schmieder K, Igel C. Registration of CT and intraoperative 3D ultrasound images of the spine using evolutionary and gradient-based methods. IEEE Trans. Evolutionary Comput, 2008;12(3):284-296.

Wu MH, Hus CC, Huang KE, Detection of congenital Mullerian duct anomalies using three-dimensional ultrasound. J. Clin. Ultrasound, 1997;25(9):487-492.

Yagel S., Cohen SM, Shapiro I, Valsky DV. 3D and 4D ultrasound in fetal cardiac scanning: a new look at the fetal heart. Ultrasound Obstet. Gynecol, 2007;29:81-95.

Yazici M, Acaroglu ER, Alanay A, Deviren V, Cila A, Surat A. Measurement of vertebral rotation in standing versus supine position in AIS. J Ped Orthop, 2001; 21:252-256.

Yong F, Wong HK, Chow KY. Prevalence of Adolescent Idiopathic Scoliosis among Female School Children in Singapore. Ann Acad Med Singapore, 2009;38:1056-1063.

Zheng YP, Cheung CW. A three-dimensional (3D) ultrasound imaging system for assessing scoliosis. US and PCT patent pending. No. 12/509,705.Jul 2009.

Zheng YP, Cheung CW, He JF, Chen X. Method and device for 3D ultrasound imaging. Chinese patent issued. No. 200810094381.9. Jan 2011.

Zheng YP, Cheung CW, Method and device for 3D ultrasound imaging. Chinese patent filed No.201210163528.1 May 2012.

Zubarev AV. Ultrasound of renal vessels. Eur. Radiol., 2001;11(10):1902-1915.